REFORM

REstoring rivers FOR effective catchment Management

Deliverable	D2.1 Part 2
Title	Thematic Annexes of the Multi-scale Hierarchical Framework

Author(s)

(authors of D2.1 Part 2 in alphabetical order*) S. Bizzi[1], B. Blamauer[2], G. Braca[3], M. Bussettini[3], B. Camenen[4], F. Comiti[5], L. Demarchi[1], D. García De Jalón[6], M. González Del Tánago[6], R.C. Grabowski[7], A.M. Gurnell[7], H. Habersack[2], B. Lastoria[3], A. Latapie[4], V. Martínez-Fernández[6], J.O. Mountford[8], L. Nardi[9], M.T. O'Hare[8], C. Percopo[3], M. Rinaldi[9], N. Surian[10], C. Weissteiner[1], L. Ziliani[10]

[1]JRC, [2]BOKU, [3]ISPRA, [4]IRSTEA, [5]Free University of Bozen-Bolzano, [6]UPM, [7]QMUL, [8]NERC, [9]UNIFI, [10]University of Padova

PU	Public	X
PP	Restricted to other programme participants (including the Commission Services)	
RE	Restricted to a group specified by the consortium (including the Commission Services)	
CO	Confidential, only for members of the consortium (including the Commission Services)	

* Please cite the whole of Deliverable 2.1 as follows:

A.M. Gurnell, B. Belletti, S. Bizzi, B. Blamauer, G. Braca, T.Buijse, M. Bussettini, B. Camenen, F. Comiti, L. Demarchi, D. García De Jalón, M. González Del Tánago, R.C. Grabowski, I.D.M. Gunn, H. Habersack, D. Hendriks, A. Henshaw, M. Klösch, B. Lastoria, A. Latapie, P. Marcinkowski, V. Martínez-Fernández, E . Mosselman, J.O. Mountford, L. Nardi, T. Okruszko, M.T. O'Hare, M. Palma, C. Percopo, M. Rinaldi, N. Surian, C. Weissteiner and L. Ziliani (2014) A multi-scale framework and indicators of hydromorphological processes and forms. Deliverable 2.1, a report in four parts of REFORM (REstoring rivers FOR effective catchment Management), a Collaborative project (large-scale integrating project) funded by the European Commission within the 7th Framework Programme under Grant Agreement 282656.

Please cite Part 2 of Deliverable 2.1 as follows:

S. Bizzi, B. Blamauer, G. Braca, M. Bussettini, B. Camenen, F. Comiti, L. Demarchi, D. García De Jalón, M. González Del Tánago, R.C. Grabowski, A.M. Gurnell, H. Habersack, B. Lastoria, A. Latapie, V. Martínez-Fernández, J.O. Mountford, L. Nardi, M.T. O'Hare, C. Percopo, M. Rinaldi, N. Surian, C. Weissteiner and L. Ziliani (2014) Thematic Annexes of the Multi-scale Hierarchical Framework. Deliverable 2.1, Part 2, of REFORM (REstoring rivers FOR effective catchment Management), a Collaborative project (large-scale integrating project) funded by the European Commission within the 7th Framework Programme under Grant Agreement 282656.

Summary

Background and Introduction to Deliverable 2.1.

Work Package 2 of REFORM focuses on hydromorphological and ecological processes and interactions within river systems with a particular emphasis on naturally functioning systems. It provides a context for research on the impacts of hydromorphological changes in Work Package 3 and for assessments of the effects of river restoration in Work Package 4.

Deliverable 2.1 of Work Package 2 proposes a hierarchical framework to support river managers in exploring the causes of hydromorphological management problems and devising sustainable solutions. The deliverable has four parts. Part 1 provides a full description of the hierarchical framework and describes ways in which each element of it can be applied to European rivers and their catchments. Part 2 (this volume) includes thematic annexes which provide more detailed information on some specific aspects of the framework described in Part 1. Part 3 includes catchment case studies which present the application of the entire framework described in Part 1 to a set of European catchments located in different biogeographical zones. Part 4 includes catchment case studies which present a partial application of the framework described in Part 1 to a further set of European catchments.

Summary of Deliverable 2.1 Part 2.

Part 2 of Deliverable 2.1 provides fuller details concerning some specific topics outlined in Part 1.

A method for automating delineation of river reaches is described and tested (Annex A). Information on the natural riparian and aquatic plant communities of Europe is tabulated (Annex B). Flow regime analysis (Annex C) is explored in far greater detail than in part 1, with indicators fully defined and several different methods described. Quantifying the calibre and structure of river sediments is a challenging task, so Annex D goes into this topic in depth, providing the information required for sampling regimes to be designed. In Annex E, some additional information on the classification of rivers and floodplains is provided.

Following a brief description of sediment budgets (Annex F), a more extended description of empirically defined threshold conditions between rivers of different type (Annex G), and a description of a range of sediment transport formulae (Annex H), Annex I presents a series of modelling applications that have been developed for network, reach and habitat scale applications. These are presented in the form of applications of particular models to individual European rivers, many of which are the focus of catchment case studies in Parts 3 and 4 of Deliverable 2.1.

Deliverable 2.1 Part 2 concludes with a review of how remote sensing can contribute to assessment of particular features, processes and characteristics that are required during the application of the hierarchical framework.

Table of Contents

This document is part 2 of a 4 part report and contains Thematic Annexes to the Hierarchical Framework proposed in Part 1.

Annex A
Automated Delineation of River Reaches
(Case Study: Upper Esla River, North West Spain)

Vanesa Martínez-Fernández, Marta González del Tánago, Diego García de Jalón
E.T.S. Ingenieros de Montes, Universidad Politécnica de Madrid (UPM), Spain

Summary

This work aims to explain the general procedure for developing automated delineation of river reaches and to provide an alternative to the traditional delineation approach based on expert criteria. This methodology has been applied to three Spanish rivers to illustrate the procedure. The use of automated delineation to identify spatial discontinuities has recently become very common due to the increase in the availability of GIS and remote sensing information. The principles indicate that the automated delineation approach seems to be more objective and statistically reliable than expert criteria. Among the large number of algorithms that could be considered to identify spatial discontinuities of river reaches, the Pettit´s test was used. The limitations and advantages of this algorithm are briefly discussed.

A.1   Introduction

Identification of spatial discontinuities along the continuum of the fluvial systems is necessary for many purposes. Physical characterization, sampling design, monitoring, or reference assignment are examples of current procedures that have to be based on specific river reaches or segments, which need to be delineated in advance.

To date, expert criteria and graphical methods have been the main procedures to detect different types of discontinuities and delineate nested spatial units for characterizing stream networks (Schumm *et al.*, 1994; Seelbach *et al.*, 2006). Nevertheless, the automated segmentation of a river using different types of algorithm is a procedure that is becoming more frequently applied, because it is efficient and objective. The segmentation of the Mississippi River made by Shumm *et al.* (1994) based on expert criteria was improved by Orlowski *et al.* (1995), who applied multi-response permutation procedures proposed previously by Mielke (1991). Brenden *et al.* (2008) proposed a spatially constrained clustering program for river valley segmentation from GIS digital river networks. They applied it to the Michigan and Wisconsin River networks based on seven physicochemical stream attributes. The results were compared with previous classifications based on expert criteria (Seelbach *et al.*, 2006), and showed a greater number of segments with the automated method. More recently, spatial disaggregation and aggregation procedures for characterizing fluvial features at the network-scale have been applied to the Rhone basin in France by Alber and Piégay (2011). Their innovative procedure for obtaining homogeneous spatial units was carried out by applying Pettitt´s test (Pettitt, 1979) to a set of data measured on the streamline, the valley bottom and the active channel. More recently, this spatial aggregation method has been applied in

other research as a necessary step for achieving different objectives (Toone *et al.*, 2014; Notebaert & Piégay, 2013), including being used as a tool for management aquatic resources and fishing (Wang *et al.*, 2012). New and improved methods are being developed for identifying appropriate spatial units for sampling design, data interpolation, formulation of management actions (Wang *et al.*, 2006) and for application of morphological (Rinaldi *et al.*; 2013) and biological indices, where automated segmentation procedures have enormous potential for objectively and efficiently detecting homogeneous units within complex fluvial systems.

In this report an example of automated delineation of homogeneous spatial units is presented. The objective has been to present a potential tool for discretizing the spatial heterogeneity in stream networks from spatially continuous data related to the hierarchical framework described in Deliverable 2.1 Part 1. To illustrate application of this tool, we have applied the methodology to the Upper Esla River (Duero Basin, North West Spain). In this example application, only geomorphic variables related to fluvial processes have been used (Kondolf *et al*, 2003; Brierley and Fryirs, 2000), but other hydrologic or biologic variables could be used for the same purpose.

A.2   Methodology

We have applied a method for automatically delineating river reaches to the Upper Esla Basin, Duero Basin, North West Spain (Figure A.1), including the Upper Esla river and the Porma and Curueño rivers. This methodology is based on that of Alber and Piégay (2011) with some modifications which are explained below.

We used two types of raw data available at the scale of the catchment: (i) a DEM with a 5 m spatial resolution (IGN, 2011); and (ii) orthophotograph cover with a 0.25 – 0.5 m spatial resolution, dated 2007. From these we extracted relevant variables using ESRI Arcmap version 9.3, with the ArcHydrotools, 3DAnalysis, Spatial analyst and Xtoolspro extensions.

In this example application, we selected three geographic elements commonly used for spatial analysis of stream networks: the channel planform, the valley bottom zone and the active channel, from which we extracted measurements of three variables: the channel slope, the valley bottom width and the active channel width, respectively. To achieve this, we followed four steps: (1) Delineation of the three geographic elements; (2) Delineation of the reference axis of each element; (3) Systematic measurement of the three variables and creation of a database; (4) Application of an algorithm for detecting significant discontinuities along each analyzed geographical element, according to the values of the three variables. Having completed these four stages, segments need to be delineated manually according to specific objectives, including the potential to consider additional criteria such as a minimum segment length or a maximum number of segments. Although this final delineation may be based on practical or relatively subjective constraints, the characterization of the segments is always supported by statistical data.
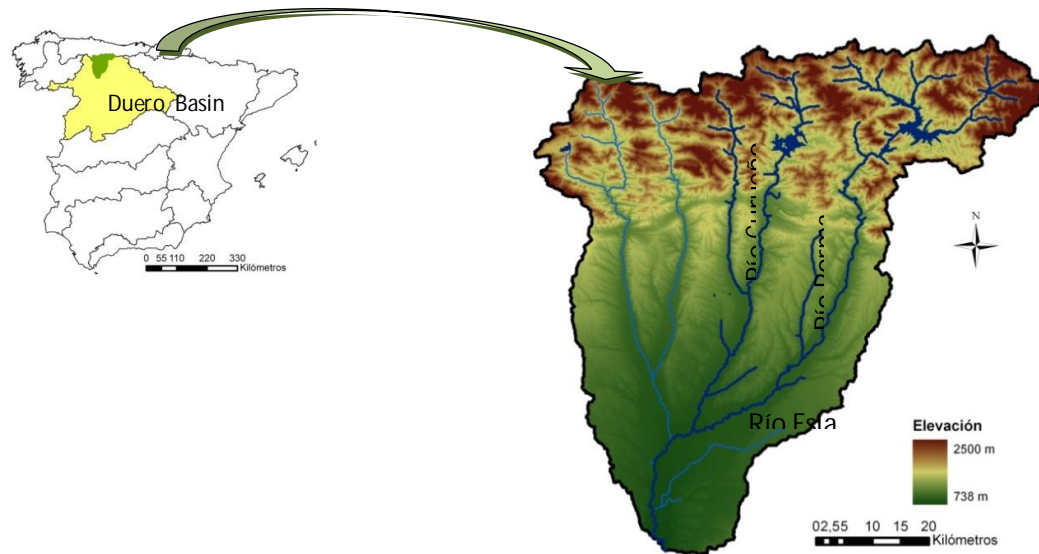
Figure A.1   Location of the study area (Upper Basin of the Esla River, Duero Basin).

A.2.1 Delineation of geographic elements in which segmentation procedures are to be applied

Once the geographic elements are selected, their delineation by means of polylines (channel planform) or polygons (valley bottom zone and active channel) represents the first stage in the procedure (Figure A.2).

The polyline to schematize the river channel planform was manually extracted from DEM and orthophotograph information. The polygon to delineate the valley bottom defines the alluvial zone inside which geographical objects required for subsequent analysis are located (e.g. active channel, erodible corridor, riparian forest, geomorphic units…). The polygon was extracted manually, combining information from a DEM and orthophotographs, and the layout of cross sections. Some semi-automated methods are available for extracting a valley bottom polygon from a DEM (Williams *et al.*, 2000; Gallant and Dowling, 2003; Hall *et al.*, 2007) but the results require careful examination after processing. Finally, the polygon delineating the active channel was manually extracted from orthophotographs. In this study we considered the single or multiple channel(s) and adjacent unvegetated gravel bars as the active channel, following recommendations by Gurnell (1997).
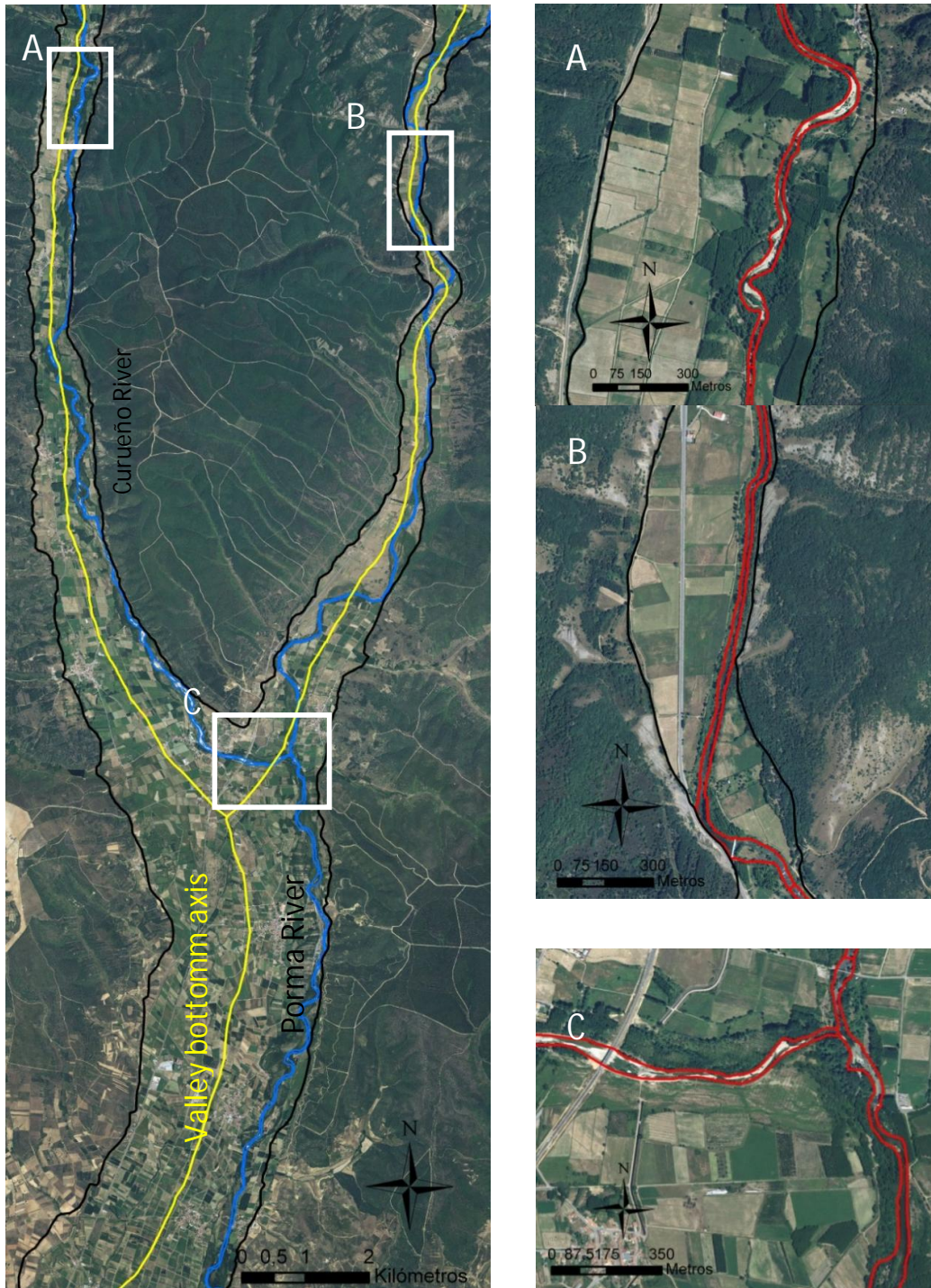
Figure A.2 Polygons (valley bottom in black and active channel in red) and polylines (valley axis in yellow, channel planform in blue) delineated in the study area.

A.2.2 Delineation of the referencing axis

Systematic measurement along the selected geographic objects requires, first, the creation of a referencing axis on which all the measurements are based. For the channel planform the reference axis coincides with its polyline. For the valley bottom, the reference axis is defined using the valley bottom polygon. A semi-automatic procedure was used, following Alber and Piégay (2011), which is based on Thiessen polygonalization, and extracts the skeleton of every polygonal and ramified polygon (Figure A.3). Lastly, the reference axis for the active channel was the same polyline that schematized the channel planform.
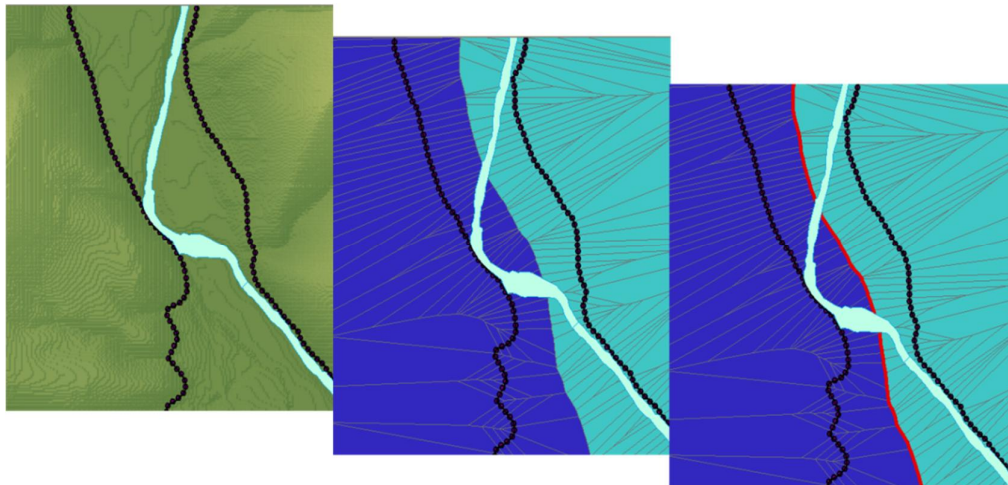
Figure A.3   Thiessen polygonalization procedure to define the axis of the valley bottom (in red).

A.2.3 Data gathering: Systematic measurements of selected variables in the geographic elements

Once the respective reference axes have been defined, systematic measurements of the relevant variables are undertaken at a specific spatial resolution, which is limited by the resolution of the available data. In the present case a resolution of 200 m was selected, which is more than 10 times the spatial resolution of the DEM and orthophotographs.

Many different variables could be measured to support the automated delineation procedure. In the present case we measured the elevation along the polyline schematizing the channel planform to derive the channel slope and longitudinal profile, and the width of the valley bottom and the active channel polygons.

Channel slope and longitudinal profile.

First, we measured the elevation along the river channel polyline with a uniform spacing of 200 m, generating a GIS layer of channel elevations. With the elevation and distance data we created the longitudinal profile. We corrected this long profile following a method described in Jain *et al.* (2006). For example, from the obtained long profiles, we located

elevation values exceeding upstream elevation values, and then corrected them based on extrapolation from upstream and downstream "correct" values. Then, we calculated the channel slope value by dividing the difference between upstream and downstream elevation corrected values by the measurement interval, which is 200 m.

Valley bottom width and active channel width.

Valley bottom width (Figure A.4) and active channel width (Figure A.5) were systematically measured every 200 m along the respective polygons. The measurements were taken orthogonally to the respective reference axis. In the case of the dams, both variables were recorded as the width of the water surface.
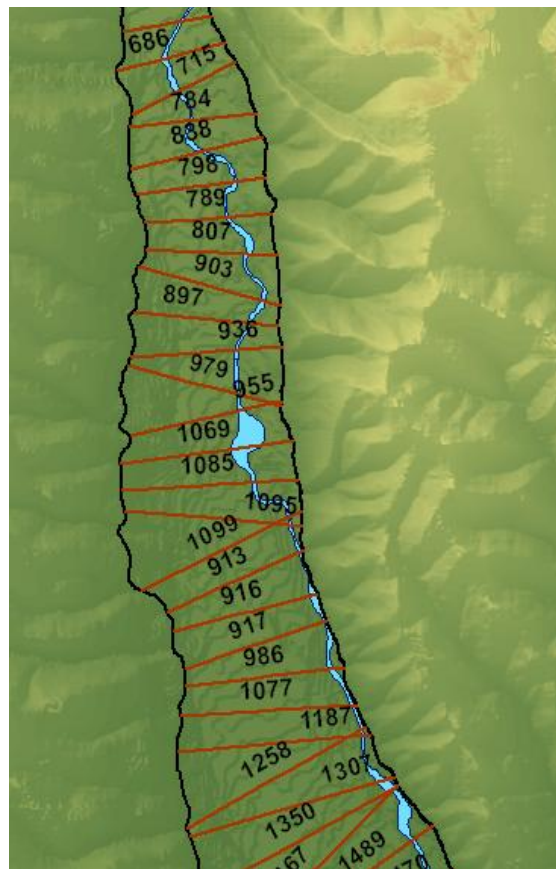
Figure A.4   Valley bottom width measurements.

Figure A.5   Active channel width measurements.

A.2.4 Application of an algorithm for detecting significant discontinuities

The procedure continues by applying spatial aggregation algorithms to the data created for the variables measured in the preceding stages, to delineate homogeneous segments or reaches. Many different algorithms and statistical techniques can be applied to delineate river reaches. Leviander *et al.* (2012), compared seven algorithms belonging to four families: tests of homogeneity methods (Pettitt, 1979; Hubert, 2000; Kehagias *et al.*, 2005); contrast enhancing methods (Leviandier *et al.*, 2000), spatially constrained classification methods (Brenden et al., 2008), and hidden Markov models (Kehagias, 2004). They concluded that all methods produced similar segmentations. Notebaert and Piégay (2013) used a test of homogeneity method employing the Pettitt test to achieve segmentation of a fluvial system from a geomorphic variable, the floodplain width.

The Pettitt test ($\alpha = 0.05$) was also used in the present application. This non-parametric, univariate test detects a unique change point in data series that are non stationary, following iterative runs of the algorithm. We chose this method because of its low complexity and easy implementation of the software. A full description of the test can be found in Pettitt (1979) and Leiviandier *et al.* (2012).   In the present research the algorithm was implemented using a script by Pascal Haenggi written in R (version 2.15.1).

We identified segments as the portions between two discontinuity and consecutive points detected by the Pettitt test. The number of segments obtained using each of the three variables and the average values of segment length were then compared.

A.3   Results

Figures A.6, A.7 and A.8 show the spatial variability of the measured variables along the three geographical elements of the rivers, together with the points where significant changes in this variability were identified according to the Pettit´s test. It is apparent that each variable produces different results, with the channel slope detecting only four breaks in the series while the other variables detect many more. The valley-bottom width showed much greater variability than the active channel width, contrary to what might be expected, and as a result, analysis of this variable yielded a larger number of smaller length segments than the other variables.

Table A.1 summarizes the number of discontinuities obtained for each variable, and the average values of the segment lengths between consecutive discontinuities. Analysis of channel slope detected four discontinuities in the three rivers resulting in quite different segment lengths (91 km for the Esla river, 80 km for the Porma river and 48 km for the Curueño river). This result reflects the relatively homogenous topography within the study area, and could be the basis for delineating landscape units or river segments at a relatively coarse scale. Analysis of the valley-bottom width identified a number of discontinuities in proportion to the river length (the greater the length, the greater the number of segments). Finally, analysis of the active channel width detected a larger number of discontinuities along the Curueño River than the Porma river, which could be related to flow regulation by the Porma dam that decreases the heterogeneity of the channel downstream. Both variables (valley width and channel width) detect a higher spatial variability than the channel slope, and could contribute to delineating river reaches or sectors at a relatively fine scale.

The geographical location of variable discontinuities along the studied rivers is shown in figures A.9 and A.10. In the case of the channel slope (Figure A.9) the results are very well correlated with topography and with tributary confluences, indicating that the segments correspond with different landscape units.

Regarding the valley bottom width (Figure A.10 left), the number of discontinuities is very large, indicating that a post-analysis aggregation stage is needed to produce a practical segmentation. On the contrary, analysis of the active channel width (Figure A.10 right) produced a reasonable number of river discontinuities that could be used for delineating reaches, although once again, some post-analysis aggregation is needed to yield a practical number of reaches.

Table A.1: Number of discontinuities (N) and values (mean and standard deviation) of the length of the resulting segments (L)

	Channel slope		Valley bottom width		Active channel width	
	N	L (km) ± SD	N	L (km) ± SD	N	L (km) ± SD
Esla	4	10.5 ± 6.46	37	2.82 ± 1.87	10	26.45 ± 22.45
Porma	4	13.0 ± 14.9	20	3.1 ± 2.04	5	18.0 ± 8.55
Curueño	4	5.7 ± 3.36	15	2.81 ± 1.76	8	11.3 ± 10.68
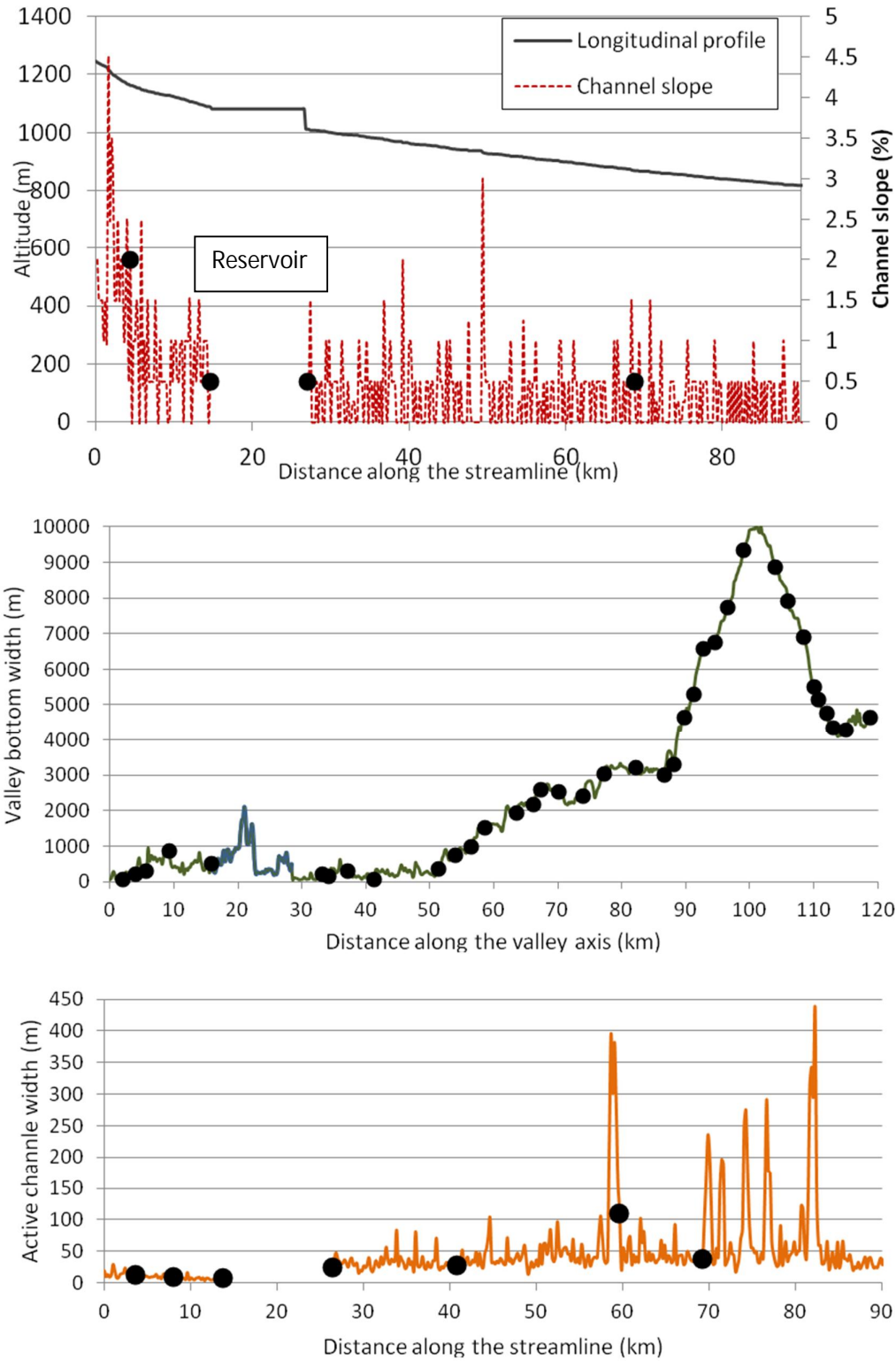
Figure A.6 Automated delineation of discontinuities along the river Esla based on spatial variability in three variables.
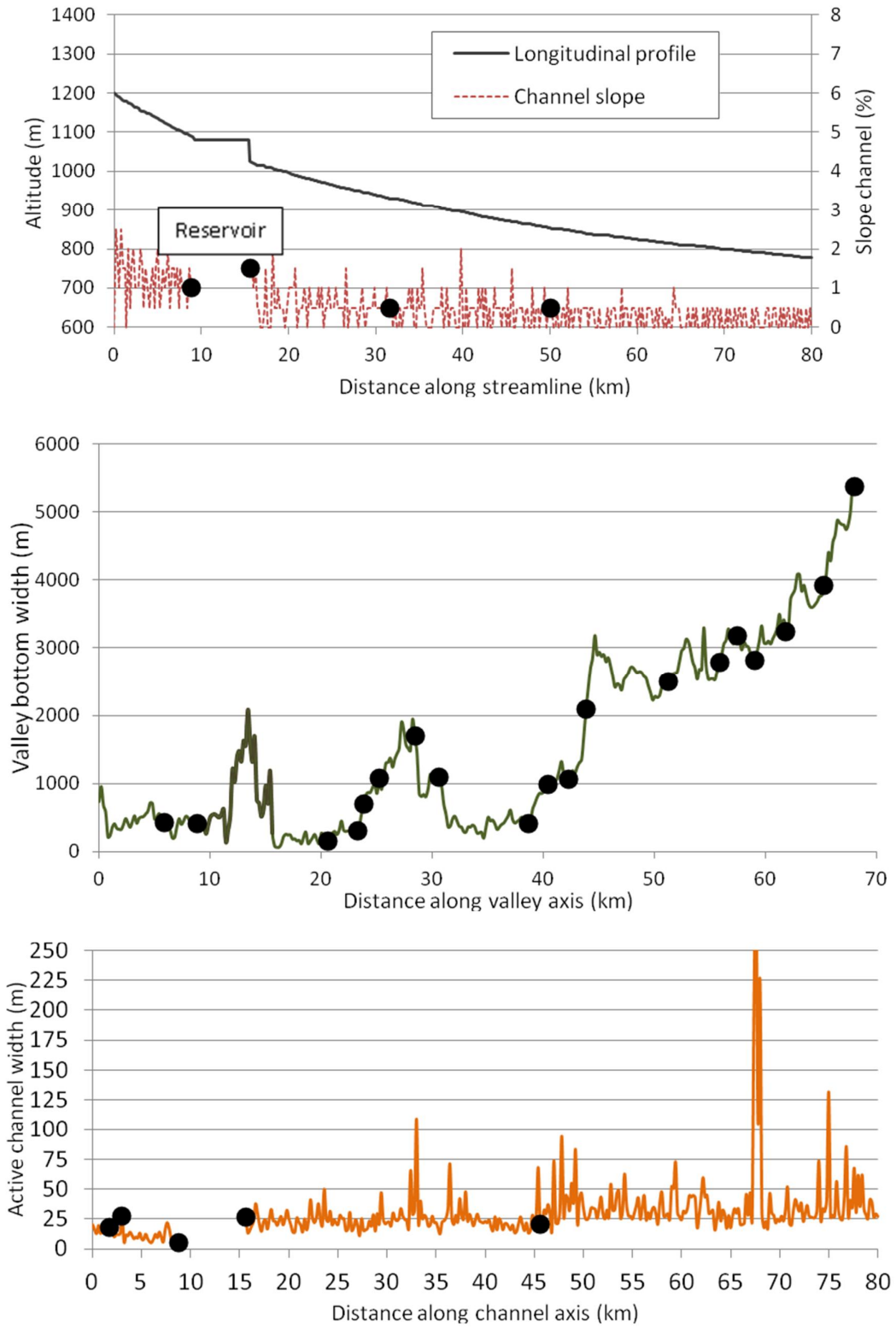
Figure A.7   Automated delineation of variable discontinuities along the river Porma, based on spatial variability in three variables.
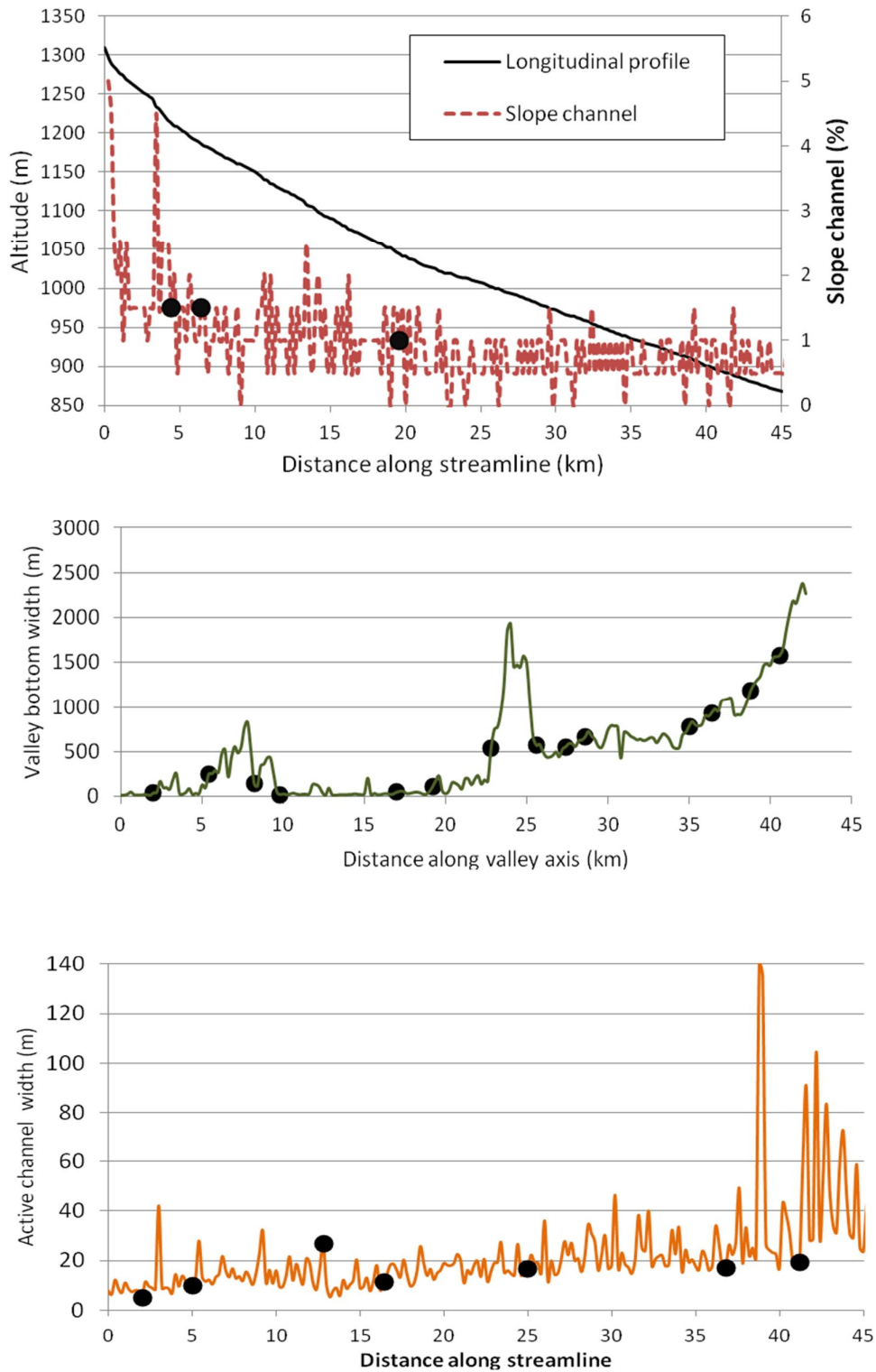
Figure A.8   Automated delineation of variable discontinuities along the river Curueño, based on spatial variability in three variables.
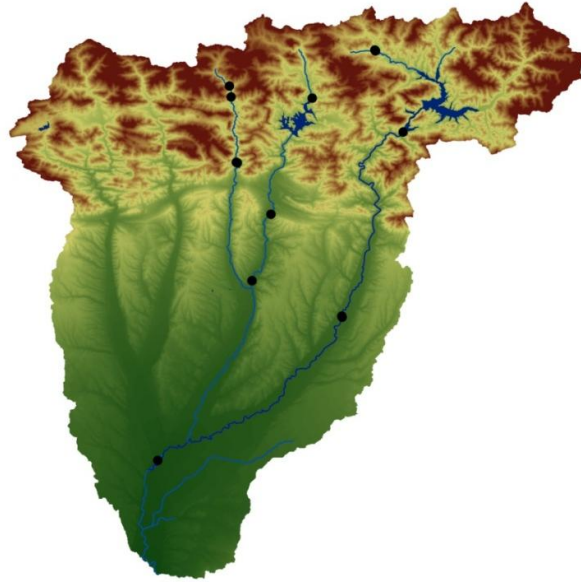
Figure A.9   Location of the channel slope discontinuities along the studied rivers, which are closely related to the different landscape units (based on topography) and river segments (based on tributary confluences).
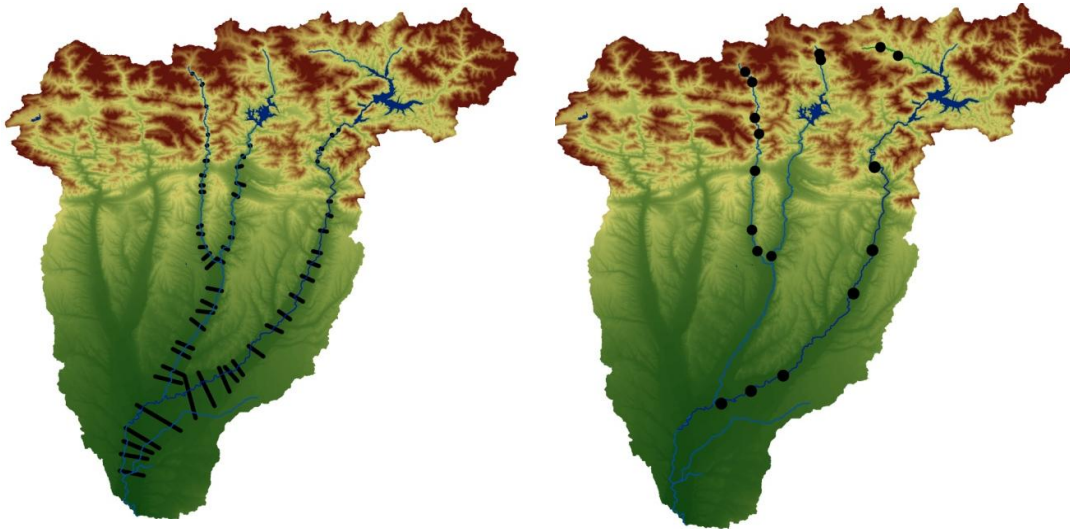
Figure A.10   Location of the valley-bottom width discontinuities (left) and active channel width discontinuities (right) along the studied rivers.

A.4   Discussion

A.4.1 Applicability of the automated delineation procedure

The purpose of this example was to show the applicability of the automated delineation procedure for segmenting the river network into statistically homogeneous reaches, in the present case based on three geomorphic variables. This methodology could be applied with other types of variables, and not only for a downscaling discretization of the river into small portions, but also for upscaling by aggregating previously identified reaches into larger segments or river sectors.

Following the hierarchical framework proposed within Deliverable 2.1 Part 1, the procedure could be applied at different spatial scales and according to different criteria. At the landscape unit scale it might be feasible to segment the catchment area according to the dominant land use; whereas at segment, reach or smaller scales, segmentation according to different hydrologic or geomorphic variables could be investigated according to the purpose of the segmentation. Also physiochemical variables like water temperature and the grading of the bed, or biotic attributes like the existence of specific macroinvertebrates or fishes could be used (Rice *et al.*, 2001; Knispel and Castella, 2003; Hitt and Angermeier, 2008, Parker *et al* 2012). The use of these water quality or biotic variables would need field work and so would be much more expensive than geomorphic variables, which can be extracted from DEMs and orthophotographs.

In our work we introduced some variations to the Alber and Piégay (2011) proposal. These variations included, measuring the variable every 200 m instead of calculating an average value for the variable every 200 m, allow us to consider the measurement as a point on the system or a transversal transect of the river (valley bottom width, active channel width, valley confinement or land use in the watershed), without referencing each measurements to an area (the disaggregated geographic object) as proposed by Alber and Piégay. This methodological variation makes the method easier and simpler to apply, by considering the measurements as systematic samples taken at a defined interval along the fluvial system.

The spatial data base of variable measurements along the rivers that is generated by our approach provides geographical information defined at a specific spatial resolution, in our case every 200 m. This geomorphic database can be enlarged or improved with an increase of spatial resolution progressing in the disaggregation procedure, or used at coarse scale by means of aggregating values of the series. Also the database created with this approach has the potential to be very useful for monitoring long-term changes of geomorphic variables.

A.4.2 Limitations of Pettit´s test

The Pettitt (1979) test, which was used in this research, has some advantages in relation to other algorithms, particularly its simplicity and the fact that it does not require normally-ditributed data. However, it also has some limitations. First, this test is univariate, which means that it is not possible to obtain one statistically significant segmentation across several variables simultaneously as with others tests (Bizzi & Lerner, 2012). In this case, the results from the application of the test could be combined using the expert criteria to take account of additional variables. Secondly, the Pettitt test

detects a single point of discontinuity in the data series and the two resultant subseries have to be subjected to the test iteratively, until the discontinuities are no longer significant depending of the α risk that was chosen (in the present case α=0.05). A final limitation of the Pettitt test, pointed out by Alber and Piégay (2011), is its strong dependence on the amount of data. In an attempt to address this question in our case study, all the variables were sampled with the same intensity, every 200 m. In this way, the effect of the amount of data on the number of segments identified with respect to each variable, is reduced.

With the widespread availability of GIS and increasingly large quantities of remote information, the use of algorithms, like the Pettitt test, provide objective alternatives to delineating and characterizing geographic features. The procedure acquires special significance when fuzzy boundaries exist along the continuous gradients of natural fluvial forms and processes at any scale.

A.5   REFERENCES

Alber A, Piégay H. 2011. Spatial disaggregation and aggregation procedures for characterizing fluvial structures at the network-scale: application to the Rhône basin (France). Geomorphology 125 (4), 343–360.

Bizzi S, Lerner DN. 2012. Characterizing physical habitats in rivers using map-derived drivers of fluvial geomorphic processes. *Geomorphology*, *169-170*, 64–73.

Brenden T, Wang L, Seelbach P, Clark R, Wiley M, Sparks-Jackson B. 2007. A spatially constrained clustering program for river valley segment delineation from GIS digital river networks. Environmental Modelling and Software 23: 638–649.

Brierley GJ, Fryirs KA. 2000. River styles, a geomorphic approach to catchment characterization: implications for river rehabilitation in Bega catchment, New South Wales, Australia. Environmental Management 25: 661–679.

Gallant JC, Dowling TI. 2003. A multi-resolution index of valley bottom flatness for mapping depositional areas. Water Resources Research 39: 1347–1360.

Gurnell A. 1997. Channel change on the river dee meanders, 1946-1992, from the analysis of air photographs. Regulated Rivers Research & Management, 13: 13-26.

Hall JE, Holzer DM, Beechie TJ. 2007. Predicting river floodplain and lateral channel migration for salmon habitat conservation. Journal of the AmericanWater Resources Association 43: 786–797.

Hitt NP, Angermeier PL 2008. Evidence for fish dispersal from spatial analysis of stream network topology. Journal of North American Benthological Society 27:304–320

Hubert P. 2000. The segmentation procedure as a tool for discrete modeling of hydrometeorological regimes. Stochastic Environmental Research and Risk Assessment 14 (4), 297–304

Jain V, Fryirs KA, Preston N, Brierley GJ. 2006. Comparative assessment of three approaches for deriving stream power plots along long profiles in the upper HunterRiver catchment, New South Wales, Australia. Geomorphology 74: 297–317.

Kehagias A. 2004. A hidden Markov model segmentation procedure for hydrological and environmental time series. Stochastic Environmental Research and Risk assessment 18, 117–130.

Kehagias A, Nidelkou E, Petridis V. 2005. A dynamic programming segmentation procedure for hydrological and environmental time series. Stochastic Environmental Research and Risk Assessment 20 (1), 77–94

Knispel S, Castella E. 2003. Disruption of a longitudinal pattern in environmental factors and benthic fauna by a glacial tributary. Freshwater Biology 48:604–618

Kondolf GM, Montgomery DR, Piégay H, Schmitt L. 2003. Geomorphic classification of rivers and streams. In: Kondolf, G.M., Piégay, H. (Eds.), Tools in Fluvial Geomorphology. J. Wiley and Sons, Chichester, UK, pp. 169–202.

Leviandier T, Lavabre J, Arnaud P. 2000. Rainfall contrast enhancing clustering processes and flood analysis. Journal of Hydrology 240: 62–79.

Leviandier T, Alber A, Le Ber F, Piégay H. 2012. Comparison of statistical algorithms for detecting homogeneous river reaches alog a longitudinal continuum. Geomorphology 138: 130-144.

Mielke PW. 1991. The application of multivariate permutation methods based on distance functions in the earth sciences. Earth-Science Review 31, 55–71.

Notebaert B, Piégay H. 2013. Multi-scale factors controlling the pattern of floodplain width at a network scale: The case of the Rhone basin, France, *Geomorphology* 200, 155-171

Orlowski LA, Schumm SA, Mielke PW. 1995. Reach classifications of the lower Mississippi River. Geomorphology 143, 221–234.

Parker C, Clifford NJ, Thorne CR. 2012. Automatic delineation of functional river reach boundaries for river research and applications. River Research and Applications 28:1708-1725

Pettitt AN. 1979. A non-parametric approach of the change-point problem. Applied Statistics 28 (2), 126–135.

Rice SP, Greenwood MT, Joyce CB. 2001. Tributaries, sediment sources, and the longitudinal organization of macroinvertebrate fauna along river system. Canadian Journal of Fisheries and Aquatic Science 58:824–840

Rinaldi M, Surian N, Comiti F, Bussettini M. 2013. A method for the assessment and analysis of the hydromorphological condition of Italian streams: The Morphological Quality Index (MQI), Geomorphology, Geomorphology 180–181: 96–108

Schumm SA, Rutherfurd I, Brooks J. 1994. Pre-Cutoff Morphology of the lower Mississippi River. In: S.A. Schumm and B.R. Winkley (Editors), The Variability of Large alluvial Rivers. American Society of Civil Engineers, New York.

Seelbach PW, Wiley MJ, Baker ME, Wehrly KE. 2006. Initial classification of river valley segments across Michigan's lowers peninsula. In: Hughes, R.M., Wang, L., Seelbach, P.W. (Eds.), Landscape Influences on Stream Habitats and Biological Assemblages. American Fisheries Society, Special Publication 48,Bethesda

Toone J, Rice SP, Piégay H. 2014) Spatial discontinuity and temporal evolution of channel morphology along a mixed bedrock-alluvial river, upper Drôme River, southeast France: Contingent responses to ext.rnal and internal controls. Geomorphology 205: 5-16.

Wang L, Seelbach PW, Hughes RM. 2006. Introduction to landscape influences on stream habitats and biological assemblages. In: Hughes, R.M., Wang, L., Seelbach, P.W. (Eds.), Landscape Influences on Stream Habitats and Biological Assemblages. American Fisheries Society, Bethesda, Maryland, pp. 1-23.

Wang L, Brenden T, Cao Y, Seelbach P. 2012. Delineation and validation of river network spatial scales for water resources and fisheries management. Environmental Management 50:875-887.

Williams WA, Jensen ME, Winne JC. Redmond RL. 2000. An automated technique for delineating and characterizing valley-bottom settings. Environment Monitoring Assessment 64: 105–114.

Annex B Riparian and Aquatic Plant Communities of Europe

J.O. Mountford and M.T. O'Hare, Centre for Ecology and Hydrology, UK

This annex contains tables of aquatic (B1) and riparian (B2) vegetation types which are considered natural and may therefore indicate natural hydrological and fluvial geomorphological conditions. The vegetation communities are taken from EUNIS / PHYSIS and the Natura 2000 (N2K) coding systems.

Table B1: Aquatic Vegetation Types

A first attempt at a Pan-European classification of aquatic vegetation likely to occur in rivers under natural geomorphic conditions. The classification is based on EUBIS/PHYSIS or a Natura 2000 description.

EUNIS / PHYSIS code	EUNIS / PHYSIS Sub-code	N2K code	EUNIS / PHYSIS or N2K description	Geographic extent
n/a		3210	Fennoscandian natural rivers [N2K manual page 44]. Defined as "Boreal and hemiboreal natural and near-natural river systems or parts of such systems containing nutrient-poor water. The water level shows great amplitude, up to 6 m during the year. Especially during the spring, the water level is high. The water-dynamics can vary and contain waterfalls, rapid streams, calm water, and small lakes adjacent to the river. The water erosion causes a higher amount of nutrients towards the river-mouth, where sedimentation starts. In higher levels the rivers are characterised by great, very cold water flows, coming from glaciers, deep snow-beds and large snow-covered areas in mire- and woodlands. In addition the water surface in placid river sections is frozen to ice every winter. These circumstances create ecosystems unique to this part of Europe. [Mainly Scandinavian and Russian taiga eco–region	boreal

EUNIS / PHYSIS code	EUNIS / PHYSIS Sub-code	N2K code	EUNIS / PHYSIS or N2K description	Geographic extent
C2.2			Permanent non-tidal, fast, turbulent watercourses	
	C2.2/ P-24.12		Epirhithral and metarhithral streams (mountain streams)	
	C2.2/ P-24.13		Hyporhithral streams (lower reaches of mountain sections)	
		3220	Alpine rivers and the herbaceous vegetation along their banks [N2K manual page 44 – equivalent to PHYSIS 24.221 and 24.222].	Alpine Bio-geographic region
	P-24.221		· Open assemblages of herbaceous or suffrutescent pioneering plants, rich in alpine species, colonising gravel beds of streams with an alpine, summer-high, flow regime, (Epilobion fleischeri p.)	· formed in northern boreal and lower Arctic mountains, hills and sometimes lowlands, as well as in the alpine and subalpine zones of higher, glaciated, mountains of more southern regions, sometimes with abyssal stations at lower altitudes (Epilobion fleischeri p.)
	P-24.222		Open or closed assemblages of herbaceous or suffrutescent pioneering plants, colonising, within the montane or sub-montane levels, gravel beds of streams with an alpine, summer-high, flow regime, born in high mountains (Epilobion fleischeri p., Calamagrostion pseudophragmitis).	[Includes eco-regions of a) Scandinavian montane birch forest & grasslands; b) Alps conifer & mixed forests; c) Carpathian montane coniferous forests; d) Pyrenees conifer & mixed forests; and maybe e)Dinaric Mountains mixed forests; and f) Urals Montane tundra & taiga]
	P-24.223	3230	Alpine rivers and their ligneous vegetation with Myricaria germanica [N2K Manual page 45 – equivalent to PHYSIS 24.223 x 44.111]. Communities of low shrubby pioneers invading the herbaceous formations of 24.221 and 24.222 on gravel deposits rich in fine silt, of mountain and northern boreal streams with an alpine, summer-high, flow regime. Myricaria germanica and	Eco-regions presumably as for type 3220

EUNIS / PHYSIS code	EUNIS / PHYSIS Sub-code	N2K code	EUNIS / PHYSIS or N2K description	Geographic extent
			Salix spp. are characteristic (Salici-Myricarietum	
	P-24.224	3240	Alpine rivers and their ligneous vegetation with Salix elaeagnos [N2K Manual page 46 – equivalent to PHYSIS 24.224 x 44.112]. Defined as: Thickets or woods of, among others, Salix spp., Hippophae rhamnoides, Alnus spp., Betula spp., on stream gravels of mountain and northern boreal streams with an alpine, summer-high, flow regime. Formations of Salix elaeagnos, Salix purpurea ssp. gracilis, Salix daphnoides, Salix nigricans and Hippophae rhamnoides of higher gravel shoals in Alpine and peri-Alpine valleys	Salix elaeagnos is confined to Pyrenees, Alps, Carpathians, Apennines and Dinaric mountains – so assume relevance to those eco-regions
	P-24.225	3250	Constantly flowing Mediterranean rivers with Glaucium flavum. [N2K Manual page 46 – equivalent to PHYSIS 24.225]. Defined as: Communities colonising gravel deposits of rivers with a Mediterranean, summer-low, flow regime, with formations of the Glaucion flavi. [	Various eco-regions – see EEA map
	P-24.4	3260	Water courses of plain to montane levels with the Ranunculion fluitantis and Callitricho-Batrachion vegetation [N2K manual page 46 – equivalent to PHYSIS 24.4]. Defined as: Water courses of plain to montane levels, with submerged or floating vegetation of the Ranunculion fluitantis and Callitricho-Batrachion (low water level during summer) or aquatic mosses. [Widespread through Atlantic and Continental and at least the southern Boreal biogeographic regions (probably further afield but certainly from Ireland to Romania and north to Sweden) – including many eco-regions]	Widespread
	C2.2/ P-24.41(p)		Acid oligotrophic vegetation of fast-flowing streams ***	
	C2.2/ P-24.42(p)		Lime-rich oligotrophic vegetation of fast-flowing streams ***	
	C2.2/ P-24.43(p)		Mesotrophic vegetation of fast-flowing streams ***	
	C2.2/ P-24.44(p)		Eutrophic vegetation of fast-flowing streams ***	
C2.3			Permanent non-tidal, slow, smooth-flowing watercourses	
	C2.3/		Epipotamal streams	

EUNIS / PHYSIS code	EUNIS / PHYSIS Sub-code	N2K code	EUNIS / PHYSIS or N2K description	Geographic extent
	P-24.14			
	C2.3/ P-24.15		Metapotamal and hypopotamal streams	
	C2.3/ P-24.43(p)		Mesotrophic vegetation of slow-flowing rivers ***	
	C2.3/ P-24.44(p)		Eutrophic vegetation of slow-flowing rivers ***	
C2.4			Tidal rivers, upstream from the estuary	
	C2.4/ P-13.11		Brackish water tidal rivers	
	C2.4/ P-13.12		Freshwater tidal rivers	
	C2.4/ P-24.43(p)		Mesotrophic vegetation of tidal rivers ***	
	C2.4/ P-24.44(p)		Eutrophic vegetation of tidal rivers ***	
C2.5			Temporary running waters (wet phase)	
	P-24.52	3270	Rivers with muddy banks with Chenopodion rubri p.p. and Bidention p.p. vegetation [N2K manual page 46 – equivalent to PHYSIS 24.52]. Defined as: Muddy river banks of plain to sub-montane levels, with annual pioneer nitrophilous vegetation of the Chenopodion rubri p.p. and the Bidention p.p. alliances. During the spring and at the beginning of the summer, sites look like muddy banks without any vegetation (develops later in the year). If the conditions are not favourable, this vegetation has a weak development or could be completely absent. [Distribution probably similar to 3260 though possibly absent from the Boreal biogeographic region	Widespread
	P 24.53	3280	Constantly flowing Mediterranean rivers with Paspalo-Agrostidion species and hanging curtains of Salix and Populus alba [N2K Manual page 47 – equivalent to PHYSIS 24.53]. Defined as: Nitrophilous annual and perennial grass and sedge formations of the alluvial banks of large Mediterranean	Assume in all/most eco-regions within this Mediterranean biogeographic region]

EUNIS / PHYSIS code	EUNIS / PHYSIS Sub-code	N2K code	EUNIS / PHYSIS or N2K description	Geographic extent
			rivers, with Paspalum paspaloides, P. vaginatum, Polypogon viridis (= Agrostis semiverticillata), Cyperus fuscus, and hanging curtains of Salix spp and Populus alba	
	P-24.53 & P-24.16	3290	Intermittently flowing Mediterranean rivers of the Paspalo-Agrostidion [N2K manual page 46 – equivalent to PHYSIS 24.16 and 24.53]. Defined as: Intermittently flowing Mediterranean rivers with Paspalo-Agrostidion communities. They correspond to the river type 24.53, but with the particularity of an interrupted flow and a dry bed during a part of the year. The bed of the river can be completely dry or left with some pools	Assume in all/most eco-regions within this Mediterranean biogeographic region]
	C2.6		Films of water flowing over rocky watercourse margins	

Table B2: Riparian Vegetation Types

The focus for this table is on (semi-) natural woody vegetation, though some attention is paid to herbaceous vegetation where that might exist naturally in an undisturbed floodplain. Especially in the upland and montane areas, many different types of forest may be found directly adjacent to rivers and overlapping with the riparian zone.

EUNIS / PHYSIS code	EUNIS / PHYSIS Sub-code	N2K code	EUNIS / PHYSIS or N2K description	Geographic extent
53.1			Reed beds (Phragmition australis and Scirpion maritimi)	
	53.11		Common Reed-beds (Phragmitetum etc) – 3 subdivisions	
	53.12		Common Clubrush beds (Scirpetum lacustris)	
	53.13		Reedmace beds (Typhetum angustifoliae and Typhetum latifoliae)	
	53.14		Medium-tall Waterside Communities. Ten subdivisions, most characterised by a single major dominant Sagittaria sagittifolia (and Sparganium emersum), Sparganium neglectum, Sparganium erectum, Acorus calamus, Butomus umbellatus, Oenantho-Rorippetum amphibae community, Equisetum fluviatile, Sium latifolium, Hippuris vulgaris, and Eleocharis palustris	
	53.15		Reed sweet-grass beds (Glycerietum maximae)	
	53.16		Reed Canary-grass beds (Phalaridetum arundinaceae)	
	53.17		Halophile club-rush beds (Scirpion maritimi)	
53.2			Large sedge communities (Magnocaricion)	
	53.21		Large Carex beds. Ten major subdivisions (some of which further split) with man dominants for those most likely to occur in riparian zone being Carex acuta, C. acutiformis, C. riparia, C. rostrata, C. vesicaria, C. elata, C. paniculata etc	
	53.22		Tall galingale beds (Cyperetum longi – mainly Mediterranean)	mainly Mediterranean
53.3			Fen-sedge beds (Cladietum marisci i.a.) at land-building zone of calcareous lakes in north and general watersides in Mediterranean.	
	53.33		Riparian Cladium beds is the most typical type by rivers, and mainly in Mediterranean region.	mainly in Mediterranean region

EUNIS / PHYSIS code	EUNIS / PHYSIS Sub-code	N2K code	EUNIS / PHYSIS or N2K description	Geographic extent
***53.4			Small reed-beds of fast-flowing waters (Glycerio-Sparganion). Formations of smaller helophytes found throughout Europe. Typical dominants include Glyceria fluitans, G. notata, G. nemoralis, G. declinata, Leersia oryzoides, Catabrosa aquatica, Sparganium neglectum, S. microcarpum, Nasturtium officinale, N. microphyllum, Veronica beccabunga, V. anagallis-aquatica, Apium nodiflorum and Berula erecta at banks of small rivers.	
53.5			Tall rush swamps (Agropyro-Rumicion crispi p). See also 37.2 Eutrophic Humid grasslands	
53.6			Riparian cane formations. Two types of Mediterranean region	
	53.61		Ravenna Cane communities. Dominants Imperata, Saccharum spp, Arundo plinii	
	53.62		Provence Cane beds dominated by long-introduced Arundo donax	
37.1		6410	37.1: Meadowsweet stands and related communities (Filipendulion ulmariae. Defined as: hygrophile tall herb strips of fertile alluvial stream banks, often dominated by Filipendula ulmaria, and tall herb stands (F. ulmaria, Angelica sylvestris) colonising humid hay meadows and pastures after more or less long discontinuation of mowing or grazing; characteristic species are Filipendula ulmaria, Achillea ptarmica, Angelica sylvestris, Cirsium palustre, Deschampsia cespitosa, Epilobium hirsutum, Geranium palustre, Veronica longifolia, Scutellaria hastifolia, Eupatorium cannabinum, Lysimachia vulgaris, Lythrum salicaria, Phalaris arundinacea, Persicaria bistorta and Valeriana officinalis. When occurring as a hygrophile tall herb strip, this habitat type is of central importance to REFORM *** Molinia meadows on calcareous, peaty or clayey-silt-laden soils (Molinion caeruleae) [N2K manual page 76 – equivalent to PHYSIS 37.31]. Defined as: Molinia meadows of plain to montane levels, on more or less wet nutrient poor soils (nitrogen, phosphorus). They stem from extensive management, sometimes with a mowing late in the year or, they correspond to a deteriorated stage of draining peat bogs. Sub-types:	[Widespread through Atlantic and Continental and at least the southern Boreal biogeographic regions (probably further afield but certainly from Ireland to Romania and north to Sweden) – including many eco-regions]
	37.311		·: on neutro-alkaline to calcareous soils with a fluctuating water table, relatively rich in species (Eu-molinion). The soil is sometimes peaty and becomes dry in summer.	

EUNIS / PHYSIS code	EUNIS / PHYSIS Sub-code	N2K code	EUNIS / PHYSIS or N2K description	Geographic extent
	37.312:		· on more acid soils of the Junco-Molinion (Juncion acutiflori) except species-poor meadows or on degraded peaty soils.	
		6430	Hydrophilous tall herb fringe communities of plains and of the montane to alpine levels [N2K manual page 78 – equivalent to PHYSIS 37.7 and 37.8]. Defined as:37.7: Wet and nitrophilous tall herb edge communities, along water courses and woodland borders belonging to the Glechometalia hederaceae and the Convolvuletalia sepium orders (Senecion fluviatilis, Aegopodion podagrariae, Convolvulion sepium, Filipendulion). [Distribution likely to similar to 6410 – see also Alpine Bio-geographic region]According to CORINE/PHYSIS, this watercourse veil and shady woodland edge type may be divided into 37.71 Watercourse Veils and 37.72 Shady woodland edge fringes. Only the former is especially relevant to REFORM***. Watercourse veils comprise screens or veils of perennial tall herbs, small bushes and lianas lining lowland watercourses (and often have many ruderal and invasive alien plants). Type includes those alliances underlined above and may be further subdivided:	
	37.711:		Angelica archangelica fluvial communities. Angelica archangelica ssp littoralis formations of great formation of great northern rivers, presently rare & threatened.	
	37.712:		Angelica heterocarpa fluvial communities. Angelica heteropcarpa formations of the tidal estuaries of the Loire, the Charente and the Gironde [Species is a rare and very narrow endemic of south-western France]	very narrow endemic of south-western France
	37.713:		Marsh Mallow screens. Althaea officinalis formations of river banks and marsh edges, particularly on somewhat saline soils ***	
	37.714:		Butterbur riverine communities. Formations of Petasites hybridus and Cirsium oleraceum of the banks of small streams *** [Also locally by large rivers]	
	37.715:		Mixed riverine screens. Formations of Senecio fluviatilis, Calystegia sepium, Eupatorium cannabinum, Epilobium hirsutum, Sonchus palustris, Urtica dioica and others species, lining lowland watercourses ***	

EUNIS / PHYSIS code	EUNIS / PHYSIS Sub-code	N2K code	EUNIS / PHYSIS or N2K description	Geographic extent
37.2		6440	Eutrophic humid grasslands. Includes the N2K Manual type 6440 Cnidion dubii (see below under Continental biogeographic region) but also Molinetalia, Calthion palustris, Bromion racemosi, Deschampsion cespitosae, Juncion acutiflorae, Agrostietalia stoloniferae and Agropyro-Rumicion p. Most of these occur in meadows developed on moderately to very nutrient-rich, alluvial or fertilised, wet or damp swards, often inundated at least in winter, and relatively lightly mowed or grazed – in lowland, collinar and montane western and Central Europe, south to western Iberia [Hence occurring in Atlantic, Continental and parts of Mediterranean biogeographic regions]. Although all types listed in CORINE biotopes manual may be found in the riparian zone, the following are especially typical:	
37.24			Flood swards and related communities. Agropyro-Rumicion crispi p. Defined as: grasslands of occasionally flooded river and lake banks, of depressions where rain water collects, of disturbed humid areas and pastures submitted to intensive grazing	
	37.241:		Tall rush pastures. Rush (Juncus effusus, J. conglomeratus, J. inflexus) colonies of intensively grazed pastures	
	***37.242:		Creeping bent and tall fescue swards. Flood swards with Agrostis stolonifera, Carex hirta, Schedonorus arundinaceus, Juncus inflexus, Alopecurus geniculatus, Rumex crispus, Mentha longifolia, M. pulegium, Potentilla anserina, P. reptans and Ranunculus repens.	
38.2		6510	Lowland hay meadows (Alopecurus pratensis, Sanguisorba officinalis) [N2K manual page 80 – equivalent to PHYSIS 38.2]. Defined as: Species-rich hay meadows on lightly to moderately fertilised soils of the plain to sub-montane levels, belonging to the Arrhenatherion and the Brachypodio-Centaureion nemoralis alliances. These extensive grasslands are rich in flowers and are not cut before the grasses flower and then only one or two times per year. CORINE/PHYSIS subdivides the type into three, none of which is strictly riparian or confined to floodplains	Distribution similar to 6410 and in the Continental biogeographic region as far as Nn Italy]

EUNIS / PHYSIS code	EUNIS / PHYSIS Sub-code	N2K code	EUNIS / PHYSIS or N2K description	Geographic extent
	38.31	6520	Mountain hay meadows [N2K manual page 81 – equivalent to PHYSIS 38.31]. Defined as: Species-rich mesophile hay meadows of the montane and sub-alpine levels (mostly above 600 metres) usually dominated by Trisetum flavescens and with Heracleum sphondylium, Viola cornuta, Astrantia major, Carum carvi, Crepis mollis, C. pyrenaica, Bistorta major, (Polygonum bistorta), Silene dioica, S. vulgaris, Campanula glomerata, Salvia pratensis, Centaurea nemoralis, Anthoxanthum odoratum, Crocus albiflorus, Geranium phaeum, G. sylvaticum, Narcissus poeticus, Malva moschata, Valeriana repens, Trollius europaeus, Pimpinella major, Muscari botryoides, Lilium bulbiferum, Thlaspi caerulescens, Viola tricolor ssp. subalpina, Phyteuma halleri, P. orbiculare, Primula elatior, Chaerophyllum hirsutum and many others. [Possibly of marginal relevance, although the UK variant (NVC MG3) certainly does occur in the floodplain locally –]	distribution straddles Atlantic, Continental and Alpine biogeographic regions and numerous eco-regions
		7210	Calcareous fens with Cladium mariscus and species of the Caricion davallianae [N2K manual page 86 – equivalent to PHYSIS 53.3]. Defined as: Cladium mariscus beds of the emergent-plant zones of lakes, fallow lands or succession stage of extensively farmed wet meadows in contact with the vegetation of the Caricion davallianae or other Phragmition species [Cladietum marisci (Allorge 1922) Zobrist 1935	Distribution similar to 6410
54.3				
		7240	Alpine pioneer formations of Caricion bicoloris-atrofuscae [N2K manual page 88 – equivalent to PHYSIS 54.3]. Defined as: Alpine, peri-Alpine and northern British communities colonising neutral to slightly acid gravelly, sandy, stony, sometimes somewhat argilous or peaty substrates soaked by cold water, in moraines and on edges of springs, rivulets, glacial torrents of the alpine or sub-alpine levels, or on alluvial sands of pure, cold, slow-flowing rivers and calm backwaters. A permanent or continuous soil frost over a long period is essential for the existence of this habitat type. Low vegetation composed principally of species of Carex and Juncus (Caricion bicoloris-atrofuscae).	Confined to Arctic, Boreal and Alpine biogeographic regions, though rarely on higher mountains in Atlantic

EUNIS / PHYSIS code	EUNIS / PHYSIS Sub-code	N2K code	EUNIS / PHYSIS or N2K description	Geographic extent
	41.24	9160	Sub-Atlantic and medio-European oak or oak/hornbeam forests of the Carpinion betuli [N2K manual page 108 – equivalent to PHYSIS 41.24] Defined as: Forests of Quercus robur (or Quercus robur and Q. petraea) on hydromorphic soils or soils with high water table (bottoms of valleys, depressions or in the vicinity of riparian forests). The substrate corresponds to silts, clayey and silt-laden colluvions, as well as to silt-laden alterations or to siliceous rocks with a high degree of saturation. Forests of Quercus robur or natural mixed forests composed of Quercus robur, Q. petraea, Carpinus betulus and Tilia cordata. Hyacinthoides non-scripta is absent or rare.	Apparently occurring in Continental, eastern part of Atlantic and southern portion of Boreal biogeographic regions
44.9			Alder, willow and bog-myrtle swamp woods. This main category includes some Natura 2000 types of restricted distribution (see type 9080 in Boreal region below). The more widespread types include:	
	44.91		Alder swamp woods. Woods and scrubs of marshy ground, waterlogged for most of year, colonising fens and marshy or permanently inundated alluvial terraces of rivers. 3 main subdivisions, one of which is further subdivided into 2 sub-units. ***	Atlantic and Continental regions, as well as Boreal etc.
	44.92		Mire willow scrub (Salicion cinereae). Willow dominated formations with Salix aurita, S. atrocinerea, S. cinerea, S. pentandra, Frangula alnus and Betula humilis of fens, marshy floodplains and fringes of lakes and ponds. 4 sub-divisions.	
	44.93		Swamp bog-myrtle scrub. Myrica gale thickets of fringes of fens, drying fens and nascent or regenerating bogs of middle Europe, mostly characteristic of the Atlantic sector.	middle Europe, mostly characteristic of the Atlantic sector.

EUNIS / PHYSIS code	EUNIS / PHYSIS Sub-code	N2K code	EUNIS / PHYSIS or N2K description	Geographic extent
	44.A1 - 44.A4	91D0	91D0 * Bog woodland [N2K manual page 111 – equivalent to PHYSIS 44.A1 to 44.A4]. Defined as: Coniferous and broad-leaved forests on a humid to wet peaty substrate, with the water level permanently high and even higher than the surrounding water table. The water is always very poor in nutrients (raised bogs and acid fens). These communities are generally dominated by Betula pubescens, Frangula alnus, Pinus sylvestris, Pinus rotundata and Picea abies, with species specific to bogland or, more generally, to oligotrophic environments, such as Vaccinium spp., Sphagnum spp., Carex spp. [Vaccinio-Piceetea: Piceo-Vaccinienion uliginosi (Betulion pubescentis, Ledo-Pinion) i.a.]. In the Boreal region, also spruce swamp woods, which are minerotrophic mire sites along margins of different mire complexes, as well as in separate strips in valleys and along brooks. Sub-types:	
	44.A1:		Sphagnum birch woods. Three subdivisions.	
	44.A2:		Scots pine mire woods. Almost confined to north and east Germany	
	44.A3:		Mountain pine bog woods. Alps, Jura and higher Hercynian ranges of Germany	
	44.A4:		Mire spruce woods [Mainly in Boreal biogeographic region]. Two subdivisions	
44.1			/PHYSIS type 44.1 comprises the Riparian Willow formations, of which several subdivisions are described under N2K types – subdivisions of this riparian type are listed under the relevant biogeographic region(s). They are all united by being Salix spp brush or aborescent formations, lining flowing water and submitted to periodic flooding.	
	44.12		44.12: Lowland, collinar and Mediterraneo-montane willow brush: linear shrubby willow formations of river banks in plains, hills and low mountains of middle Europe and the Mediterranean region, with Salix triandra, S. viminalis and S. purpurea.	
			There are 7 sub-divisions which are simply listed under below or under other biogeographic regions if more restricted.	
			· 44.121: Almond willow-osier scrub (Salicetum triandro-viminalis) – Continental and Atlantic	

EUNIS / PHYSIS code	EUNIS / PHYSIS Sub-code	N2K code	EUNIS / PHYSIS or N2K description	Geographic extent
		9.10E+01	Alluvial forests with Alnus glutinosa and Fraxinus excelsior (Alno-Padion, Alnion incanae, Salicion albae) [N2K manual page 113 – equivalent to PHYSIS 44.3, 44.2 and 44.13]. Defined as: Riparian forests of Fraxinus excelsior and Alnus glutinosa, of temperate and Boreal Europe lowland and hill watercourses.44.3: Alno-Padion); riparian woods of Alnus incanae of montane and sub-montane rivers of the Alps and the northern Apennines (44.2: Alnion incanae); arborescent galleries of tall Salix alba, S. fragilis and Populus nigra, along medio-European lowland, hill or sub-montane rivers (44.13: Salicion albae). All types occur on heavy soils (generally rich in alluvial deposits) periodically inundated by the annual rise of the river (or brook) level, but otherwise well-drained and aerated during low-water. The herbaceous layer invariably includes many large species (Filipendula ulmaria, Angelica sylvestris, Cardamine spp., Rumex sanguineus, Carex spp., Cirsium oleraceum) and various vernal geophytes can occur, such as Ranunculus ficaria, Anemone nemorosa, A. ranunculoides, Corydalis solida. This habitat includes several sub-types:	of temperate and Boreal Europe lowland and hill watercourses
	44.31		· ash-alder woods of springs and their rivers (44.31: Carici remotae-Fraxinetum) – type is subdivided into 5 units by CORINE-PHYSIS distributed by small streams in Atlantic, sub-Atlantic and sub-Continental Middle Europe	small streams in Atlantic, sub-Atlantic and sub-Continental Middle Europe
	44.32		· ash-alder woods of fast-flowing rivers (44.32: Stellario-Alnetum glutinosae) – said to occur by CORINE/PHYSIS hills of northern and western Europe (assume Atlantic and Boreal)	hills of northern and western Europe (assume Atlantic and Boreal)
	44.33		· ash-alder woods of slow-flowing rivers (44.33: Pruno-Fraxinetum, Ulmo-Fraxinetum) – subdivided into 2 units by CORINE-PHYSIS and found in central and locally western Europe (Atlantic but mainly Continental)	central and locally western Europe (Atlantic but mainly Continental)
	44.21		montane grey alder galleries (44.21: Calamagrosti variae-Alnetum incanae Moor 58	
	44.22		· sub-montane grey alder galleries (44.22: Equiseto hyemalis-Alnetum incanae Moor 58)	
	44.13		· white willow gallery forests (44.13: Salicion albae)	

EUNIS / PHYSIS code	EUNIS / PHYSIS Sub-code	N2K code	EUNIS / PHYSIS or N2K description	Geographic extent
	?		· Spanish types belong to alliance Osmundo-Alnion (Cantabric-Atlantic & SE Iberia peninsula)	[Distribution may be partly inferred from description of sub-types, but clearly found throughout the Atlantic, Continental, Alpine biogeographic regions, as well as parts of the Mediterranean, Pannonian and Boreal regions
	44.34		type 44.34: Northern Iberian Alder galleries. Various communities and sub-divided into 3 major units and two sub-units with Alnus glutinosa and Fraxinus excelsior. Includes Pyrenees (Alpine region) and Galicia (Atlantic region)	Includes Pyrenees (Alpine region) and Galicia (Atlantic region)
	44.12		44.12: Lowland, collinar and Mediterraneo-montane willow brush types	atlantic
	44.125		· 44.125: Cantabrian willow scrub (Salicetum cantabricae) – Cordillera Cantabrica	atlantic
		6450	Northern boreal alluvial meadows [N2K manual page 79]. Defined as: Along large rivers with placid river sections which are frozen every winter, the type is affected by flooding in spring. The traditional management as hay meadows has usually ceased. Type includes areas that are not yet severely overgrown with trees and bushes [Mainly Scandinavian and Russian taiga eco–region]	Mainly Scandinavian and Russian taiga eco–region

EUNIS / PHYSIS code	EUNIS / PHYSIS Sub-code	N2K code	EUNIS / PHYSIS or N2K description	Geographic extent
		6530	6530 Fennoscandian wooded meadows [N2K manual page 81]. Defined as: A vegetation complex consisting of small copses of deciduous trees and shrubs and patches of open meadows. Ash (Fraxinus excelsior), birch (Betula pendula, B. pubescens) and Quercus robur, Tilia cordata, Ulmus glabra or Alnus incana are the common tree species. Nowadays very few areas are managed but traditionally these areas were managed by a combination of raking, hay-cutting, grazing of grassland and pollarding or lopping of trees. Species-rich vegetation complexes with rare and threatened meadow species and well developed epiphytic flora of mosses and lichens are characteristic. Many threatened species preferring old pollarded deciduous trees of semi-open habitats occur. The habitat type includes managed areas and overgrown areas with old pollarded or lopped deciduous trees. The type does not include abandoned meadows being invaded by trees. [Presumably as 6450 – this habitat type is probably rare in the riparian/floodplain zone]	Presumably as 6450 – this habitat type is probably rare in the riparian/floodplain zone
	N2K manual page 104 – equivalent to PHYSIS 44.9112, 44.915, 44.A14 (1997 version	9080	9080 *Fennoscandian deciduous swamp woods [N2K manual page 104 – equivalent to PHYSIS 44.9112, 44.915, 44.A14 (1997 version)]. Defined as: Deciduous swamps are under permanent influence of surface water and usually flooded annually. They are moist or wet, wooded wetlands with some peat formation, but the peat layer is usually very thin. Ash (Fraxinus excelsior) in the hemi-boreal zone and black alder (Alnus glutinosa) reaching the middle boreal zone are typical tree species. Grey alder (Alnus incana), silver birch (Betula pubescens) and willows (Salix spp.) are also common. A mosaic of patches with different water level and vegetation is typical for the type. Around the tree stems are small hummocks, but wet flooded surfaces are dominant. Deciduous swamp woods are most common in Finland in the south-western archipelago and other coastal areas. On the mainland they are rare. In Sweden they are common throughout the whole region. [Eco-regions include Scandinavian and Russian taiga and Baltic mixed forests	[Eco-regions include Scandinavian and Russian taiga and Baltic mixed forests

EUNIS / PHYSIS code	EUNIS / PHYSIS Sub-code	N2K code	EUNIS / PHYSIS or N2K description	Geographic extent
	37.8 & 37.7	6430	Hygrophilous perennial tall herb communities of montane to alpine levels of the Betulo-Adenostyletea class. 6430 Hydrophilous tall herb fringe communities of plains and of the montane to alpine levels [N2K manual page 78 – equivalent to PHYSIS 37.7 and 37.8]. Defined as:	Probably includes eco-regions of a) Scandinavian montane birch forest and grasslands; b) Alps conifer & mixed forests; c) Carpathian montane coniferous forests; d) Pyrenees conifer and mixed forests; and possibly e)Dinaric Mountains mixed forests]
	44.12		44.12: Lowland, collinar and Mediterraneo-montane willow brush types	mediterranean
	44.124		· 44.124: Ibero-montane willow scrub (Salicetum triandrae-elaeagni) – Pyrenees, Iberian Range and Sierra Nevada (thus also Mediterranean region)	mediterranean
	37.23	6440	6440 Alluvial meadows of river valleys of the Cnidion dubii [N2K manual page 78 – equivalent to PHYSIS 37.23]. Defined as: Alluvial meadows with natural flooding regime belonging to the Cnidion dubii alliance, under continental to subcontinental climatic conditions. [	Principally in Germany, Czech Republic, Slovakia, Hungary, Poland and into Romania – Eco-regions include Central European mixed forests (and into Western too) and Pannonian mixed forests]

EUNIS / PHYSIS code	EUNIS / PHYSIS Sub-code	N2K code	EUNIS / PHYSIS or N2K description	Geographic extent
	44.4	91F0	Riparian mixed forests of Quercus robur, Ulmus laevis and Ulmus minor, Fraxinus excelsior or Fraxinus angustifolia along the great rivers (Ulmenion minoris) [N2K manual page 114 – equivalent to PHYSIS 44.4]. Defined as: Forests of hardwood trees of the major part of the river bed, liable to flooding during regular rising of water level or, of low areas liable to flooding following the raising of the water table. These forests develop on recent alluvial deposits. The soil may be well drained between inundations or remain wet. Following the hydric regime, the woody dominated species belong to Fraxinus, Ulmus or Quercus genus. The undergrowth is well developed.	
	44.41		· 44.41: Rhine, Danube, Emst, Elbe, Saale, Weser, Loire and Rhône-Saône systems	· 44.41: Rhine, Danube, Emst, Elbe, Saale, Weser, Loire and Rhône-Saône systems
	44.42		· 44.42: Residual fragments in the same systems	as for 44.41
	44.43		· 44.43: Sub-Mediterranean regions of SE Europe (Balkanic) – sub-units in NE Italy and Nn Greece	· 44.43: Sub-Mediterranean regions of SE Europe (Balkanic) – sub-units in NE Italy and Nn Greece
	44.44		· 44.44: Po and its tributaries	· 44.44: Po and its tributaries

EUNIS / PHYSIS code	EUNIS / PHYSIS Sub-code	N2K code	EUNIS / PHYSIS or N2K description	Geographic extent
	41.2A	91L0	Illyrian oak–hornbeam forests (Erythronio-Carpinion) [N2K manual page 117 – equivalent to PHYSIS 41.2A]. Defined as: Forests of Quercus robur or Q. petraea, sometimes Q. cerris, and Carpinus betulus on both calcareous and siliceous bedrocks, mostly on deep neutral to slightly acidic brown forest soils, with mild humus in the SE-Alpine-Dinaric region, West- and Central Balkans extending northwards to Lake Balaton mostly in hilly and sub-montane regions, river valleys and the plains of the Drava and Sava. The climate is more continental than in sub-Mediterranean regions and warmer than in middle Europe; these forests are intermediate between oak-hornbeam woods (e.g. 9170) of central Europe and those of the Balkans and merge northwards into the Pannonic oak woods (91G0). They have much higher species richness than the Central European oak woods. Outliers of these forests also occur in Frioul and the northern Apennines. [Though centred in the Continental biogeographic region of Serbia, Croatia and Bosnia-Herzegovina, this type clearly enters the Alpine and Pannonian regions, and the outliers are in the Mediterranean region]	SE-Alpine-Dinaric region, West- and Central Balkans extending northwards to Lake Balaton mostly in hilly and sub-montane regions, river valleys and the plains of the Drava and Sava. The climate is more continental than in sub-Mediterranean regions and warmer than in middle Europe; these forests are intermediate between oak-hornbeam woods (e.g. 9170) of central Europe and those of the Balkans and merge northwards into the Pannonic oak woods (91G0). They have much higher species richness than the Central European oak woods. Outliers of these forests also occur in Frioul and the northern Apennines. [Though centred in the Continental biogeographic region of Serbia, Croatia and Bosnia-Herzegovina, this type clearly enters the Alpine and Pannonian regions, and the outliers are in the Mediterranean region]

EUNIS / PHYSIS code	EUNIS / PHYSIS Sub-code	N2K code	EUNIS / PHYSIS or N2K description	Geographic extent
	44.162 & 44.6	92A0	92A0 Salix alba and Populus alba galleries [N2K manual page 128 – equivalent to PHYSIS 44.141, 44.162 and 44.6]. Mostly found in Mediterranean biogeographic region (see below) – certainly it reaches its greatest diversity there	Mostly found in Mediterranean biogeographic region (see below) – certainly it reaches its greatest diversity there
	37.4	6420	6420 Mediterranean tall humid herb grasslands of the Molinio-Holoschoenion [N2K manual page 78 –equivalent to PHYSIS 37.4]. Defined as: Mediterranean humid grasslands of tall grasses and rushes, widespread in the entire Mediterranean basin, extending along the coasts of the Black Sea, in particular in dunal systems [P	Passes from Mediterranean region into Black Sea region – covering numerous eco-regions – may be mostly coastal rather than riparian]
	44.12		PHYSIS 44.12: Lowland, collinar and Mediterraneo-montane willow brush types	
	44.122		· 44.122: Mediterranean purple willow scrub (Saponario officinalis-Salicetum purureae) – Southern France, Mediterranean eastern Spain and south to Rio Seguara basin (Italy)	Southern France, Mediterranean eastern Spain and south to Rio Seguara basin (Italy)
	44.123		· 44.123: Balkanic purple willow scrub (various communities with Salix purpurea and other willows)	Balkans?
	44.124		· 44.124: Ibero-montane willow scrub (Salicetum triandrae-elaeagni) – Pyrenees, Iberian Range and Sierra Nevada (thus also Alpine region)	Pyrenees, Iberian Range and Sierra Nevada (thus also Alpine region)
	44.126		· 44.126: Iberian sage-leaved willow scrub (Salicetum purpureo-salvifoliae) – Central and southern Iberia	Central and southern Iberia
	44.127		· 44.127: Pedicellated willow scrub – subdivided into 4 types confined to a) Andalusia; b) Sardinia; c) Sicily; and d) Calabria	a) Andalusia; b) Sardinia; c) Sicily; and d) Calabria
	44.142		44.142: Olive-leaved and ashy willow riparian woods (Rubo corylifolii-Salicetum atrocinereae and Viti-Salicetum atrocinereae) which occurs with four variants from central and southern Iberia via Sardinia to Italy and Greece	from central and southern Iberia via Sardinia to Italy and Greece

EUNIS / PHYSIS code	EUNIS / PHYSIS Sub-code	N2K code	EUNIS / PHYSIS or N2K description	Geographic extent
	44.162 & 44.6	92A0	***92A0 Salix alba and Populus alba galleries [N2K manual page 128 – equivalent to PHYSIS 44.141, 44.162 and 44.6]. Defined as:	
	44.141		· Riparian forests of the Mediterranean and Black Sea basins dominated by Salix alba, Salix fragilis or their relatives (44.141)	[Distribution may be partly inferred from description of types, but clearly found throughout the Continental, Black Sea, Mediterranean and Black Sea biogeographic regions, as well as parts of the Pannonian and possibly Steppic region]
	44.6		· Mediterranean and Central Eurasian multi-layered riverine forests with Populus spp., Ulmus spp., Salix spp., Alnus spp., Acer spp., Tamarix spp., Juglans regia, Quercus robur, Quercus pedunculiflora, Fraxinus angustifolia, Fraxinus pallisiae, lianas. Tall poplars, Populus alba, Populus caspica, Populus euphratica (Populus diversifolia), are usually dominant in height; they may be absent or sparse in some associations which are then dominated by species of the genera listed above (44.6). Type is subdivided by CORINE/PHYSIS into 4 major units:	Mediterranean and Central Eurasian
	44.61		o 44.61: Mediterranean Riparian poplar forests – further subdivided into five major units in Iberia, Provence/Languedoc, Corsica/Sardinia, Italy and Greece (Greek stands are themselves classified into four minor sub-units)	Mediterranean
	44.62		o 44.62: Mediterranean Riparian Elm forests	Mediterranean
	44.63		o 44.63: Mediterranean Riparian Ash woods: further subdivided into six units distributed from Iberia (3 units) through southern France and northern Italy (1 unit) to Adriatic Italy and Sicily (1 unit) and Greece (1 unit)	Mediterranean
	44.64		o 44.64: Hop-Hornbeam galleries: Ostrya dominated and only in SE France	SE France
	44.52 & 44.54	92B0	92B0 Riparian formations on intermittent Mediterranean watercourses with Rhododendron ponticum, Salix & others [N2K manual p. 128: equivalent to PHYSIS 44.52 & 44.54]. Types:	

EUNIS / PHYSIS code	EUNIS / PHYSIS Sub-code	N2K code	EUNIS / PHYSIS or N2K description	Geographic extent
	44.52		· Distinctive, relict thermo- and meso-Mediterranean alder galleries of deep, steep-sided valleys, with Rhododendron ponticum ssp. baeticum, Frangula alnus ssp. baetica, Arisarum proboscideum and a rich fern community including Pteris incompleta, Diplazium caudatum, #Culcita macrocarpa (44.52).	
	44.54		· Relict Betula parvibracteata riparian galleries. The dominant species, an extremely local endemic, is accompanied by Myrica gale, Frangula alnus, Salix atrocinerea, Galium broterianum, Scilla ramburei (44.54) [Found in Montes de Toledo only]	Found in Montes de Toledo only]
			CORINE/PHYSIS lists in addition to these N2K types the following further units:	
	44.51		· 44.51: Southern Black Alder galleries in Italy, Cévennes, Iberia and Greece (4 sub-units)	Italy, Cévennes, Iberia and Greece
	44.53		44.53: Corsican Black and Cordate Alder galleries (2 sub-units both in Corsica	Corsica
		92C0	92C0 Platanus orientalis and Liquidambar orientalis woods (Plantanion orientalis) [N2K manual page 129 – equivalent to PHYSIS 44.71 and 44.72]. Defined as: Forests and woods, for the most part riparian, dominated by Platanus orientalis (oriental plane) or Liquidambar orientalis (sweet gum), belonging to the Platanion orientalis alliance. Sub-types:	
	44.71		· 44.71: Oriental plane woods (Platanion orientalis) Forests of Platanus orientalis.	

EUNIS / PHYSIS code	EUNIS / PHYSIS Sub-code	N2K code	EUNIS / PHYSIS or N2K description	Geographic extent
	44.711		o 44.711: Helleno-Balkanic riparian plane forests. Platanus orientalis gallery forests of Greek and southern Balkanic watercourses, temporary rivers and gorges; they are distributed throughout the mainland and archipelagos, colonising poorly stabilised alluvial deposits of large rivers, gravel or boulder deposits of permanent or temporary torrents, spring basins and particularly, the bottom of steep, shady gorges, where they constitute species-rich communities. The accompanying flora may include Salix alba, S. elaeagnos, S. purpurea, Alnus glutinosa, Celtis australis, Cercis siliquastrum, Populus alba, P. nigra, Juglans regia, Fraxinus ornus, Alnus glutinosa, Crataegus monogyna, Cornus sanguinea, Ruscus aculeatus, Vitex agnus-castus, Nerium oleander, Rubus spp, Rosa sempervirens, Hedera helix, Clematis vitalba, Vitis vinifera ssp sylvestris, Ranunculus ficaria, Anemone blanda, Aristolochia rotunda, Saponaria officinalis, Symphytum bulbosum, Hypericum hircinum, Melissa officinalis, Calamintha grandiflora, Helleborus cyclophyllus, Cyclamen hederifolium, C. repandum, C. creticum, Galanthus nivalis ssp reginae-olgae, Dracunculus vulgaris, Arum italicum, Biarum tenuifolium, Brachypodium sylvaticum, Dactylis glomerata and may be rich in mosses, lichens and ferns, among which Pteridium aquilinum is often abundant. Various associations have been described reflecting regional and ecological variation in composition of the under-growth. Plane tree galleries are particularly well represented along the Ionian coast and in the Pindus; other important local complexes exist in Macedonia, in Thrace, around the Olympus massif, in the Pelion, in the Peloponnese, particularly in the Taygetos, where luxuriant gorge forests reach 1300m, in Euboea and in Crete; local, distinctive, representatives occur in other Aegean islands e.g. Rhodes, Samos, Samothrace, Thasos. Restriction to gorges is increasingly pronounced towards the south.	Greece & Baltics
	44.712		o 44.712: Hellenic slope plane woods. Platanus orientalis woods on colluvions, detritus cones, ravine sides or other poorly stabilised substrates, of Greece.	greece

EUNIS / PHYSIS code	EUNIS / PHYSIS Sub-code	N2K code	EUNIS / PHYSIS or N2K description	Geographic extent
	44.713		o 44.713: Sicilian plane tree canyons. Relict Platanus orientalis-dominated or P. orientalis -rich galleries of the Cassabile, the Anapo, the Irminio and the Carbo rivers, in the Iblei range of south-eastern Sicily, of the gorge of the Sirmeto, in the vicinity of the Nebrodi. Some of these formations, in particular, in the gorges of the Cassabile and of the Anapo, are true plane tree woods. Others, such as on the Sirmeto, are Populus alba, Fraxinus angustifolia, Salix spp. formations with Platanus orientalis; as they grade into each other, and because of the very isolated occurrence, and great biogeographical and historical interest of Platanus orientalis in Sicily, they are all listed here. Plane tree woods have had a much greater extension in Sicily and probably in Calabria. A large forest has, in particular, existed on the Alcantara, where the species is now extinct.	sicily
	44.72		· 44.72: Sweet gum woods. Riverine forests dominated by the Tertiary relict Liquidambar orientalis, with very limited range in south Asia Minor and Rhodes.	south Asia Minor and Rhodes
	44.721		o 44.721: Rhodian sweet gum woods. Liquidambar orientalis gallery forest of the Petaloudhes Valley, on Rhodes, with poorly developed undergrowth and a ground layer dominated by Adiantum capillus-veneris in damp areas. This forest constitutes the only European formation of this species and harbours the unique, concentrated aggregation of Jersey Tiger Moths, Panaxia quadripunctaria.	Petaloudhes Valley, on Rhodes
	44.81 to 44.84	92D0	92D0 Southern riparian galleries and thickets (Nerio-Tamaricetea and Securinegion tinctoriae) [N2K manual page 130 – equivalent to PHYSIS 44.81 to 44.84]. Defined as: Tamarisk, oleander, and chaste tree galleries and thickets and similar low ligneous formations of permanent or temporary streams and wetlands of the thermo-Mediterranean zone and south-western Iberia, and of the most hygromorphic locations within the Saharo-Mediterranean and Saharo- Sindian zones. Includes formations of Tamarix smyrnensis (syn. Tamarix ramosissima) of stream sides and coastal localities of the Pontic and Steppic regions of western Eurasia. The formations with Tamarix africana should not be taken into account.	

EUNIS / PHYSIS code	EUNIS / PHYSIS Sub-code	N2K code	EUNIS / PHYSIS or N2K description	Geographic extent
	44.81		· 44.81: Oleander (Nerium), Chaste-tree (Vitex) and Tamarix galleries. 3 units defined by the dominant shrub, with Tamarix galleries being further sub-divided into 4 major sub-units and 4 subsidiary units. Throughout Mediterranean region	mediterranean
	44.82		· 44.82: South-western Iberian tamujares: characterised by Securinega tinctoria and found in southern Spain and southern Portugal.	southern spain and portugal
	44.83		· 44.83: Oretanian lauriphyllous galleries: Montes de Toledo (southern Spain) only – Prunus lusitanica and Viburnum tinus.	southern spain
	44.84		· 44.84: Oretanian bog myrtle & willow scrub: Montes de Toledo (southern Spain) only – Frangula, Myrica gale, Salix atrocinerea, S. salvifolia.	southern spain
		9370	9370 * Palm groves of Phoenix[N2K manual page 133 – equivalent to PHYSIS 45.7]. Defined as: Woods, often riparian, formed by the two endemic palm trees, Phoenix theophrasti and Phoenix canariensis.· The palm groves of Crete are restricted to damp sandy coastal valleys; they include the extensive forest of Vai, where the luxuriant palm growth is accompanied by a thick shrubby undergrowth rich of Nerium oleander, and about four other smaller coastal groves, notably on the south coast of the prefectorate of Rethimnon (Plakias etc).· The Canarian palm groves are mostly characteristic of the bottom of barrancos and of alluvial soils, below 600 metres; particularly representative examples are found at Fragata, Maspalomas and Barranco de Tirajana in the Gran Canary, Valle Gran Rey in La Gomera, Masca in Ténérife and Brena Alta in La Palma.[Geographical range clearly indicated in description of the sub-types]	Fragata, Maspalomas and Barranco de Tirajana in the Gran Canary, Valle Gran Rey in La Gomera, Masca in Ténérife and Brena Alta in La Palma.[Geographical range clearly indicated in description of the sub-types]

Annex C
Flow Regime Analysis and Hydrological Alteration

Martina Bussettini, Carlo Percopo, Barbara Lastoria, Giovanni Braca
ISPRA, Italy

C.1   Flow regime analysis

A river classification into flow regime types is proposed with representative characteristics for application across European continent. In this classification scheme, the following characterization criteria are considered: (i) intermittency; (ii) river-aquifer interaction (Boni *et al.*, 1993-A); (iii) prevailing type of water sources (Poff and Ward, 1989; Poff, 1996; Poff *et al.*, 1997). Furthermore, the classification scheme takes into account the ecological relevance of hydrological indicators, with the aim of giving an eco-hydrological overview of European river systems.

C.2   Groundwater and river-aquifer interaction

In order to classify river flow regimes into types, one of the most relevant factors to be considered is the degree of river-aquifer interaction since it influences the hydrological response of fluvial systems. Groundwater plays a very different role than surface water in the hydrological, morphological and ecological processes of fluvial systems.

Several methods for river-aquifer characterization have been developed in the last two decades. Among these, the "characteristic discharges" method (Boni *et al.*, 1993-B) was selected since it is one of the most useful approaches starting from daily and/or monthly flow data. This method describes the quantitative interaction and variation in time between surface water and groundwater, providing a unified view of the river-aquifer system.

The baseflow-runoff characterization method is based on the following assumptions:

(i) Discharge in a river gauging section is fed only by groundwater (baseflow) when surface runoff (quick-flow) ceases;

(ii) Quick-flow ends after the rainfall ends and after a concentration time (the estimated time required to reach a gauging section starting from the farthest point on the watershed);

(iii) Baseflow consists of the sum of the contributions of both linear and point springs located in the catchment area draining to the gauging station. This component has a relatively regular flow regime and sustains total discharge during minimum flow.

Data required for the calculation consists of long-term time series of daily discharge recorded at a gauging station for a "representative" number of years. For statistical representativeness, at least 20 years of continuous records are needed (Huh *et al.*, 2010).

For each month of the hydrological average year, some "characteristic discharges" can be derived. For the description of the characteristic discharge it is useful to define daily and monthly discharge.

- *Daily discharge, QD*, is the mean value of all elementary, equally spaced, values recorded during a day.

- *Monthly discharge, QM*, is the mean value of daily discharges recorded during a month.

In the following definitions we use the following:

- k: index of day in the month; k = **1,…,M_j**, where M_j is the number of days in j^{th} month;

- j: index of month in the year; j = **1,…,12**;

- i: index of year in the data series; i = **1,…,N** where N is the number of all years in data series.

1.   The "mean monthly discharge" of the jth month, *meanQM_j*, is the arithmetic mean (over N years) of the monthly discharge values of the jth month and it consists of the total discharge, that is the sum of runoff and baseflow, for each month.

$$meanQMj = \frac{\mathbf{1}}{N}\sum_{i=\mathbf{1}}^{N} QM_{j,i} \quad j = \mathbf{1,…,12}$$

2.   The "mean of minimum daily discharge" of the jth month, *meanQD_{min,j}* is the arithmetic mean (over N years) of the minimum of the daily discharge values in j^{th} month. During drought periods it is representative of baseflow, while in the wet season it represents baseflow plus runoff due to precipitation events with a duration shorter than the time of concentration of the basin.

$$meanQDmin,j = \frac{\mathbf{1}}{N}\sum_{i=\mathbf{1}}^{N} QD_{min,j,i} \quad j = \mathbf{1,…,12} \quad where \quad QD_{min,j,i} = \min_{1\leq k\leq M_j}\left(QD_{k,i}\right)$$

3.   The "minimum of the monthly discharge" of the jth month, $QM_{min,j}$, is the minimum (over N years) of the monthly discharge values and it represents the calculated baseflow.

$$QM_{min,j} = \min_{1\leq i\leq N}\left(QM_{j,i}\right) \quad j = \mathbf{1,…,12}$$

4.   The "lowest value of the minimum daily discharge" of the jth month, $QD_{lowest,j}$, is the absolute minimum daily value (observed throughout the recordings series) for each month and it represents the minimum baseflow during the most severe droughts.

$$QD_{lowest,j} = \min_{1 \leq i \leq N} \left(\min_{1 \leq k \leq M_j} QD_{k,i} \right) \quad j = 1, \dots, 12$$

In the annual hydrograph, these four "characteristic monthly discharges" identify four distinct water volumes, corresponding to (Figure C.1):

A. Runoff;
B. Runoff+Baseflow: the "undetermined field", which consists of discharge that cannot be divide into baseflow or runoff. It depends on watershed features and climatic conditions. It should be assigned to runoff in wet periods, while to baseflow in dry periods;
C. Baseflow;
D. Minimum baseflow, during the most severe droughts. It consists of water resources that are always available.

The *characteristic monthly discharge* method provides a simple quantification of groundwater availability within the watershed. The water volumes identified represent the groundwater that a catchment yields during its average hydrological year. Furthermore, these volumes represent the maximum amount of withdrawable groundwater.
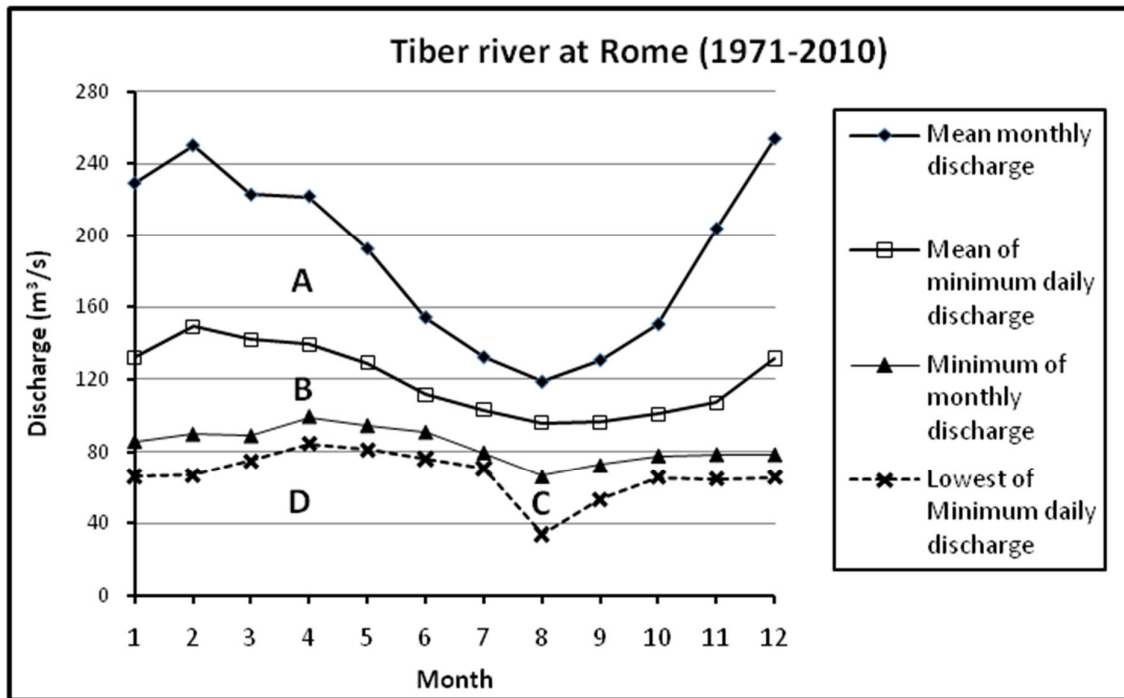

Figure C.1   Characteristic monthly discharge (1971-2010) for Tiber river at Rome ('Ripetta' gauging station). Source: *Former Servizio Idrografico e Mareografico Nazionale database (Hydrological Yearbooks – Second part) and Lazio Region database.*

This method is able to represent and quantify interactions between the aquifer and river and their changes over time. In particular, it provides useful information to evaluate alteration imposed on water resources by human exploitation.

To correctly apply this method, discharge time series of at least 20 years of data are needed. When using shorter time series it is possible that the "mean of minimum daily

discharge" values are less than the "minimum of the monthly discharge". In such a case, a hydrogeological interpretation is needed.

A baseflow index (BFI) is proposed for classifying river-aquifer interaction. This index is calculated as the annual mean of the monthly ratio between the "minimum of the monthly discharge" and the "mean monthly discharge" (see C and A values in Figure C.1).

C.3 Characterising rivers according to the predominant flow sources

Natural streams are fed by liquid or solid precipitation (rainfall or snowmelt) through surface or underground pathways.

Surface runoff is represented by overland flows or channelled flows draining slopes. Surface runoff occurs discontinuously and ends after a variable time interval at the end of the rain.

Groundwater flow consists of the effective infiltration that feeds the stream network through underground pathways as follows:

- Point springs: point groundwater sources located in specific locations near to riverbeds and at defined altitudes;

- Linear springs: dispersed groundwater inputs through river banks and bed and distributed along river reaches, which are identified with the proper methods of quantitative hydrogeology (e.g. upstream to downstream discharge measurement series).

It must be noted that "hypodermic outflow" is included in the "groundwater flow". It represents the portion of the groundwater flow that does not reach the aquifer but flows at shallow depth through the soil (order of meters). Examples are provided by the hypodermic runoff through thawed soil, and the debris and alluvial deposits feeding the stream network.

In terms of their water supply typology, rivers can be described as:

1. Groundwater fed: where the discharge is predominantly fed by baseflow through:

    a. point springs;
    b. linear springs.

2. Surface runoff fed: where the river is prevailingly fed by surface runoff during rainy periods. When runoff ceases, perennial rivers of this type are fed by groundwater (base flow);

3. Snow melt fed: where the river is prevailingly fed by snow melt. When snow melt ceases, perennial rivers of this type are fed by groundwater (base flow);

C.4 Flow regime classification

Starting from the classification scheme proposed by Poff and Ward (1989) and Poff (1996) for the streams in the United States, flow regime classification schemes have been devised, with some adaptations, for application to European streams (see for example Oueslati *et al.*, 2010). These methods are based on eco-hydrological indicators and provide nine flow regime types on the basis of (i) intermittency, (ii) river-aquifer interaction, and (iii) predominant flow source types (surface water, groundwater, snow melt).

Intermittent rivers: In the original scheme, a temporary flow regime was based on the extent of intermittency, with the threshold for perennial flows fixed at 10 days/year of zero-flow conditions (zero discharge). However, for European streams, we adopt a more restrictive threshold between perennial and temporary streams, whereby "perennial" or "permanent" flowing rivers are those that have continuous flow in their channels throughout the year. Poff (1996) also recognises a "*harsh intermittent*" regime for those streams with zero-days (days with no flow) for more than 90 days/year. This threshold is ecologically representative in North America. However, in the European context, and particularly in Mediterranean areas, arid conditions heavily affect the flow intermittency intervals. Therefore, we recognise three types of intermittent stream: (i) *harsh intermittent*, (ii) *intermittent flashy* and (iii) *intermittent runoff.* These reflect the thresholds proposed in the intermittency hydrological indicators of Oueslati *et al.* (2010), which were calibrated on Mediterranean rivers:

1. *Harsh Intermittent*: temporary streams having more than 240 zero-days/year;
2. *Intermittent Flashy*: temporary streams having between 120 and 240 zero days/year;
3. *Intermittent Runoff*: temporary streams having less than 120 zero days/year.

Perennial rivers: Perennially-flowing streams are classified according to their predominant source of flow by (i) groundwater ("stable" and "superstable groundwater" rivers), (ii) surface runoff ("perennial flashy" or "perennial runoff" rivers) and (iii) snow melt processes ("snowmelt" or "snow-rain" rivers). The hydrological indicators are reported below as "characterization indicators" of fluvial systems in Table C.4.

Based on these characterization indicators, a conceptual model of flow regime classification has been developed (Figure C.2). The data required consists of a long-term series of daily flow data (average daily flow), and at least 20-years of records should be considered (Huh *et al.*, 2010). The classification model assigns a hydrological type to each river in a gauging station or to river-segments.

Threshold values of hydrological indicators to define these river types are shown in Table C.1. These are based on the original values reported in Poff and Ward (1989) and Poff (1996), with some modifications for European and Mediterranean regions. The conceptual flowchart for assigning a flow regime class to a river is shown in Figure C.2. The nine flow regime classes are described in Table C.2 (perennial streams) and Table C.3 (temporary streams).

In Tables C.1, C.2 and C.3, and in Figure C.2 (see also Table C.4):

BFI   is a baseflow index (BFI) calculated as the annual mean of the monthly ratio between the "minimum of the monthly discharge" and the "mean monthly discharge":

ZERODAY   is the number of days without channel flow in a year.

FLDFREQ   is the average number of floods per year having discharge higher than the mean of maximum daily discharge (this is a fixed flood threshold).

FLDPRED   is the maximum proportion of all floods over the fixed flood threshold that falls in one of six "60-day seasonal windows", divided by the total number of floods. It ranges from 0.167 (absence of seasonality) to 1 (complete predictability of floods).

FLDTIME   is the day number of the first day within the seasonal 60-day windows when FLDPRED is highest. For the day count, note that the first 60-day period is January-February and the last one is December-January.

DAYCV   is the average (across all years) of the standard deviation of daily discharge divided by the annual mean discharge (x 100):

Table C.1   Threshold values of hydrological indicators to define flow regime types.

|	Flow regime Types	Thresholds
HI	Harsh Intermittent	ZERODAY > 240
IF	Intermittent Flashy	120 ≤ ZERODAY ≤ 240 or (ZERODAY≤ 120 and FLDFREQ ≥ 0.60)
IR	Intermittent Runoff	ZERODAY ≤ 120 and FLDFREQ < 0.60
SN	Perennial Snowmelt	ZERODAY < 1 and FLDPRED ≥ 0.70 and 121 ≤ FLDTIME ≤ 182
SR	Perennial Snow + Rain	ZERODAY < 1 and 121 ≤ FLDTIME ≤ 182 and 0.60 ≤ FLDPRED < 0.70
SS	Perennial Superstable	ZERODAY < 1 and FLDPRED < 0.60 or/and (FLDTIME<121 or FLDTIME>182) and BFI≥50 and DAYCV≤100
SG	Perennial Stable	ZERODAY < 1 and FLDPRED < 0.60 or/and (FLDTIME<121 or FLDTIME>182) and 30≤BFI<50 and DAYCV≤100
PF	Perennial Flashy	ZERODAY < 1 and FLDPRED < 0.60 or/and (FLDTIME<121 or FLDTIME>182) and BFI<30 or/and DAYCV>100 and FLDFREQ≥0.60
PR	Perennial Runoff	ZERODAY < 1 and FLDPRED < 0.60 or/and (FLDTIME<121 or FLDTIME>182) and BFI<30 or/and DAYCV>100 and FLDFREQ<0.60
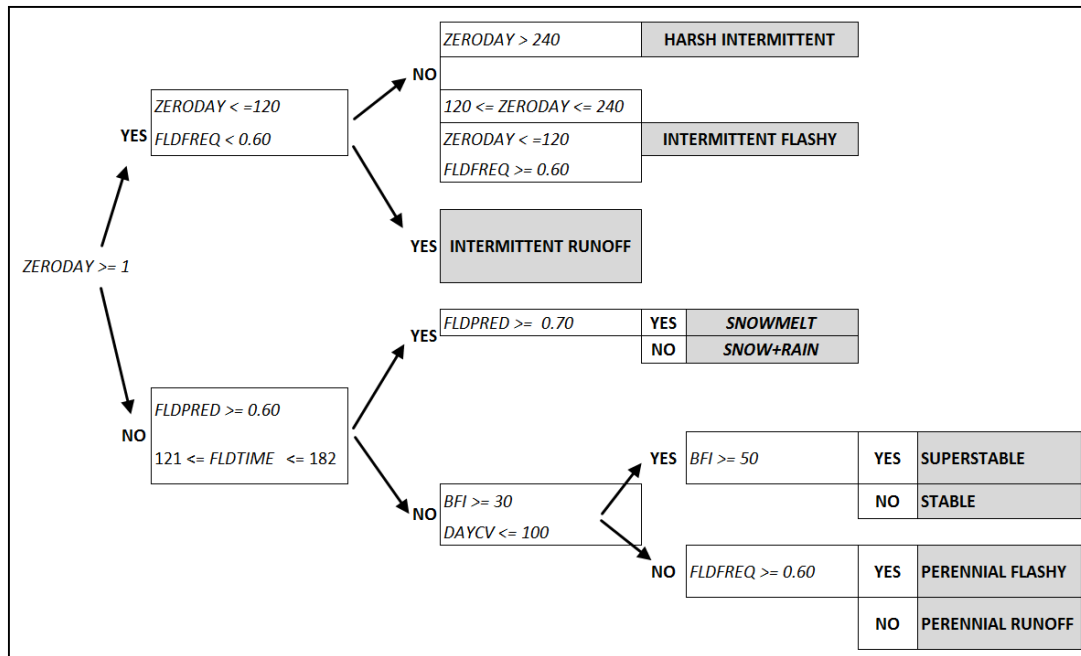
Figure C.2   Conceptual model of flow regime classification.

Table C.2   Classes of Perennial Stream.

Hydrological classes	Flow regime	Hydrological indicators
Perennial Runoff	Perennial rivers fed predominantly by surface runoff (quick flow) and groundwater (baseflow) in the second place. Flow regime is characterized by low seasonal variability.	High contribution by surface runoff to total discharge: BFI < 30 % and FLDFREQ < 0.60
Perennial flashy	Perennial rivers fed predominantly by surface runoff (quick flow), with high flashiness of floods. Flow regime is highly influenced by intense flood events and seasonal droughts.	High contribution by surface runoff to total discharge: BFI < 30 % and FLDFREQ > 0.60
Perennial Stable (*groundwater*)	Rivers having a stable flow regime, due to the regulation effect of groundwater. In the case of unregulated rivers, flow is predominantly fed from groundwater (baseflow).	High contribution by baseflow to total discharge: 30 < BFI < 50 % and DAYCV ≤ 100
Perennial Super-stable (*groundwater*)	Rivers having very low variability in flow regime. In the case of unregulated rivers (natural regime), flow is predominantly fed from groundwater (baseflow).	Very high contribution by baseflow to total discharge: BFI ≥ 50% and DAYCV ≤ 100
Perennial Snow+rain	Perennial streams fed by a mix of surface runoff and snow melt.	High seasonal flood predictability: 0.60≤FLDPRED<0.70 and *121 ≤ FLDTIME ≤ 182*
Perennial Snowmelt	Perennial streams prevailingly fed by snow and glacier melt.	Very high seasonal flood predictability: FLDPRED > 0.70 and *121 ≤ FLDTIME ≤ 182*

Table C.3   Classes of Temporary Stream

Hydrological classes	Flow regime	Hydrological indicators
Harsh intermittent	Temporary streams without flow for almost the whole year. Flow is activated during intense rainfall. No river-aquifer interaction. Streams exclusively fed by surface water (R > 90%).	ZERODAY > 240 and FLDFREQ ≥ 0.60
Intermittent flashy	Temporary streams having runoff in the river bed for less than 8 months/year; streams predominantly fed by surface runoff. Runoff is present occasionally, because of rainfall, snowmelt or seasonal fluctuations of the aquifer level.	120 ≤ ZERODAY ≤ 240 or (ZERODAY≤120 and FLDFREQ ≥ 0.60)
Intermittent runoff	Temporary stream having runoff in the river bed for more than 8 months/year. Streams are fed by surface runoff and groundwater, due to variations in water table levels within the aquifer.	1 ≤ ZERODAY ≤ 120 and FLDFREQ < 0.60

The scheme proposed in Tables C.2 and C.3 classifies all gauged streams or river segments into nine classes on the basis of ecologically-relevant hydrological indicators:

I – Temporary streams

1. Harsh Intermittent - temporary streams without flow for almost the whole year. Flow is activated during intense rainfall (e.g., streams of the Southern Europe and Mediterranean areas);

2. Intermittent Flashy - temporary streams with runoff in the river bed for less than 8 months/year; runoff is present occasionally because of rainfall, snowmelt or seasonal fluctuations of the aquifer level;

3. Intermittent Runoff: temporary stream with runoff in the river bed for more than 8 months/year;

II – Perennial rivers fed predominantly by snowmelt

4. Snowmelt - perennial streams prevailingly fed by snow and glacier melt;

5. Snow-rain - perennial streams fed by a mix of surface runoff and snow melt;

III- Perennial rivers fed predominantly by groundwater

6. Super-stable rivers - rivers with very low variability of the flow regime; in the case of unregulated rivers (natural regime) these are predominantly groundwater fed (baseflow);

7. Stable rivers - rivers having a stable flow regime, due to the regulation effect of groundwater; in the case of unregulated rivers, flow is predominantly fed from groundwater (baseflow);

IV – Perennial rivers fed predominantly by surface runoff

8. Perennial flashy - perennial rivers fed predominantly by surface runoff (quick flow), with high flashiness of floods. Flow regime is highly influenced by intense flood events and seasonal droughts;

9. Perennial runoff - perennial rivers fed predominantly by surface runoff (quick flow) and groundwater (baseflow). Flow regime is characterized by low seasonal variability.

To assign one of the nine hydrological classes to a stream within a particular segment, an algorithm based on the flow indicators reported in Table C.4 (characterization indicators) is used. This algorithm has been tested on approximately 50 Italian river sections, selected on the basis of altitude and latitude, watershed geology and availability of long discharge time series in order to incorporate a wide range of hydrologic and climatic conditions.

C.5   Calculation of the flow regime indicators

All calculation of the following indicators refers to the 'mean daily discharge' of the data series.

ZERODAY [days]: Extent of intermittency. It is the average annual number of days having zero discharge.

QThreshold   [m^3/s]:   is the fixed discharge used to identify flood events over a threshold. It is the mean of annual maximum daily discharges (i.e. 1 maximum value per year in the discharge record). In Figure C.3 an example of maximum flood events over threshold is shown for the River Frome - UK.
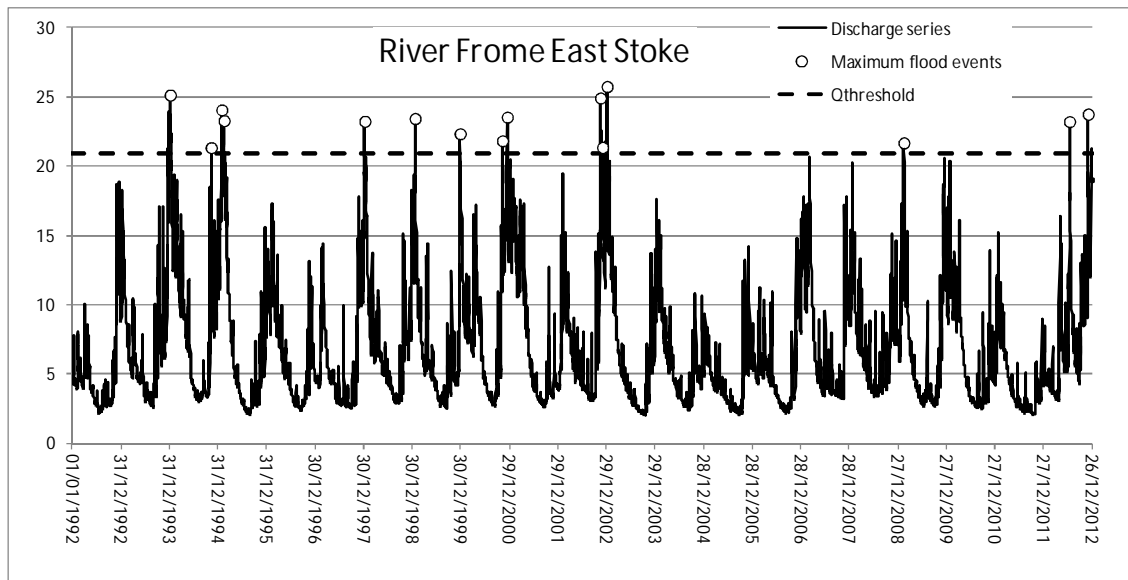

Figure C.3   Maximum flood events over threshold discharge for River Frome (UK) at the East Stoke gauging station.

FLDPRED *[-]: seasonal predictability of flooding* is the maximum proportion of all floods over the threshold that falls in one of the twelve "60-day seasonal windows" (Jan-Feb, Feb-March, …, Dec-Jan) divided by the total number of floods (Table C.4 - C.5). It ranges from 0.167 (absence of seasonality) to 1 (complete predictability of floods). A 10-day period separating individual events over threshold is used to identify separate events (Figure C.3).

Calculation method: identify each daily discharge exceeding the flood threshold and the corresponding date. Select only the maximum discharge value for each flood event and verify that the maximum values are separated by a lag time of at least 10 days. Calculate the total number of these exceedance values. Then assign each maximum flood event to the 60-day seasonal windows. Calculate the ratio of number of maximum events in each window to the total number of the exceedance values. FLDPRED is the highest ratio value.

Table C.4 Flood events over threshold for River Frome (UK) at the East Stoke gauging station.

Date	Month	Peak discharge over threshold
06/01/1994	1	25.13
10/11/1994	11	21.34
28/01/1995	1	24.06
15/02/1995	2	23.28
08/01/1998	1	23.24
20/01/1999	1	23.43
25/12/1999	12	22.34
07/11/2000	11	21.84
13/12/2000	12	23.54
14/11/2002	11	24.92
29/11/2002	11	21.36
02/01/2003	1	25.74
10/02/2009	2	21.68
09/07/2012	7	23.22
26/11/2012	11	23.76

Table C.5 FLDPRED and FLDTIME calculation for River Frome (UK) at the East Stoke gauging station.

Two-month periods	I	II	III	IV	V	VI	VII	VIII	IX	X	XI	XII
First month / Second month	1 / 2	2 / 3	3 / 4	4 / 5	5 / 6	6 / 7	7 / 8	8 / 9	9 / 10	10 / 11	11 / 12	12 / 1
N. POT in 2 month	7	2	0	0	0	1	1	0	0	5	7	7
FLDPRED (n. POTs in 2 month/ Total n. POTs)	0.47	0.13	0.00	0.00	0.00	0.07	0.07	0.00	0.00	0.33	0.47	0.47
periods with same FLDPRED	Jan-Feb	-	-	-	-	-	-	-	-	-	Nov-Dec	Dec-Jan
FLDTIME	1	32	60	91	121	152	182	213	244	274	305	335

FLDTIME *[day]: timing of flooding*; it is the first day of the 60-days seasonal windows where the FLDPRED is highest (Figure C.5). FLDTIME possible values are:

Seasonal window	FLDTIME
1 (Jan-Feb)	1
2 (Feb-Mar)	32
3 (Mar-Apr)	60
4 (Apr-May)	91
5 (May-Jun)	121
6 (Jun-Jul)	152
7 (Jul-Aug)	182
8 (Aug-Sep)	213
9 (Sep-Oct)	244
10 (Oct-Nov)	274
11 (Nov-Dec)	305
12 (Dec-Jan)	335

FLDFREQ *[yr^{-1}]: flood frequency* is the average number of flood events over the threshold per year. A 10-day period separating individual events over threshold is used to identify separate events. Calculation method: identify each daily discharge exceeding the flood threshold and the corresponding date. Select only the maximum discharge value for each flood event and verify that maximum values are separated by a lag time of 10 days (Figure C.3). Calculate the total number of these exceedance values. FLDFREQ is the ratio of the total number of exceedance values to the number of years of the record period.

BFI *[%] Base flow index.* For each month of each year calculate the mean discharge values. Calculate the mean and minimum values for each month (12 mean monthly values + 12 minimum monthly values). Then calculate the ratio of minimum monthly values to mean monthly values. Multiply the ratios by 100. BFI is the average of these 12 values.

$$BFI = 100 \times \frac{1}{M} \sum_{j=1}^{M} \left[\frac{\min_{1 \le i \le N}(QM_{j,i})}{\frac{1}{N} \sum_{i=1}^{N}(QM_{j,i})} \right]$$

where:

N = number of years

M = number of months (12)

$QM_{j,i}$ = monthly discharge for the jth month of the ith year.

DAYCV *[%]: coefficient of variation* is the average (across all years) of the ratio of the annual standard deviation of mean daily discharge to the annual mean discharge multiplied by 100.

$$AYCV = 100 \times \frac{1}{N} \sum_{i=1}^{N} \left(\frac{\sigma_{QD,i}}{\mu_{QDd,i}} \right)$$

where:

N = number of years

QD = mean daily discharge

$\sigma_{QD,i}$ = annual standard deviation of mean daily discharge for the ith year

$\mu_{QD,i}$ = annual mean of mean daily discharge for the ith year.

C.6   Hydrological alteration

After classifying the streams according to their flow regime, as described in the previous section (C.4), a hydrological alteration method can be applied to investigate and assess the degree of alteration of the hydrological regime. This hydrological alteration assessment also provides a useful set of indicators to help identify differences and similarities between rivers classified within the same type.

The proposed hydrological indicators (Table C.5) are grouped in relation to their scale of representation (catchment/network, segment, reach), and to the type of hydrological indication that they are able to provide. They are also labeled with *A* or *C* depending on the type of information they provide regarding the flow regime (i.e., indicators of characterization – *C*; or indicators of alteration – *A* of the flow regime).

C.7   Characterization indicators

Characterization (C) and hydrological alteration (A) indicators shown in Table C.4 allow hydrological characterisation and hydrological alteration to be assessed. Together they provide information about hydrological response of the river-watershed system, given a series of expected hydrological features, as a function of rainfall variability.

Morphometric characterization is conducted at the catchment scale while flow regime characterization and type of water supply are built at the catchment or segment scale if flow data (or hydrological simulation models, e.g. rainfall-runoff model) are available. Analysis of hydrological alteration is built at the reach scale.

Most of the characterization indicators are based on physical properties of the catchment upstream of the reach: surface extension (S), length (L), slope, shape, land use, geology, geomorphology, etc.. All these properties affect the way runoff is generated and so the amount and variability of stream discharges. Changes in their values could affect discharges even though it is not the only way flow regime becomes altered.

Hydrological indicators are used to classify streams into nine flow regime types. They give information about the predominant sources of water to the segment or reach and river-aquifer interaction in space and time.

C.8   Alteration indicators

The flow regime of a natural river is a product of the set of expected characteristics, both quantitative and temporal, through which water flow occurs in that river. Flow regime description related to a time interval (usually 1 year) is generally conducted with reference to the chronological discharge diagram or *hydrograph* in which flow discharges at a given time-aggregation are shown in their temporal event sequence (Figure C.4).

Although the description of flow regime alteration is really complex, it is recognized that the identification of the 5 main flow components (magnitude, frequency, duration, timing, rate of change) is important for an effective characterization of the degree of hydrological alteration.

Hydrological alteration is the deviation between:

- the "current" hydrological regime (measured or estimated through models. In the latter case uncertainties can affect the estimation)

and

- the "natural" hydrological regime. This refers to unaltered conditions: pre-impact (in the past) or now without impacts (reconstruction from current flow regime "removing" anthropogenic pressures)

The hydrological regime is usually represented by (Figure C.3):

- The hydrograph (stream discharges vs time);

- The flow duration curve (stream discharge plotted against the time interval in which that discharge value is exceeded).

The hydrological regime identifies those aspects or components that describe the peculiar behaviour of river discharges at different time-scales.

The flow regime is effectively described by 5 main flow components, relevant for their effects on ecological processes:

1. Magnitude – *how much?*

2. Frequency – *how often?*

3. Timing – *when?*

4. Duration – *how long?*

5. Rate of change – *how fast?*[1]

Hydrological Alteration assessment methods all refer to the main 5 flow components in terms of stream discharges, to derive a suite of parameters / indicators of the flow regime. They all characterize hydrological conditions (current and natural) by the value of those indicators, and assess the hydrological alteration by comparing the values of homologous parameters representing unaltered and impacted conditions.

Table C.5 Proposed hydrological indicators

Scale	Hydrological Indicator	Description	Characterization / Alteration	Calculation
REGION	ARIDITY INDEX	e.g. De Martonne	C	
CATCHMENT – NETWORK (upstream of the reach; draining through the reach's outlet section) MORPHOMETRIC INDICATORS	GLACIER RATIO		C	
	IPSOMETRIC CURVE		C	
	MORPHOMETRY	Rc (circularity ratio)	C	$Rc = 0.89*L/[(4*S/\pi)^{0.5}]$
	PERMEABILITY	Flow coefficient	C	ψ, CN
	TRAVEL TIME	Time of concentration	C	$(h_{max}-h_{min})/L$, S
	HIERARCHY	Horton's laws (set threshold for minimum area to be considered)	C	
	DRAINAGE DENSITY		C	
	AREA	Basin drainage area, Km2	C	
CATCHMENT – SEGMENT HYDROLOGICAL (FLOW REGIME) INDICATORS	QMEAN	Daily mean discharge, m^3/s	C	
	DAYCV	Daily discharge coefficient of variation, %	C	Average (across all years) of standard deviation of daily discharge divided by the annual mean discharge (x 100).
	FLDFREQ	Flood frequency, 1/yr	C	The average number of floods per year having discharge higher than the mean of maximum daily discharge (fixed flood threshold).
	FLDPRED	Seasonal flood predictability	C	The maximum proportion of all floods over the threshold that falls in one of the six "60-day seasonal windows", divided by the total number of floods. It ranges from 0.167 (absence of seasonality) to 1 (complete predictability of floods).
	FLDTIME	Timing of floods; day	C	The first day of the 60-day period when FLDPRED is highest. The first 60-day period is January-February and it includes February 29.
	BFI	Base Flow index, %	C	Proportion between the "minimum of monthly discharge" and "mean monthly discharge' (see chap. II – Groundwater and river-aquifer interaction), multiplied by 100

| Scale	Hydrological Indicator	Description	Characterization / Alteration	Calculation
	ZERODAY	Extent of intermittency (number of days)	C	The average annual number of days having zero discharge.
REACH — HYDROLOGICAL ALTERATION INDICATORS	MEAN FLOW CONDITIONS	1. Magnitude of monthly discharge	A	Mean or median value for each calendar month
	EXTREME FLOW CONDITIONS	2. Magnitude and duration of discharge	A	Annual minima, 1-day mean Annual minima, 3-day means Annual minima, 7- day means Annual minima, 30-day means Annual minima, 90-day means Number of zero-flow days Base flow index: 7-day minimum flow/mean flow for year Annual maxima, 1-day mean Annual maxima, 3-day means Annual maxima, 7-day means Annual maxima, 30-day means Annual maxima, 90-day means
		Channel forming discharge	A	Qp_2: 2 year return period peak discharge Qp_{10}: 10 year return period peak discharge
		3. Timing of annual extreme discharge	A	Julian date of each annual 1-day maximum Julian date of each annual 1-day minimum
	DISCHARGE FLUCTUATIONS	4. Frequency and duration of high and low pulse	A	Number of low pulses within each water year Mean or median duration of low pulses (days) Number of high pulses within each water year Mean or median duration of high pulses (days)
	RATE OF FLOW CONDITION CHANGES	5. Rate and frequency of discharge values	A	Rise rates: Mean or median of all positive differences between consecutive daily values Fall rates: Mean or median of all negative differences between consecutive daily values Number of hydrologic reversals
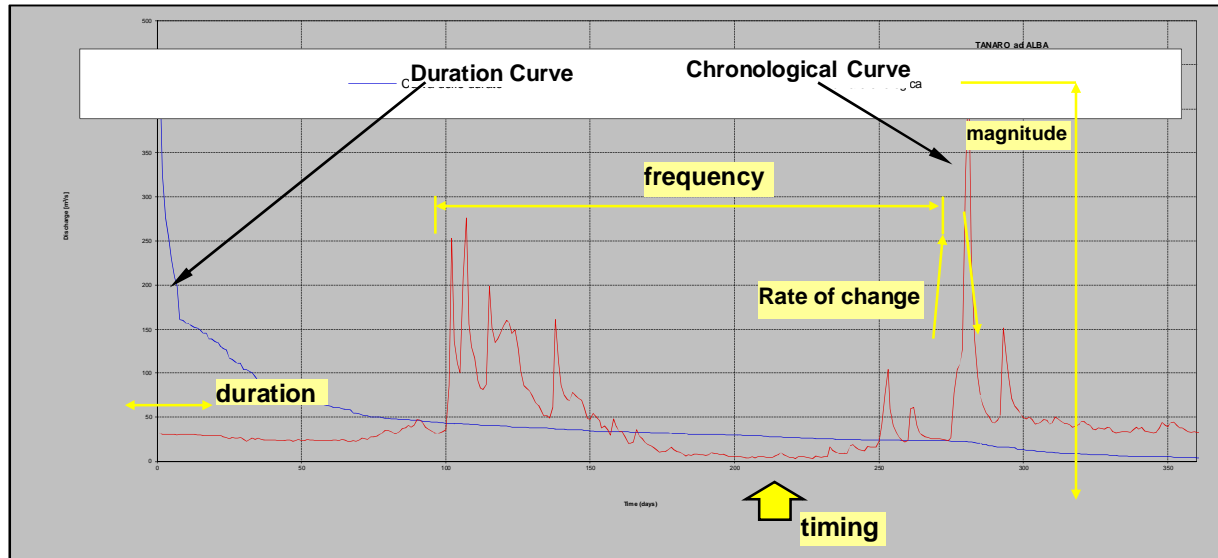
Figure C.4 Example of a hydrograph and a flow duration curve.

Indicators of alterations are obtained by comparing the value of certain flow regime characterization indicators for different periods of time (e.g. pre-impact and post impact periods) or for current (altered) and naturalised flow series. These indicators have already been developed and presented in the literature. They share a common basis and have some critical aspects that are analyzed in the following section (C.9). The same descriptive approach (listing the PROS and CONS of specific indicator applications) is used to analyze the indicators suggested for alteration.

C.9   Methodologies for hydrological alteration assessment

In this section, several approaches to the assessment of hydrological alteration are described:

(i)   Indicators of Hydrological Alteration - IHA (Richter et al. 1996)

The IHA methodology considers 33 indicators describing the 5 flow components mentioned above (Figure C.5). It uses the Range of Variability Approach (Richter et al. 1996) to estimate the overall alteration:

- IHA defines 33 indicators (parameters) to be estimated in pre/post impact conditions
- In the RVA analysis the full range of pre-impact data for each parameter is divided into 3 different categories (High, Middle, Low).
- The boundaries between categories are based on either percentile values (e.g. 25% and 75%) or a number of standard deviations away from the mean.
- The frequencies with which the "pre and post-impact" annual values of IHA parameters fall within each of the 3 categories are calculated.

Hydrologic Alteration is calculated for each of the 3 categories comparing an "expected frequency" (or a pre-development natural variation) based on "pre-impact" or "naturalised" values with the "observed frequency" based on "post-impact" values.

PROS:

- The method is easy to apply
- The results are readily interpretable
- Software is available.

CONS:

- It needs a minimum of a 15 year daily discharge series..
- It estimates the alteration in terms of frequency but not in terms of size of deviation.
- It results in 33 indicators.
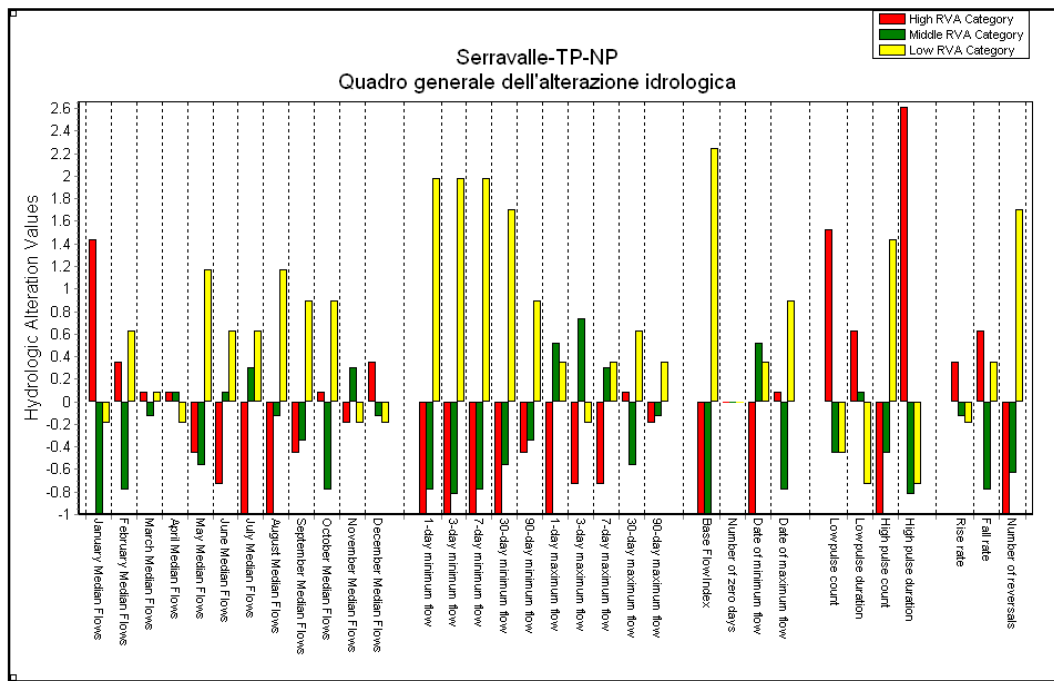
Figure. C.5 IHA indicators.

(ii)   IAHRIS developed by UPM and CEDEX (ES)

This method defines indicators (parameters) to be estimated in pre and post impact conditions according to 3 global components:

1. *habitual regime*
2. *flood regime*
3. *drought regime*

REGIME COMPONENT		ASPECT	PARAMETER			
HABITUAL DATA	MONTHLY OR ANNUAL VOLUMES	MAGNITUDE	Average of the annual volumes	Type of year		Wet year
						Normal year
						Dry year
				WEIGHTED year (P1)		
		VARIABILITY	Difference between the maximum and the minimum monthly volume along the year	Type of year		Wet year
						Normal year
						Dry year
				WEIGHTED year (P2)		
		SEASONALITY	Month with the maximun and minimum water volume along the year	Type of year (P3)		Wet year
						Normal year
						Dry year
	DAILY FLOW	VARIABILITY	Difference between the average flows associated to the percentiles 10% and 90%	Type of year (P4)		Wet year
						Normal year
						Dry year
EXTREME DATA	MAXIMUM VALUES OF THE DAILY FLOWS (FLOODS)	MAGNITUDE & FREQUENCY	Average of the maximum daily flows along the year Effective discharge Connectivity discharge Flushing flood	Qc (P5) QGL (P6) QCONEC (P7) Q 5% (P8)		
		VARIABILITY	Coefficient of variation of the maximun daily flows along the year Coefficient of variation of the flushing flood series	CV (Qc) (P9) CV (Q 5%) (P10)		
		DURATION	Maximum number of consecutive days in the year with q≥ Q 5%	Flood duration (P11)		
		SEASONALITY	Average number of days in the month with q ≥ Q 5%	12 values (one for each month) (P12)		
	MINIMUM VALUES OF THE DAILY FLOWS (DROUGHTS)	MAGNITUDE & FREQUENCY	Average of the minimum daily flows along the year Ordinary drought discharge	Qs (P13) Q 95% (P14)		
		VARIABILITY	Coefficient of variation of the minimun daily flows along the year Coefficient of variation of the ordinary droughts series	CV (Qs) (P15) CV (Q 95%) (P16)		
		DURATION	Maximum number of consecutive days in the year with q≤ Q 95%	Drought duration (P17)		
			Average days per month with no daily flow	12 values (one for each month) (P18)		
		SEASONALITY	Average number of days in the month with q ≤ Q 95%	12 values (one for each month) (P19)		

Figure C.6 – IAHRIS parameters.

| INDICATOR	Natural Reg.	Altered Reg.
I_j	1	a_j
I_k	1	a_k
I_l	1	a_l
I_m	1	a_m
I_n	1	a_n
I_p	1	a_p
I_q	1	a_q
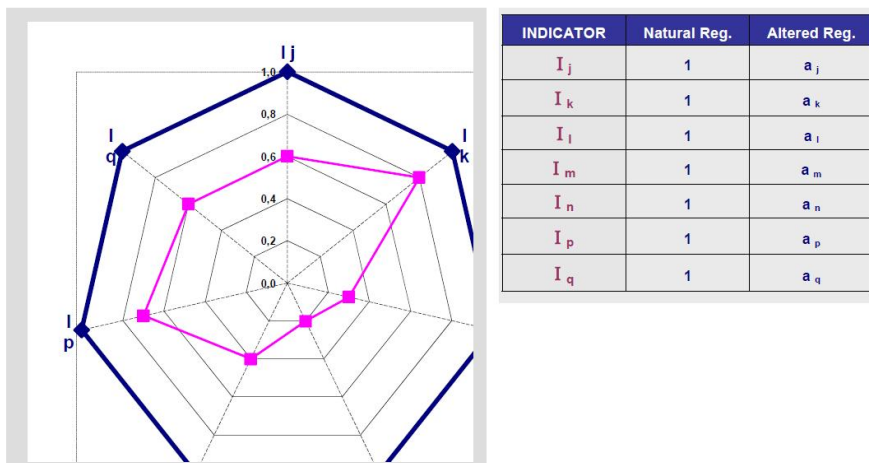
Figure C.7 Polygons showing indicator values for reference and actual conditions.

For each of the 3 global components, it defines suites of indicators for characterizing pre-post hydrological conditions (Figure C.6).

It then represents the value of each indicator of the suite of indicators in a polar diagram. This generates two polygons (e.g. Figure C.7): one, representing the reference conditions, and the other representing the actual (altered) ones. It eventually calculates the hydrological alteration as the deviation of the areas of the two polygons.

PROS:

• IAHRIS distinguishes between wet, dry, and normal years and weights the indicators accordingly.

- It considers also parameters related to geomorphological aspects such as "channel forming" discharges.
- It defines floods as those events whose discharge exceeds the 5% percentile of annual maximum.

CONS:

- It needs a minimum of a 15 year daily discharge series.
- It results in three final indicators.

(iii)   IARI developed by ISPRA

This method first selects a procedure on the basis of data availability.

If only a limited data set is available, it estimates alteration on the basis of monthly discharges. If this generates values that indicate hydrological conditions that are less than good, then a further analysis is required.

If daily data are available, the method calculates IHA parameters but then uses the deviation of each parameter representing actual conditions from the 25 and 75 percentiles of the natural (pre-impact or naturalised) discharge condition.

PROS:

- It can be performed even with a short time series
- It uses degree of deviation to calculate alteration
- It summarises the alteration using only one index.
- It distinguishes between wet, dry, and normal years and weights the indicators accordingly.

CONS:

- It averages all the 33 deviations into one value (one index of alteration)

(iv) REFORM Hydrological Alteration Indicators

For REFORM, we propose a methodology that incorporates the IHA 33 parameters together with several 'geomorphologically significant discharges' (Qp_2 – the two year return period peak discharge'; Qp_{10} – the10 year return period peak discharge). This is elaborated in section 5.4 of this report for application at the segment scale (to maximise the chance of accessing a gauging station with sufficient length and temporal resolution of records)

The methodologies for hydrological alteration assessment share some critical aspects regarding:

1. Data: stream discharge series are often discontinuous or short, stage-discharge relationship are not updated frequently, modelling discharges implies uncertainties and, above all, data on hydrological pressures (withdrawals, abstractions) are very rare or lacking.

2. Reference condition: Should we consider the system as it is now but without pressures (i.e. naturalized) or should we refer to the system as it was in the past, when no pressures were in place? In the latter case we could have a mistaken

vision of the reference system because, especially from a geomorphic point of view, the system could have changed considerably.

3. The (necessary) time-unit of assessment: monthly to daily to hourly series are needed.

C.10 References

Boni C, Petitta M, Preziosi E, Sereni M. 1993-A. Genesi e regime di portata delle acque continentali del Lazio. Roma, CNR – Italian National Research Council.

Boni CF, Mastrorillo L, Petitta M, 1993-B. Scomposizione della portata dei corsi d'acqua dell'Appennino Marchigiano con il metodo delle portate mensili caratteristiche. Geologia Applicata e Idrogeologia, 28, Bari, 121-129.

European Communities, 2000. Directive 2000/60/EC of the European Parliament and of the Council of 23 October 2000 establishing a framework for Community action in the field of water policy. Official Journal of the European Communities 43 (L327), 75 pp.

Huh S, Dickey DA, Meador MR, Ruh KE. 2005. Temporal analysis of the frequency and duration of low and high streamflow: years of record needed to characterize streamflow variability, Journal of Hydrology 310, 78–94.

ISPRA. 2011. Implementazione della Direttiva 2000/60/CE. Analisi e valutazione degli aspetti idromorfologici. Versione 1.1. Istituto Superiore per la Protezione e la Ricerca Ambientale, Roma.

Olden JD, Poff NL, 2003. Redundancy and the choice of Hydrologic Indices for characterizing streamflows regimes, River research and applications, 19, 101–121.

Oueslati O, De Girolamo AM, Abouabdillah A, Lo Porto A. 2010. Attemps to flow regime classification and characterization in Mediterranean streams using multivariate analysis. International Workshop 'Advances in Statistical Hydrology'; May 23-25, 2010, Taormina, Italy.

Poff NL. 1996. A hydrogeography of unregulated streams in the United States and an examination of scale-dependence in some hydrological descriptors, Freshwater Biology, 36, 71–91.

Poff NL, David Allan J, Bain MB, Karr JR, Prestegaard KL, Richter BD, Sparks RE, Stromberg J. 1997. The Natural Flow Regime, A paradigm for river conservation and restoration, Bioscience, 47, 769–784.

Poff NL, Ward JV, 1989. Implications of streamflow variability and predictability for lotic community structure: a regional analysis of Streamflow Patterns, Canadian Journal of Fisheries and Aquatic Sciences, 46, 1805–1818.

Richter BD, Baumgartner JV, Powell J, Braun DP. 1996. A method for assessing hydrologic alteration within ecosystems, Conservation Biology, 10, 1163–1174.

Annex D
Sampling Bed and Bank Sediments in Streams and Rivers

Francesco Comiti,

Faculty of Science and Technology,

Free University of Bozen-Bolzano, Italy

Acknowledgment:

The following text draws heavily on Bunte and Abt (2001), including Tables and Figures from this source, to provide a brief review of the issues involved in sampling sediments in streams and rivers. The review emphasizes approaches to obtaining average reach particle size distributions and D_{50} estimates, since such estimates are most relevant to broad reach-scale assessments. Readers are strongly recommended to refer to Bunte and Abt (2001) to obtain full details on any specific aspect of the following and to find more information on how the particle size characteristics of particular landform or patches can be estimated. If not specified differently, Figures and Tables are from Bunte and Abt (2001).

D.1   Introduction

Some simple methods for characterizing bed and bank materials are presented in the main report (Deliverable 2.1, Part 1, section 5.5.3). However, when reaches are being specifically surveyed to characterize their hydromorphology, there is an opportunity to undertake a more thorough characterization of river channel sediments. Such a characterization will underpin a stronger and more process-based interpretation of this extremely important property of river channels. This section presents a range of methods that could be adopted in such surveys.

River beds often display distinct sedimentary structures and a distinction is often drawn between the surface and subsurface layers (Figure D.1), because river beds may become armoured (fine particles are mobilised and removed leaving a layer of coarse particles that protect fine particles in the subsurface layer from erosion) or buried and clogged by the deposition of a layer of fine sediment. These layers are often sampled and characterized separately.

- When the bed has a coarse (gravel, cobble or boulder) surface layer, the particle size distribution is determined from a pre-selected number (see D.2.3) of surface particles

obtained from a predefined sampling area of the bed. The sampled surface layer is one particle deep.

- *When the coarse bed is buried in fine sediments*, the depth of this surface layer can be measured by inserting a pointed probe until it hits the coarser material beneath and then bulk sample(s) of the fine layer can be obtained for particle size analysis (see D.3.1).

- *When the subsurface layer or the integrated surface and subsurface sediments are of interest*, a pre-selected sediment volume is extracted from the required sediment layer(s). Unstratified bed-material samples are useful only when the bed material is not markedly stratified (e.g no armour layer of fine sediment veneer) or when such strata are not relevant to the study being undertaken.
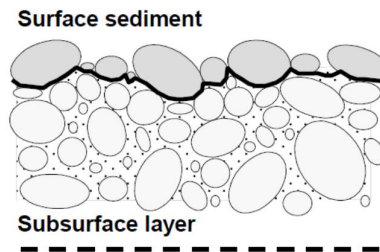
Figure D.1   Surface and subsurface sediment layers within a river bed.

While coarse particles are usually sampled individually by hand, there are numerous samplers available for obtaining grab and volumetric samples from river beds, with different designs available to suit different sediment calibres and river sizes (depths). Freeze coring can also be used to obtain intact bed sediment profiles. These sampling devices are fully described by Bunte and Abt (2001).

Once samples of sediment have been obtained a particle size distribution can be estimated. Particles per size class can be either counted or weighed, and size distributions may be explained in terms of frequency-by-number or frequency-by weight. The comparability of number- and weight-based particle-size analyses is briefly presented in the next section.

D.2   Surface sampling

For fine sediments, a few bulk samples will provide a sufficiently accurate assessment of the particle size distribution. The samples are dried and then past through a nest of sieves to determine the weight of sediment within different size ranges from gravel through to fine sand and silt. If finer sediment sizes are to be assessed, then a small sub-sample of the material that passes through the finest sieve can be analysed using a laser-sizer or settlement techniques. In this way a size by weight analysis is performed.

Coarse bed-surface sediment can be sampled by three methods:

Line counts select a preset number of surface particles at evenly-spaced increments along transects that may be parallel and span a relatively large sampling area ($\approx$ 100 m^2)

Grid counts select particles at a preset number of evenly-spaced grid points that span a relatively small sampling area (≈ 1-10 m^2), handpicking particles or measuring particle sizes on photographs.

Areal samples include *all* surface particles contained within a small preset area (≈ 0.1 - 1 m^2) of the streambed. Adhesives are often used to ensure that small particles are included representatively in the sample.

Number-based particle-size distributions obtained from line counts and grid samples are mutually comparable and combinable. Both distributions are also comparable and combinable with distributions obtained by volume-by-weight in unstratified beds. In contrast, particle-size distributions of areal samples need to be converted, applying the appropriate conversion factors as indicated in Bunte and Abt (2001), before making a comparison or combination with size distributions from pebble counts or volumetric samples.

Differences between the three surface sampling methods are summarized in Table D.1. <u>NOTE: areal samples are not discussed any further in this Annex.</u>

Table D.1   A comparison of the properties of line, grid and areal samples

Line Counts	Grid Counts	Areal Samples
Sample a pre-determined number of particles at approximately evenly spaced intervals at least Dmax size apart along lines / transects	Sample a pre-determined number of particles across a an approximately even grid of points at least Dmax size apart	Sample all surface particles within a small pre-defined sampling area
Samples a large area	Samples relatively small areas (e.g. single geomorphic units in large rivers or integrate more units in small streams).	Samples several specific point locations across a sampling area
Suitable for cobble-gravel sediments (not sand)	Suitable for cobble-gravel sediments (not sand)	Suitable for medium gravel to sand (not coarse gravel or cobbles)

D2.1   Line and Grid Counts: Procedures and Operator Bias

Line and gird counts sample a preset number of particles in evenly-spaced increments along transects or across grids. Two methods are usually used: a heel-to-toe walk and sampling at evenly-spaced marks along a measuring tape.

The first technique was proposed by Wolman (1954) (see also Leopold 1970). An operator traverses a gravel surface along a grid pattern. The grid may be established by pacing or laid out by lines or a tape. A particle is collected in the vicinity of each grid point – it must be selected at random. As a means to achieve this randomness, Wolman proposed picking up a particle from beneath the tip of the boot while looking away. The spacing between selected particles is determined by the size of the grid needed to cover the sampling area with 100 grid points. Heel-to-toe walks were invented for sampling

streambeds of medium gravel. If applied to coarser beds, heel-to-toe sampling may bring about bias both for and against large clasts.

A more systematic way of sampling surface bed-material with pebble counts is to stretch a measuring tape in several transects across the sampling area. Particles are selected at intersections with evenly-spaced marks along the edge of the tape, for example at 0.5 m intervals. The spacing between particles depends on the bed-material particle size and is set to a value larger than the b-axis of the D_{max} particle size being sampled, in order to prevent double counting of large particles and bias towards large particle sizes

Operator error is likely to be introduced into pebble counts through favouring middle-sized, easily collected particles, by sampling areas that have a systematic spatial variation in particle sizes, or by preferentially sampling at the most accessible stream bed locations. The bias against fine or coarse particles has the most pronounced effect on the cumulative particle-size distribution and presents an opportunity for neglecting fines or under-representing cobbles and boulders for coarser river beds (Figure D.2).
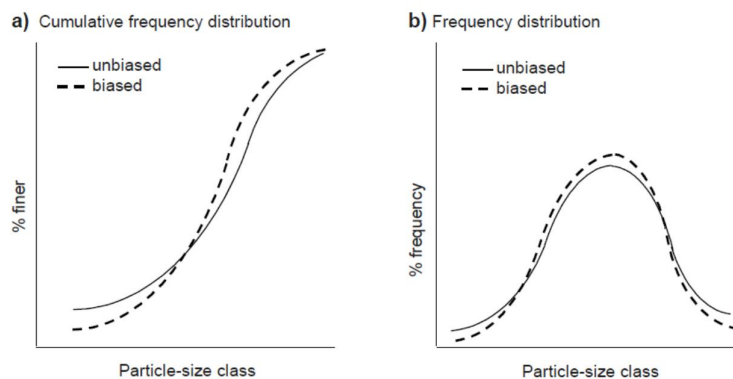
Figure D.2   Impacts of operator bias on particle size frequency distributions

D.2.2   Statistical errors in pebble and grid counts

The ideal way to describe the particle-size distribution of a streambed would be to count and measure every particle within the reach. Since this is impossible, bed material has to be sampled to estimate the bed material characteristics of the sampled area, and a balance has to be achieved between the number of particles or quantity of sediment sampled and the related effort involved in obtaining and processing the samples.

As the number of particles collected increases, the precision with which the bed material can be described also increases. Furthermore, when there is little variability in the sampled material (i.e., when the bed is well sorted or homogenous), smaller samples are sufficient to precisely describe the bed material. With greater variability, the sample sizes must be increased to obtain the same precision. The precision achieved needs to be sufficient to measure the effects being investigated.

Because sample size determines both the cost and the benefits of field measurements, _careful attention should be paid to the minimum sample size needed to ensure the necessary sampling precision_ _before going out into the field_. It is necessary to have at least an approximate estimate of the bed-material standard deviation or sorting to estimate the required sample size. Such an estimate can be based on prior studies of

other streams with similar bed material or on a brief _pilot data-collection_ exercise at the field site.

Particle size data are often expressed in φ (phi) units rather than in mm, where φ is the negative logarithm to the base 2 of the particle size in mm (Wentworth, 1922, Table D.2). This transformation often produces an approximately normal (Gaussian) particle-size distribution.

For normal (Gaussian) distributions the required sample size (n) to obtain a desired precision of the sample mean is

$$n = \left(\frac{t \cdot \sigma}{e}\right)^2 \qquad (1)$$

where t is the relevant value of Students' t for the required confidence level, σ is the population standard deviation, and e is the acceptable error around the mean.

Table D.2   Particle size units, categories and descriptions (after Wentworth, 1922)

Particle size (phi)	Particle size (mm)	Particle size (microns)	Size class description
<-8	>256		Boulder
-6 to -8	64 to 256		Cobble
-2 to -6	4 to 64		Gravel (pebble)
-1 to -2	2 to 4	2000 to 4000	Gravel (granule)
0 to -1	1 to 2	1000 to 2000	Sand (very coarse)
4 to -1	0.0625 to 2	63 to 2000	Sand
9 to 4	0.00195 to 0.0625	2 to 63	Silt
>9	<0.00195	<2	Clay

The value of Student's t is selected for a range of sample sizes and the required confidence level for the estimated sample mean (e.g. ɑ = 0.05 for a 95% confidence level). Values for t for different confidence levels and samples sizes can be obtained from statistical tables available in standard statistics books. Since the population standard deviation is not known, it is replaced by an estimate of the standard deviation (s) derived from the pilot sample - the Inman sorting coefficient s_I (describes the range of particle sizes contained within the central 68% of all the pilot sample data) is often used:

$$s_I = \frac{|\phi_{84} - \phi_{16}|}{2} \qquad (2)$$

The error around the mean can be expressed in absolute or in percentage terms. An acceptable error for the sample mean can be specified (e.g., ±0.15 φ around the mean in φ-units) and then the sample size necessary to attain this can be calculated.
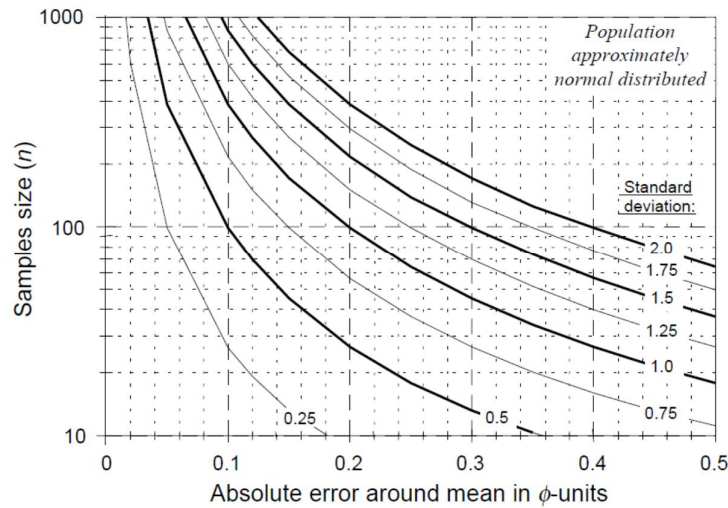
Figure D.3   Relationships among standard deviation (S), error around the mean (e) and sample size (n).

D.2.3   Sample Size in Pebble and Grid Counts

Sampling precision increases with the reciprocal of the square root of sample size n (standard error ≈ 1/SQRT(n)). Thus, sampling precision improves dramatically as sample size (n) increases at small values of n, but the improvement becomes very small for high values of n. For the bed material of the Mamquam River with σ = 1.17 φ, Rice and Church (1996) determined the cutoff point beyond which further sampling does not significantly improve sampling precision is at a sample size of 400 particles.

A 400-particle surface sample in moderately-sorted bed material (s = 1 φ) yields an approximate absolute error of ± 0.1 φ around the mean, whereas sampling only 100 particles increases the absolute error margin to approximately ±0.2 φ. In more poorly sorted bed material with s = 2 φ, sampling 400 particles leads to an absolute error around the mean of ±0.2 φ, and 100 particles to an error of ±0.4 φ.

The statistical error associated with estimates of small percentiles is usually relatively large, and so a considerably larger sample size is required to accurately characterize low percentiles (e.g., D_5, D_{16}) than high percentiles (e.g., D_{84}, D_{95}) in distributions skewed towards a fine tail. Percentiles between D_{50} and D_{95} require nearly the same sample size for any given precision.

If the underlying distribution of the bed material is symmetrical and normal, and has a sorting coefficient of 1.2 φ, the sample size required for estimating the D_5 and D_{95} is approximately 2.6 larger than the sample size needed for the D_{50}. Thus, if 400 particles are required to estimate the D_{50} to within ±0.15 φ, more than 1,000 particles are needed to estimate the D_5 or D_{95} with the same precision.

These sample-size considerations do not take account of spatial heterogeneity, and are only valid for homogeneous sampling reaches / areas. For heterogeneous reaches, required sample sizes are likely to be larger.

D.2.4   Recording pebble count data

Particle sizes from pebble counts should always be recorded in a systematic manner, so that the approximate location of each counted particle can be traced. To achieve this, all transects should start on the same side of the stream, beginning at the downstream end of the reach and working upstream. All particle-size data from one transect should be recorded sequentially in one column (or row).

A spatially systematic particle-size record permits the user to analyze whether particle sizes vary in a longitudinal direction by comparing individual transects, or sets of adjacent transects. Lateral particle-size variability can be estimated from moving averages over 5 to 9 consecutively counted particle sizes. A spatially systematic particle size record can also be used to delineate, retrospectively, sedimentary or even geomorphological units. Particle-size data can then be consolidated for each sedimentary unit to achieve an approximate, spatially segregated bed material size analysis.

D.3   Volumetric sampling

Volumetric samples extract a pre-defined volume or mass of sediment from the bed. Volumetric samples are three-dimensional and may be taken from various strata of the sediment column or may represent unstratified bulk sediment. However, the two-dimensional properties of prevent a single particle layer of surface sediment from being sampled volumetrically. Unstratified volumetric samples of the bed material can include combined armour and subarmour, or surface and subsurface, sediments sediment sampling. Such samples are useful for providing bed material characterization at-a-site only when the bed material has negligible stratification.

Volumetric bed sampling is easiest in dry river beds or on exposed bed features such as bars, but particle sizes on bars (both surface and the subsurface), tend to be finer than bed material in other parts of the streambed. Therefore, representative sampling that will characterize the river bed of a reach requires sampling all areas of the bed, both wet and dry.

D.3.1   Volumetric sampling depth of unstratified beds

The sampling depth of unstratified deposits does not usually have a lower boundary. This offers the opportunity to take a sample to a sufficient depth to avoid bias against large particle sizes. Diplas and Fripp (1992) and Simons and Sentürk (1992) suggest that volumetric sampling of unstratified sediment should extend to a minimum depth of twice the D_{max}.

D.3.2   Volumetric sampling mass

Samples need to be sufficiently large to gain a representative assessment of the particle size distribution including the largest particles. The sample mass required to obtain representative volumetric samples can be computed by three methods:

• As an empirical function of the D_{max} particle size,
• By computing the number of subsamples required (two-stage approach)

• By analytical means based on an assumed underlying distribution type.

A large number of empirical equations exist in which sample mass is expressed as a function of the Dmax particle size. These equations are simple to apply and there are numerous national standards. Sample-mass recommendations based on the D_{max} particle size do not require assumptions about an underlying frequency distribution type. However, different equations predict widely different sample sizes, sample sizes are generally large, and do not provide information about the relationship between sample mass and error. Therefore, the precision of a sample remains unknown.

Sample-size statistics that assume an underlying normal distribution indicate that a larger sample size is required to accurately describe the distribution tails than the central parts of the distribution. Consequently, a sample size that is sufficiently large to describe the distribution tails will also be sufficient to accurately describe the entire particle-size distribution. The coarse tails of bed-material samples from gravel- and cobble bed streams are comprised of only a few large particles per size class, but they contribute a large proportion of the total sample weight. Consequently, presence or absence of a few large particles influences the percentiles of the coarse tail, and also the central and fine percentiles as well. Therefore, a volumetric sample needs to be sufficiently large that coarse particles are representatively sampled, and sample mass is determined as a function of the D_{max} particle size. Because particle mass is a function of the third power of particle size, sample-size equations for volumetric samples are (usually) a function of the third power of D_{max} (Table D.3).

The D_{max} particle size used for determining the mass of volumetric samples should be the size of the largest particles to be represented in the sample, which depends on the study objective. For example, when determining the D_{50} or another percentile for computations of bedload transport rates in a given streambed, untransportably large particles (e.g., boulders exposed from glacial deposits or supplied from rock fall) should not be included in the sample. However, if the objective is to determine stream bed roughness, untransportably large particles should be included.

When applied to a normally-distributed particle size distribution, a 0.1% criterion for the proportion of the sample mass represented by a D_{max} particle provides a precision of at least $\pm 0.4\varphi$ for all percentiles up to the D_{95}. Estimated sample mass can easily amount to 100s to 1000s of kg in coarse gravel-bed streams, even if the less stringent 1% criterion is applied (Figure D.4).

Table D.3   Example relationships that estimate the required sample mass from D_{max}.

Regression Function	Author, *Criterion*	Equation Number	Sample Mass (kg) for D_{max} of:	
			16 mm	180 mm
Cubic sample-mass equations:				
$m_s = 26,500,000\,D_{max}^3$	De Vries (1970), ISO (1977), *high prec.*	5.37	108	(154,550)
$m_s = 2,775,073\,D_{max}^3$	Ibbeken (1974), *5 D_{max} particles*	5.45	11.4	16,180
$m_s = 2,650,000\,D_{max}^3$	De Vries (1970), ISO (1977), *norm. prec.*	5.38	10.9	(15,450)
$m_s = 1,388,000\,D_{max}^3$	Church et al. (1987), $D_{max} = 0.1\%\,m_s$	5.40	5.7	8,090
$m_s = 1,380,000\,D_{max}^3$	Fripp and Diplas (1993), *400 particles*	5.44	5.7	8,050
$m_s = 460,000\,D_{max}^3$	Diplas and Fripp (1992), *100 particles*	5.43	1.9	2,680
$m_s = 265,000\,D_{max}^3$	De Vries (1970), ISO (1977), *low prec.*	5.39	1.1	(1,550)
$m_s = 138,800\,D_{max}^3$	Church et al. (1987), $D_{max} = 1\%\,m_s$	5.41	(0.60)	810
$m_s = 138,000\,D_{max}^3$	Neumann-Mahlkau (1967), $m_s = 100\,D_n$	5.32	0.57	805
$m_s = 27,751\,D_{max}^3$	Church et al. (1987), $D_{max} = 5\%\,m_s$	5.42	(0.11)	160
$m_s = 13,800\,D_{max}^3$	Neumann-Mahlkau (1967), $m_s = 10\,D_n$	5.33	0.06	80
Non-cubic sample-mass equations:				
$m_s = 5,750\,D_{max}$	Anastasi (1984); Fehr (1987)	5.50	(92)	1030
$m_s = 2,069\,D_{max} - 6.7$	ASTM D75-71	5.46	26	(370)
$m_s = 2,882\,D_{max} - 47.6$	Church et al. (1987), *adjusted*	5.51	1.1	472
$m_s = 2,596\,D_{max}^{1.5}$	ASTM C136-71	5.47	5.2	200
$m_s = 712.4\,D_{max}^{1.43}$	DVWK (1988)	5.48	1.9	(61)
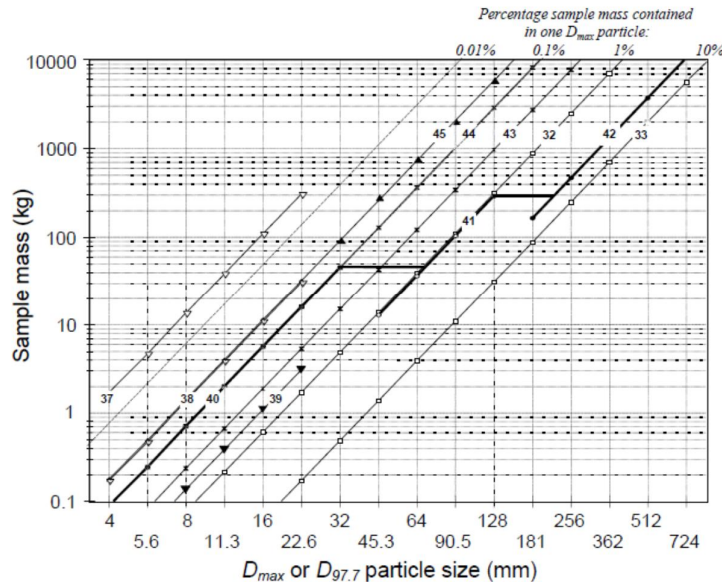
Figure D.4   Sample mass estimates for cobble-gravel samples with varying proportions of the total mass attributable to one D_{max} particle

Figure D.5 illustrates relationships between minimum sample weights and D_{max} proposed by Church et al. (1987). For river beds with D_{max} greater than 32 mm, Church et al (1987) proposed the following equation for the sample mass:

$$m = (2.87 \cdot D_{max} - 44.8) \qquad\qquad (3)$$

where sample mass m is in kg and D_{max} in mm.
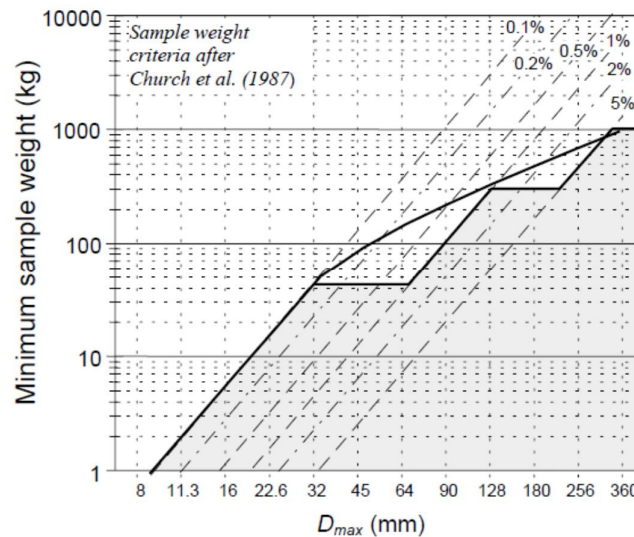
Figure D.5   Minimum sample weight for bed sediments with different D_{max} (Church et al., 1987)

D.4   Spatial sampling schemes

Spatial sampling schemes refer to the spatial patterns by which individual particles (in pebble counts) or groups of particles (in areal or volumetric samples) are taken from the streambed to produce a sample. Sampling schemes affect the outcome of a sample and different sampling schemes may produce different results when used in the same stream reach. One of three main spatial sampling schemes are usually applied:

- *Spatially integrated (= unstratified sampling)* Covers the entire reach with the same sampling pattern, and ignores sedimentary or geomorphological units. A reach averaged bed-material size is obtained

- *Spatially segregated (= stratified sampling)* Distinguishes between geomorphological or sedimentary units and may use a separate sampling pattern for each unit

- *Spatially focused sampling* Focuses on a small area of interest, such as an area near a hydraulic structure, a particular geomorphic unit such as a riffle or sediment patch such as fines deposited in a pool

Statistical analyses of bed-material samples assume that samples are collected at random locations. Randomization of sampling locations is obtained by several sampling patterns (Figure D.6):

- Completely random – samples are collected at random locations within the sampling area;

- Systematic grid – samples are collected at the intersections of a single systematic grid with a random starting point;

- Overlapping grid systems – subsamples are collected at the intersections of several systematic grids that are offset from one another,

- Random within systematic cells – samples are collected at random locations within systematic grid cells that have a random starting point.
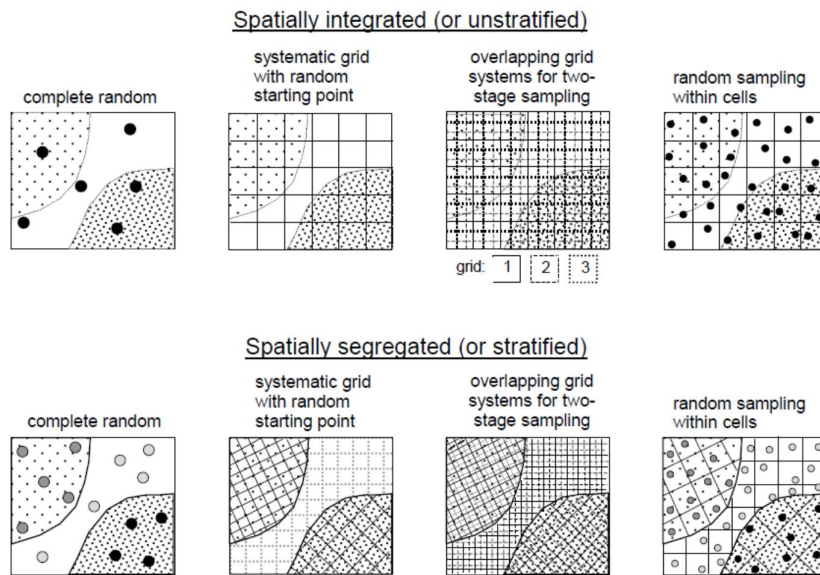
Figure D.6   Spatial sampling designs that may be used to sample river bed material.

D.4.1   Spatially integrated pebble counts

Spatially integrated pebble counts cover the reach evenly with a preset sampling pattern. The resulting particle-size information is reach-averaged, unless a spatially distinct record permits spatial segregation of the data at a later time. Reach-averaged information on bed-material particle size may be used for a variety of purposes which include the computation of reach-averaged bedload transport rates, a comparison of bed-material sizes between reaches, or to detect a change over time when sediment supply to the reach has been altered.

The density of points within a sampling pattern used within a spatially integrated sampling scheme should reflect the spatial variability of bed-material size. For streambeds with relatively homogeneous beds, widely-spaced sampling patterns are appropriate. As the degree of spatial variability of particle sizes over the reach increases,

the sampling must become more closely spaced to ensure that all sedimentary units present are sampled in a representative manner.

The ideal sampling scheme for a reach should reflect the degree of sediment heterogeneity and the ease of sampling (i.e., wadability, ease of particle selection and retrieval). Where a reach has relatively homogenous, well sorted gravel beds and is easily wadable, widely-spaced, random, unsystematic sampling would be appropriate, such as widely-spaced paced transects and unplanned zigzag walks. Where a reach contains, heterogeneous, poorly sorted particles that are difficult to retrieve, a closely-spaced grid pattern should be used. If spatially integrated sampling is the selected sampling scheme for a heterogeneous reach, a tightly-spaced systematic grid pattern that evenly covers the entire sampling reach is required to obtain reach-averaged particle-size information (e.g., Figure D.7). Entire coverage implies that particles from all possible sampling locations are included in the sample. If this is physically impossible (some locations are inaccessible or particles are unretrievable), it is statistically more accurate to make an educated guess about the size class of such particles than to exclude those locations from the sample altogether.
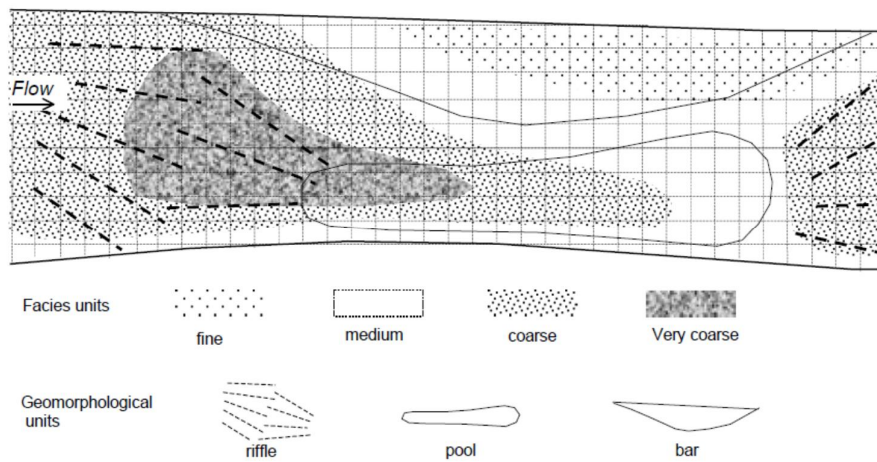
Figure D.7   Sampling grid superimposed on sediment patches of different sediment size and on geomorphological units.

For grid sampling, the grid orientation should be rectangular to ensure that each grid point represents a streambed section of the same size and transects should extend over the entire bankfull width when the sampling objective is to provide a reach-averaged estimate of channel bed conditions. In slightly sinuous reaches, transects can be adjusted to the high flow bed which is usually less sinuous than the low flow bed. In highly meandering reaches consisting of several meander bends the bed should be sampled by a rectangular grid unconnected to stream morphology, if a reach-averaged bed-material particle size is to be obtained from a joint particle-size analysis of all sampled particles. Representative spatially integrated sampling of a morphologically or sedimentologically diverse reach must ensure that a sufficient number of sampling points falls onto each unit to ensure a fair representation. A grid system with about 20 transects is required to

cover the morphological and sedimentary units within a riffle-pool section (from one riffle to the next riffle) in sufficient detail (Figure D.8).
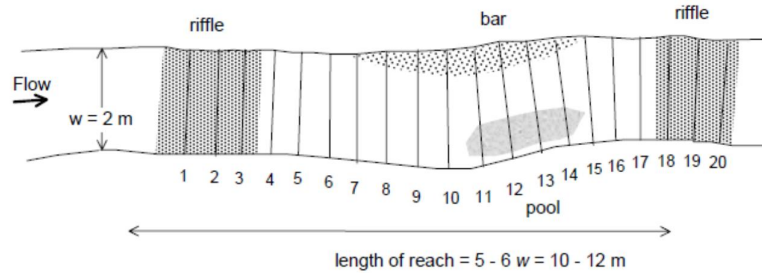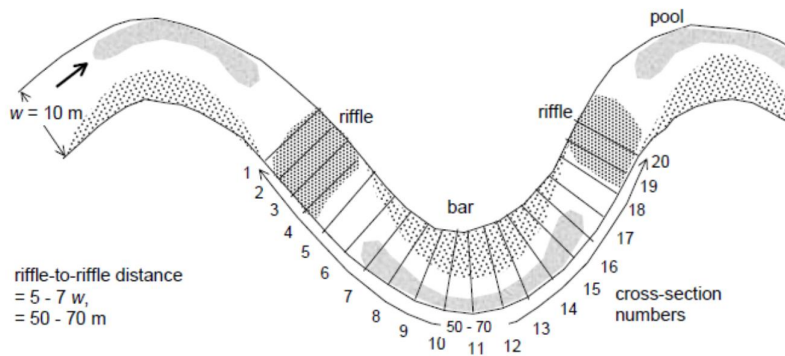

Figure D.8   Sampling grid with 20 transects in low and high sinuosity reaches.

D.4.2   Spatially integrated volumetric sampling

Spatially integrated volumetric sampling is best used for computing the reach-averaged particle size of relatively homogeneous reaches in which the number of sampling locations is relatively low. If heterogeneous reaches are sampled to obtain a reach-averaged particle size, the number of samples needed is relatively high, leading to a large total sample mass.

The most common sampling patterns used for spatially integrated volumetric sampling include random locations and systematic grid points. Random sampling is appropriate for homogeneous streambeds but spatial homogeneity is rare. Sampling at random locations is not recommended for heterogeneous reaches; a better strategy is to cover the reach by a systematic grid and to collect volumetric samples at each grid intersection (Figure D.9). However, systematic sampling will not correctly represent sediment from units that are smaller than the grid size.
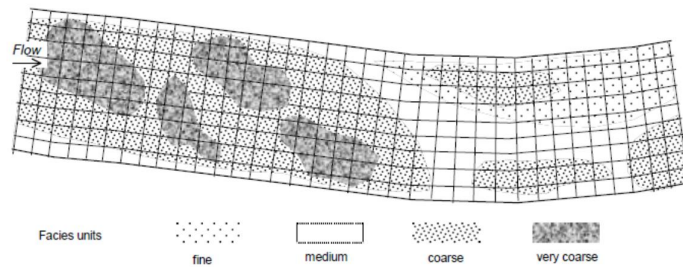
Figure D.9   Grid design for volumetric sampling of a heterogeneous reach

Once the patterns for spatially integrated sampling have been determined, the user needs to determine:

1. The number of points to be sampled in the reach;

2. The mass of sediment to be collected at each sampling location;

3. The total mass of sediment to be collected;

The number of sample points required depends on the degree of spatial variability of the sediments within the reach. Purely statistical criteria may be applied to compute this number when sampling a large area in a dry streambed, and the resulting number of sampling locations may amount to 100 or more. Wolcott and Church (1991) suggested that 100 to 300 samples collected from evenly spaced sampling points may be appropriate for an unbiased particle-size estimate of reach-averaged subsurface sediment in many gravel-bed rivers.

Another aspect to consider when determining the grid size for spatially integrated sampling, is the areal extent of each volumetric sample in relation to the size of the reach. For example, each sample may disturb a streambed area of approximately 0.5 m^2. If such samples were spaced 5 m apart in a stream 10 m wide, and the reach was 50 m long, 20 samples could be collected per reach (a relatively small sample number) but the combined area disturbed by collection of all samples is 2% of the area of reach (a relativey large area of disturbance from an ecological perspective).

Collection of "full-sized" samples at all grid points may be feasible in streams with sand or fine gravel beds, where 1 kg of sediment is an adequate sample size for the D$_{max}$. However, in poorly sorted and / or coarse gravel- or cobble-bed streams, the mass required for a single sample alone can amount to hundreds or thousands of kg, leading to a total sample mass that is impossible to collect. Under these circumstances, the sample mass needs to be reduced but the total mass collected needs to remain statistically meaningful. Reducing the number of grid points is not recommended. Other approaches to reduce the sample mass collected include:

1. Exclusion of the largest particle sizes from the analysis (truncation at the coarse end, acceptable and even recommended if the study focuses on fines);

2. Acceptance of a larger error;

3. Limitation of the analysis to the D_{50} particle-size rather than the entire particle size distribution;

4. Collection of individually small samples (grab samples) that are combined to one composite sample that is then statistically unbiased and "accurate".

In relation to 4, Wolcott and Church (1991) proposed collection of individual small grab samples while maintaining the number of sampling locations. Each grab sample must comprise at least 1% of the total sample mass required for an unbiased sample of the entire reach, and each grab sample must be at least as large as the mass of the largest particle present in the reach (D_{max}) and must be obtained with a sampling device that does not hinder collection of a particle of D_{max} size.

Remote and proximal sensing techniques are currently being developed for mapping the spatial granulometric distribution in deep, non-wadable rivers with heterogeneous sediment beds. The spatial units detected by these methods (i.e. natural radioactivity emissions, echosoundings, bathymetric LiDAR) could help in the determination of sampling locations as well as to infer their dominant grain size (e.g. from the acoustic backscatter). However, these techniques are still in the testing phase and their accuracy still to be quantified in many settings.

D.5   Sampling protocols for REFORM

This section recommends approaches to achieving a reach-averaged particle size distribution.

D.5.1   Surface or volumetric sampling ?

Performing volumetric or surface sampling should be based on the reach type, as follows:

- Sand-bed rivers: volumetric sampling (unstratified).

- Wadable gravel-bed rivers: grid pebble-counts

- Unwadable gravel-bed rivers: unstratified volumetric sampling (unless armoring is of interest)

- In the case of a comparison between a degraded unwadable reach and a restored wadable reach, the same methodology should be applied in the two, i.e. volumetric sampling.

D.5.2   Spatially-integrated or segregated scheme?

For inter-reach comparisons, particularly a comparison between a degraded and a restored reache, the evaluation of a reach-averaged grain size distribution in is most relevant and,therefore, spatially-integrated sampling scheme is suggested.

D.5.3   Random or systematic selection or sampling site?

In (relatively homogenous) sand-bed rivers, random locations for samples can be selected. In (relatively heterogeneous) gravel-bed rivers, use a systematic approach for both surface and volumetric sampling.

D.5.4   Sample size ?

For volumetric sampling, use the method proposed by Church et al (1987), i.e. if $D_{max} > 32$ mm apply equation 3; for smaller D_{max} use equation 5.40 in Table D3.

In sand-bed rivers, the full mass required should be collected at each of 30 sampling sites, selected randomly across the reach. In gravel-bed rivers, the total mass required should be collected as the sum of 100 individual small grab samples, selected systematically across the reach.

For surface sampling, the target should be an error of 10% around the mean diameter (in mm), and the sample size *n* could be roughly estimated by applying equation 1, once the standard deviation is estimated from a pilot study (i.e. a reduced pebble count with sample size of about 30) in the reach, and using *t*=1.96 (large samples). However, a minimum size of 200 pebble counts should be adopted with a grid spacing of at least $2D_{max}$.

D.6   References

Bunte K, Abt SR. 2001. Sampling surface and subsurface particle-size distributions in wadable gravel-and cobble-bed streams for analyses in sediment transport, hydraulics, and streambed monitoring. Gen. Tech. Rep. RMRS-GTR-74. Fort Collins,CO: U.S. Department of Agriculture, Forest Service, Rocky Mountain Research Station. 428 p. Downloadable at: http://www.fs.fed.us/rm/pubs/rmrs_gtr074.html

Church M, McLean DG, Walcott JF. 1987. River bed gravels: sampling and analysis. In: C.R. Thorne, J.C. Bathurst and R.D. Hey (Editors), Sediment Transport in Gravel-Bed Rivers. John Wiley and Sons, Chichester, UK, pp. 43 – 88.

Diplas P, Fripp JB. 1992. Properties of various sediment sampling procedures. Journal of Hydraulic Engineering, 118(7): 955-970.

Leopold LB. 1970. An improved method for size distribution of river bed gravels. Water Resources Research, 22: 125-145.

Rice S, Church M. 1996. Sampling surficial fluvial gravels: the precision of size distribution percentile estimates. Journal of Sedimentary Research, 66(3): 654-665.

Simons DB, Sentürk F. 1992. Sediment Transport Technology. Water and Sediment Dynamics. Water Resources Publications, Littleton, Colorado, 897pp.

Wentworth CK. 1922. A Scale of Grade and Class Terms for Clastic Sediments. The Journal of Geology, 30(5): 377-392.

Wolcott J, Church M. 1991. Strategies for sampling spatially heterogeneous phenomena: the example of river gravels. Journal of Sedimentary Petrology, 61(4): 534-543.

Wolman MG. 1954. A method of sampling coarse river-bed material. Transactions of the American Geophysical Union, 35(6): 951-956.

Annex E: Some Further Information on Classifications of Rivers and Floodplains

Angela Gurnell, Queen Mary University of London

Table E.1   Typical sediment calibre and transport regime associated with different channel configurations, their characteristic geomorphic units and stability (synthesised mainly from Church 2006; Montgomery and Buffington, 1997).

Dominant sediment calibre	Sediment transport regime	Channel morphology[1]	Channel stability
		BEDROCK AND COLLUVIAL CHANNELS	
Bedrock	Very low and variable. Sediment transport is limited by sediment supply.	Predominantly single thread straight or low sinuosity channels that generally occur on steep gradients. These, sediment supply-limited channels exhibit no continuous alluvial bed, but some alluvial material may be stored in scour holes, or behind flow obstructions such as large boulders.	Usually strongly confined and highly stable because of the low erodibility of the bedrock bed and bank material.
Highly variable colluvium	Very low and variable. The shallow flows in these headwater channels have little ability to mobilise sediment.	Predominantly single thread straight or low sinuosity channels small headwater channels at the upper extremities of the stream network that exhibit weak or ephemeral fluvial transport. Sediment delivered from adjacent hillslopes accumulates as colluvial valley fill that forms the channel bed. Therefore, bed sediment size is highly variable and irregular depending upon valley and hillslope gradient and dominant sediment delivery processes (e.g. very coarse sediment and large wood from debris flows or finer mixed sediments from less catastrophic hillslope processes). In steep locations boulder levées, sand splays and abandoned channels are common. In headwaters of gentle gradient channels are poorly defined and relatively featureless.	In very steep headwaters, the channel can be highly unstable as water is diverted around and across very coarse deposits supplied by debris flows. In low gradient headwaters where debris flows are absent, these shallow ephemeral channels are very stable as water drains over relatively fine sediments supplied by gradual mass movement down hillslopes.

Dominant sediment calibre	Sediment transport regime	Channel morphology*1	Channel stability
ALLUVIAL CHANNELS			
Boulder	Bed load dominated. Low total fluvial transport but subject to debris flows.	Predominantly single thread straight or low sinuosity channels, which occur on steep gradients (slope usually >> 3%). Relative roughness^{*2} > 1. Characterized by disorganized coarse bed material consisting mainly of boulders and local exposures of bedrock that split the flow into fast-flowing, turbulent threads (cascades). Small pools that do not span the channel are common, and are often spaced less than a channel width apart.	Stable for long periods with throughput of bed material finer than the large clasts dominating the bed structure. Subject to catastrophic destabilisation during debris flows.
Boulder-Cobble	Bed load dominated. Low total fluvial transport but subject to debris flow.	Predominantly single thread low sinuosity channels that occur on steep gradients (slope usually > 3%). Relative roughness^{*2} > 1. Characterised by a step-pool profile (relative roughness $\geq$ 1; sequence of channel spanning accumulations of boulders and cobbles supporting broken, fast-flowing, turbulent, shallow flow threads and pools that frequently span the channel, are usually lined with finer, cobble-sized, material, and support deeper, slower flowing water that is also often turbulent.	Stable for long periods with throughput of bed material finer than the large clasts dominating the bed structure. Subject to catastrophic destabilisation during debris flows.

Dominant sediment calibre	Sediment transport regime	Channel morphology[1]	Channel stability
Cobble-Gravel	Bedload dominated. Low total transport, but bedload may be less than 10% total load. Bed material is supplied predominantly by bank erosion / failure and fluvial transport from upstream reaches, although debris flows may occur in some locations.	Predominantly single thread, low sinuosity channels but secondary channels are sometimes present. They occur on steep to moderate gradients (slope usually > 1%). relative roughness[2] typically 0.3 to 1.0; w/d > 20; sinuosity low. Typically characterised by a relatively featureless plane bed, composed of predominantly cobble and gravel sized material with occasional boulders or sand patches. Where relative roughness is high, rapids may form. Obstructions (boulders, large wood) may locally forced bar and forced pool formation. Flows tend to be fairly uniform, commonly comprised of glides, runs and occasional rapids.	Relatively stable for extended periods, but floods can induce lateral instability and avulsions, with secondary channels that may be periodically reoccupied and some channels can be destabilised by debris flows.
Gravel	Bed load dominated but often a high suspended load. Bedload typically 1-10% of total load. Bed material is supplied predominantly by bank erosion / failure and fluvial transport from upstream reaches.	Occur on moderate gradients (slope usually > 0.5%); relative roughness[2] typically 0.1 to 1.0; w/d > 40; sinuosity moderate to low. Although dominated by gravel, bed material of varying size in the sand to cobble rangemay be present. Sediments are usually well sorted to reflect the flow pattern and bed morphology. Multi thread channels are characteristically braided where sediment supply is relatively higher and/or slopes are steeper and / or sediment is coarser. Occasional islands are often present. Characterised by numerous bars separating a network of channels. Larger channels usually contain riffle-pools. Single thread channels sinuous / meandering occur where sediment supply is relatively lower and/or slopes are gentler and / or sediment is finer. Characterised by an undulating thalweg reflecting an alternating longitudinal and lateral sequence of pools, riffles and bars. Transitional wandering channels are common, reflecting local changes in slope and/ or sediment supply / calibre.	Wide channels subject to avulsion and frequent channel shifting. Single thread channels subject to chute cutoffs at bends. Braided channels may be highly unstable both laterally and vertically.

Dominant sediment calibre	Sediment transport regime	Channel morphology*1	Channel stability
Sand to fine gravel	Mixed load. Much sediment moves in suspension and bed highly mobile.	Occur on moderate to low gradients (slope typically < 0.5%), Relative roughness*2 typically <0.001; sinuosity variable but generally < 2; w/d < 40. These sand to gravel bed channels are predominantly Single thread sinuous / meandering, characterised by an undulating thalweg reflecting an alternating longitudinal and lateral sequence of pools, riffles and bars. Pronounced point bar and some levée development. Sandy bedforms (ripples, dunes) may also be present. Multi-thread braided channels are also found, often with a significant island extent (i.e. island-braided channels).	Predominantly single thread laterally unstable sinuous channels subject to lateral and/or progressive migration.
Sand bed with fine sand to silt banks	Suspended load.	Occur on low gradients (slope << 0.2%), sinuosity > 1.5, w/d < 20. Predominantly Single thread meandering channels. characterised by high sinuosity and point bar, levée, and cutoff development. Multi-thread anastomosing channels also possible. Vegetation critical in stabilising islands that develop by vertical accretion of fine sediment, minor channel bedform development (e.g. sand ripples)	Single thread, highly sinuous channels show meander loop progression and extension with cutoffs common. Muti-thread anastomosing channels have very stable planform.
Sand to silt bed with silt to silt clay banks often with high organic content	Suspended load.	Occur on very low gradients (slope close to 0%), sinuosity generally > 1.5; w/d < 15. Multi-thread anastomosing channels. Characterised by extensive islands covered by wetland vegetation including peat swamps, often bordered by levées with crevasse channels, crevasse splays, and ponds. Relatively featureless channels apart from vegetation-induced bar and bench development Single thread meandering channels. Characterised by prominent levées.	Occur on very low gradients in unconfined situations. Bed material is very fine, dominated by silt but may also include coarser material, particularly sand. Bed material supplied predominantly by bank erosion / failure and transport from upstream reaches. Sediment supply is abundant relative to transport capacity, which is usually the limiting factor. In humid climates and in the lowest gradient settings, organic material forms a significant part of the bed and bank material.

*1 relative roughness is ratio of 90th percentile grain size to bankfull flow depth

Table E.2 Types of floodplain, based on bankfull flow energy, sediment calibre, level of confinement and forming channel type (after Nanson and Croke, 1992, which gives further details including block diagrams).

Floodplain class	Floodplain type	Floodplain Sediments and Geomorphic Units	1. Environment context, 2. Channel planform type, 3. Bankfull unit stream power ($W\,m^{-2}$)
High energy, non-cohesive floodplains	Confined, coarse textured	*Sediments:* Poorly sorted boulders and gravel with some sand and buried soils *Geomorphic units:* boulder levées, sand / gravel splays; back / abandoned channels, scour holes, usually covered with a thin overbank deposit of fine alluvium.	1. steep confined bedrock valleys and narrow gorges 2. single-thread straight or sinuous 3. >1000
	Confined, vertical accretion	*Sediments:* basal gravels with an overburden of abundant sand with silt. *Geomorphic units:* large levées, deep back channels, scour holes.	1. upland headwater valleys 2. single-thread straight or sinuous 3. 300 - 1000
	Unconfined, vertical accretion, sandy	*Sediments:* predominantly sands with interbedded muds *Geomorphic units:* flat floodplain surface lacking major levées around channels. Channels alternate between wide relatively straight and narrow sinuous states.	1. semi-arid open valleys 2. single-thread to transitional wandering 3. 300 - 600
	Partly confined, cut and fill	*Sediments:* sands, silts and organic sediments *Geomorphic units:* flat floodplain surface with little surface relief around channels that oscillate between shallow sinuous channels and deeply incised flat-bedded gullies.	1. semi-arid alluvial-filled valleys 2. single-thread straight or sinuous 3. ~ 300
Medium energy, non-cohesive	Braided	*Sediments:* gravels with sand and occasional silt usually showing a fining-upwards sequence *Geomorphic units:* undulating floodplain comprised of the aggrading surfaces of abandoned channels, bars, and islands.	1. abundant sediment load (in tectonically and glacially active areas) 2. multi-thread braided 3. 50 – 300
	Wandering, gravel-bed	*Sediments:* gravels, sands, silts and organic sediments *Geomorphic units:* complex undulating floodplains comprised of the aggrading surfaces of features associated with both braided and single thread river floodplains including abandoned channels; point, lateral and medial bars; and islands.	1. abundant sediment load (alternating sedimentation zones in tectonically and glacially active areas) 2. transitional, wandering with possibility of some single-thread and multi-thread anastomosing sections 3. 30 - ~200

Floodplain class	Floodplain type	Floodplain Sediments and Geomorphic Units	1. Environment context, 2. Channel planform type, 3. Bankfull unit stream power (W m-2)
	Sinuous / meandering, lateral migration, non-scrolled	*Sediments:* gravels, sands and silts *Geomorphic units:* gently undulating, smooth floodplain surface, sometimes with abandoned channels.	1. middle to lower valley reaches 2. single-thread sinuous / meandering 3. 10 – 60
	Sinuous / meandering, lateral migration, scrolled	*Sediments:* sands with some gravels *Geomorphic units:* undulating floodplain surface incorporating distinct parallel scrolls or ridges with intervening swales and occasional backswamps in lower lying areas.	1. middle to lower reaches 2. single-thread sinuous / meandering 3. 10 – 60
	Sinuous / meandering, lateral migration, backswamp	*Sediments:* sands, silts and organic sediments *Geomorphic units:* flat to undulating floodplain surface featuring ridge and swale topography close to the active channel with extensive smooth areas of vertically accreted fine sediments often associated with extensive backswamps and ponding on distal areas of the floodplain	1. middle to lower reaches 2. large single-thread sinuous / meandering rivers with insufficient power to rework more than a part of the valley fill 3. 10 – 60
	Partly-confined, sinuous / meandering, lateral migration counterpoint.	*Sediments:* sands, abundant silts and organic sediments *Geomorphic units:* series of parallel ridges arranged upstream of and parallel to tightly curving meander bends, illustrating the downstream migration of the bends. The low areas between the ridges are often poorly drained and so may contain linear wetland areas.	1. middle to lower reaches 2. partly-confined sections of single-thread meandering, forced to reduce their normal curvature because of valley side obstruction 3. 10 – 60
Low energy cohesive	Laterally stable.	*Sediments:* silts, clays and organic material *Geomorphic units:* flat floodplains with low levées, sand splays and sometimes backswamps indicative of poor drainage	1. abundant fine sediment load, middle to lower reaches 2. single-thread straight, sinuous or meandering 3. < 10
	Anastomosing, organic rich.	*Sediments:* abundant silts and clays with some sands and gravels and abundant organic / lacustrine deposits *Geomorphic units:* flat floodplains with extensive islands, often bordered by levées; crevasse-channels and splays, lakes and peat swamps.	1. very low gradient (<0.0002) in humid environments 2. multi-thread anastomosing 3. < 10

Floodplain class	Floodplain type	*Floodplain Sediments and Geomorphic Units*	1. Environment context, 2. Channel planform type, 3. Bankfull unit stream power (W m-2)
	Anastomising, inorganic.	*Sediments:* abundant silts and clays with some sands and gravels and little organic matter *Geomorphic units:* flat floodplains with extensive levees, islands and flood basins, crevasse-channels and splays. Vegetation is relatively sparse although the anastomosing channels are often tree-lined, have low width/depth ratios, transport little sand and are incised into very cohesive mud. The floodplain braid-channels are free of trees, very broad and shallow and may initiate at, terminate at or cross over the anastomosing channels.	1. very low gradient (<0.0002) in semi-arid environments 2. multi-thread anastomosing 3. < 10

References

Church M. 2006. Bed material transport and the morphology of alluvial river channels, Annu. Rev. Earth Planet. Sci. 34, 325-354.

Montgomery DR, Buffington JM. 1997. Channel reach morphology in mountain drainage basins. Geological Society of America Bulletin 109: 596-611.

Nanson GC, Croke JC. 1992. A genetic classification of floodplains. Geomorphology 4(6): 459-486.

Annex F
Sediment Budget: review of definition and principles

A. Latapie, B. Camenen

Irstea, Lyon, France

The estimation of a sediment budget requires the identification of inflow (sources of sediment to the river network / segment / reach under consideration), outflow (sediment discharge at the stream outlet or from the segment / reach under consideration) and storage within the river network or network segment / reach under consideration. This is generally expressed as:

$I = O + \Delta S$

where *I* is input, *O* is output and ΔS change in storage.

A sediment budget is a framework for integrating the various components of sediment transfer within fluvial systems including the sources, transport pathways, sinks / stores and outputs of sediment (Philips, 1991; Walling 1999). Ideally, fluvial sediment budgets should include a quantification of:

- Atmospheric dust deposition / scour

- Soil erosion (rainfall detachment, freeze, overland flow)

- Landslides and other, slower, hillslope sediment processes

- Bank erosion

- Reservoir sedimentation

- Tributary and land drainage inputs

Assembly of the above information is extremely challenging and depends upon integrating information from field survey (forms and processes), remotely-sensed and historical sources, and models (e.g. the USLE -Universal Soil Loss Equation developed by Wischmeier, 1977 - and its successors often underpin estimates of fine sediment delivery to river networks; bed material transport equations are often used to estimate inputs or outputs of sediment from reaches and segments). As a result of this complexity, estimations are often limited to a single component of the sediment budget (Walling and Collins, 2000), such as the transfer of fine sediment, and budget estimates generally only highlight broad scale generalisations of catchment sediment sources and sinks. Nevertheless, in the context of catchment management, estimates of the components of sediment budget components and their change across the spatial units within a catchment and through time, are extremely valuable for supporting understanding of catchment and river function and identifying where and when channel changes may take place. The estimation of the various elements of a sediment budget for different spatial

units can be gained using many of the methods reviewed in sections 5 and 6 of Deliverable 2.1 Part 1. Methods for development of a sediment budget are also described in detail by Reid and Dunne (1996, 2003). A further important consideration is the transit time of sediment in a river, which can be estimated by dividing the long term average input rate by the output rate (Wasson et al., 1998), while typical intermediate storage of sediment in a catchment can be expressed as the ratio of sediment yield at a catchment outlet to the total on-site rates of soil loss within the same time period, which is referred to as the Sediment Delivery Ratio (SDR) (Walling, 1983).

Although too time consuming and expensive to be applied in the context of practical catchment management, it is worth mentioning that a reliable sediment budget, particularly for a relatively small catchment, can be constructed using analysis of fallout radionuclides (Caesium 137, unsupported Lead 210 and Beryllium 7). The methodology comprising estimating residence time in rivers using the mass balance of contaminants. For example, Wallbrink et al. (1998) used ^{137}Cs and ^{210}Pb, to determine sources and transit times of suspended sediment in the Murrumbidgee river (Australia). However, even this type of approach is most effective when it is combined with other approaches, as illustrated by Walling et al. (2006) in their evaluations of fine-grained sediment budgets for two catchments in southern England.

References

Philips JD. 1991. Fluvial sediment budgets in the North Carolina piedmont. Geomorphology 4, 231-241.

Reid LM, Dunne T. 1996.. Rapid evaluation of sediment budgets. Catena, Verlag, GMBH, Reiskirchen, Germany.

Reid LM, Dunne T. 2003. Sediment budgets as an organizing framework in fluvial geomorphology. In Kondolf GM, Piégay H. (Eds.) Tools in Fluvial Geomorphology, 463 –500, John Wiley, Hoboken N. J.

Walling DE. 1983. The sediment delivery problem. Journal of Hydrology, 65, 209–237.

Walling DE. 1999. Linking land use, erosion and sediment yields in river basins. In Garnier J, Mouchel JM. (Eds.) Man and River Systems. Kluwer Academic Publishers, Netherlands, 223-240.

Walling DE, Collins AL, Jones PA, Leeks GJL, Old G. 2006. Establishing fine-grained sediment budgets for the Pang and Lambourn LOCAR catchments, UK. Journal of Hydrology, 330: 126-141.

Walling DE, Collins AL. 2000. Integrated assessment of catchment sediment budgets: a technical manual. Framework of UK Department for International Development Research Project R6868, University of Exeter. 168 pp.

Wallbrink PJ, Murray AS, Olley JM, Olive LJ. 1998. Determining sources and transit times of suspended sediment in the Murrumbidgee River, New South Wales, Australia, using fallout 137Cs and 210Pb. Water Resources Research 34 (4), 879-887.

Wasson RJ, Mazari RK, Starr B, Clifton G. 1998. The recent history of erosion and sedimentation on the Southern Tablelands of southeastern Australia: sediment flux dominated by channel incision. Geomorphology, 24: 291-308.

Wischmeier WH. 1977. Soil erodibility by rainfall and runoff. In Toy TJ. (Ed.), Erosion; Research Techniques, Erodibility and Sediment Delivery. Geo Abstr. Ltd., Norwich, United Kingdom, pp. 45–56.

Annex G
Threshold Conditions for predicting Channel Patterns

H. Habersack, B. Blamauer

University of Natural Resources and Life Sciences (BOKU), Austria

This section gives an overview of a set of threshold conditions which were developed to predict the occurrence of various river bed forms, and can be used to separate braiding channel patterns from meandering ones. Most of the thresholds were derived by observations of natural rivers or were derived empirically from flume studies.

G.1   Threshold conditions

Threshold conditions can be classified into four groups, which are discussed below:

- Thresholds based on discharge, slope and bed material size
- Specific stream power as a discriminator
- Non-dimensional (empirical) criteria, and
- Theoretical stability analysis

G.1.1 Thresholds based on discharge, slope and bed material size

The threshold condition based on discharge Q, slope S and bed material size D was first proposed by Leopold and Wolman (1957) and Lane (1957) in the form of:

$$S = aQ^{-b}$$

Where a and b are empirically derived parameters, S is the channel slope and the mean discharge (Lane, 1957) or the bankfull discharge (Leopold and Wolman, 1957) was used for the discharge (Q). Mosley (1981) adapted the equation by using the valley slope instead of channel slope, and by using the mean annual flood. Another adjustment was carried out by Henderson (1963), who recognised the importance of bed material calibre and introduced it as a parameter, yielding the following equation:

$$S = aQ^{-b}D^{c}$$

These equations are based on the assumption that at equal discharge braiding occurs at higher slopes than meandering (Figure G.1).
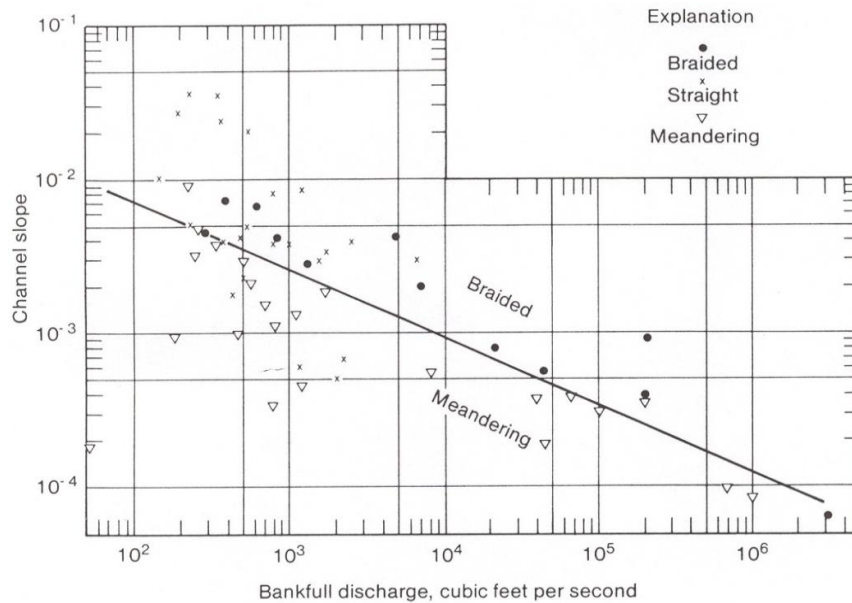
Figure G.1 : Empirical threshold condition based on channel slope and bankfull discharge (Leopold and Wolman, 1957)

G.1.2 Specific stream power as discriminator

Another threshold condition is based on specific stream power. The background to this was the introduction of the relative shear stress as a physical basis for the threshold (Begin, 1981). Enhancements of this relationship yielded the specific stream power (ω), which can be calculated as product of mean bed shear stress and mean flow velocity, as an additional parameter in the derivation of the threshold condition for channel patterns.

A general form of this relation can be given as:

$$\varpi \cong \left(\frac{\gamma}{a}\right) Q^{1-b} S$$

Where γ is the specific weight of the fluid, and a and b are empirically defined parameters. Examples for the application of specific stream power as discriminator can be found in Bray (1982) and Van den Berg (1995).

G.1.3 Non-dimensional (empirical) criteria

Different dimensionless combinations of parameters were used to predict the occurrence of different bed forms. Some examples of non-dimensional parameters are:

- the "flow intensity" – the ratio between the actual (v^*) and critical shear velocity (v^*_c) for bedload movement $v^* v^{*-1}_c$ (e.g. Ikeda, 1973; Ikeda, 1975)
- the "channel form index" – WSd^{-1}, where W is the channel width, S is channel slope and d is mean flow depth (e.g. Sukegawa, 1972)
- the "relative width" – the width to depth ratio Wd^{-1} (e.g. Muramoto and Fujita, 1978)

- or the "relative roughness" – flow depth to grain size (*D*) ratio dD^{-1} (e.g. Muramoto and Fujita, 1978)

Some authors used combinations of non-dimensional parameters for separating meandering from braided river channels. Ikeda (1973; 1975) for example combined the flow intensity with the channel form index to produce the following equation:

$$\frac{v^*}{v_c^*} = 1,4\left(\frac{WS_c}{d}\right)^{0,333}$$

And Muramoto and Fujita (1978) combined the relative width with the relative roughness to propose the following expression:

$$6,7 = \frac{\left(\dfrac{W}{D}\right)^{\frac{2}{3}}}{\dfrac{d}{D}}$$

G.1.4 Theoretical stability analysis

In theoretical stability analysis, parameters which are physical based – often derived from turbulence related processes – are introduced to the geometric data and thresholds are established. Parker (1976) for example, combined the channel form index (WSd^{-1}) with the Froude number (*Fr*) to classify bedforms and channel patterns. The derived equation is given below:

$$\frac{S_c}{Fr} \approx \frac{d}{W}$$

Other authors have applied the dimensionless bed shear stress (e.g. Fredsoe, 1978) or the Darcy Weisbach friction factor (e.g. Bridge, 1993).

A very often cited theoretical stability analysis was derived from Da Silva (1991). She developed a threshold system based on the width to depth ratio and the relative roughness to separate different bed forms (Figure G.1). The diagram representing the boundaries between the different existing regions is shown in Figure G.2. The values for the limits were derived from experiments.

The upper boundary – a discriminator between alternate (single row bars) and multiple bars (2, 3, and n-row bars) – is given as:

$$\frac{W}{d} = 24,5\left(\frac{d}{D}\right)^{\frac{1}{3}} \text{ for } dD^{-1} < 100, \text{ and } \frac{W}{d} = 120 \text{ for } dD^{-1} > 100$$

And the lower boundary – a discriminator between alternate bars and dunes / antidunes – is given as:
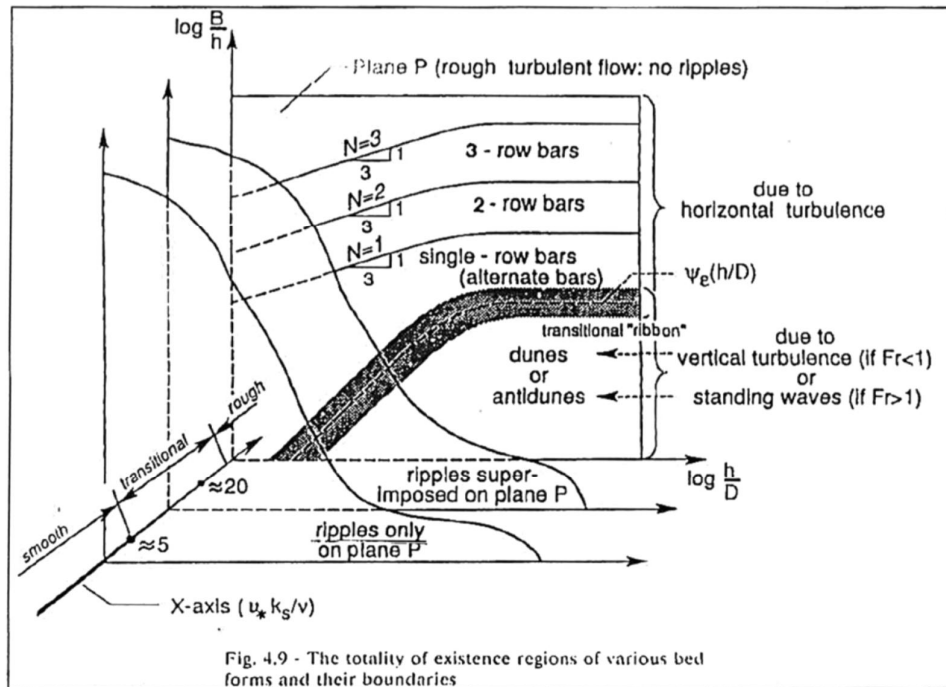
Figure G.1 Regions of various bed forms and their boundaries (Da Silva, 1991).
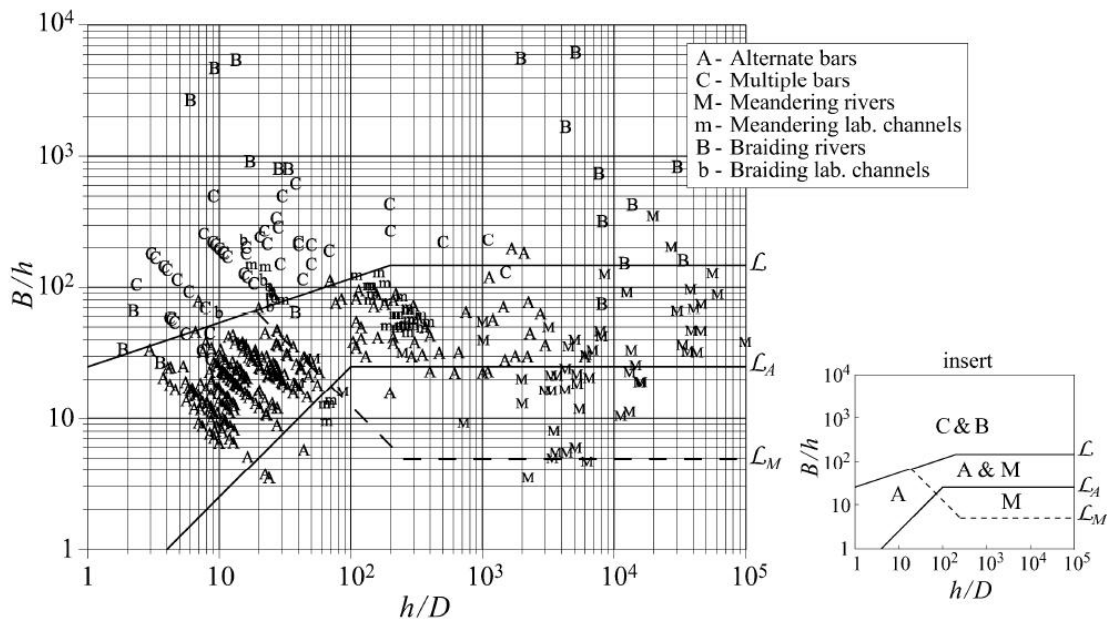
Figure G.2 The (B/h; h/D)-plan (Yalin and Da Silva, 2001)
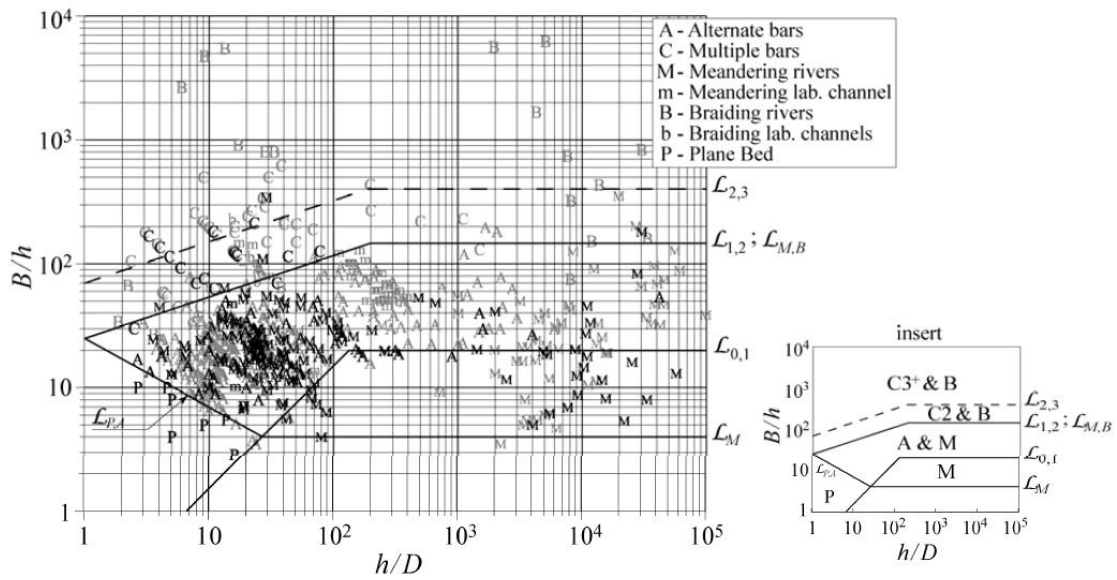
Figure 12   Revised version of the $(B/h; h/D)$-plan

Figure G.3 Revised version of the (B/h; h/D)-plan (Ahmari and Da Silva, 2011).

$$\frac{W}{d} = 0.25\left(\frac{d}{D}\right)^{\frac{1}{3}} \text{ for } dD^{-1} < 100, \text{ and } \frac{W}{d} = 25 \text{ for } dD^{-1} > 100$$

However, the boundaries between the different regions should not be interpreted as abrupt thresholds; they should rather be interpreted as gradual transitions from one bed form to another one (Ferguson, 1987).

The structure of the turbulence can only be affected by the channel geometry and roughness (Da Silva, 1991). Horizontal turbulence, which becomes more important with increasing width or width to depth ratio (Wd^{-1}; B/h in Figure G.1), initiates the formation of bars, whereas vertical turbulence and standing waves are responsible for the creation of dunes or antidunes. According to Yalin and Da Silva (2001) the revision illustrated in Figure G.3 is recommended. A further improvement is given by Ahmari and Ferreira Da Silva (2011). The relevant discriminating equations are given below.

For L$_{1,2}$:   If $\dfrac{h}{D} \leq 200$,   then $\dfrac{B}{h_{1,2}} = 25\left(\dfrac{h}{D}\right)^{\frac{1}{3}}$

           If $\dfrac{h}{D} \geq 200$,   then $\dfrac{B}{h_{1,2}} = 146(\approx 150)$

For L$_{p,A;\,0,1}$:   If $\dfrac{h}{D} \leq 25$, t   hen $\dfrac{B}{h_{0,1}} = 25\left(\dfrac{h}{D}\right)^{-0.55}$

$$If \approx 25 < \frac{h}{D} \leq 130, \quad \text{then} \quad \frac{B}{h_{0,1}} = \frac{2}{13}\left(\frac{h}{D}\right)$$

$$If \frac{h}{D} \geq 130, \quad \text{then} \quad \frac{B}{h_{0,1}} = 20$$

Crosato and Mosselman (2009) developed another method which can be used to distinguish between different planforms based on the number of stable bars in a river cross section. This method relies on the width to depth ratio, longitudinal slope, bed roughness and sediment characteristics at bankfull condition. The number of calculated bar/s per cross section indicates the channel pattern in the following way: meandering ≤ 1.5 bars, intermediate between 1.5 and 2.5 bars, and braiding ≥ 2.5 bars.

G.2   Application and testing of different approaches

In a masters thesis (Speckle, 2000), the performance of the different approaches were tested when applied to different rivers and the following conclusions were drawn:

- A classification based only on discharge and slope (e.g. Lane, 1957; Leopold and Wolman, 1957) cannot be performed with data sets originating from different environments and including various sizes. The introduction of the grain size (e.g. Henderson, 1963) might improve the classification.
- The stream power or specific stream power showed only a weak relation to channel pattern – although the rivers plot in groups according to their channel pattern;
- Classification systems based on non-dimensional parameters or theoretical stability analysis performed better. The width to depth ratio seemed to be a good indicator for delineation of channel patterns.
- Beside geometric data and grain size, the introduction of hydraulic parameters improved the classification of different bed forms.

G.3   References

Ahmari H. Da Silva AMF. 2011. Regions of bars, meandering and braiding in da Silva and Yalins plan. Journal of Hydraulic Research 46, 718-727.

Begin ZB. 1981. The relationship between flow-shear stress and stream pattern. Journal of Hydrology, 52, 307-19.

Bray DI. 1982. Regime equations for gravel-bed rivers. In: Hey, R. D., Bathurst, J. C. & Thorne, C. R. (eds.) Gravel Bed Rivers: Fluvial Processes, Engineering and Management. Wiley-Interscience Publications.

Bridge JS. 1993. The interaction between channel geometry, water flow, sediment transport and deposition in braided rivers In: Best, J. L. & Bristow, C. S. (eds.) Braided Rivers. London, UK: Geographical Society, Special Publications.

Crosato A, Mosselman E. 2009: Simple physics-based predictor for the number of river bars and the transition between meandering and braiding. Water Resour. Res., 45, W03424.

Da Silva AMF. 1991. Alternate Bars and Related Alluvial Processes. Master thesis, Queen´s University Kingston.

Ferguson R. 1987. Hydraulic and sedimentary controls of channel pattern. In: Richards, K. (ed.) River Channels. Oxford: Blackwell.

Fredsoe J. 1978. Meandering and braiding of rivers. J. Fluid Mech., 84, 609-624.

Henderson F M. 1963. Stability of alluvial channels. Transactions of the ASCE, 128, 657-686.

Ikeda H. 1973. A study of the formation of sand bars in an experimental flume. Geog. Rev. Japan, 46, 435-52.

Ikeda H. 1975. On the bed configuration in alluvial channels; their types and condition of formation with reference to bars. Geog. Rev. Japan, 48, 712-30.

Lane EW. 1957. A study of the shape of channels formed by natural streams flowing in erodible material. Omaha, NB: Tech. rep., U.S. Army Eng. Div.

Leopold LB, Wolman MG. 1957. River Channel Patterns; Braided, Meandering and Straigth. Prof. Pap. 282-B. U.S. Geological Survey, Washington, DC.

Mosley MP. 1981. Semi-determinate hydraulic geometry of river channels, South Island, New Zealand. Earth Surface Processes and Landforms, 6, 127-37.

Muramoto Y, Fujita Y. 1978. The Classification of MesoScale River Bed Configuration and the Criterion of Its Formation. Japan Soc. Civ. Eng. (in Japanese), 207, 42-47.

Parker G. 1976. On the cause and characteristic scale of meandering and braiding in rivers. Journal of Fluid Mechanics, 76, 457-480.

Speckle M. 2000. Observation on New Zealand´s River Morphology Classification, Characteristics. Master Thesis, University of Natural Resources and Life Sciences.

Van den Berg JH. 1995. Prediction of alluvial channel pattern of perennial rivers. Geomorphology, 12, 259-279.

Yalin MS, Da Silva AMF. 2001. Fluvial Processes, Delft, The Netherlands.

Annex H
Sediment Transport Formulae

A. Latapie, B. Camenen

Irstea, Lyon, France

This section gives an overview of semi-empirical sediment transport formulae that are used in numerical models or classically applied using measured field data.

H.1   Generalities

Estimation of sediment transport is generally calculated using empirical formulae. Numerous equations have been derived over the years expressing the sediment transport capacity that is the maximum amount of sediment that is likely to be transported for the slope and discharge conditions considered. The formulae are based on the assumptions that there is no sediment deficit and the river bed is active (not paved).

First, the dominant mode of sediment transport needs to be determined; the sediment load is transported in various ways (even if these distinctions are to some extent arbitrary):

a) Bed load
b) Intermittent suspension (saltation) load
c) Suspended load
d) Wash load
e) Dissolved load

In river management, only suspended load and bed load are generally considered. Suspended sediment is supported in the water column by upwardly directed turbulent water motion but still remains closely related to local hydro-sedimentary conditions (in contrast to wash load, which mainly depends on the catchment input). Such material (mainly sand) may travel a long way before being deposited. Bed load progresses by sliding, rolling or bouncing over the river bed, its weight remaining generally supported by the bed. Such material (sand and coarser) is apt to travel only a short distance in one movement.

The dominant mode of sediment transport can be evaluated by determining the Rouse number (R_o) defined as:

$$R_o = \frac{w_s}{\kappa \, u_*}$$

where w_s is the settling velocity, κ is the Von Karman's constant ($\kappa = 0.4$) and u_* is the shear velocity.

If $R_o > 2.5$ mode is bed load

If $0.8 < R_o < 2.5$ mode is bed load and suspended load

If $R_o < 0.8$ mode is suspended load

H.2 Sediment transport formulae

Once the mode of sediment transport is defined, a formula can be selected. Table H.1 provides details on the classic formulae with information on the data required and the validity. It is important to note that these formulae are often applied using section-averaged parameters (water depth, velocity, bed shear stress, which are output from 1D models) or even using rough estimations of parameters (e.g. bed slope instead of the energy slope, water depth instead of hydraulic radius). These assumptions may yield additional uncertainties (Camenen et al., 2011).

Table H.1 : Details of some classic transport formulae (adapted from Malavoi et al., 2011).

Transport mode	Formula	Data required	Validity
Bed load	Meyer-Peter and Müller (1948)	d_{50}, J, K, H	Laboratory $0.0004 < S < 0.25$ $0.4 < d_i < 29$ mm $\tau^* < 0.25$
Bed load and suspended load	Engelund and Hansen (1967)	U, R_h, d_{50}, J, K	Laboratory $S < 0.019$ $0.19 < d_i < 0.93$ mm $0.7 < \tau^* < 6$
Bed load and suspended load	Bagnold (1966)	R_h, d_{50}, J, K	Laboratory $0.001 < S < 0.096$ $0.18 < d_i < 16$ mm $0.21 < \tau^* < 8.7$
Bed load and suspended load	Van Rijn (1984)	H, R_h, d_{50}, J, K	Lab. and field $S < 0.005$ $0.1 < d_i < 2$ mm $\tau^* < 6$
Bed load	Rickenmann (1991)	d_{30}, d_{50}, d_{90}, J, U, H	Lab. and field $0.001 < S < 0.2$ $0.4 < d_i < 29$ mm $0.1 < \tau^* < 3.3$
Bed load	Camenen and Larson (2005)	d_{50}, J, K, H	Lab. and field $S < 0.2$ $0.1 < d < 100$ mm
Suspended load	Camenen and Larson (2008)	d_{50}, J, K, U, H	Lab. and field $S < 0.2$ $0.1 < d_i < 1$ mm

with :

A	Wetted area	(m²)
di	Grain size diameter (indice I indicate percent finer than in percent)	(m)
f	Friction factor: $f = (2gSh)/U^2$	(-)
g	Acceleration due to gravity ($g = 9.81$ m/s²)	(m/s²)
q_b	Unit bedload discharge	(kg/s/m)
Fr	Froude number: $Fr = U/(gH)^{1/2}$	(-)
H	Water depth	(m)

J	Energy slope	(m/m)
K	Bed roughness: $K = U/(J^{1/2}R_h^{2/3})$	(m$^{1/3}$/s)
K_p	Particle roughness: $K_p = 21/d_{50}^{1/6}$	(m$^{1/3}$/s)
W	Average channel width	(m)
Q	Flow Discharge	(m^3/s)
Q_b	Total bedload discharge	(kg/s)
Q_s	Volumetric sediment discharge	
R_h	Hydraulic radius	(-)
S	Bed slope	(m/m)
U	Average flow velocity	(m/s)
$u*$	Shear or friction velocity: $u* = \sqrt{(\tau_b/\rho)}$	(-)
w_s	Settling or fall velocity	(m/s)
ρ_w	Density of water ($\rho = 1000$ kg/m^3)	(kg/m^3)
ρ_S	Density of sediment ($\rho_s = 2650$ kg/m^3)	(kg/m^3)
γ	Density of water	(N/m^3)
γ_s	Density of sediment particles	(N/m^3)
τ_b	Average bed shear stress $\tau_b = \rho g H J$	(N/m²)
τ_{eff}	Effective bed shear stress $\tau_{eff} = \tau (K/K_p)^{(3/2)}$	(N/m²)
$\tau*$ (or θ)	Shields parameter	(-)
$\tau*_{cr}$ (or θ_{cr})	Critical shield parameter	(-)
ω	Specific stream power: $\omega = \Omega/W \sim \tau U$	(W/m²)
Ω	Total stream power	(W/m)
ν	Kinematic viscosity (1E-6)	(m²/s)

Meyer Peter and Muller (1948):

$$q_S^{cap} = 8\,(\tau_{eff} - 0.047)^{3/2}\,\sqrt{\Delta g d_{50^3}}$$

with $\quad q_s^{cap}\quad$ the sediment transport capacity (kg/ms)

$\qquad \tau*_{eff}\quad$ the effective bed shear stress

Engelund and Hansen (1967):

$$q_s^{cap} = K\,\frac{0.05\,U^2\,R_h^{3/2}\,J^{3/2}}{\Delta\,d_{50}\,\sqrt{g}}$$

Bagnold (1966)

$$q_T = K\,\rho_s\,R_{h5/3}\,J^{3/2}\left(0.17 + 0.01\,K\,R_{h2/3}\,J^{1/2}\,w_s\right)$$

with $\quad w_s\quad$ the settling velocity

Van Rijn (1984)

$$q_T = 0.053\,\sqrt{\Delta g d_{50}^3}\,\frac{T_0^{2.1}}{d_*^{0.3}} + c_a\,F_h\,U$$

with $\quad d_* = d_{50}\left(\dfrac{\Delta g}{v^2}\right)^{1/3}$, $\Delta = (s\text{-}1)$, $s = \rho_S/\rho_w$ the relative sediment density ($s \approx 2.65$),

$$T_0 = \frac{\tau' - \tau_{cr}}{\tau_{cr}}$$

c_a the reference concentration and F_h a correction factor for suspended load.

Rickenman (1991)

$$q_s^{cap} = 3.1 \sqrt{g\, d_{50}^3}\left(\frac{d_{90}}{d_{30}}\right)^{0.2} \tau^{*\ 0.5}\ (\ \tau^* - \tau^*_{c}\ )\, F_r^{1.1}$$

Camenen and Larson (2005):

$$q_{Sb}^{cap} = 12\, \tau^{*\ 3/2}_{eff}\ \exp\!\left(-4.5\frac{\tau^*_{cr}}{\tau^*_{eff}}\right)\sqrt{\Delta g d_{50}^3}$$

with $\quad q_{sb}{}^{cap}$ the sediment bedload transport capacity (kg/ms)

$\quad \tau^*_{eff}$ the effective dimensionless bed shear stress (or Shields parameter)

Camenen and Larson (2008):

$$q_{Ss}^{cap} = U c_R\, \frac{\varepsilon}{w_s}\left[1 - \exp\!\left(\frac{w_s h}{\varepsilon}\right)\right]$$

with $\quad q_{ss}{}^{cap}$ the sediment suspended load transport capacity (kg/ms),

$\quad U$ the depth averaged-current velocity (m/s), h the water depth (m),

$\quad c_R$ the reference concentration (assuming an exponential profile for the concentration):

$$c_R = 1.5 \times 10^{-3} \exp\!\left(-0.2 d_*\right)\tau^*_{eff}\, \exp\!\left(-4.5\frac{\tau^*_{cr}}{\tau^*_{eff}}\right)$$

$\quad \varepsilon$ the sediment diffusivity (m^2/s):

$$\varepsilon = \frac{\sigma \kappa}{6} u^* h$$

with $\quad \sigma \approx 1$ the Schmidt number.

H.3 Important parameters to estimate

H.3.1 Critical Shields parameter and critical stream power

The Shields parameter τ^* or θ (Shields 1936) is used to calculate the initiation of motion of sediment.

$$\tau^* = \frac{\tau}{g\,(\rho s - \rho)\,d_{50}}$$

Based on laboratory results, Shields established a curve giving a critical value of τ_c^* above which sediment moves. Numerous values have been suggested for τ_c^*, however, a consensus seems to have emerged associating variation in this parameter with the slope (Mueller, 2005; Lamb et al, 2008; Recking, 2009; Camenen, 2011).

Soulsby (1997) suggested a simple fit for the Shields curve:

$$\tau_{cr} = \tau^*\,g\,(\rho_s - \rho_w)\,d_{50}$$
$$\tau^* = \frac{0.30}{1 + 1.2\,D^*} + 0.055\ (1 - \exp(-0.02\,D^*))$$
$$D^* = d_{50}\,[\Delta g / \upsilon^2]^{1/3}$$

with υ the kinematic viscosity of water ($\upsilon = 1.0\times10^{-6}\,\text{m}^2/\text{s}$ at 20°C).

The critical stream power can be estimated using the equation derived by Bagnold (1980):

$$\omega_{cr} = 290\ d_{50}^{3/2}\ \log_{10}\left(\frac{12\,H}{d_{50}}\right)$$

Recently Parker et al. (2011) suggested a simpler estimation for ω_{cr}:

$$\omega_{cr} = 0.1\rho_w g(s-1)\sqrt{(s-1)gD_{50}^3}$$

As shown by Camenen (2012), both τ_c^* and ω_{cr} are closely related. The relative flow depth at the inception of movement $(R_h/D)_{cr}$ (which can be estimated as a function of the bed slope S) is the main term that differentiates the two parameters.

H.3.2 Settling velocity

The settling velocity w_s may be computed using the following formulae:

The Stocke's law for $d_{50} < 0.1$ mm :
$$w_s = \frac{g\,\dfrac{\rho_s - \rho_w}{\rho_w}\,d_{50}^2}{18\,\upsilon}$$

The Zanke (1977) formula for 0.1 mm $< d_{50} <$ 1 mm:

$$w_s = 10\ \frac{\upsilon}{d_{50}}\left(\sqrt{1 + 0.01\,g\,\frac{\rho_s - \rho_w}{\rho_w}\,d_{50}^3}\ - 1\right)$$

The Van Rijn (1984) formula for $d_{50} > 1$ mm :
$$w_s = 1.1\ \sqrt{g\,\frac{\rho_s - \rho_w}{\rho_w}\,d_{50}}$$

Soulsby and Whitehouse (1997) and Camenen (2007) suggested some formulae that are valid for all grain sizes (non-cohesive sediments).

H.4   References

Bagnold RA. 1966. An approach of sediment transport model from general physics US Geol. Survey Prof. Paper, 422-I: 37 pp.

Bagnold RA. 1980. An empirical correlation of bedload transport rates in flumes and natural rivers. In: Thorne CR, MacArthur RC, Bradley JB. (Eds.), The Physics of Sediment Transport by Wind and Water. American Society of Civil Engineers, New York, pp. 323-345.

Camenen B. 2007. A simple formula for the settling velocity of particles. J. of Hydraulic Eng. 133(2): 229-233.

Camenen B. 2012. Discussion of "Understanding the influence of slope on the threshold of coarse grain motion: Revisiting critical stream power" by C. Parker, N.J. Clifford, and C.R. Thorne, Geomorphology 126: 51-65.

Camenen B, Holubova K, Lukac M, Le Coz J, Paquier A. 2011. Assessment of the methods using 1D modelling for computing bedload transport in a large river: the Danube River in Slovakia. Journal of Hydraulic Engineering 137(10): 1190-1199.

Camenen B, Larson M. 2005. A bed-load transport formula for the nearshore, Estuarine Coastal and Shelf Science, 63: 249-260.

Camenen B, Larson M. 2008. A suspended load sediment transport formula for the nearshore. Journal of Coastal Research, 24(3): 615-627.

Engelund F, Hansen E. 1967. A Monograph on Sediment Transport in Alluvial Streams, Technical Press.

Lamb MP, Dietrich WE, Venditti J-G. 2008. Is the critical Shields stress for incipient sediment motion dependent on channel-bed slope? J. Geophys. Res. 113: F02008.

Malavoi JR, Garnier CC, Landon N, Recking A, Baran Ph. 2011. Eléments de connaissance pour la gestion du transport solide en rivière. Guide Onema. (in French)

Meyer Peter E, Müller R. 1948. Formulas for bed-load transport. Proceedings of the 2nd IAHR congress, Stockholm, 39-64.

Mueller ER, Pitlick J, Nelson JM. 2005. Variation in the reference Shields stress for bed load transport in gravel-bed streams and rivers. Water Resources Research, 41: W04006 (1-10).

Recking A. 2009. Theoretical development on the effects of changing flow hydraulics on incipient bedload motion. Water Resources Research 45: W04401, 1-16

Rickenmann, D., 1991. Hyperconcentrated flow and sediment transport at steep slopes J. Hydraulic Eng. 117: 1419-1439.

Shields A. 1936. Anwendung der Ahnlichkeits-mechanik und der turbulenzforschung auf die geshiebebewegung [Application of similarity principles and turbulence research to bed-load movement]. Mitteilungen der Preussischen Versuchsanstalt für Wasserbau und Schiffbau, Heft 26, Berlin.(in German)

Soulsby RL. 1997. Dynamics of marine sands, a manual for practical applications Thomas Telford.

Soulsby RL, Whitehouse RJSW. 1997b. Threshold of sediment motion in coastal environment. Proc. Pacific Coasts and Ports'97 Conf., University of Canterbury, pp. 149-154.

Van Rijn LC. 1984. Sediment transport, part I: bed load transport. Journal of Hydraulic Engineering 110(10): 1431-1456 and Sediment transport, part II: suspended load transport. Journal of Hydraulic Engineering 110(11): 1613-1641.

Zanke U. 1977. Computation of the settling velocity of sediments Mitteilung des Franzius-Instituts für Wasserbau. (in German)

Annex I
Models tested at Catchment Case Study Sites

Annex I1
Network-scale sediment budgeting using the Sediment Impact Analysis Method (SIAM): Application to the lowland River Frome

Robert C. Grabowski, Angela Gurnell

School of Geography, Queen Mary University of London, London, UK

Summary

A 1-D sediment continuity model was used to explore network-scale spatial patterns in bedload transport within the River Frome (Dorset, UK). The modelling work supports the hydromorphological assessment of the lowland, gravel-bed river as presented in the catchment case study annexes (Deliverable 2.1 Part 3). Information on the channel network, channel cross-sections, river flows, bed sediment size and sediment sources outside the channel were input into the HEC-RAS modelling environment and sediment budgets were calculated using the Sediment Impact Analysis Methods (SIAM). SIAM is best used to explore general patterns in aggradation and degradation at a network scale, which can help to assess the potential impacts of different management scenarios on sediment erosion or deposition within the channel. The outcomes of the modelling show that sediment transport potentials are low for coarse sediment in the entire main stem of the River Frome (Segments 2-6), and delivery of sand and gravel to the river would result in aggradation. These results are supported by field observations of algae-covered, compacted gravels and colmation or smothering of the gravel bed by silt and sand in many reaches.

I1.1 Introduction

Sediment transport is a fundamental hydromorphological process that controls the forms and processes occurring within the river channel and floodplain. Alterations in natural sediment delivery to and transport within the channel can lead to changes in bed levels, channel pattern, erosion / migration rates, and the presence and type of geomorphic features within the channel and floodplain, amongst others.

Where they exist, monitoring data for suspended sediment and bedload are vital datasets to support the hydromorphological assessment of a river. Whilst suspended sediment is frequently measured as part of water quality monitoring, bedload transport is more difficult to quantify and is only monitored in areas with significant coarse sediment management problems (e.g. Alpine regions). In many rivers, the only way to assess bedload sediment transport is through the use of hydraulic and sediment transport models. In this paper, we present a case study application of a tool developed to quantify bedload transport, and which allows for the formulation of network-scale sediment budgets that can be used to explore the impacts of management scenarios on the net loss or gain of sediment within the river network.

I 1.2   What is SIAM?

The Sediment Impact Assessment Method (SIAM) is a tool developed by the US Army Corps of Engineers Research and Development Center and Colorado State University. It was designed to evaluate reach-scale transport processes within a catchment and to function as a quick screening tool to assess the potential impacts of alternative sediment management options on downstream reaches. It is freely available online as part of the 1-D modelling software HEC-RAS[2].

SIAM generates a simple sediment budget that identifies network-scale patterns in sediment accumulation or loss within the channel. It is a 1-D sediment continuity model based on reach-averaged hydraulic and sediment information. SIAM is simpler than a mobile bed sediment transport model and requires less data, and is well suited to support the preliminary data analysis conducted within the hydromorphological assessment method. For many systems, this level of analysis will be sufficient for the methodology proposed in Deliverable 2.1 Part 1, however if bedload transport is a significant management problem in a river (either too much or too little sediment), more complex sediment transport models are recommended to accurately estimate transport rates when empirical measurements are not available.

SIAM requires data on the channel network, flow duration curve, sediment sources in the catchment, and the particle size distributions of sediment sources and channel sediment. Using this information, the model calculates the transport potential (tonnes day^{-1}) for each sediment size fraction and flow profile (i.e. discharge) based on a sediment transport equation. The sediment transport potentials are then multiplied by the duration of each profile and compared with the channel bed sediment supply from the upstream reach and local sources to determine the local balance for each sediment size (Figure I1.1). Balances for each sediment size fraction are then combined to estimate a total sediment balance per reach, which indicates whether a reach is aggrading, at equilibrium or degrading.
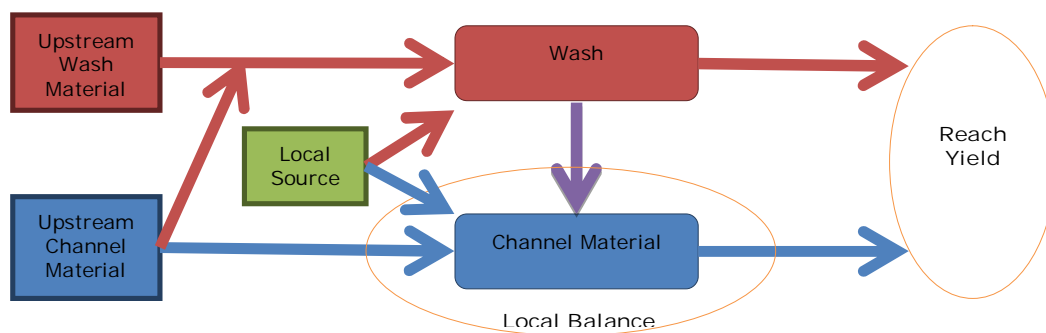
Figure I1.1 SIAM calculates the net gain or loss of channel bed sediment in each reach based on reach-averaged hydraulics and the sediment inputs from upstream and local sources. Adapted from Mooney (2006).

---

[2] http://www.hec.usace.army.mil/software/hec-ras/, accessed on 29 May 2013

The SIAM model incorporates wash load and bed load in the analysis. However only bed load will impact the local sediment balance in a reach (Little and Jonas, 2010). Channel bed load is the sediment size fractions that are found on the river bed, and for which transport is typically hydraulically limited. Wash load is sediment that originates from sources further upstream in the catchment and is transported through a reach without interacting significantly with the channel bed. Wash load is typically composed of clays and silts but can include fine sand. The particle sizes found in the wash load and bed load can vary within a catchment. Wash load would be composed of coarser sediment in steeper headwater reaches than in lower gradient ones downstream. In other words, fine sediment may not be an issue in the headwaters of a river network because it is passed through the reaches as wash load, but it may cause a problem in downstream reaches when it deposits on the river bed. SIAM allows users to define the maximum wash load diameter in each reach, and to vary it between reaches to simulate this phenomenon.

I1.3 Case Study

The sediment budget analysis was conducted on the River Frome (Dorset, UK). The River Frome catchment is a medium-sized, lowland, calcareous catchment according to the Water Framework Directive typology (catchment area = 457 km^2, median elevation = 104 m). It has a gravel/sand bed and a baseflow dominated hydrology stemming from the underlying chalk aquifer (baseflow index = 0.83-0.89). Fine sediment infiltration into and accumulation onto the channel bed has been identified as a significant problem for the management and restoration of the river. For more information on the River Frome, please see the River Frome Case Study in Deliverable 2.1 Part 3.
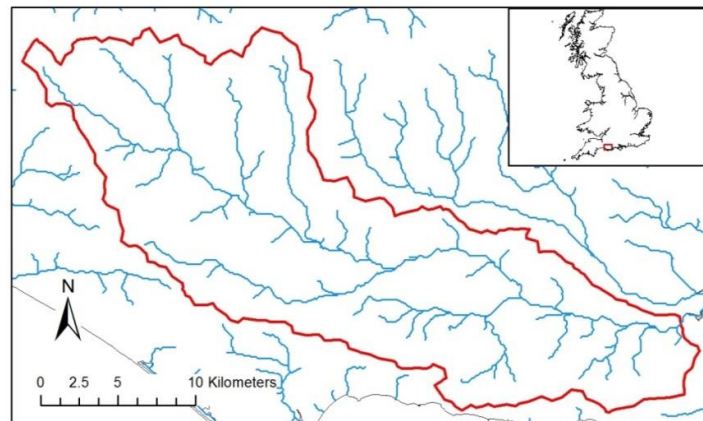
Figure I1.2 The Frome catchment is a medium-sized, lowland, calcareous catchment according to the Water Framework Directive typology (catchment area = 457 km^2, median elevation = 104 m). Profile DTM: © Crown database right 2009.

I1.4 Materials and methods

The SIAM sediment budget analysis is divided into 2 main stages: (1) the development of a 1-D steady-state hydraulics model of the river network and (2) the SIAM analysis based on sediment reaches. A general description of the methods is included below. For

detailed step-by-step methods, please refer to the HEC-RAS user manual and the hydraulic reference manual (US Army Corps of Engineers, 2010a, b).

I1.4.1   1-D Hydraulics model input

The first step of the development of a 1-D steady state hydraulics model is the definition of river geometry. The geometry file in HEC-RAS describes the river network and includes information on tributary junctions, elevations, cross-sections and anthropogenic features (e.g. bridges and weirs) (Error! Reference source not found.). The file can be created directly in HEC-RAS or extracted from ArcGIS using the HEC-GeoRAS extension.

Table I1.1 The data requirements for the 2 stages of the SIAM analysis, and the specific datasets used for the Frome catchment.

Analysis stage	Data type	Data	Frome dataset
1-D steady-state hydraulics model	River Geometry	River network	Ordnance survey map (1:1250)
		Elevation	Profile DTM - 10 m resolution (Edina)
			LiDAR - 1 m resolution (Env. Agency)
		Cross sections	Detailed cross sections (Env. Agency)
			Water depths (RHS, Env. Agency)
	Steady-state data	Discharge profiles	Gauging stations (Env. Agency)
		Boundary conditions	Normal depth based on slope
SIAM	Bed Material	Size distribution	Dominant substrate (RHS, Env. Agency)
			Mean trophic rank physical data (CEH)
	Hydrology	Flow duration	Gauging stations (Env. Agency)
		Temperature	UK average (8 C)
	Sediment properties	Transport function	Yang
		Fall Velocity	Default
		Wash load maximum diameter	5, CM, 0.0625 mm
		Specific gravity	Default: 2.65
	Sources	Sediment sources	Pesera soil erosion model (JRC)

The Frome river geometry file was created in ArcGIS using Ordnance Survey maps (1:1250) to describe the river network[3], the Profile Digital Terrain Model (DTM) [4] and 1-m resolution LiDAR surveys for elevation, and detailed engineering cross-sections and River

---

[3] MasterMap data obtained from Edina Digimap Ordnance Survey Service © *Crown database right 2012*

[4] Profile DTM data obtained from Edina Digimap Ordnance Survey Service © *Crown database right 2009*

Habitat Survey data for cross-section information (Environment Agency, UK) (Figure I1.3). Only significant tributaries were included in the river network, defined as those with upstream catchment areas greater than 20% of the main stem catchment area at the confluence. River cross sections were spaced approximately 1 km apart, which is appropriate for a catchment scale analysis of sediment transport dynamics (US Army Corps of Engineers, 2010b). Manning's n was set at 0.1 for the river channel, representing a mid-value from the range of Manning's n values measured in UK rivers with *Ranunculus* spp. (O'Hare et al., 2010) and 0.03 for the floodplain, based on the values for high grass pasture and mature field crops (US Army Corps of Engineers, 2010a, Table 3-1).
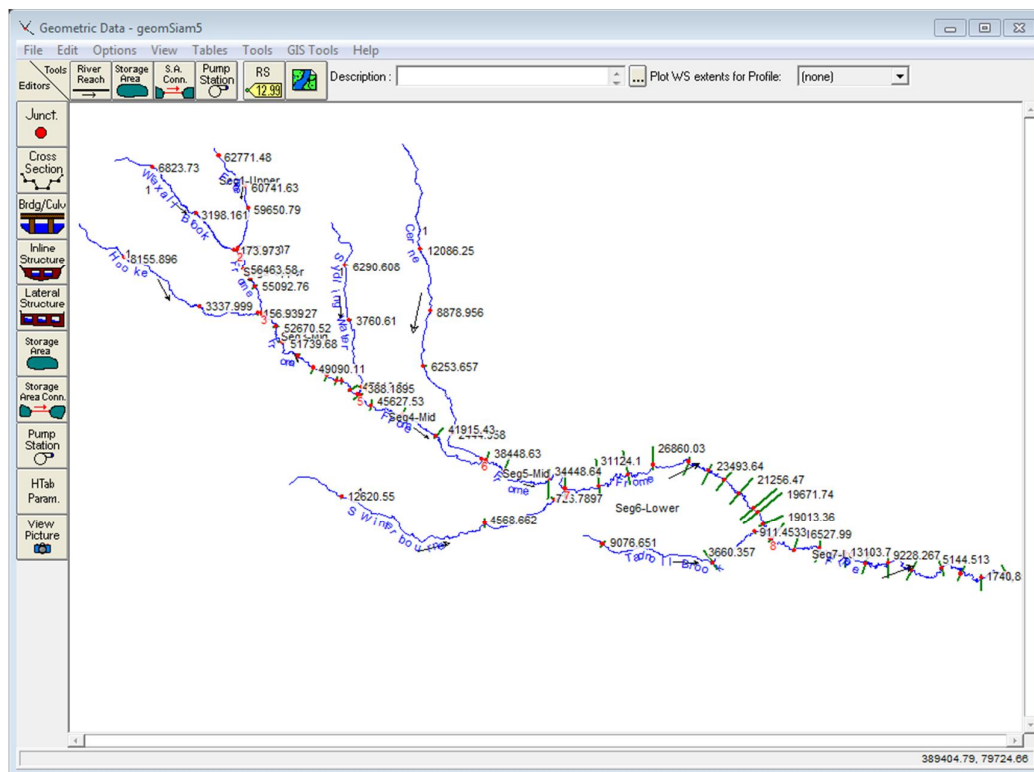
Figure I1.3 HEC-RAS geometry file for the River Frome catchment. Blue lines: river centre lines, red and green lines indicate cross sections, and red circles indicate tributary junctions

No anthropogenic structures were included in this analysis because of insufficient data on the dimensions of structures such as bridges and weirs, and channel cross sections upstream and downstream of the structures. Similarly, the channel network was represented as single-thread because of insufficient data on secondary channel cross-sections and flow separation at bifurcations. In reality, the River Frome has a very high number of engineering structures, particularly water level control structures and bridges, and is anabranching in the middle and lower catchment. Therefore, the geometry file represents a river system that has higher energy than in reality, and the resulting sediment budget serves as an 'upper limit' or a 'maximum sediment transport scenario'.

The hydrology data used to conduct a steady-state hydraulic model included discharge profiles for all stream reaches and steady state boundary conditions. Stream discharge data was obtained from the Environment Agency for 5 gauging stations in the River Frome catchment (Table I1.2). Six discharge profiles were used in the HEC-RAS steady-state model to ensure a good temporal coverage of the annual variation in flow (Table I1.3). Water level data was not available to parameterise the model at these discharges, but the flood extent of the 1 in 100 year flood was used as an external check on the model calibration.

Table I1.2   Gauging station data used to create the discharge profiles for the 1-D hydraulics model of the Frome catchment

Gauge number	River	Grid Reference	Data type	Period of Record	Catchment Area
445210	Hooke	353820, 100000	15 min flow	1992 - 2012	11.60
44006	Sydling Water	363270, 99640	Mean daily flow	1970 - 2011	12.06
445930	Win at Winfrith	380640, 84880	15 min flow	1999 – 2012	18.18
44004	Frome at Dorchester	370920, 90550	Mean daily flow	1970 - 2011	205.54
44001	Frome at East Stoke	386760, 86860	Mean daily flow	1966 - 2011	413.46

Table I1.3   Discharge profile, used in the steady-state hydraulic model, and their duration in days per year, used in the later SIAM model step.

Discharge profile	Duration (days)
Q95	96.05
Q70	76.84
Q50	153.68
Q10	30.74
Q2	3.85
Q1	3.84

Reliable hydrology data was not available for all reaches in the catchment. In order to estimate discharges for ungauged reaches, a linear regression analysis was conducted for discharge based on catchment area for each discharge profile (R^2 = 0.97–0.99). Discharge was estimated for cross sections in ungauged reaches based on the upstream catchment area, which was estimated using the flow accumulation procedure in the Hydrology toolset in ArcGIS 10.0.

Boundary conditions must be assigned for the ends of reaches that are not connected to another reach. Therefore upstream boundary conditions were assigned for all tributaries and the upper reach of the main Frome, and downstream conditions were assigned for the outlet of the Frome. Due to the paucity of detailed hydrological data, boundary conditions were mostly defined based on normal slope, for which friction slope was approximated using the channel gradient. Boundary conditions for the River Hooke were set as known water level at depth based on the stage and flow data reported from the gauging station for the upstream cross section.

I1.4.2 SIAM data input

As the SIAM analysis is based on 'reach'-averaged hydraulic and sediment data, the first step is to define sediment reaches. At a minimum, there must be at least one sediment reach for each of the reaches defined in the river geometry file. All cross sections must be included in a sediment reach, and no cross section can be in more than one sediment reach. HEC-RAS 'reaches' in the initial geometry file are automatically delineated at river confluences/bifurcations. In the case of the River Frome, only the tributaries that increased flow by greater than 20% were included in the analysis, which resulted in HEC-RAS reaches that were coincident with segments. An additional tributary was included in the lower catchment to split the long Segment 6 in half. Thus the River Frome was split into 7 reaches in the geometry file. Sediment reaches for SIAM are based initially on the river geometry reaches, but can be further subdivided to account for significant changes in channel characteristics (e.g. gradient) or sediment delivery to the channel. These changes in valley setting are already picked out in the initial delineation, so the River Frome catchment has a total of 13 sediment reaches (7 in the Frome and 1 for each of the 6 main tributaries).

Bed material data is input as particle size frequency (% finer). SIAM lists 20 size classes from clay to large boulder, but calculations are only done for classes input by the user. Bed material for the River Frome was estimated from substrate data recorded during River Habitat Surveys (Environment Agency) and Mean Trophic Rank surveys (MTR; Centre for Ecology and Hydrology) (Error! Reference source not found.). The closest RHS or MTR survey was identified for each cross section in the geometry file. MTR surveys record percent cover for substrate classes along a 100 m stretch of river (clay, silt/mud, sand, gravel, pebbles/gravels, pebbles, boulders/cobbles). RHS surveys record 10 point estimates of dominant substrate over a 500 m reach. These point estimates were averaged together to simulate a particle size distribution for the RHS survey reach. An average was then calculated for the entire sediment reach using both the MTR and RHS data. No substrate data was available for the tributaries, and the bed particle size distribution estimate for Frome Segment 1 was used for all tributaries.

Reach averaged hydraulic data is automatically calculated for each of the discharge profiles based on the 1-D hydraulics model. The only data inputs required from the user at this stage are to specify the duration of each profile in days and to set a water temperature. Flow durations for discharge profiles used in the Frome are listed in Table I1.3, and water temperature was set at an average UK temperature of 8 $^{\circ}$C for all profiles. The flow profiles were selected because they are used for flow analyses in the UK (e.g. Q95 and Q70) or were needed to capture high flows (Q1). Duration was calculated as the number of days with flow greater than the percentile (e.g. 95th percentile for Q95) but less than the next flow profile (e.g. Q70), and then scaled to 100% to account for the 5% unaccounted for at the lower end of the profile (95-100%)

The next dataset needed to run the SIAM model is local sediment source information. Sediment sources are defined as the amount of sediment delivered to the river for each particle size class (tonnes/year). Any number of sources can be included. The program allows users to use a sediment source for multiple reaches and apply a multiplier (e.g. a set bank erosion rate multiplied by length of meander bends in each reach). In this base SIAM model for the River Frome, the only sediment source included was soil erosion as estimated by the Pesera soil erosion model, a 1-km resolution model of erosion rates

(tons/ha/year) (http://eusoils.jrc.ec.europa.eu/ESDB_Archive/pesera/pesera_download.html). A river buffer shapefile was created from the river network (500 m buffer). The Pesera raster was converted to a shapefile and clipped with the buffer. Areas were tabulated in the attributes table in ArcGIS for each value in the reach, and multiplied by the erosion rates to estimate sediment loads. Particle size data was not available for this sediment source and was assumed to be composed of 3% clay and 97% silt for the SIAM model.

Table I1.4 Bed material used for the base SIAM model for the 7 sediment reaches in the main stem of the River Frome, by size classes and maximum particle diameter (mm). Particle size distributions were estimated from River Habitat and Mean Trophic Rank surveys. The size categories used in the surveys were matched with the SIAM size class with the maximum particle diameter (mm) for that type, e.g . sand at 2mm. The coarse gravel class was used for entries reported in the surveys as Pebble/Gravel.

	Clay	Silt	Sand	Gravel		Pebble	Cobble
				Medium	Coarse		
	0.002	0.063	2	16	32	64	256
1	0%	10%	20%	37%	85%	95%	100%
2	2%	15%	30%	47%	88%	100%	100%
3	0%	6%	24%	34%	86%	98%	100%
4	3%	4%	7%	40%	83%	100%	100%
5	0%	3%	21%	30%	89%	100%	100%
6	0%	3%	13%	38%	85%	99%	100%
7	0%	0%	4%	49%	100%	100%	100%

Finally, the user must specify what the program terms 'sediment properties'. These properties include the sediment transport function, the sediment fall velocity, the wash load maximum diameter and the sediment specific gravity. Three of the 6 transport equations are appropriate for gravel-bed rivers: Laursen (Copeland), Meyer-Peter Muller, and Yang (US Army Corps of Engineers, 2010a, Ch. 12, p 37 – 45). Laursen (Copeland) is a total load predictor based on mean channel velocity, depth of flow, energy gradient and the sediment gradation and fall velocity. It was originally designed for silt-sized sediments but was extended up to gravel-sized sediments (0.011 to 29 mm). Meyer-Peter Muller is an empirically derived equation for bedload transport based on excess shear stress. It is applicable to sediment grain sizes ranging from 0.4 to 29 mm, and is used for well-graded sediment. Yang is a total load equation based on unit stream power, was derived from field measurements and flume experiments, and is applicable to sand and gravel. The Yang formula was used in the base model. The sediment fall velocity was set at default for the sediment transport equation, wash load maximum diameter at 0.0625 for all reaches, and the specific gravity of the sediment at 2.65.

I1.5   Results

The SIAM analysis found a general pattern of sediment loss in all tributaries and Segment 1 of the River Frome, and aggradation in the main stem (Figure I1.4). The greatest annual loss of sediment was found in the South Winterbourne tributary, whilst Segment 6 immediately downstream of the confluence with South Winterbourne had the greatest annual gain of bed sediment (Figure I1.5).
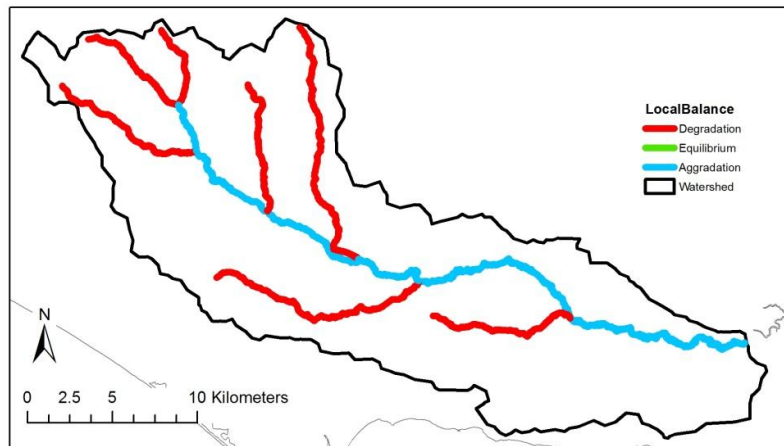
Figure Figure I1.4 Predicted aggradation or degradation of bed material by sediment reach for the base SIAM model. The threshold for equilibrium are 10% of maximum and minimum sediment balance. (Yang transport equation, wash load maximum diameter = 0.062 mm, Pesera soil erosion source)
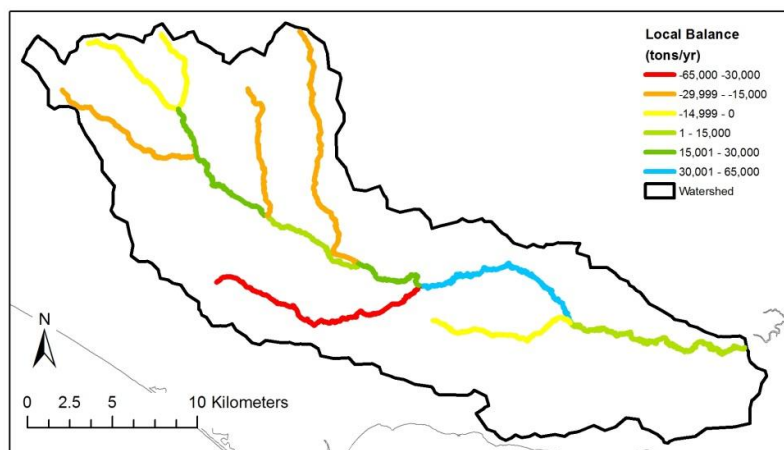
Figure I1.5 Local balance of bed material by sediment reach for the base SIAM model (Yang transport equation, wash load maximum diameter = 0.062 mm, Pesera soil erosion source)

An examination of the results by grain size show that most of the bed sediment that was transported in the network was sand (Figure I1.6). The only reach that had sediment transport potential for medium gravel was the South Winterbourne at Q2 and Q1 discharges, which resulted in a small volume of sediment being transferred to Segment 6 (Figure I1.6). The results suggest that the gravel bed is not actively reworked by average yearly flows. This is consistent with observations from several reaches that the gravel bed is compacted and often covered in algae and suffering from colmation or smothering by sand and silt.
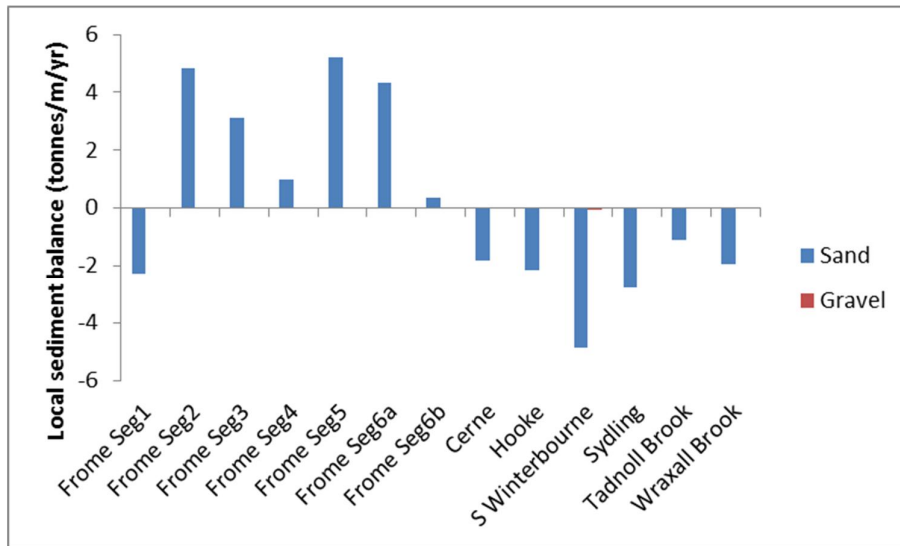
Figure I1.6 Local sediment balance per m of river length by bedload grain size.

I1.6   Model testing

The initial base model was varied in several ways to test the validity of the results: (i) cross-sectional form of the floodplain was simplified to ensure flow remained principally within the channel at less than bankfull discharges and (ii) the sediment transport model was varied. Parameters were not tested in a systematic fashion as would be the case for a sensitivity analysis, and consequently this work constitutes an exploration of the impacts of variations in model parameters rather than a thorough sensitivity analysis.

An examination of the water level results of the 1-D hydraulic modelling revealed that some of the flow was being diverted through the floodplain even at low discharges. This outcome was caused by a combination factors: the low gradient of the channel; the wide, flat floodplain; the high resolution elevation data for the floodplain cross-sections; and the wide spacing of cross sections. In short, water flow is directed downstream perpendicular to cross-sections in a 1-D hydraulics model. Since the floodplain is so flat and cross sections are 1 km apart on average, flow in the model was directed into depressions in the floodplain rather than staying in the channel. To determine how this was impacting the results, the floodplain was smoothed and its elevation adjusted slightly (on the order of decimeters) to make sure that flow was kept within the channel. While creating this new geometry file, two new tributaries were incorporated into the analysis and the duration of the flow profiles was adjusted to correct for an over dominance of low flows (Table I1.5). Because of the low number of profiles and the uneven intervals, the calculation of duration was complicated. In this analysis, duration was calculated by determining the geometric mean between the discharge profiles (e.g. 81.5% for Q95 and Q70), calculating the percent between the means or endpoints (e.g. 100% - 81.5% for Q95), and then multiplying by 365 days. This flow profile duration was used for all subsequent analyses, but was not tested on the original geometry file used in the base model. The underlying 1-D hydraulics model on which SIAM calculations are based remained unchanged from the base model.

Table I1.5 Discharge profiles and duration used to test the effects of sediment transport function on the model outcome.

Discharge profile	Duration (days)
Q95	67.35
Q70	81.71
Q50	134.32
Q10	65.29
Q2	11.16
Q1	5.16

The change in cross-sectional geometry and flow profile durations had no impact on the general trends in aggradation and degradation by reach (Figure I1.7), and little impact on the amounts of sediment deposited or eroded (Figure I1.8). As would be expected, the results of the model showed that more sediment would be transported within the channel when all of the flow remained in the channel at less than bankfull discharge. More sediment was eroded in the tributaries than in the base model and less was deposited in the main stem of the River Frome (Segments 2-6) (Figure I1.8a).

The HEC-RAS user manual states that the choice of sediment transport function will have a significant effect on the results of the SIAM analysis, and that users should carefully identify the most appropriate sediment transport function. Unfortunately, none of the functions are ideal for the gravel-bed River Frome. The Yang transport function based on unit stream power was originally selected, however it is very sensitive to stream velocity and sediment fall velocity. Also, after further reading of the manual, an upper sediment size limit of 7 mm diameter was noticed, which is well below the size of bed sediment in the River Frome. The other two transport functions that are applicable to gravel sediments are the Meyer-Peter Müller (MPM) and Laursen (Copeland). MPM is based on excess shear stress and applicable to sediment with an 'overall' size up to 29 mm, whilst Laursen (Copeland) is based on mean water velocity and depth and is applicable to sediment size with a median size up to 29 mm (US Army Corps of Engineers, 2010a, ch. 12, p. 42). Both of these functions were tested with the smoothed geometry and revised flow profile durations.

The general pattern of sediment erosion vs deposition remains the same regardless of the transport function used (Figure I1.7), but the amount of sediment transported is substantially greater with MPM and Laursen (Figures I1.8 and I1.9), as is the amount of gravel (Figure I1.9). The incredibly high sediment transport in Laursen is very suspect for the lowland, low energy River Frome. An examination of the model outputs shows that sediment transport potentials for some of the reaches are predicted to be exceptionally high (Table I1.6). For example, Segment 1 on the main stem of the River Frome is estimated to have high transport potentials for coarse gravel, cobble and even small boulders when estimated using the Laursen equation (e.g. 3131 tonnes of coarse gravel per day at a discharge of 0.08 m^3 s^{-1}). Furthermore, transport potentials are higher for many of the low flow profiles than they are for the high flow ones. Sediment transport potentials are more realistic for the main stem of the River Frome for both the Laursen and MPM functions (e.g. Segment 6a, Table I1.7). There are two possible reasons for the results: (1) the empirical relationships used to calculate sediment transport potential are

not suitable for the Frome because model variables (e.g. sediment grain size) lie outside of the empirical relationships or (2) boundary conditions were not calibrated sufficiently for the tributaries (and Frome Segment 1) because of insufficient river flow and level data.
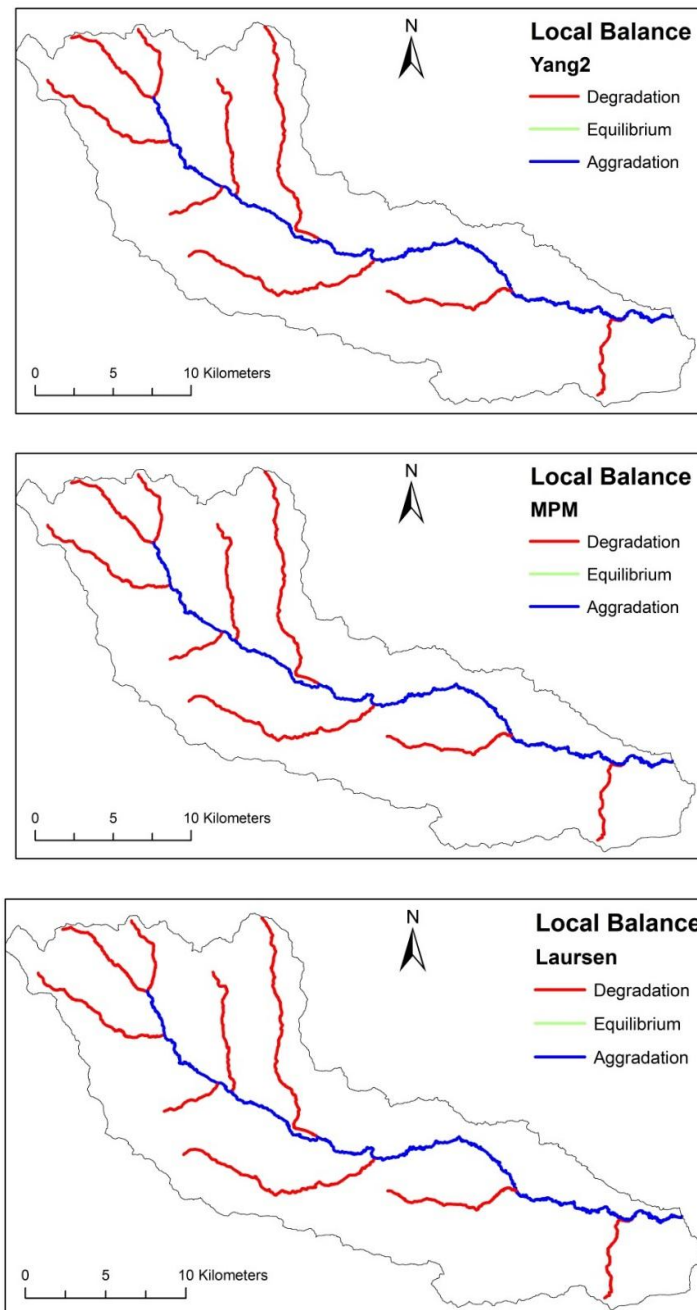
Figure I1.7   Predicted aggradation or degradation of bed material by sediment reach calculated using (top) Yang, (middle) Meyer-Peter Müller and (bottom) Laursen sediment transport functions. The threshold for equilibrium are 10% of maximum and minimum sediment balance.
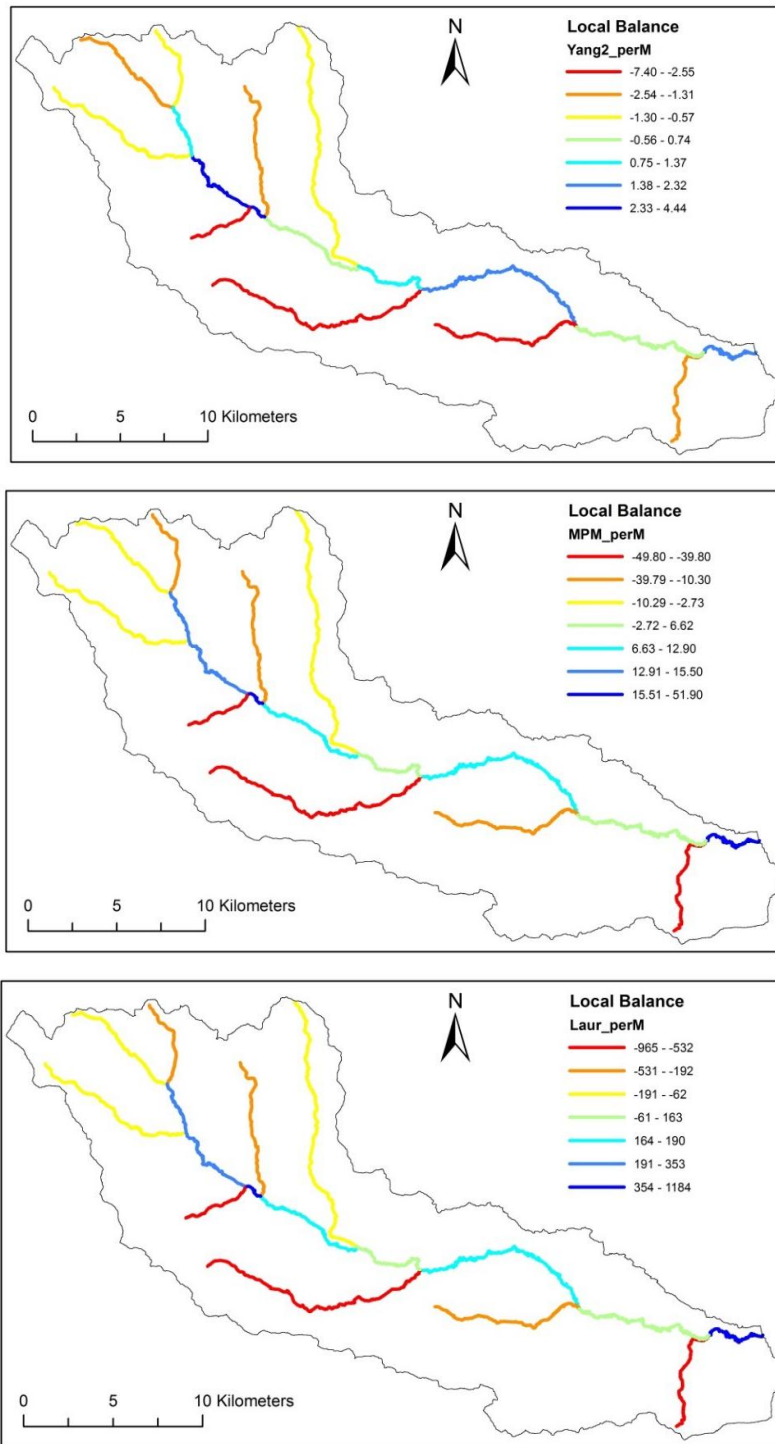
Figure I1.8   Predicted loss or gain of sediment per meter of channel length per year calculated using (top) Yang, (middle) Meyer-Peter Müller and (bottom) Laursen sediment transport functions. N.B. patterns are similar but amounts vary depending on the transport function. Red, sediment erosion; blue, sediment deposition; and green, little or no change.
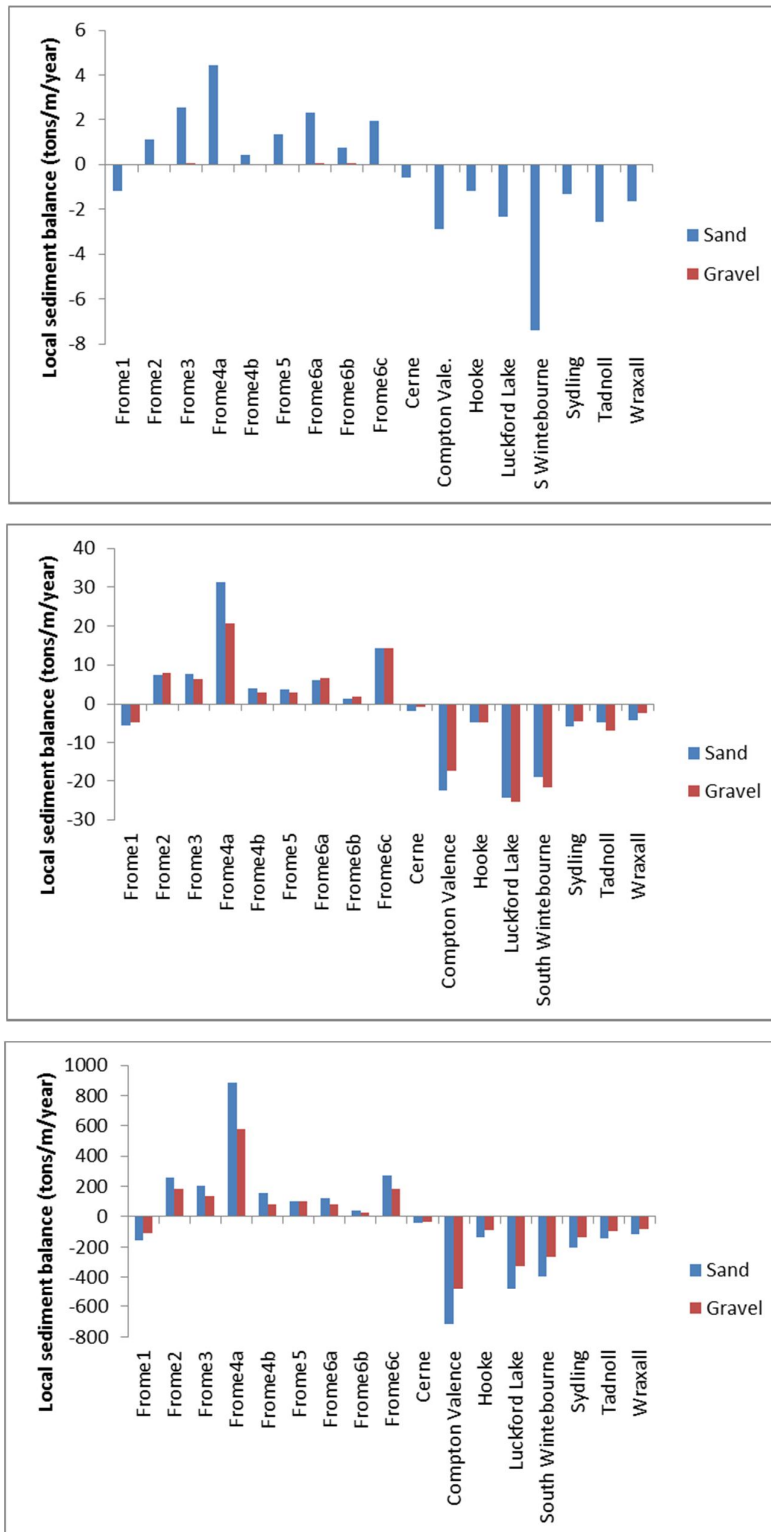
Figure I1.9   Predicted loss or gain of sediment per meter of river length by bedload grain size calculated using (top) Yang, (middle) Meyer-Peter Müller and (bottom) Laursen sediment transport functions.

Table I1.6 Sediment transport potential (tonnes per day) for different grain sizes (upper size limit in mm) and flow profiles (i.e. discharges) for Segment 1 on the main stem of the River Frome calculated using 3 different transport functions. FS – fine sand, MS – median sand, CS – coarse sand, VCS – very coarse sand, VFG – very fine gravel, FG – fine gravel, MG – medium gravel, CG – coarse gravel, VCG – very coarse gravel, SC – small cobble, LC – large cobble, SB – small boulder.

	Discharge (m³ s⁻¹)	Duration (days)	FS 0.25	MS 0.5	CS 1	VCS 2	VFG 4	FG 8	MG 16	CG 32	VCG 64	SC 128	LC 256	SB 512
Yang	0.08	67	1595	412	174	92	0	0	0					
	0.12	82	2427	638	277	152	0	0	0					
	0.17	134	2792	758	340	193	0	0	0					
	0.4	65	1677	528	272	176	0	0	0					
	0.57	11	1189	400	221	152	0	0	0					
	0.63	5.2	1147	391	220	153	0	0	0					
MPM	0.08	67	836	828	812	779	715	593	374	55				
	0.12	82	948	939	921	886	816	682	440	80				
	0.17	134	896	887	868	832	760	623	379	37				
	0.4	65	485	476	459	427	363	247	67	0				
	0.57	11	368	360	344	313	253	148	8	0				
	0.63	5.2	356	347	331	300	241	136	3	0				
Laursen	0.08	67	6.11E+05	1.28E+05	4.89E+04	2.46E+04	1.37E+04	7840	4504	3131	2213	1331	393	8
	0.12	82	6.95E+05	1.45E+05	5.55E+04	2.80E+04	1.55E+04	8910	5116	3583	2525	1506	453	7
	0.17	134	5.91E+05	1.24E+05	4.72E+04	2.38E+04	1.32E+04	7551	4317	3193	2198	1217	420	1
	0.4	65	1.43E+05	3.00E+04	1.14E+04	5725	3138	1889	1382	916	441	183	0	0
	0.57	11	7.54E+04	1.58E+04	5983	2988	1622	1131	791	462	144	1	0	0
	0.63	5.2	6.81E+04	1.42E+04	5403	2695	1461	1044	722	407	136	0	0	0

Table I1.7 Sediment transport potential (tonnes per day) for different grain sizes (upper size limit in mm) and flow profiles (i.e. discharges) for Segment 6a on the main stem of the River Frome calculated using 3 different transport functions. FS – fine sand, MS – median sand, CS – coarse sand, VCS – very coarse sand, VFG – very fine gravel, FG – fine gravel, MG – medium gravel, CG – coarse gravel, VCG – very coarse gravel, SC – small cobble, LC – large cobble, SB – small boulder.

	Discharge (m^3 s^{-1})	Duration (days)	FS 0.25	MS 0.5	CS 1	VCS 2	VFG 4	FG 8	MG 16	CG 32	VCG 64	SC 128	LC 256	SB 512
Yang	1.5	67	68	26	16	7	0	0	0					
	2.4	82	133	54	35	22	0	0	0					
	3.4	134	226	94	65	47	0	0	0					
	6.8	65	886	384	278	236	0	0	0					
	8.9	11	2484	1051	733	628	1	0	0					
	9.6	5.2	3416	1428	981	837	1	0	0					
MPM	1.5	67	89	79	61	29	0	0	0	0				
	2.4	82	131	118	95	53	1	0	0	0				
	3.4	134	178	163	135	84	11	0	0	0				
	6.8	65	378	357	317	242	113	0	0	0				
	8.9	11	656	630	581	486	313	57	0	0				
	9.6	5.2	780	753	700	599	410	115	0	0				
Laursen	1.5	67	3409	700	260	173	108	46	8	0	0	0	0	0
	2.4	82	5339	1099	405	264	169	80	33	0	0	0	0	0
	3.4	134	7673	1582	585	369	241	123	47	0	0	0	0	0
	6.8	65	2.07E+04	4294	1603	897	619	376	125	5	0	0	0	0
	8.9	11	4.93E+04	1.03E+04	3859	1888	1346	902	469	177	0	0	0	0
	9.6	5.2	6.53E+04	1.36E+04	5122	2516	1719	1177	659	222	1	0	0	0

I 1.7   Conclusions

For the purpose of supporting the hydromorphological assessment of the River Frome, the main conclusion from all of the SIAM tests is that river flows are insufficient to transport the coarse bed sediment in any significant manner. Sediment transport potentials are low for both sand and gravel in the main stem of the river Frome. Consequently, the delivery of coarse sediment to the main channel results in net sediment deposition. This conclusion is supported by field observations in many reaches of compacted gravels covered in algae or the smothering of gravels by silt and sand, as well as by the general setting of the river (a low gradient, low energy, lowland river). Furthermore, recall that the River Frome was modelled as a single-thread system based on the dimensions of the main channel, but it is anabranching in many reaches particularly in the middle and lower catchment. Therefore, flow velocities and unit stream powers would be substantially lower than estimated in the model because the total width of the multiple channels would be significantly wider than the single main channel, thereby reducing sediment transport potentials even further. Consequently, without the routine reworking of the gravel bed, the River Frome will continue to suffer from problems of persistent fine sediment storage that impact the ecological communities in the river.

I 1.8   References

Little C, Jonas N. 2010. Sediment impact analysis methods (SIAM): Overview of model capabilities, applications, and limitations. 2nd Joint Federal Interagency Conference: Las Vegas, NV, USA.

Mooney DM. 2006. Siam, sediment impact analysis methods, for evaluating sedimentation causes and effects. Eighth Federal Interagency Sedimentation Conference (8th FISC). US Department of the Interior, Bureau of Reclamation: Reno, NV, USA.

O'Hare MT, McGahey C, Bissett N, Cailes C, Henville P, Scarlett P. 2010. Variability in roughness measurements for vegetated rivers near base flow, in England and Scotland. Journal of Hydrology 385: 361-370.

US Army Corps of Engineers. 2010a. HEC-RAS River analysis system: Reference manual (Version 4.1). Hydrologic Engineering Center UACoE (ed).

US Army Corps of Engineers. 2010b. HEC-RAS River analysis system: User's manual (Version 4.1). Hydrologic Engineering Center UACoE (ed).

Annex I2
Discussion of the sediment dynamics on a long reach using 1D modelling

Audrey Latapie and Benoît Camenen
Irstea, Lyon, France

I2.1   Methodology

The methodology proposed here is twofold:

-   The first step consists in delineating a long reach into homogeneous subreaches.
-   Then, a 1D hydraulic model is applied to estimate several hydraulic parameters at chosen discharges, and so the sediment transport capacity.

Upstream and lateral inputs of sediments are not taken into account in this study since each homogeneous subreach is assumed to be in equilibrium.

I2.2   Data and methods

I2.2.1   The Middle Loire River case study

The reach studied is the Middle Loire, France, which extends from the confluence with the Allier River to the confluence with the Maine River (Figure I2.1). The length of the study reach is about 450 km.
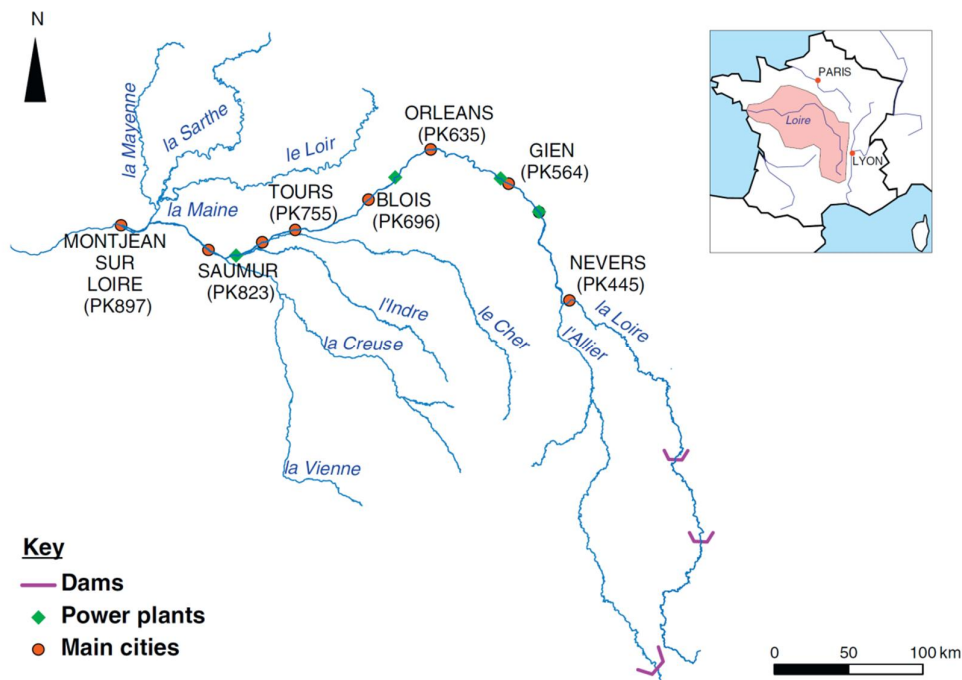
Figure I2.1 Location map showing the study reach.

The Middle Loire River is characterized by a section with a multiple channel configuration downstream of the confluence with the Allier River, a short meandering section upstream of Orléans, and a multiple channel system with the presence of numerous vegetated islands and sand bars in the downstream section. The Middle Loire River has a highly variable hydrologic regime: very low discharge during the summer and high magnitude flows in winter and spring. At Gien, located 564 km downstream from the source, flood events with a return period of 2 years correspond to a discharge of 1600 m^3/s. In Figure I2.2, the evolution of the discharge along the river for specific return periods is presented. The significant inputs of the Cher, Vienne and Maine tributaries, respectively, can be clearly seen.
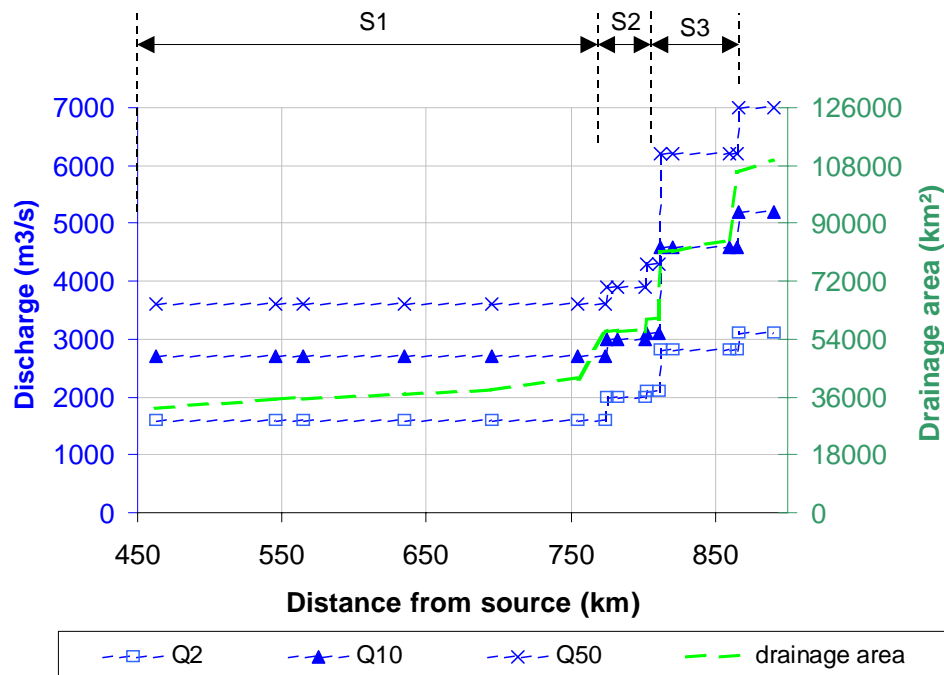
Figure I2.2 Contribution from the tributaries to the Loire's discharge for specific return period (S1, S2, S3 correspond to main geological units).

On the Middle Loire, four geological units can be distinguished: Jurassic limestones from the confluence with the Allier River to 90 km downstream, then Tertiary formations (lacustrine limestones and alluvial formation) to downstream of Blois (located at a distance of 696 km from source), Cretaceous chalks to the confluence with the Maine River, and Hercynian metamorphic rocks in the downstream section. The first two geological units are characterized by similar mean slope ($s_{b1} \approx s_{b2} \approx 0.4$ m/km), whereas units 3 and 4 have a lower mean slope value ($s_{b3} = 0.29$ m/km; $s_{b4} = 0.18$ m/km).

The Loire River has been intensively modified over the centuries. Flood embankments were constructed between the 13th and 18th century. Oblique groynes were erected in the 19th century to maintain a single channel. As intended, these structures have caused the deepening of the main channel, but sediments have accumulated behind them, inducing the development of vegetation, closing secondary channels and thus reducing

flood conveyance (Rodrigues et al., 2006). The construction of infrastructure along the river (bridges, dams, power plants) also influences the river by confining the flow and stabilizing the river bed. Sand and gravel extraction in the main channel started in an industrialized manner at the beginning of the 1950s and was formally prohibited in 1995. Extractions had and still have a significant impact on the river dynamics (Latapie et al., 2014).

I2.2.2   Data available

The regional environment agency (DREAL Centre) have regularly monitored two hundred sites to record water levels at low and high flows since 1978. Aerial photographs taken during low flow conditions are available for 1955, 1984, 1995, 2002 and 2010. A topographic survey of the Middle Loire River was undertaken in 1995. Cross sections, surveyed every 2 km on average, cover the main channel and can be completed with floodplain data extracted from Lidar data collected in 2003. These data have allowed the determination of geomorphic characteristics and the construction of a hydraulic model.

Only a small amount of data is available for the description of the sediment grain size in the main channel. A downstream fining exponential law in the form of the Sternberg (1875) formulation was adopted and fitted to these data (Figure I2.3):

$$d_{50} = 4.4 \times 10^{-3} \exp(-4.65 \times 10^{-6} x)$$
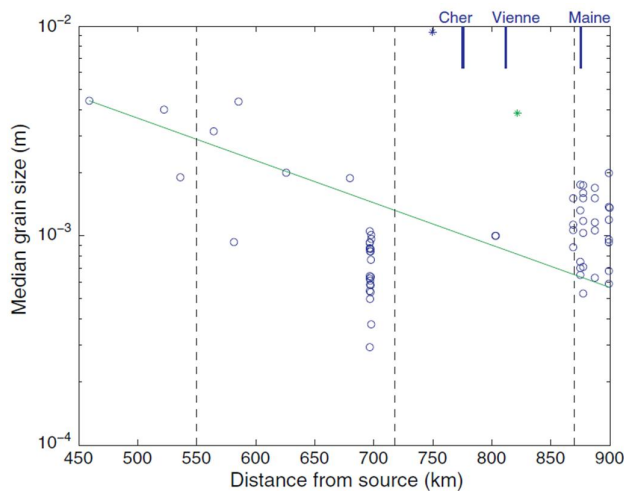
Figure I2.3   Downstream variation in median grain size for the main channel (circles indicate measured values, crosses are measured d50 which have been excluded from the analysis). The solid line represents the exponential law in the form of the Sternberg formulation. The vertical dotted lines indicate the four geological units and the blue segments the location of major tributaries.

I2.2.3   Use of a 1D model

The one dimensional hydraulic model RubarBE, developed by Irstea (El Kadi Abderrezzak and Paquier, 2009) was used for this study. The model allows the consideration of two

roughness coefficients: one for the main channel ($K_{mc} \approx 30$ m$^{1/3}$/s for our case) and one for the floodplain ($K_{fp} \approx 15$ m$^{1/3}$/s for our case).

Adjustments to the resistance coefficient were made locally in order to obtain a good reproduction of the available measured water levels. Once calibrated, the model can be run for a succession of steady discharges from low flows to extreme events. Using the model outputs, several parameters were computed for different discharges:

- The river width to mean water depth ratio (*W/D*)

- The effective bed shear stress:

$$\tau_{eff} = \left(\frac{K}{K_g}\right)^{3/2} \rho g R_h S$$

with *K* and *K$_g$* the total and grain related Stickler coefficients, respectively, ρ the water density, *g* the acceleration of gravity, *R$_h$* the hydraulic radius, and *S* the energy slope.

The specific stream power:

$$\omega = \rho g \frac{QS}{W}$$

with *Q* the water discharge and *W* the river width.

12.2.4   Comparison of approaches to detect reach boundaries

Some statistical tests have been implemented on the geomorphic and hydraulic parameters in order to detect discontinuities. The results obtained with these automated reach delineations are compared with the spatial units identified in the previous paragraphs.

(i) Visual distinction of changes

The delineation of reaches along the fluvial continuum is generally based on a visual distinction of changes (Orr et al., 2008). A first division of the river into homogeneous geomorphic reaches was conducted in two steps (Latapie et al., 2009):

1. Identifying discontinuities in low water profiles (1978, 1986, 1995, 2002, 2011).

2. Assessing the presence of singularities affecting the flow, sediment transport and thus river behaviour. The presence of artificial structures (bridges, dams, groynes, …), bedrock outcrops, confluences and transitions from a single channel to a multiple channel configuration (presence of vegetated islands) was checked on the 1995 aerial photographs.

The 1995 aerial photography dataset was selected in step 2. It is represents an intermediate date in the period analysed, which corresponds to the official end of the mining period on the Middle Loire. The hydraulic model is based on topographic data surveyed in 1995. This visual delineation is pertinent but the location of reach boundaries could be corroborated by implementing of some statistical tests.

(ii) Spatial autocorrelation tests

Spatial autocorrelation tests are performed in order to assess if similarity between values as a function of their spatial position along the stream profile can be inferred. The spatial distribution of the data are explored using the *c* of Geary (Geary, 1954). This test is derived from the semi-variance $\gamma(h)$, defined as the spatial dissimilarity between a parameter separated by a distance *h* divided by the variance of the variable:

$$\gamma(h) = \frac{1}{2N(h)} \sum \left[u(a) - u(a+h) \right]^2$$

$$c(h) = \frac{\gamma(h)}{s^2}$$

where *N(h)* is the number of data pairs separated by the distance *h,* and *u(a)* and *u(a+h)* are the parameter values at location *(a)* and some distance *(a+h)* away, and s^2 is the variance. The difference in distance between each data point and every other data point is calculated and the pairs of data are binned. The x-axis represents the separation distance between pairs of binned data points while the y-axis plots the corresponding c of Geary. The value of c is 1 in the absence of spatial autocorrelation. A low value of c (0<c<1) represents a positive spatial autocorrelation, which approaches zero for strong autocorrelation, whilst when c varies between 1 and $+\infty$, it implies negative autocorrelation.

In addition, an experimental semi-variogram can be fitted on the $\gamma(h)$ curve to determine the range, that is the distance at which the variable is no longer correlated. The range value gives an indication of the spatial dependence and can thus be regarded as the maximum length of a river reach.

The variogram analysis was performed on the active channel width, floodplain width, changes in bed level, and hydraulic parameters calculated with a 1D hydrodynamic model for bankfull flow condition. Results illustrated that the active channel width, floodplain width and the hydraulic parameters are not spatially correlated. Changes in bed level considered between 1986 and 1995 and between 1995 and 2002 provided a range value equal to 4 km and 5 km, respectively.

(iii) Non parametric statistical tests

In order to dismiss discontinuities linked to uncertainties associated with the derivation of the parameters and to limit the detection to main discontinuities, threshold values have been defined as ±50 m for the active channel width B, ±6 cm for the bed variations Δz and ±20 % for the hydraulic parameters. Results of these tests are referred to as "Data Over Threshold" or DOT.

Finally, a non-parametric test was then used to detect discontinuities along the stream network. The test of Pettitt (1979) was implemented on all the parameters available to identify discontinuities along the stream network. This test was initially designed to detect a single point of change. However, Alber and Piégay (2011) implemented the approach on the Rhône basin and ran the algorithm iteratively as long as a change point was detected to define homogeneous river reaches (with an risk equal to 0.05). The test can be briefly described as follows. Once a change point is detected through the test then the dataset is divided into two intervals. The intervals before and after the change point then form homogeneous groups, which take heterogeneous characteristics from each

other. Let *k* be the rank and *U(k)* the non-parametric statistic and let s_0 be the value taken by *U(k)* on the distribution and *p* the significance probability associated with s_0:

$$U(k) = \sum_{i=1}^{k} \sum_{j=k+1}^{N} \text{sgn}(x_i - x_j)$$

$$S = \max |U(k)|$$

$$p(S \geq s_0) = 2 \exp^{(-6s0/N^3 + N^2)}$$

If p is inferior to the risk α, defined as 0.05 in this study, the null hypothesis is rejected and a change point is localized at the rank *k* for which *S* occurs.

Combining these approaches to detect changes on the longitudinal plots of the geomorphic and hydraulic parameters allowed the identification of the most significant discontinuities (see Table I2.1 and Figure I2.4).

Table I2.1 Number of discontinuities identified on the geomorphic and hydraulic parameters and on temporal lateral and vertical changes with the Data Over Threshold approach (noted DOT in the table) and the Pettitt's test.

							Hydraulic parameters			
	Geomorphic parameters									
	B					B_f	τ_{eff}	ω	W/D	U
Date	1955	1984	1995	2002	2010	2003	1995			
Nb. Values	858						1827			
DOT	357	370	343	339	311	366	655	748	265	41
Pettitt	20	20	17	21	24	56	70	72	106	107
	Temporal changes									
	ΔB					Δz				
Date	55-84	84-95	95-02	02-10		78-86	86-95	95-02	03-11	
Nb. Values	858					86	145	145	184	
DOT	177	95	121	76		34	74	62	70	
Pettitt	13	5	13	9		70	62	53	47	

I2.3 Results

I2.3.1 Reach definition

The first delineation based on a visual detection of discontinuities on the low water long profile and aerial photographs differentiated 167 reaches with lengths ranging from 250 m to 4,750 m and an average length of 2,500 m. Due to the presence of numerous structures in the cities of Orléans and Tours, all singularities were not accounted for in those areas; reaches corresponding to those locations have simply been characterized as heavily influenced by human disturbance.

Results from variogram analysis illustrated that the active channel width, floodplain width and the hydraulic parameter data are not spatially correlated. On the other hand, changes in bed levels between 1986 and 1995 and between 1995 and 2002 provided a range value equal to 4 and 5 km, respectively, which is consistent with the length of the reach identified using the preliminary visual approach.

(a)

(b)
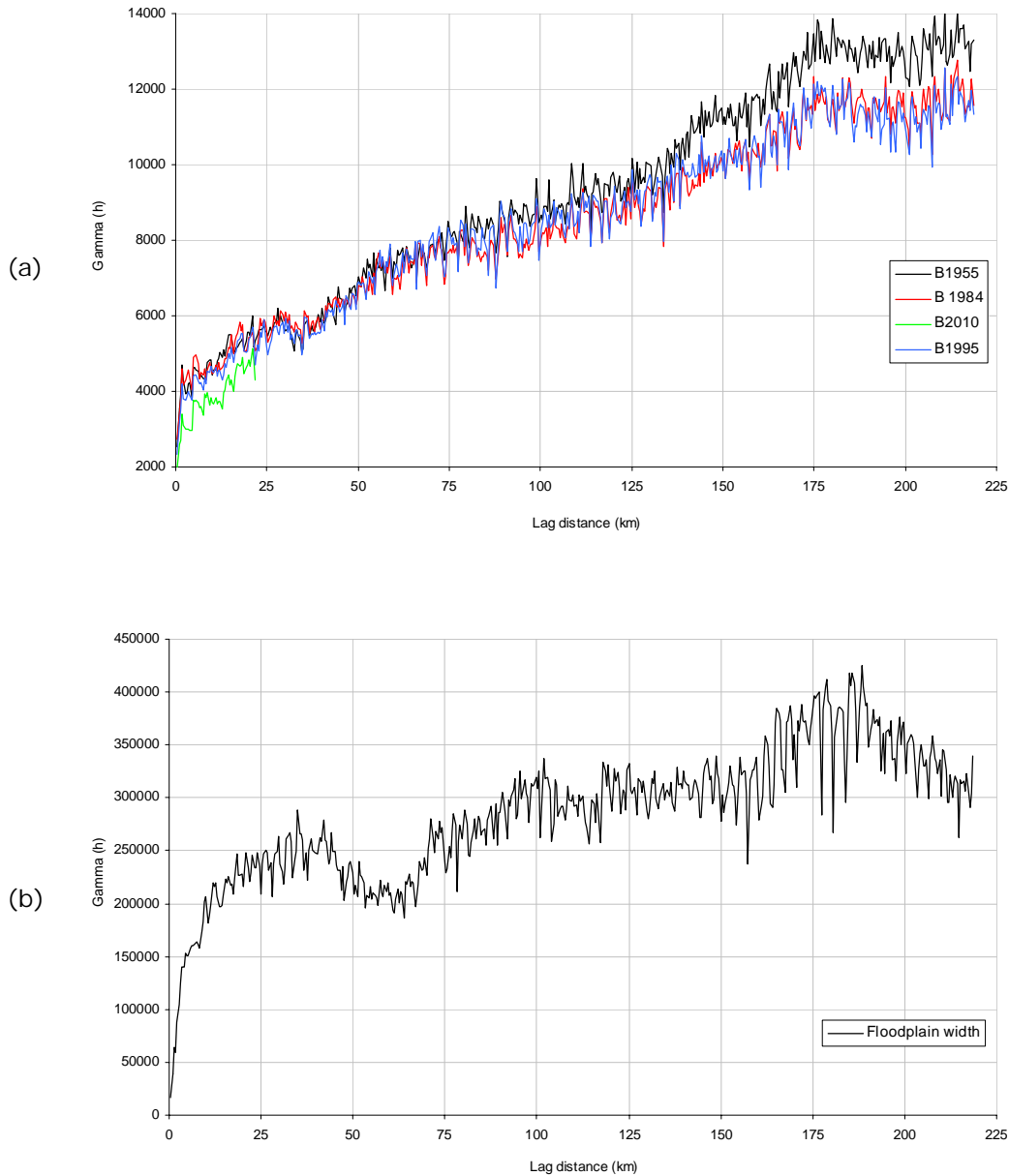
Figure I2.4 Variograms considering (a) the active channel widths measured in 1955, 1984, 1995 and 2010 and (b) the floodplain width.

The number of inflection points detected with the DOT approach is highly dependent on the spatial resolution used for calculation. Except for the velocity, the number of discontinuities identified using the hydraulic parameters is nearly twice the values calculated using the geomorphic parameters. If discontinuities in lateral and vertical changes are considered, the results appear to be very sensitive to the period considered. However, the "multi-temporal" analysis allows the distinction of permanent structures

from transitory ones. The permanent structures identified with the DOT approach were then combined with results from Pettitt's test to detect robust discontinuities. If we assume a tolerance of 250m to account for differences in the data resolution, 170 reaches are identified. With the exception of three boundaries, they all coincide with the boundaries of the 167 reaches previously defined. The additional discontinuities identified correspond to structures located in the cities of Orléans and Tours; and as previously mentioned, those reaches are merged.

12.3.2   Longitudinal evolution of hydraulic parameters

The implementation of a 1D hydraulic model to calculate parameters provides major advantages: multiple modelling scenarios can be envisaged and the derivation is more rigorous; in particular, specific stream power is generally calculated using the energy slope S assimilated to the bed (or low water) slope S_b (Nanson and Knighton, 1996 among others). This assumption can be discussed as the slope should be estimated for the bankfull discharge. Based on the results of the 1D model for the biennial discharge, we found $0.17 < S_{Q2}/S_b < 19$. Significant scatter reflects the presence of artificial and natural singularities, which have a high influence at low to intermediate discharges (such as Q_2).

The hydraulic parameters obtained for the biennial discharge, Q_2, which may be assimilated to the bankfull discharge, are reported in Figure I2.5. Q_2 is nearly constant for the first 300 km of the Middle Loire before being affected by the main tributaries which double the discharge (Figure I2.5a).

The river width-depth ratio, W/D, computed for Q_2 varies between 57 and 421. It is higher in the upstream and downstream part of the studied area where multiple channels predominate (Figure I2.3b). As the mean water depth does not vary significantly from the upstream to the downstream part of the Middle Loire River (from $D_{Q2} \approx 3$ m *to* $D_{Q2} \approx 4$ m), it appears logical that the W/D ratio behaves similarly to the active channel width B ($W_{Q2}/B \approx 1.5$). In geological unit 1, W/D decreases as the Middle Loire changes from a multiple channel system to a single (constrained) channel. In the middle part of the studied area (geological unit 2), the width-depth ratio is nearly constant and $W/D \approx 100$. In geological units 3 and 4, W/D increases simultaneously with discharge and the presence of multiple channels. A larger dispersion is observed in the downstream part of the model (second part of unit 3 and unit 4). This is mainly due to the presence of multiple channels. The difference in water levels between the two channels cannot be rigorously integrated in our model, inducing a larger dispersion in the hydraulic results.

The calculated effective bed shear stress τ_{eff} is within the range of 0.9 to 8.2 N/m^2 (Figure I2.3c). In terms of sediment transport magnitude, the results may be affected by the high entrainment threshold. The increasing τ_{eff} in unit 1 indicates a potential for erosion. A maximum is observed for τ_{eff} at a distance of approximately 550 km from source. This forms the boundary between unit 1 and unit 2. Finally, the decreasing τ_{eff} in units 2, 3 and 4 indicates a potential for sediment deposition.

(a)

(b)

(c)

(d)
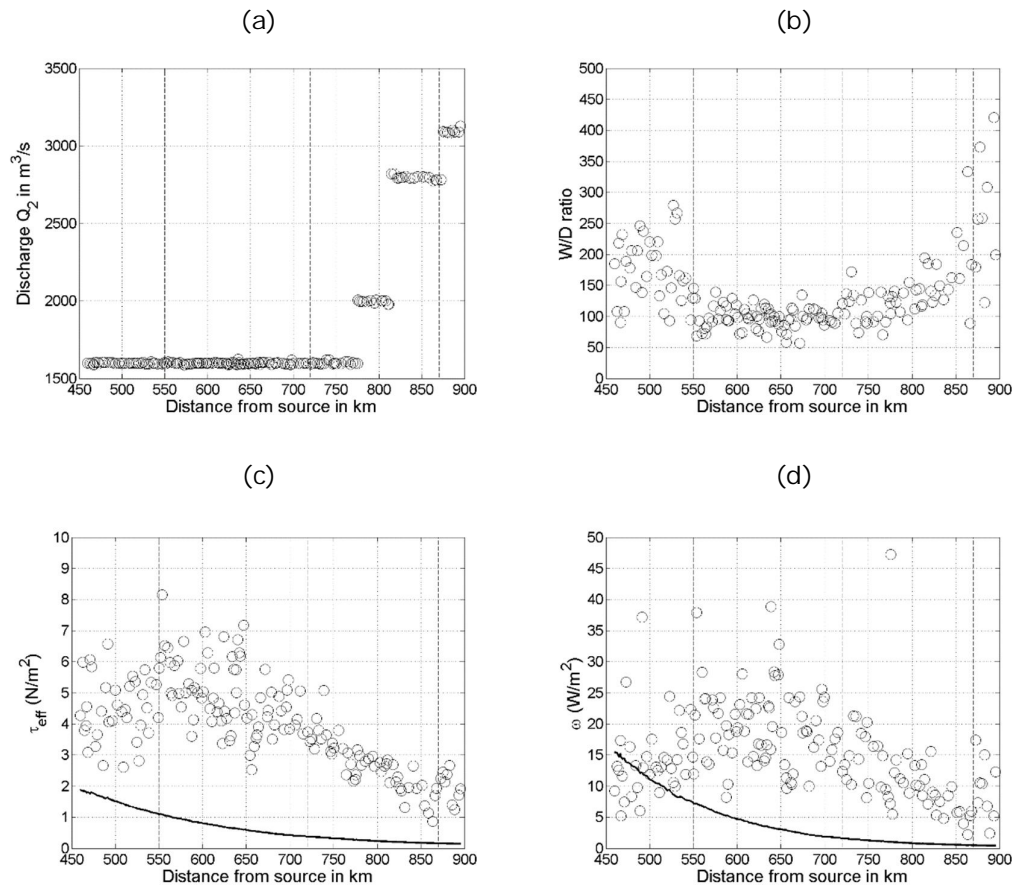
Figure 12.5 Longitudinal variation of (a) modeled bankfull discharge ($Q_{bf} \approx Q_2$), (b) river width-depth ratio, (c) effective bed shear stress (τ_{cr} in plain line), (d) specific stream power (ω_{cr} in plain line). The vertical dotted lines delineate the four geological units.

The calculated specific stream power ω is within the range of 4 to 47 W/m^2. Downstream patterns of change in ω are highly correlated to downstream changes in channel slope and width. The general trend of the curve is the direct opposite of the width-depth ratio plot. As observed by Knighton (1999), a maximum specific stream power is evident, in this instance approximately 650 km from the river's source. Then, ω decreases to values of less than 10 (except at confluences where a slight increase is noticed). Channel changes have often been associated with specific stream power (e.g. Brookes, 1987; Bledsoe et al., 2002; Orr et al., 2008). Since threshold values are specific to a catchment, the analysis of downstream changes in stream power should be considered as an indicator of zones of potential sediment transport. Large changes in stream power from one reach to the next are generally associated to erosion (increase of ω) or sediment accumulation (decrease of ω), whereas high values alone are not necessary indicative of changes (Reinfelds et al. 2004; Vocal-Ferencevic and Ashmore 2012). It should be noted that, based on the Strickler (1923) concept, we can derive $\omega \propto \tau^{1.5}$,

which explains the similar behaviour of ω and τ albeit the larger dispersion in the specific stream power.

To be more accurate in characterizing the potential sediment transport, the bed shear stress or specific stream power was compared to its critical value for inception of sediment transport. The critical bed shear stress (τ_{cr}) was obtained from the Shields curve based on the grain size estimates. The critical specific stream power (ω_{cr}) was estimated using the development of Bagnold (1980). As the river bed median grain size decreases (from $d_{50} \approx$ 4mm to $d_{50} \approx$ 0.6mm), the critical bed shear stress decreases from τ_{cr} = 3.6 to 0.3 N/m^2; and the critical specific stream power from ω_{cr} = 15 to 0.4 W/m^2 (see plain line in Figure I2.5(c) and (d), respectively). Despite uncertainties in the estimation of the critical bed shear stress and specific stream power, especially due to some sensitivity to the slope (Camenen, 2012) but also because of the scatter in the grain size measurements, Figure I2.5(c) and (d) indicate that critical values are generally exceeded all along the river. Results indicate that sediment transport occurs at flows lower than the biennial discharge, which is consistent with measurements and analysis realized around the site of Bréhémont (776 km from source; see Claude et al., 2012). This behaviour is typical in sand-gravel bed rivers where sediment transport is influenced by flood events but also by lower discharges occurring over a longer period.

I2.3.3   Effective bed shear stress and width-depth ratio

The effective bed shear stress made dimensionless by its critical value for inception of transport and the width-depth ratio computed for the biennial discharge is presented in Figure I2.6. These two parameters allow a clear distinction between the four geological units. For units 1 and 4, the large *W/D* values are directly connected to the presence of multiple channels and islands. Since d_{50} is larger in unit 1 than in unit 4, τ_{eff}/τ_{cr} differs in those two units.

- *Unit 1*: The τ_{eff}/τ_{cr} ratio is relatively small ($\tau_{eff}/\tau_{cr} \approx$ 1.5) and slightly decreases with the *W/D* ratio (80 < *W/D* < 280);
- *Unit 2:* The τ_{eff}/τ_{cr} ratio is intermediate (2 < τ_{eff}/τ_{cr} < 6.5) but decreases rapidly with the W/D ratio (60 < W/D < 130);
- *Unit 3:* The τ_{eff}/τ_{cr} ratio is relatively high (3 < τ_{eff}/τ_{cr} < 7.5), increasing with the *W/D* ratio (70 < *W/D* < 330);
- *Unit 4:* The τ_{eff}/τ_{cr} ratio is high (5 < τ_{eff}/τ_{cr} < 9) and slightly decreases with the *W/D* ratio (120 < *W/D* < 420).

I2.3.4   Application of the da Silva (1991) analysis

The theoretical stability analysis made by da Silva (1991) and improved by Ahmari and da Silva (2011) has been presented in section G.1.4. Results from the 1D model can be easily associated with the diagram by Ahmari and da Silva (2011) to distinguish the main fluvial patterns (Figure I2.7). Subreaches from Units 1 and 4 should mainly correspond to braided rivers or multiple bar systems whereas subreaches from Units 2 and 3 should correspond to alternate bar systems or meandering rivers (Figure I2.7a). The few observed meandering subreaches are indeed located in Unit 2 (Figure I2.7b). Also, Units 2 and 3 are characterised by the presence of alternate bar systems. The large amount of straight subreaches may be explained since the Loire River has been significantly

straightened with the construction of flood protection measures. On the other hand, there are many subreaches characterised by a multiple channel system (red color in Figure I2.7b). If this observation is in agreement with the C & B zone (multiple bar system and braided rivers), which could have developed in a more anastamosing system, it is not as coherent for the A & M zone (alternate bar system and meandering river). One reason for such evolution could be the general erosion of the Middle Loire River for the last 50 years (mainly due to the sand extraction from the 60s to the 80s) and the reduction of the active width with the encroachment of vegetation.
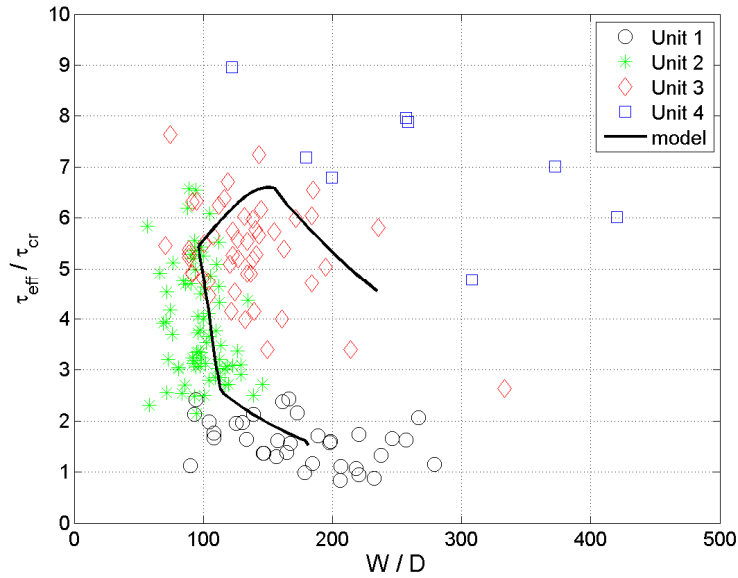
Figure I2.6   Effective bed shear stress made dimensionless by its critical value for inception of transport versus the width-depth ratio computed for Q_2.
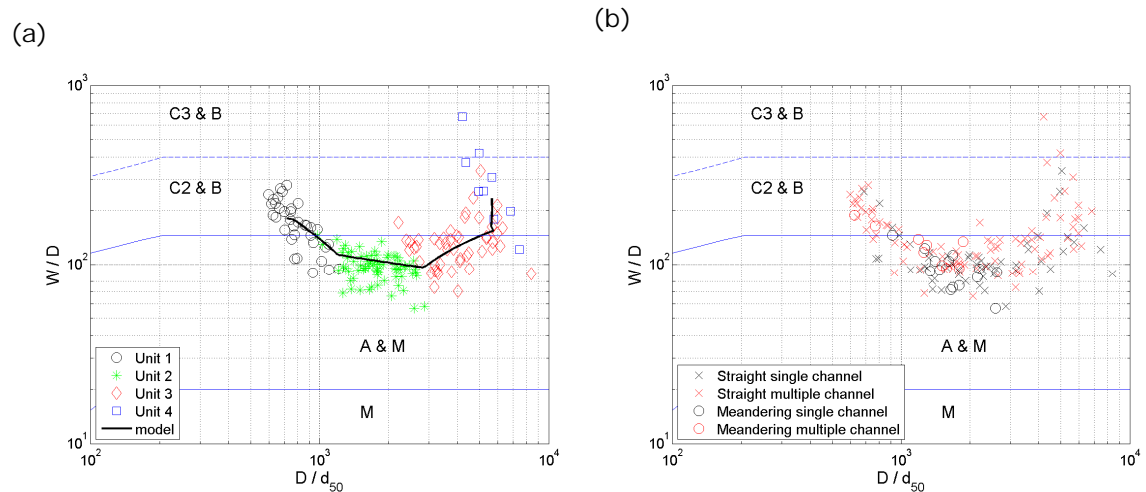
Figure I2.7: Width-depth ratio W/D versus the relative water depth D/d_{50} together with the existence region plan by Ahmari and da Silva (2011) (M: meandering rivers, A: alternate bars C2 and C3: multiple bars (2 and 3 rows, respectively), and B: braided rivers) distinguishing the 4 different units (a) or major river patterns observed (b).

12.4   Conclusions

The use of a 1D model is of interest for delineating a long reach into homogeneous subreaches and calculating accurately several hydraulic parameters at chosen discharges such as the width-depth ratio, effective bed shear stress, and so the sediment transport capacity. Thus, it provides figures to be compared,for example, with the existence region plan by Ahmari and da Silva (2011). A sediment budget for a typical discharge could be achieved as well.

12.5   References

Ahmari H, da Silva AMF. 2011. Regions of bars, meandering and braiding in da Silva and Yalins plan. Journal of Hydraulic Research 46: 718-727.

Alber A, Piégay H. 2011. Spatial disaggregation and aggregation procedures for characterizing fluvial features at the network scale: application to the Rhône basin (France). Geomorphology 125: 43–360.

Bagnold RA. 1980. An empirical correlation of bedload transportrates in flumes and natural rivers. Proc. Royal Society of London, A, 372(1751): 453–473.

Bledsoe BP, Watson CC, Biedenham DS. 2002. Quantification of incised channel evolution and equilibrium. J. American Water Resources Assoc. 38:861-870.

Brookes A. 1987. River channel adjustments downstream from channelization works in England and Wales. Earth Surface Processes and Landforms 12: 337–351.

Camenen B. 2012. Discussion of "understanding the influence of slope on the threshold of coarse grain motion: Revisiting critical stream power" by C. Parker, N.J. Clifford, and C.R. Thorne. Geomorphology 139-140: 34–38.

Claude N, Rodrigues S, Bustillo V, Bréhéret J-G, Macaire J-J, Jugé P. 2012. Estimating bedload transport in a large sand-gravel bed river from direct sampling, dune tracking and empirical formulas. Geomorphology 179: 40–57.

Da Silva AMF. 1991. Alternate Bars and Related Alluvial Processes. Master thesis, Queen´s University Kingston.

El Kadi Abderrezzak K, Paquier A. 2009. One-dimensional numerical modelling of sediment transport and bed deformation in open channels. Water Resources Research 45: W05404.

Latapie A, Camenen B, Paquier A, Rodrigues S, Moatar F, Bouchard J-P. 2009. Morphological evolution of the middle Loire River (France): definition of geomorphic homogeneous reaches. In Proc. 6th IAHR symposium on River, Coastal and Estuarine Morphodynamics, volume I, pages 43–50, Santa Fe, Argentina.

Knighton AD. 1999. Downstream variation in stream power. Geomorphology 9(3-4): 293–306.

Latapie A, Camenen B, Rodrigues S, Paquier A, Bouchard JP, Moatar F. 2014. Assessing channel response of a long river influenced by human disturbance. Catena (in press).

Nanson GC, Knighton AD. 1996. Anabranching rivers: their cause, character and classification. Earth Surface Processes and Landforms 21: 217–239.

Orr HG, Large ARG, Newson MD, Walsh CL. 2008. A predictive typology for characterising hydromorphology. Geomorphology 100: 32–40.

Pettitt A. 1979. A non-parametric approach to the change point problem. Applied Statistics 28: 126–135.

Reinfelds I, Cohen T, Batten T, Brierley G. 2004. Assessment of downstream trends in channel gradient, total and specific stream power: a GIS approach. Geomorphology 60: 403–416.

Rodrigues S, Bréhéret JG, Macaire JJ, Moatar F, Nistoran D, Jugé P. 2006. Flow and sediment dynamics in the vegetated secondary channels of an anabranching river : the Loire River (France). Sedimentary Geology 186: 89–109.

Strickler A. 1923) Beiträge zur frage der geschwindigkeitsformel und der rauhigkeitszahlen für ströme, kanäle und geschlossene leitungen   [Contributions to the questions of velocity

formulations and roughness values for rivers, canals, and closed ducts]. Mitteilung 16, Amt für Wasserwirtschaft, Bern, Switzerland. (in German).

Vocal-Ferencevic MV, Ashmore P. 2012) Creating and evaluating digital elevation model-based stream-power map as a stream assessment tool. River Research and Applications 28: 1394–1416.

Annex I3
Hydraulic modelling of the Magra river (Italy)

Laura Nardi, Massimo Rinaldi

Dipartimento di Scienze della Terra, Università di Firenze, Italy

I3.1 Introduction

In this example, we present some numerical modelling conducted on a portion of the Magra river (Italy). The aim is to show the spatial pattern of a series of hydraulic variables at segment scale. This knowledge can be used to develop a better understanding of hydraulic conditions controlling channel morphology and processes. Following the delimitation of spatial units along the Magra river included within the Catchment Case Study (Deliverable 2.1 Part 3), 1D numerical modelling was performed along the segment M3 (Figure I3.1). Hydraulic data were averaged according to the different spatial scales as described in the following sections.
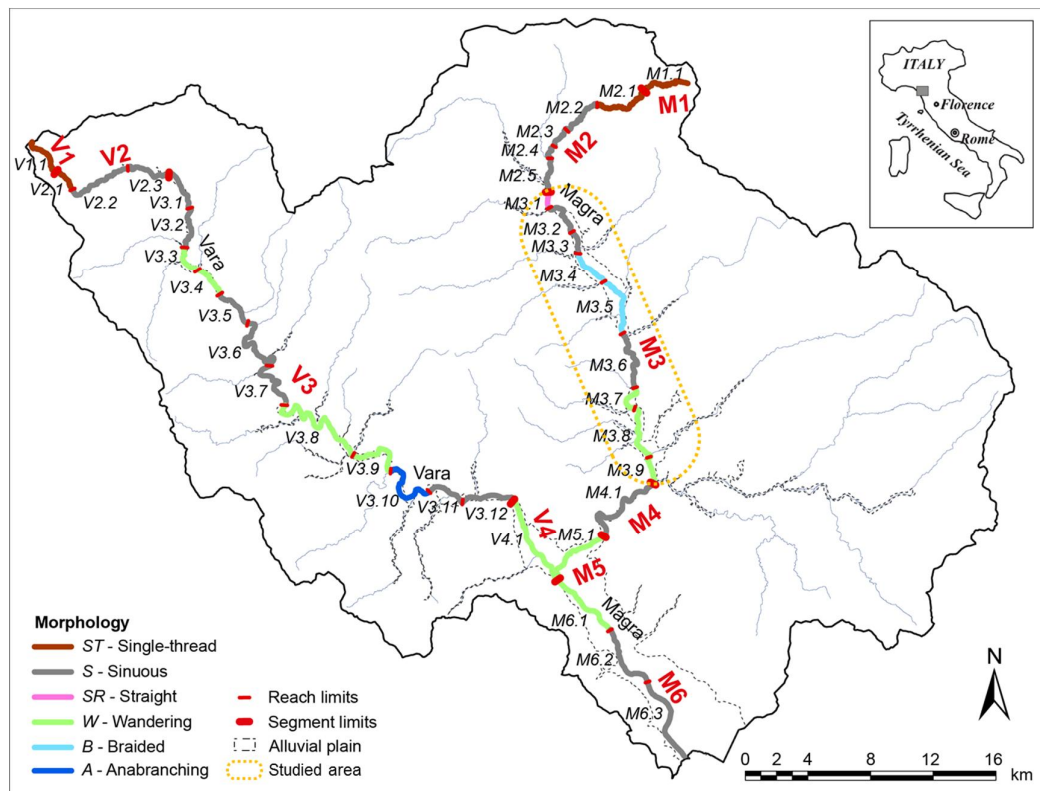
Figure I3.1 Identification of Magra and Vara segments and reaches.

I3.2 Spatial distribution of the stream power along the Magra River

Stream power (or total stream power) is widely recognized as a key parameter controlling channel morphologies, their spatial distribution over a catchment and channel changes (e.g. Bull, 1979; Lawler, 1992; Nanson and Croke, 1992; Knighton, 1999; Fonstad, 2003; Barker et al. 2009; Eaton et al., 2010; Vocal Ferencevic and Ashmore, 2012). It refers to the time rate of expenditure of potential energy (or supply) in a channel as water travels downstream (Rhoads, 1987), and it is mathematically defined as following:

$$\Omega = \rho g Q S$$

where ρ is the fluid density (kg m^{-3}), g is the acceleration due to gravity (m s^{-2}), Q is the channel-forming discharge (m3 s^{-1}) and S the energy slope (m m^{-1}).

Compared to the total stream power, the unit stream power has the advantage of being a predictor of bedload transport (Eaton and Church, 2011) and thus a suitable indicator of stream-channel stability (Thorne et al., 2011). Unit stream power expresses the amount of energy expended per unit area and can be obtained by dividing the total stream power by the active channel width ($\omega = \Omega/w$). In this study, it was calculated by dividing the stream power by the channel width in 2010.

In the present study, the channel-forming discharge was assumed to be the discharge with a recurrence interval of 1.5 years. The empirical equation developed by the Basin Authority of the Magra River and obtained by a regionalisation of flow discharges at the catchment scale was adopted. It is expressed as:

$$Q_{1.5} = 11.997 \, A^{0.7}$$

where $Q_{1.5}$ (m^3/s) is the discharge with a recurrence interval of 1.5 years, and A (km^2) is the drainage area.

Measurements of the drainage area at the downstream limit of each reach were made using the *Hydrology* toolbox of ArcGIS 10.1 on the 10-m resolution DEM, which includes the use of the *Fill*, *Flow Direction*, *Flow accumulation* and *Watershed* tools.

At a first stage of detail, data were averaged at the reach scale, with reach lengths ranging from 1 to 6.6 km (see the relevant Catchment Case Study in Deliverable 2.1part 3). Channel slope for each reach was measured using topographic maps, under the hypothesis of uniform flow (i.e. assuming the slope of the channel bed equals the slope of the water surface). The active channel width, required to calculate the unit stream power, was calculated using aerial photos collected in 2010, by dividing the active channel area (excluding islands) by the reach length. The results of these analyses are presented in Figure I3.2.

The choice of the distances over which the slope is measured can be a critical task, since the calculated slope is very sensitive to the integration step length. For this reason, at a second level of detail, data were integrated at a finer spatial scale than the length of the reaches. In fact, measuring the slope or slope-dependent parameters over a large distance can mask channel-scale geometric and hydraulic variations. Following the approach of Vocal Ferencevic and Ashmore (2012) the water surface slope was selected as the key parameter for a further division of the original reaches. Starting from the DEM, the main streamflow was firstly identified by the Soil and Water Assessment Tool

(SWAT) in ArcGIS 10.1. Then, the water surface slope was calculated for the following longitudinal distances along the main streamflow: 100, 200, 500, 1000 and 2000 m. The results of this analysis (Figure I3.3), revealed that distances of 100 m and 200 m were too short as they showed peaks in the slope that were dependent on local conditions, while a distance of 2000 m almost completely masked any slope change. Based on these findings, each initial morphological reach was divided into equal parts, here named sub-reaches, having lengths within the range of 500-1000 m. In this way, each sub-reach had homogeneous morphological characteristics and, at the same time, presented a meaningful length for averaging hydraulic parameters.

In Figure I3.4 the spatial distribution of stream power computed at the reach scale is compared to the spatial distribution of stream power obtained by averaging values at the sub-reach scale.
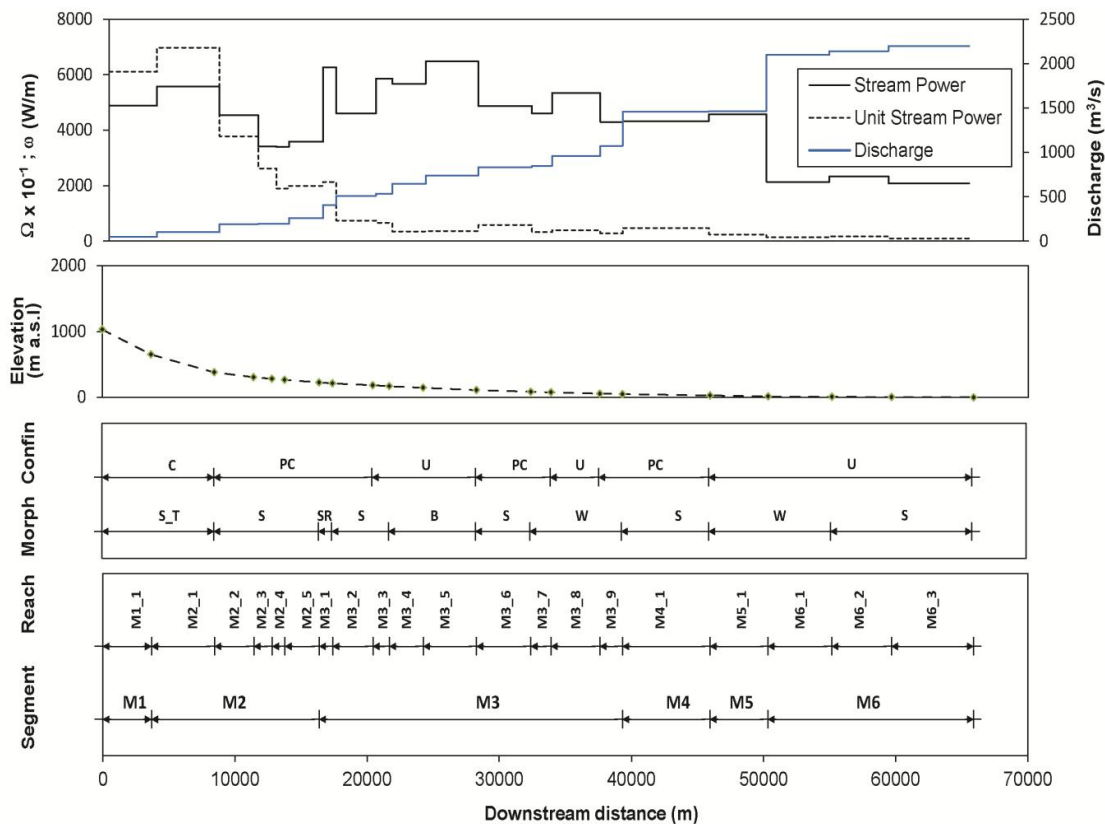
Figure I3.2   Spatial distribution of the total and unit stream power along the Magra river compared to the spatial distribution of channel slope, confinement and morphology.

I3.3 Spatial distribution of the hydraulic variables along the Magra River

Doyle et al. (2000) demonstrated that purely quantitative assessment methods, aiming to define the sediment flux in a reach or basin using measures of shear stress or stream power, were significantly better at predicting channel stability and instability than

qualitative assessments (Vocal Ferencevic and Ashmore, 2012). For this reason, besides the total and unit stream power, additional hydraulic variables were computed using the 1D model HEC-RAS and performing steady flow analysis for different discharges. The geometry used for this analysis is represented by topographic cross sections that were surveyed in 1990. More recent geometry was not available. Furthermore, due to the inability of LiDAR to detect submerged areas, Lidar-DEM data from 2008 could not be used for the modelling.

Different discharges were considered: the mean, the bankfull and the overbank flow discharge. As mentioned above, Q1.5 was taken as the bankfull discharge, whereas Q10 was taken as the overbank flow, being recognised in the geomorphology literature as a useful flow for channel form as well as floodplain inundation in rivers with highly variable flows.
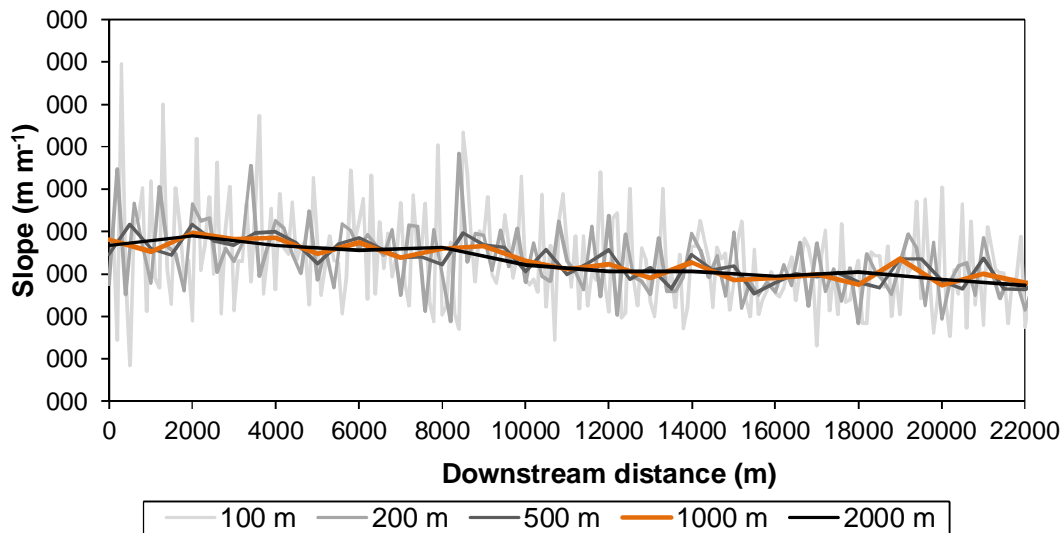
Figure 13.3 Slope profiles computed using different distances.
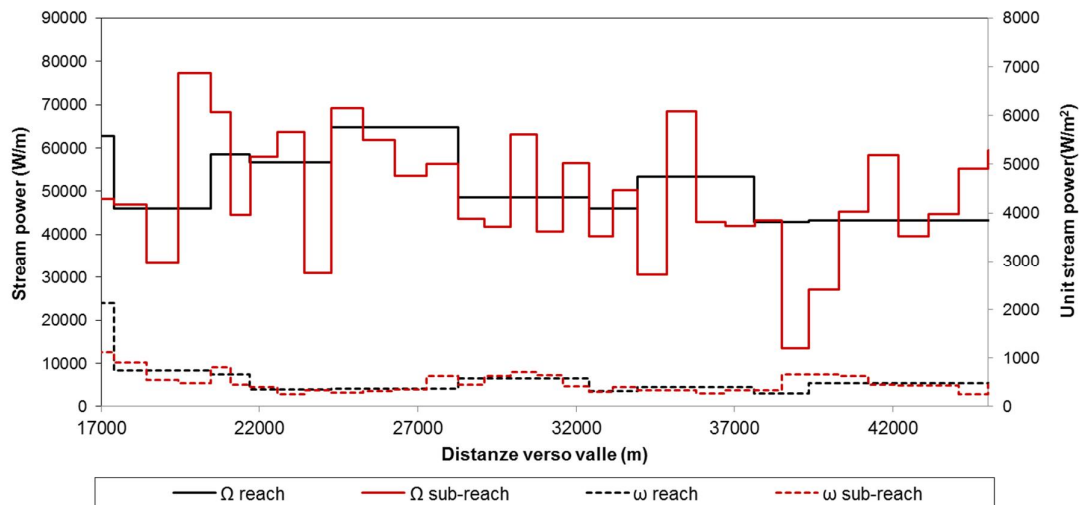
Figure 13.4 Comparison of the total and unit stream power computed at different spatial scale.
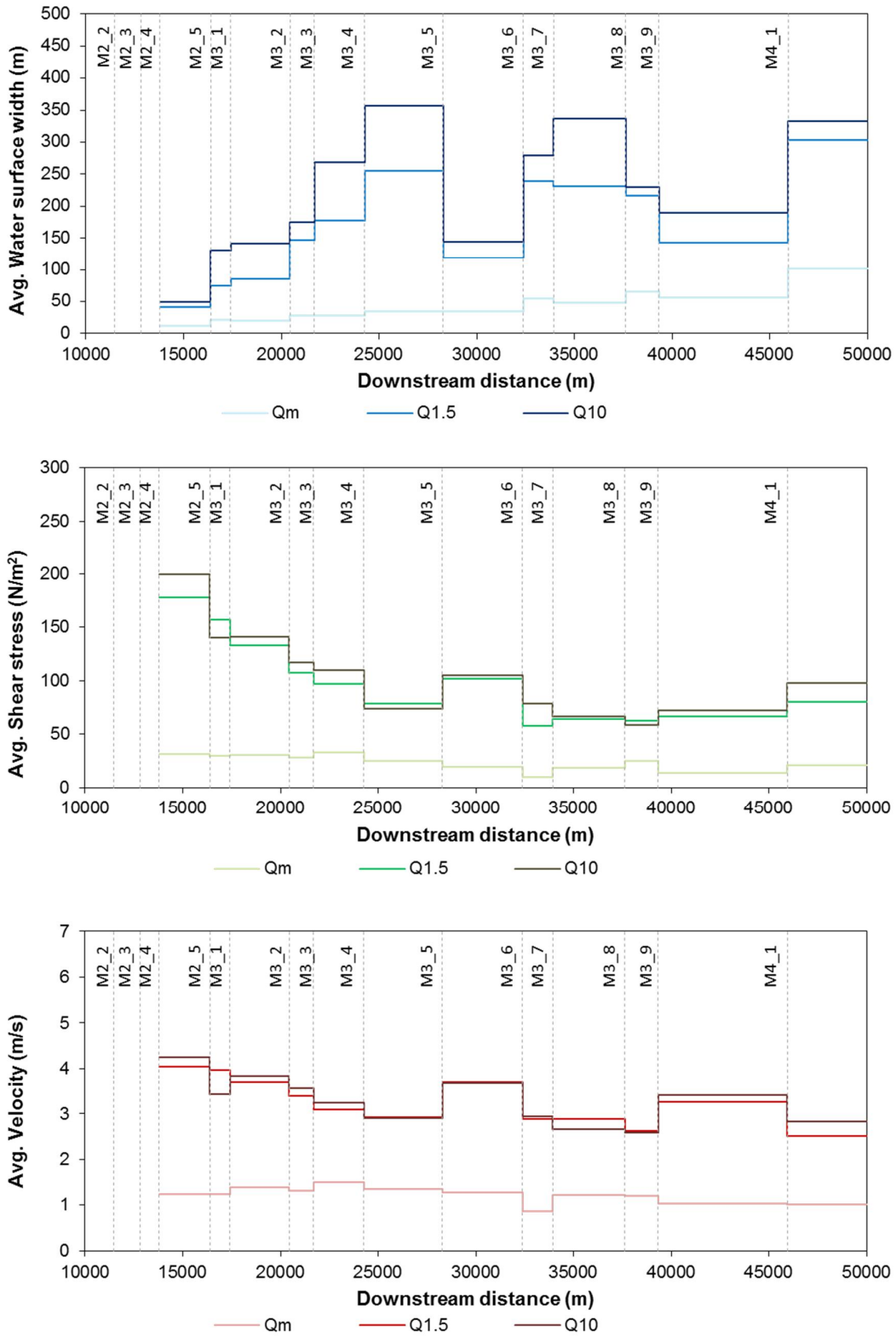
Figure I3.5   Results of the 1D modelling. Data are averaged at the reach scale.
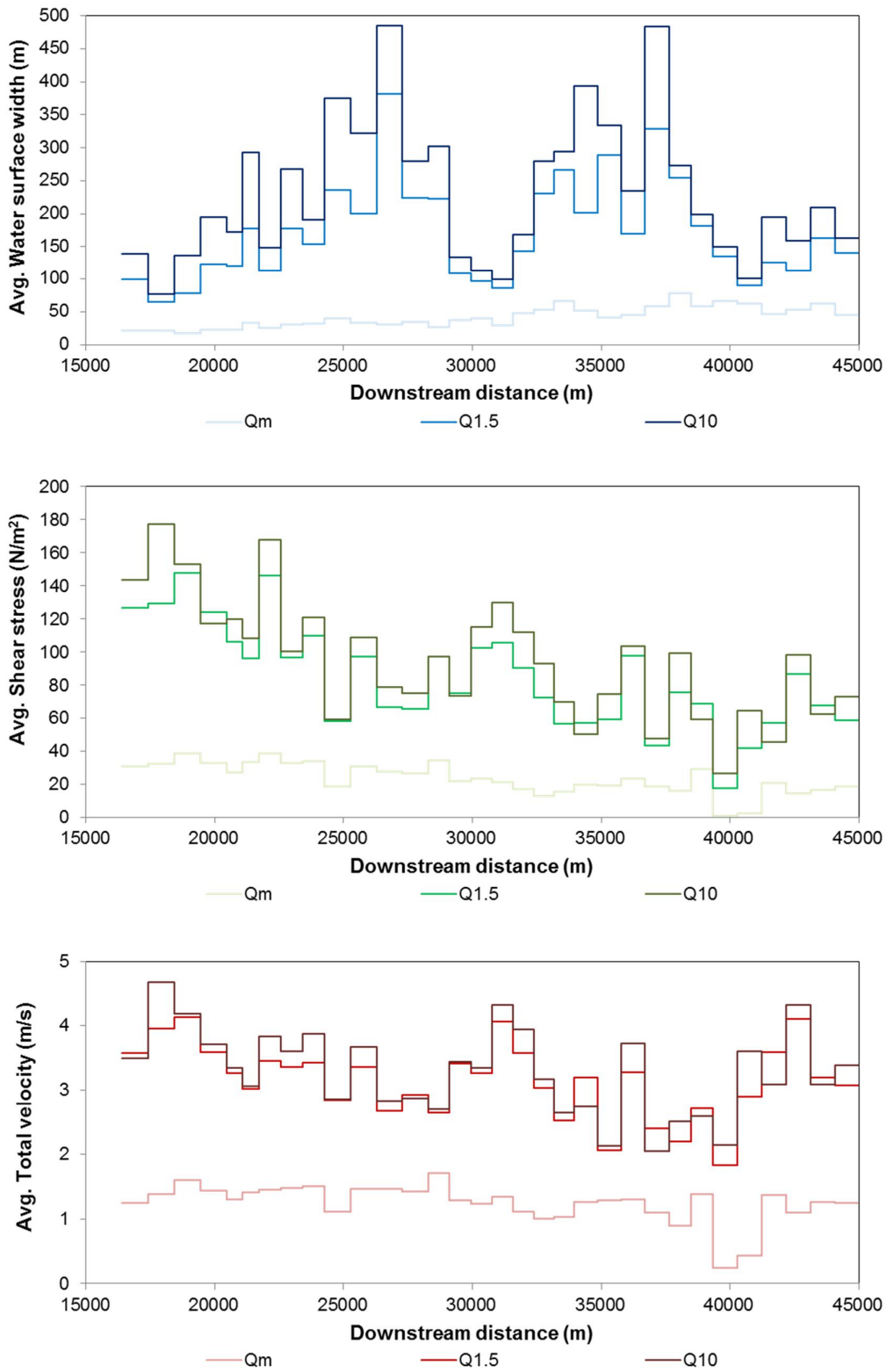
Figure I3.6 Results of the 1D modelling. Data are averaged at the sub-reach scale.
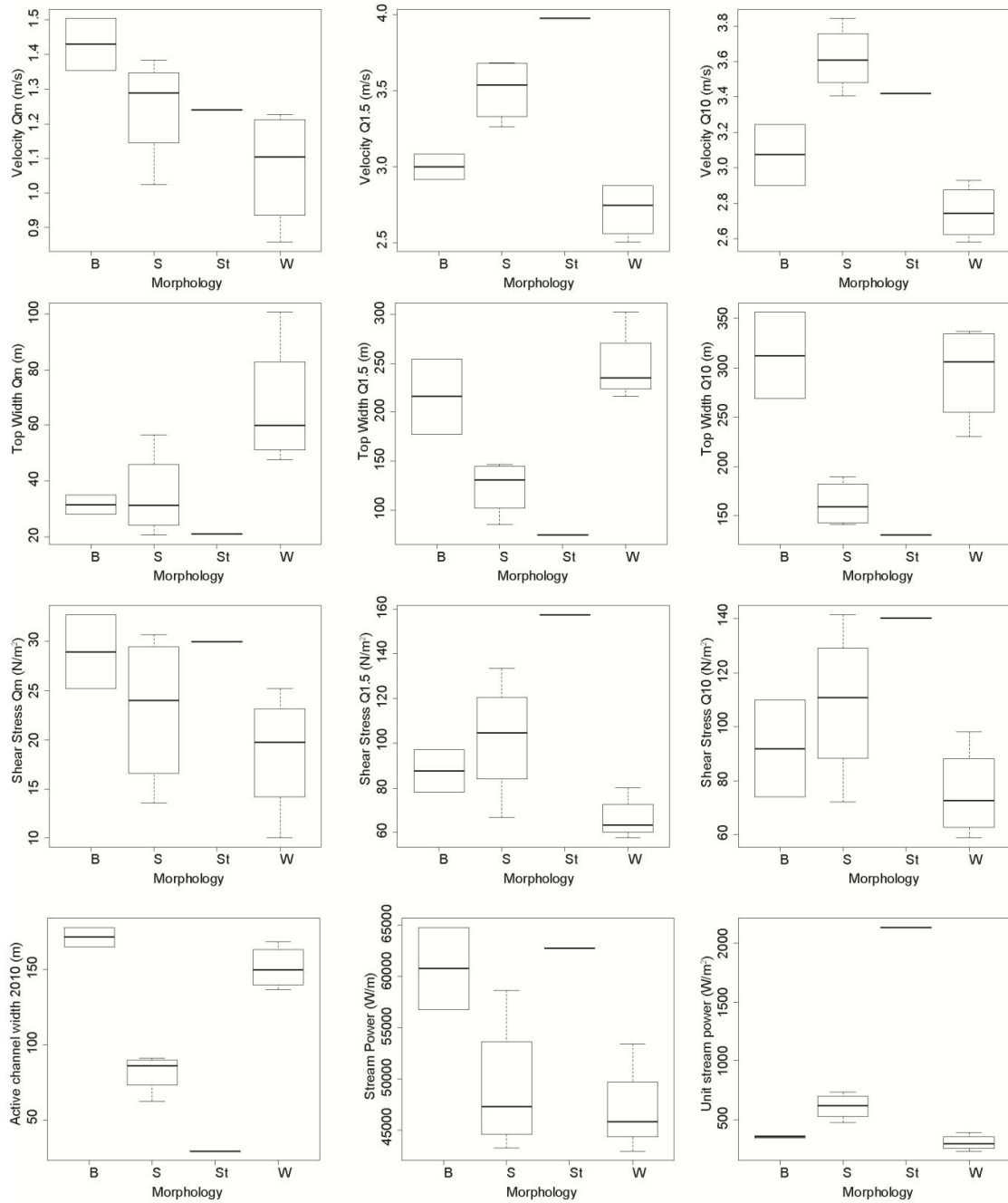
Figure I3.7 Ranges of hydraulic parameters averaged at the reach scale in relation to channel morphology.
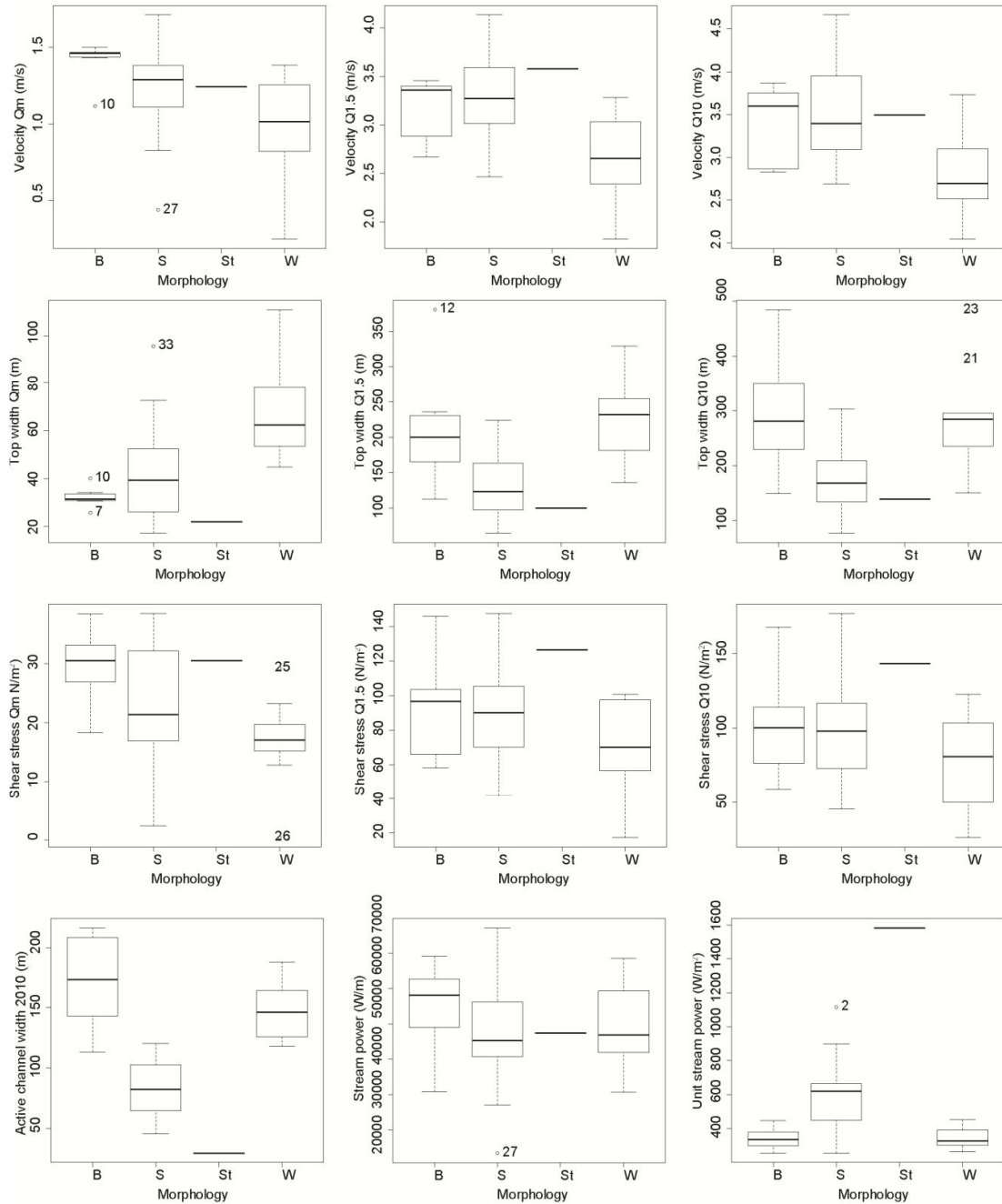
Figure I3.8 Ranges of hydraulic parameters averaged at the sub-reach scale in relation to channel morphology.

Similarly to the analyses of the stream power, the hydraulic variables resulting from the modelling were averaged according to two different data aggregations: the reach and the sub-reach scale. Results of these analyses, which are summarized in Figures I3.5 and I3.6, show a decreasing trend in the average bed shear stress with distance downstream,

mirroring the longitudinal pattern in channel gradient, whereas the average width of the water surface reflects the average active channel width.

Aiming at better understanding of the relationship among hydraulic variables, total and unit stream power, and the different channel patterns, results of the modelling were aggregated based on the channel morphologies. Box plots in Figures I3.7 and I3.8 indicate that aggregating data according to the channel morphology and using different integration step lengths for hydraulic parameters may provide different results. This especially occurs with increasing discharge. For instance, in the case of Q_m, the velocity of braided morphology obtained by averaging at the reach and sub-reach scale is the highest compared to the velocities of the other channel morphologies. This is due to the narrowest water surface width being related to the discharge Q_m. Looking at the results of Q_{10}, it is possible to observe that the distribution of velocities varies by averaging the velocity at the two spatial scale. In fact, at the reach scale, the sinuous morphology exhibits the highest velocity, whereas averaging at the sub-reach scale, higher velocities are reached by braided channels. These outcomes confirm the importance of selecting a proper integration step length for the interpretation of modelling results with the purpose of understanding condition and functioning of the river system.

I3.4 References

Alber A, Piégay H. 2011. Spatial disaggregation and aggregation procedures for characterizing fluvial features at the network-scale: Application to the Rhône basin (France). Geomorphology 125: 343-360.

Barker DM, Lawler DM, Knight DW, Morris DG, Davies HN, Stewart EJ. 2009. Longitudinal distributions of river flood power: the Combined Automated Flood, Elevation and Stream power (CAFES) methodology. Earth Surface Processes and Landforms 34: 280–290.

Bull WB. 1979. Threshold of critical power in streams. Geological Society of America Bulletin 90: 453-464.

Eaton BC, Church M. 2011. A rational sediment transport scaling relation based on dimensionless stream power. Earth Surface Processes and Landforms 36: 901–910.

Eaton BC, Millar RG, Davidson S. 2010. Channel patterns: braided, anabranching, and single-thread.Geomorphology 120: 353–364.

Fonstad MA. 2003) Spatial variation in the power of mountain streams in the Sangre de Cristo Mountains, New Mexico. Geomorphology 55: 75-96.

Knighton AD. 1999. Downstream variation in stream power. Geomorphology 29: 293-306.

Lawler DM. 1992. Process dominance in bank erosion systems. In: Carling PA, Petts GE. (Eds.), Lowland Floodplain Rivers: Geomorphological Perspectives, Wiley, 117-143.

Nanson GC, Croke JC. 1992. A genetic classification of floodplains. Geomorphology 4: 459-486.

Rhoads BL. (1987). Stream power terminology. The Professional Geographer 39: 189–195.

Thorne CR, Wallerstein NP, Soar PJ, Brookes A, Wishart D, Biedenharn DS, Gibson SA, Little CD, Mooney DM, Watson CC, Green APE, Coulthard TJ, Van de Wiel MJ. 2011. Accounting for sediment in flood risk management. In Pender G, Faulkner H. (Eds.). Flood Risk Science and Management, Wiley-Blackwell, Chichester, 87–113.

Vocal Ferencevic MV, Ashmore P. 2011. Creating and evaluating digital elevation model-based stream-power map as a stream assessment tool. River Research and Applications 28: 1394-1416.

Annex I4
Modelling of the Tagliamento River (Italy): prediction of channel morphology and estimation of bedload transport

Luca Ziliani, Nicola Surian

Department of Geosciences, University of Padova, Italy

I4.1 Introduction

Prediction of future channel evolution has several practical implications because it may represent a key tool to guide management strategies. Prediction requires use of models (e.g. conceptual, physical, analytical or numerical models) (Wilcock and Iverson, 2003). Uncertainty associated with any kind of model and with the complexity of fluvial systems, specifically of braided rivers, are major issues to be taken into account. This means that we should be aware that prediction of channel morphology has inherent limitations since results of any model are affected by a degree of uncertainty and braided rivers are very complex systems that exhibit self-organized critical behaviour.

This report deals with modelling carried out on the Tagliamento River (north-eastern Italy), specifically on two segments of the river having a total length of 33 km (Figure I4.1). This large gravel-bed river has undergone notable channel adjustments due to human interventions (i.e. sediment mining and channelization) in the past (Ziliani and Surian, 2012). Channel adjustments are described in the relevant Case Study in Deliverable 2.1 Part 3. The aim of modelling was to explore future channel evolution taking into account different scenarios of sediment supply at catchment and reach scale. Two different modelling approaches were combined to predict channel morphology: (i) a conceptual model based on a historical analysis of channel changes and controlling factors and (ii) numerical modelling, using a reduced complexity model (CAESAR; Coulthard et al., 2007). In this report the main focus is on the numerical modelling. Full details of the modelling applications are reported in Surian and Ziliani (2012) and Ziliani et al. (2013). Therefore, this section provides a brief overview of this work, mainly focussing on the outcomes of the modelling.

I4.2 CAESAR application to the Tagliamento River

A cellular model (CAESAR) was used to predict channel morphology over the period 2001-2081. The approach that was used included the following steps: sensitivity analysis, calibration, validation, and, finally, long-term simulations. This approach allowed us to analyse 12 input factors initially and then to focus calibration only on the factors that the model identified as most important. Sensitivity analysis and calibration were performed on a 7.5 km reach, using a hydrological time series of 20 months.

Validation and long-term simulations on the whole 33 km of the two study segments, were conducted over a period of 8 years (2001 - 2009) and 80 years (2001 - 2081).

The model was applied using constant conditions for flow regime and different conditions (i.e. scenarios) for sediment supply. Flow regime in the period 2000-2010 was replicated several times, assuming no changes in flow regime. As for sediments, several different possible scenarios of management were explored. In two scenarios bed load supply was increased (for instance assuming removal of bank protection structures), in one scenario upstream bed load input was reduced, in the fourth scenario no change in sediment supply was assumed, representing the present condition.
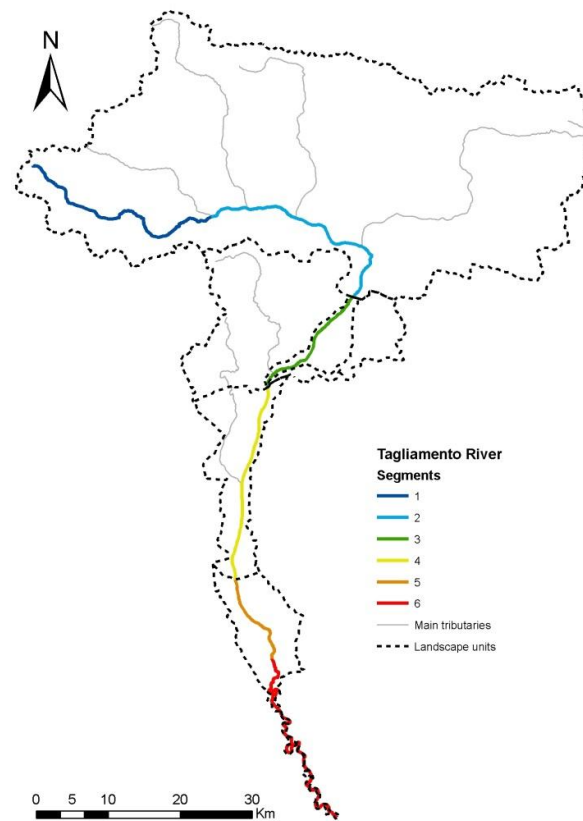
Figure 14.1 The Tagliamento River: identification of landscape units and segments. Modelling was carried out on the whole of segment 4 (yellow) and the upper part of segment 5 (orange).

14.3 Prediction of channel morphology

The numerical modelling showed that channel widening will continue in the future (up to 2080), independently of sediment management strategies (Figure 14.2). As expected, channel width (w) was larger in the scenario (SC) where bank protections were removed (w = 1230 m in SC2) and smaller in the scenario where upstream sediment input was reduced (w = 1130 m in SC4). SC1 (scenario with no interventions) and SC3 (scenario with an increase of upstream sediment input) produced very similar results in terms of

channel width (Figure I4.2), confirming a low influence of upstream sediment input on channel dynamics in the study segments.

There were clearly some differences between the results derived from applying the numerical model and those of the conceptual model, but overall the results can be considered satisfactory. Both models predict that channel widening will continue in the future and the magnitude of widening in the five scenarios is comparable. Besides inherent errors associated with both models (e.g. it is possible that the cellular model underestimated the effect of vegetation growth on channel dynamics), some differences were also due to input data. Specifically, the flow regime of the periods 1993-2009 and 2000-2010 were used as input data for the conceptual and the numerical model, respectively.
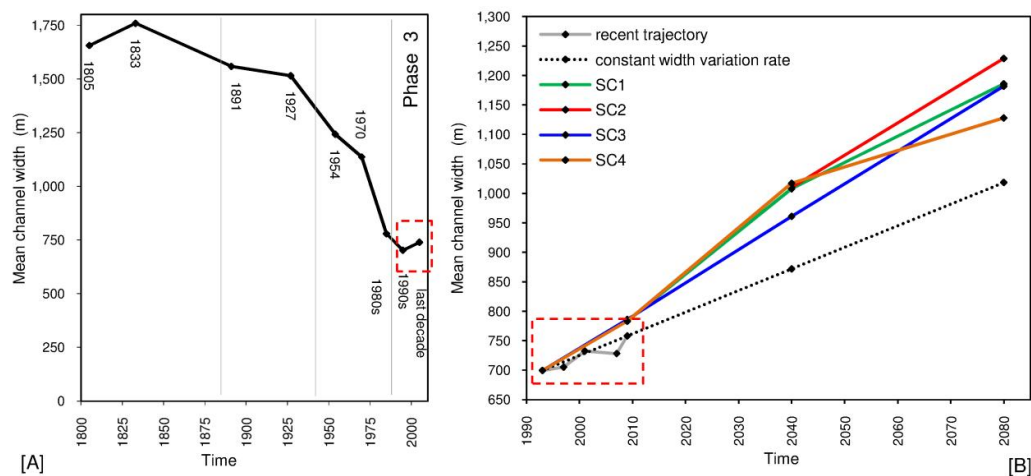
Figure I4.2 (A) Changes in channel width over the period 1805-2009; (B) Prediction of channel width for the period 2009-2080; recent trajectory: channel width measured from aerial photos; constant width variation rate: derived from the conceptual model; SC1, SC2, SC3, SC4: simulations of different scenarios of sediment management using a numerical model (CAESAR), assuming no intervention (SC1), removal of bank protections (SC2), increase of upstream sediment input (SC3), and decrease of upstream sediment input (SC4) (from Surian and Ziliani, 2012).

I4.4 Assessment of sediment transport

In order to integrate the morphological performance evaluations, an estimate of the mean annual bedload sediment yield along the whole of the studied segments was carried out (Figure I4.3). Because field measurements of sediment transport were not available, reference values of sediment transport were derived from other, similar, case studies. At the downstream end, mean annual bedload yields obtained from the two validation runs were 60 x 10^3 and 62 x 10^3m^{3}yr^{-1}, which are comparable to those estimated in other similar rivers. Modeled mean annual sediment yield varied significantly along the study segments (up to 40%), but differences also existed between the maximum and minimum annual sediment transport. The 2005 minimum corresponds to an averaged segment mean annual sediment yield of about 10 x 10^3 m^{3}yr^{-1} in comparison with the 2002 maximum average value of about 200 x 10^3 m^{3}yr^{-1} (Figure

I4.3). Sediment transport values obtained from the model have a very good correspondence with estimates reported by Nicholas (2000) and Griffiths (1979) for the braided Waimakariri River (60 / 310 x $10^3 m^3 yr^{-1}$) which displays morphological characteristics very similar to the Tagliamento River.
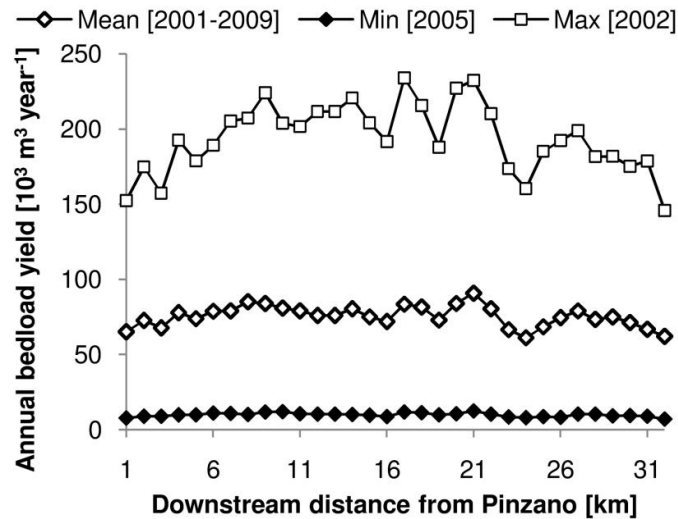
Figure I4.3 Mean, maximum (in 2002) and minimum (in 2005) modeled annual bedload sediment transport estimated for the 2001-2009 period along the whole study segments (from Ziliani et al., 2013).

I4.5 References

Coulthard TJ, Hicks DM, Van De Wiel MJ. 2007. Cellular modelling of river catchments and reaches: advantages, limitations and prospects. Geomorphology 90: 192-207.

Griffiths GA. 1979. Recent sedimentation history of the Waimakariri river, New Zealand. Journal of Hydrology (New Zealand) 18(1): 6-28.

Nicholas AP. 2000. Modelling bedload yield braided gravel bed rivers. Geomorphology 36(1-2): 89-106.

Surian N, Ziliani L. 2012. Prediction of channel morphology in a large braided river. In: Proceedings of the 1st International Conference on Integrative Sciences and Sustainable Development of Rivers (ISRivers 2012), 26-28 June 2012, Lyon, France, pp. 1-3, published on-line
(http://www.graie.org/ISRivers/actes/a_index.htm).

Wilcock PR, Iverson RM. 2003. *Prediction in geomorphology.* In: Wilcock PR, Iverson RM. (Eds.) Prediction in geomorphology, Geophysical Monograph 135, American Geophysical Union, 3-11.

Ziliani L, Surian N. 2012. Evolutionary trajectory of channel morphology and controlling factors in a large gravel-bed river. Geomorphology 173-174: 104-117.

Ziliani L, Surian N, Coulthard TJ, Tarantola S. 2013. Reduced-complexity modeling of braided rivers: Assessing model performance by sensitivity analysis, calibration, and validation. Journal of Geophysical Research: Earth Surface 118: 2243-2262.

Annex I5
Sediment transport and bed evolution modelling: application to the middle Loire river

Audrey Latapie and Benoît Camenen
Irstea, Lyon, France

I5.1   Methodology

The methodology proposed here to study sediment dynamics along several reaches of the Middle Loire River is based on 1D modelling.

I5.1.1   1D modelling

The one dimensional hydraulic and bed-evolution model RubarBE, developed by Irstea (El Kadi Abderrezzak and Paquier, 2009), was used for this study. The model allows the consideration of two roughness coefficients: one for the main channel ($K_{mc} \approx 30$ m$^{1/3}$/s for our case) and one for the floodplain ($K_{fp} \approx 15$ m$^{1/3}$/s for our case).

Adjustments to the resistance coefficient were made locally in order to obtain a good reproduction of the measured water levels that were available. Once calibrated, the model can be run for a succession of steady discharges from low flows to extreme events.

Bed evolution is computed using the mass conservation equation (or Exner equation), which in 1D reads:

$$(1-p)\frac{\partial S_s}{\partial t} + \frac{\partial Q_s}{\partial x} = q_{s,lat}$$
Equation 1

where p is the porosity of the bed, $S_s = B_a Z_b$ the solid section (B_a: active width and Z_b bottom level), Q_s the solid discharge and $q_{s,lat}$ the lateral sediment input. Q_s is generally calculated using capacity formula such as those suggested by Meyer-Peter and Muller (1948) or Camenen and Larson (2005). However, the equilibrium state may not be immediate. We used the non-equilibrium model of Daubert and Lebreton (1967):

$$\frac{\partial Q_s}{\partial x} = \frac{Q_{s*} - Q_s}{L_a}$$
Equation 2

where Q_{s*} is the sediment transport capacity and L_a the adaptation length. If $\frac{\partial Q_s}{\partial x} = \frac{Q_{s*} - Q_s}{L_a}$ **Equation 2**

has a scientific meaning and L_a is generally assumed small for bedload regime (Phillips & Sutherland, 1989), it is often used in 1D modelling as a diffusion term including effects not included in the model due to the relatively loose description of the geometry. As a consequence, much larger values are often used in 1D modelling (Wu et al., 2000).

Another very important aspect in 1D bed-evolution modelling is the way in whih the river sections are modified. A 1D model computes a mass of sediment eroded or deposited for each reach. The way in which this mass is distributed throughout the river reach will

significantly influence the results. Generally, a symmetric option is used; i.e. the same repartition is assumed for both erosion and deposition and this repartition is often assumed proportional to the bed shear stress or water depth. However, for some energetic systems, one can assume that sediment is mainly eroded in the middle of the section and deposited on the sides of the river (Latapie, 2011).

I5.1.2   Simplification of the geometry

Using the results from the delineation (see section I2) and in order to improve the efficiency of the numerical computation, a simplification of the geometry is proposed. For each homogeneous reach, a smooth geometry is built such that the main hydraulic parameters are preserved whatever the discharge. The approach consists of creating a symmetrical section which maintains the river width whatever the discharge in comparison to the original geometry (see Figure I5.1). For each discharge Q, water depths H are adjusted following the Manning-Strickler law:

$$Q = K \frac{S^{5/3}}{P^{2/3}} \sqrt{J} \qquad\qquad \text{Equation 3}$$

with K representing the Strickler coefficient, S the wetted area, P the wetted perimeter, and J the energy slope. If the computation is made with n discharges (or n water lines), it results in a section described by $2n$ points (see Figure I5.1).
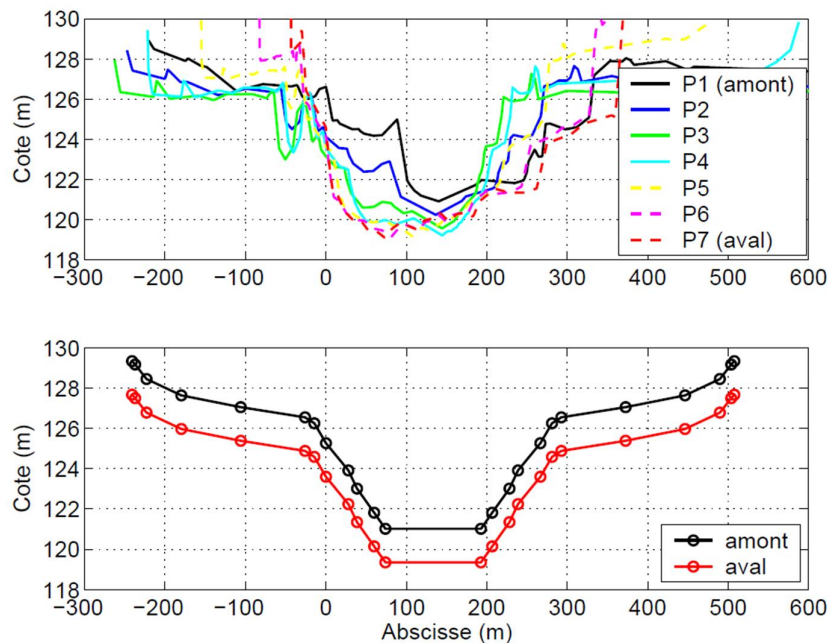
Figure I5.1 Example of simplified geometry for a reach using n=12 water lines.

I5.2   Studied cases

I5.2.1   Middle Loire River

The reaches studied are located on the Middle Loire, France (See Figure I5.1), which extends from the confluence with the Allier River to the confluence with the Maine River. The length of the Middle Loire river is about 450 km. The three reference sites detailed in this document are:

- Belleville
- Guilly
- Bréhémont

The Belleville reference site is 37 km long, from Myennes (PK 526.8) to the hydrometric station of Gien (PK 564.0). It is an anthropogenic reach, which includes the nuclear power plant of Belleville, four bridges, a navigation channel, and several islands. This segment contains 14 homogeneous sub-reaches (see section I2).

The Guilly reference site is 25 km long, from St-Père-sur-Loire (PK 590.5) to St-Denis-de-l'Hotel (PK 616.5). It is the only reach of the Middle Loire River with meanders (see photo Figure I5.2) and it contains 11 homogeneous sub-reaches (see section I2). Despite the low level of human disturbance, there are four old sediment mining sites.

The Bréhémont reference site is 13km long, starting at the hydrometric station at Langeais (PK 782.0) and extending to La Chapelle-sur-Loire (PK 795.0). It contains four homogeneous sub-reaches (see section I2). It is characterized by the presence of three secondary channels, which contain flowing water during flood periods. This site has been particularly studied by Rodrigues (2004) and Claude (2012).
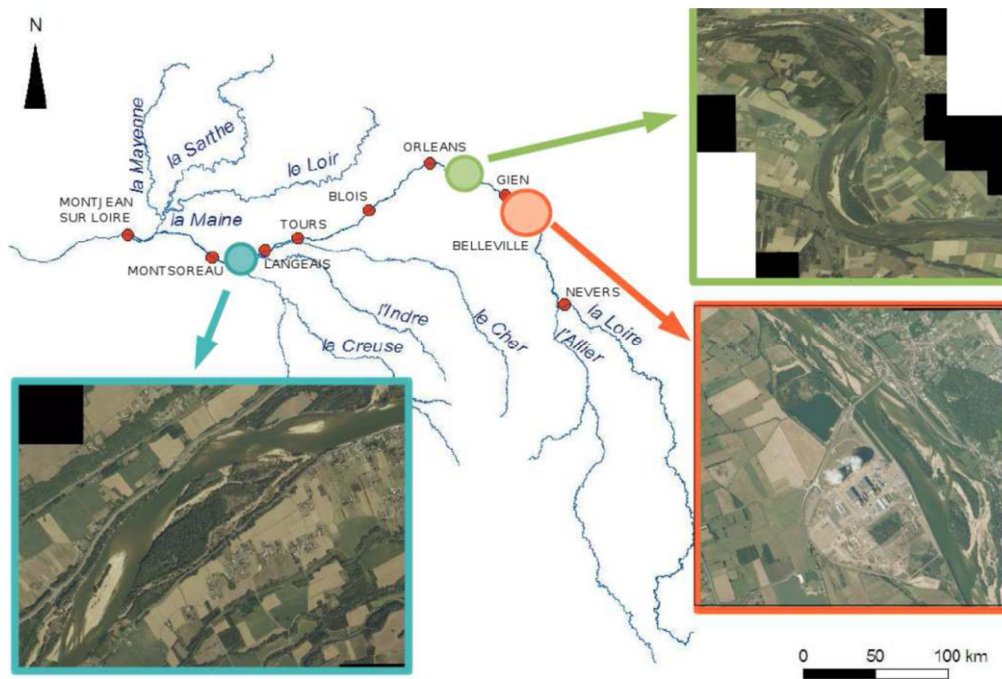
Figure I5.2   Location map showing the three different study reaches.

I5.2.2   Data

(i) Topographic and bathymetric data
The regional environment agency (DREAL Centre) have regularly monitored two hundred sites to record water levels at low and high flows since 1978. Aerial photographs taken during low flow conditions are available for 1955, 1984, 1995, 2002 and 2010. A topographic survey of the Middle Loire River was undertaken in 1995. Cross sections, surveyed every 2 km on average, cover the main channel and can be extended using floodplain data extracted from Lidar data collected in 2003. These data have allowed the determination of geomorphic characteristics and the construction of a hydraulic model.

(ii) Sediment data

Only a small amount of data is available for the description of the sediment grain size in the main channel. A downstream fining exponential law in the form of the Sternberg (1875) formulation was adopted and fitted to these data (see section I2):

$$d_{50} = 4.4 \times 10^{-3} \exp(-4.65 \times 10^{-6} x)$$
Equation 4

Belleville. Bouchard & Courivaud (2000) found the following grain size characterictics based on samples collected during the construction of the nuclear power plant: d_{50} = 1.9 mm and σ=8 (standard deviation). These value are however smaller than those observed by Babonaux (1970) at Cosnes-sur-Loire (d_{50} = 3,9 mm). Both of these observations are however consistent with the variability observed. Following the exponential law (equation 4), we used d_{50} =3.1 mm.
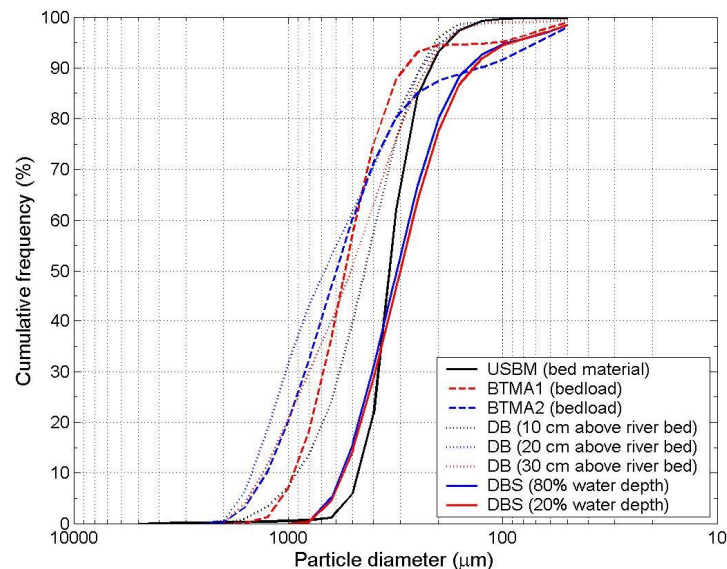
Figure I5.3 Evolution of the sediment size in one vertical (fraction less than 40 microns was eliminated). USBM-54 = bed material, BTMA = bedload, DB = Delft Bottle with indicative location of measure above river bed and DBS = Delft Bottle Surface with indicative location along the water column (data compiled by the University of Tours; Gautier, 2007).

Guilly. This site is poorly described, with a series of cross-section made only in 1995 and 2008 and nearly no sediment description. Again, we used equation 4 for estimating d_{50}=2.3 mm.

Bréhémont. Many sediment transport measurements have been achieved around this site (Gautier et al., 2008; Claude et al., 2012). Figure I5.3 presents some grain size analyses of samples collected during bedload and suspended load sampling campaigns. Rodrigues (2004), Gautier etal. (2008), and Claude et al., (2012) observed a significant tranversal and longitudinal variation of the median grain size. In the main channel, it was observed to be around 1mm, which is coherent with the results from equation 4 (d_{50}=0.95 mm).

I5.3   Results

In this section, we present some results obtained by Latapie (2011) for the three reference sites.

I5.3.1   Influence of the sediment repartition

Before talking about the final results from the three reference sites, it is important to have in mind the influence of the sediment repartition on the section bed evolution. In Figure I5.4 some typical results are presented for different hypotheses concerning deposition repartition. While these options do not affect significantly the average bed level evolution (in the short term), they significantly affect the thalweg evolution. Indeed, assuming horizontal layers for the deposition (pink line in Figures I5.4 and I5.5) results in a filling of the main channel, whereas adopting the option for which sediments are deposited in zones where bed shear stresses are low results an overestimated erosion of the main channel and overestimation of the deposition in the side of the channel (blue line in Figures I5.4 and I5.5).

I5.3.2   Results obtained for the different reference sites

In order to be coherent, all the results below are presented in the form of a sediment budget for all homogeneous reaches describing the different reference sites.

Belleville. The Belleville reference site is described by 11 homogeneous reaches (tronçon in French) but only 8 were used for the comparison of the modelling period. The modelling was achieved for a 2 year-period from November 1996 to November 1998, which included two large floods in December 1996 and April 1998 (Q_{pic} = 1700 m^3/s and Q_{pic} = 2100 m^3/s, respectively) .

As discussed above, the final results are clearly influenced by the hypotheses concerning the repartition of the deposited or eroded sediment. The option that yields the best results compared with the measurements (mesures in French) corresponds to a non-symmetric option for which erosion occurs mainly in the deepest parts and deposition in the shallowest parts (blue line in in Figures I5.4 and I5.5). As a consequence, even though the final description of the cross-section is not very accurate, this option yields the best results in term of the sediment budget for this specific case.
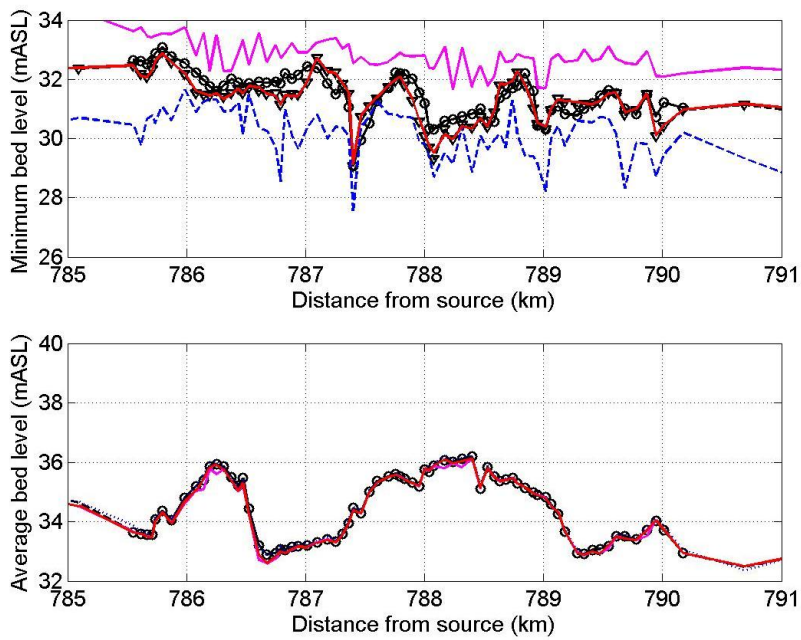
Figure 15.4 Comparison of the measured bed level (triangles for 2000 and circles for 2002) and calculated levels for the period 2000 – 2002 considering : (above) the minimum bed level (i.e. lowest point in the cross section) and (below) the average bed level (i.e. average bed level between the river banks).
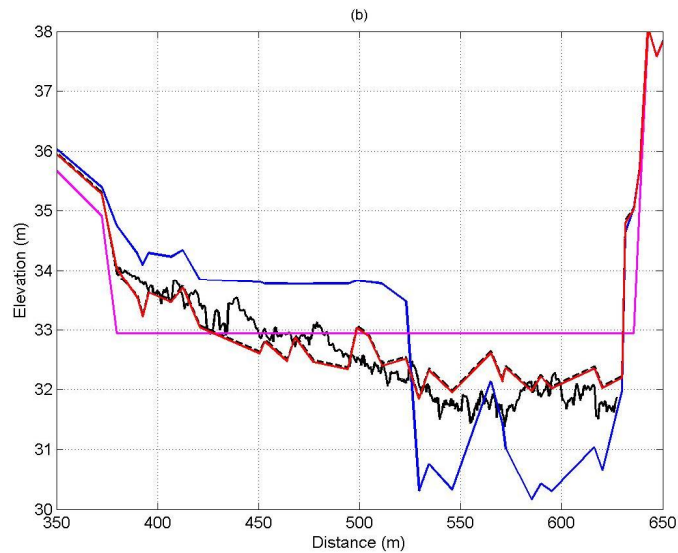
Figure 15.5 Example of cross sections obtained at the end of the calculation (dotted black line : initial bed level and plain black line : measured bed level in 2002).

Several sediment transport formulae were tested and it appeared that the main effect of this choice was the amplitude of the variations but not the general trend of the results.

On the other hand the adaptation length had a significant impact on the final results. If a small value for L_a is used, volumes of sediments deposited or eroded are significantly overestimated and a longitudinal system of erosion/deposition is observed. A much larger value (L_a = 1 km) was eventually used since it provided much better results, especially for the general trend.

The simplified geometry had some effects on the modelling of the anthropogenic Belleville sector. As a consequence, the results were poorer especially in the upstream and downstream boundaries.

A classical approach using the flow duration curve and a direct computation of the volume transported (giving the sediment budget) was also tested. This approach yielded relatively poor results in comparison to the measurements both in terms of the general trend (large erosion observed in reaches 4 and 5 whereas deposition was observed) but also in terms of the volume (two to three times larger whereas volumes tends to be underestimated with the 1D model).
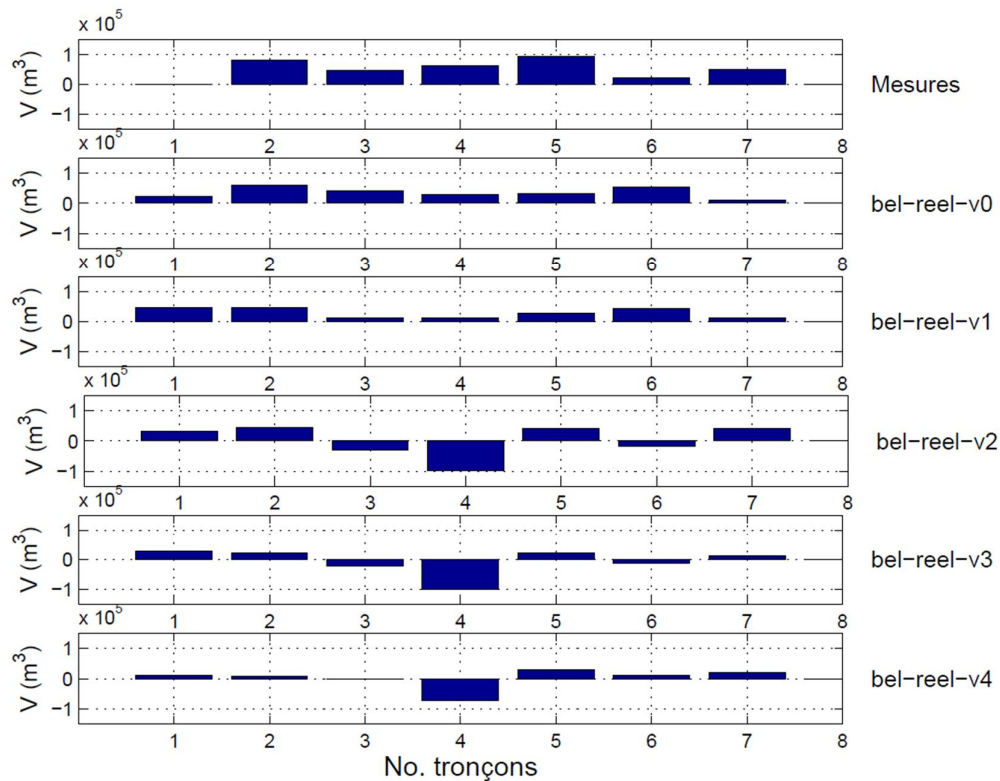
Figure 15.6 Example of different sediment budgets obtained with the 1D modelling for Belleville reference site (option v0 to v4 corresponds to different option for the repartition of the deposits.

Guilly. The sector described by 11 sub-reaches was modelled for the period of 12 years since bathymetric data were available only partially and for two dates (February 1996 to

June 2008). Since bathymetric data were available in 2008 only for a part of the sector, results are presented for 5 reaches only. Moreover, only computations with a simplified geometry were achieved for this sector. Computational results are in agreement with observation: significant erosion is observed in this sector (cf. Figure I5.7).
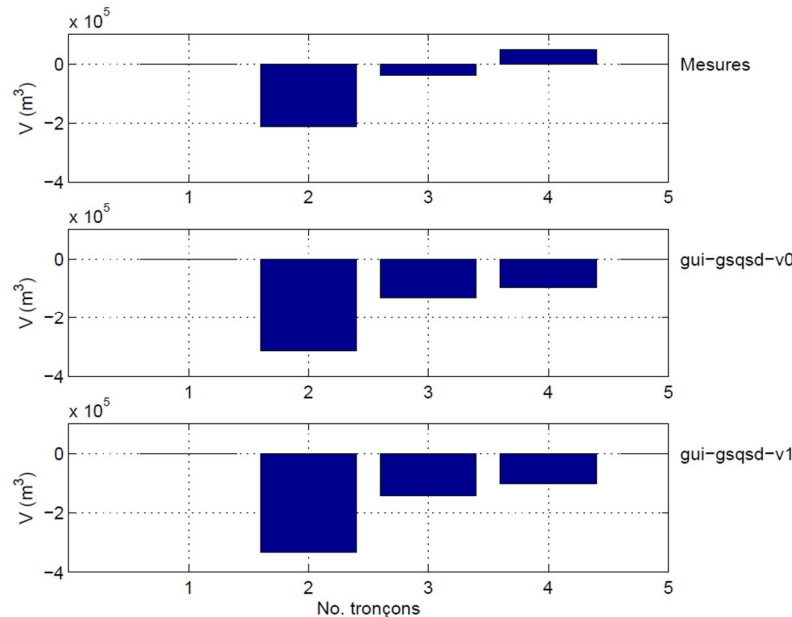
Figure I5.7 Example of different sediment budgets obtained with the 1D modelling for Guilly reference site.

Bréhémont. The Bréhémont reference site is described by 4 homogeneous reaches. The modelling was achieved for a 2 year period from November 2000 to November 2002, which includes one large flood in April 2001 (Q_{pic} = 3000 m^3/s).

Similar conclusions as for the Belleville test case can be made in term of influence of the hypotheses for the erosion and deposition distribution throughout the river section. The option that yields the best results compared to the measurements corresponds to a non-symmetric option for which erosion occurs mainly in the deepest parts and deposition in the shallowest parts (blue line in Figures I5.4 and I5.5). This sector presents a generally dynamical equilibrium apart for one reach where significant deposition is observed (Figure I5.8).

In Figure I5.8, the influence of simplification of the discharge-time series was tested. A critical discharge Q_{cr} = 200 m^3/s was estimated based on the bed shear stress computations at different discharges. The value for Q_{cr} was chosen such that the bed shear always exceeds the critical bed shear stress for inception of movement. As observed by Claude et al. (2012), notable differences could be observed according to whether this critical dischargeis used or not (Figure I5.8) since there still exists some non-negligible residual sediment transport. However, final results remain in agreement with the observations.

Tests with the simplified geometry were not very good although the system is "natural" (no human disturbance apart from the flood protection). The simplified geometry led to a systematic erosion in the two last reaches. One explanation could be the influence of the boundary condition.
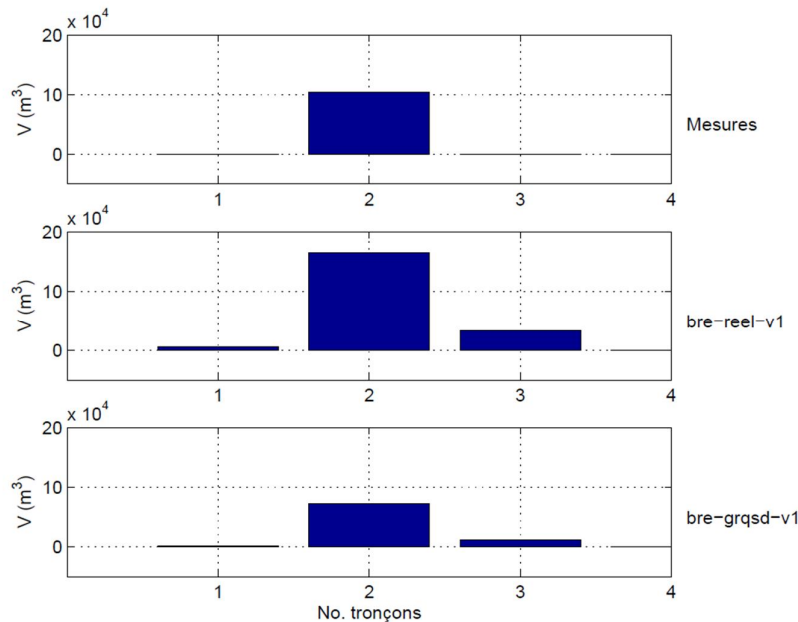
Figure 15.8 Example of different sediment budgets obtained with the 1D modelling for Bréhémont reference site.

15.4   Conclusions

The use of a 1D morphodynamical model is capable of correctly reproducing bed evolution in terms of the sediment budget. It appears however unrealistic to try to reproduce local bed evolution as well, since 2D or 3D effects are important for local bed evolution. On the other hand, the numerical model is very sensitive to several parameters such as the repartition of the deposited or eroded volumes or to the adaptation length. Thus, it is necessary to properly validate a 1D model for the specific study site. Simplified geometric or simplified discharge time-series may be of interest for long-term simulations. However,once more it is necessary to validate these simplifications since they may not always be accurate depending on the river dynamics and type of sediment involved. Such a model also showed that the position of the major floods in the discharge time-series (at the beginning or at the end of the simulation period) significantly affects the final results. As a consequence, any model based on a flow duration curve can only provide rough estimations for the sediment budget.

15.5   References

Babonaux Y. 1970. Le lit de la Loire, Etude hydrodynamique fluviale. Thèse de doctorat, Ministère de l'éducation nationale. Comité des travaux historiques et scientifiques. Mémoires de la Section de géographie. (in French)

Bouchard J, Courivaud J. 2000. Diagnostic morphologique de la Loire à Belleville. Rapport technique, EDF. Rapport EDF HP-73/200/020/A. (in French)

Camenen B, Larson M. 2005. A bedload sediment transport formula for the nearshore Estuarine, Coastal and Shelf Science 63: 249-260

Claude N. 2012. Processus et flux hydro-sédimentaires en rivière sablo-graveleuse : influence de la largeur de section et des bifurcations en Loire moyenne (France) [Hydro-sedimentary processes in a sand-gravel river : influence of the river width and bifurcations in the Loire River(France)]. Université F. Rabelais, Tours.

Claude N, Rodrigues S, Bustillo V, Bréhéret JG, Macaire JJ, Jugé P. 2012. Estimating bedload transport in a large sand gravel river from direct sampling, dune tracking and empirical formulas. Geomorphology 179: 40-57

Daubert A, Lebreton J-C. 1967. Study with a mathematic model on some erosion processes in alluvial rivers for steady and unsteady regimes, in 12th IAHR congress, Fort Collins, Colorado, USA. (in French).

El Kadi Abderrezzak K, Paquier A. 2009. One-dimensional numerical modelling of sediment transport and bed deformation in open channels. Water Resources Research 45: W05404.

Gautier J, Rodrigues S, Peters J, Peeters P, Jugé P. 2008. Transport solide en Loire moyenne lors des crues. Justification des mesures in situ et quantification. *La Houille Blanche* 5 : 71-78 (in French)

Latapie A. 2011. Modélisation de l'évolution morphologique d'un lit alluvial: application à la Loire Moyenne [Modelling the morphological evolution of the Middle Loire River (France)] PhD thesis. F. Rabelais University, Tours.

Meyer-Peter E, Müller R. 1948, Formulas for bed-load transport, in 2nd Meeting of the International Association for Hydraulic Structures Research, IAHR, Stockholm, Sweden, pp. 39–64.

Phillips B, Sutherland A. 1989. Spatial lag effects in bed load sediment transport, J. Hydraulic Res. 27(1): 115–133.

Rodrigues S. 2004. Dynamique sédimentaire et végétation : évolution de chenaux fluviatiles en Loire moyenne (France) [Sediment and vegetation dynamics : evolution of some Middle Loire channels]. PhD thesis, F. Rabelais University, Tours. (in French)

Rodrigues S, Bréhéret JG, Macaire JJ, Moatar F, Nistoran D, Jugé P. 2006. Flow and sediment dynamics in the vegetated secondary channels of an anabranching river: the Loire River (France). Sedimentary Geology 186: 89–109.

Wu W, Rodi W, Wenka T. 2000. 3D numerical modeling of flow and sediment transport in open channel. Journal of. Hydraulic Engineering 126(1): 4–15.

Annex I6
Discussion concerning the sediment dynamics of the lowland River Frome using 1D modelling

Audrey Latapie and Benoît Camenen

Irstea, Lyon, France

Summary

To complement the application of the SIAM model at the network scale (Annex I1), a more detailed 1-D model was constructed for the Frome River (Dorset, UK). The present study gives an indication of the difficulties encountered in building an accurate model when data are missing. Following the methodology, some hydraulic parameters obtained from the 1D model are discussed.

I6.1 Site description

I6.1.1 Location

The river Frome catchment (Dorset, UK) covers an area of 414 km² and extends from the village of Evershot to Poole Harbor (Figure I6.1). The underlying geology of the study area is Cretaceous Chalk. The land use within the catchment is primarily agricultural (mainly grassland and cereals) and the town of Dorchester is the only significant urban area in the catchment.

From Dorchester to Wareham, the river Frome is designated as a Site of Special Scientific Interest (SSSI) due to the important chalk river and lowland, low gradient river habitats it supports. The habitat assessment undertaken in 2009 by Natural England revealed that the SSSI is in unfavourable condition. The reasons for this condition include historical modifications to the physical structure of the river channel, its banks and riparian zone, and the way in which flow is divided between multiple channel sections. These have resulted in a straightened, over deepened channel that has very little geomorphological diversity, uniform flows and enhanced siltation[5].

The SSSI report highlights the presence of in channel structures altering the flow regime and disrupting the downstream transport of sediment (AKA impounding regime). In addition, the river Frome is affected by unsuitable apportionment of flows between different channels by in channel structures.

The present study focuses on a shorter reach (about 14 km) located between Dorchester and Wool, corresponding to the Middle Frome River.

---

[5] Map available online : http://www.natureonthemap.naturalengland.org.uk
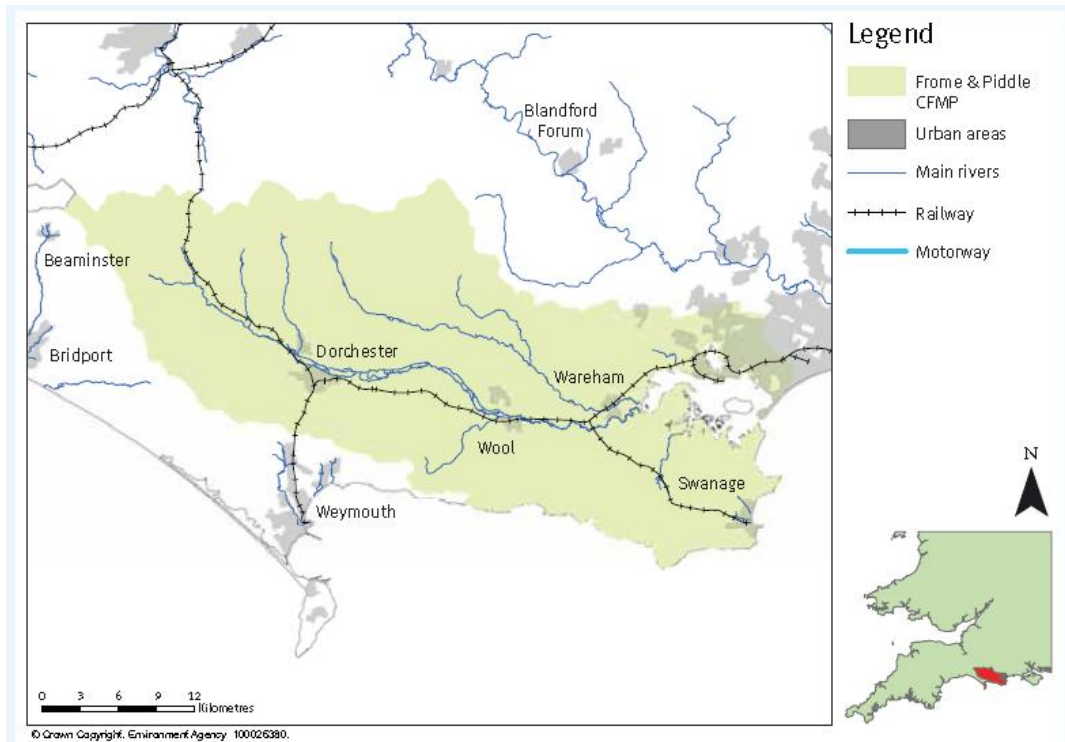
Figure 16.1 Location map of the Frome catchment (source: Environment Agency)
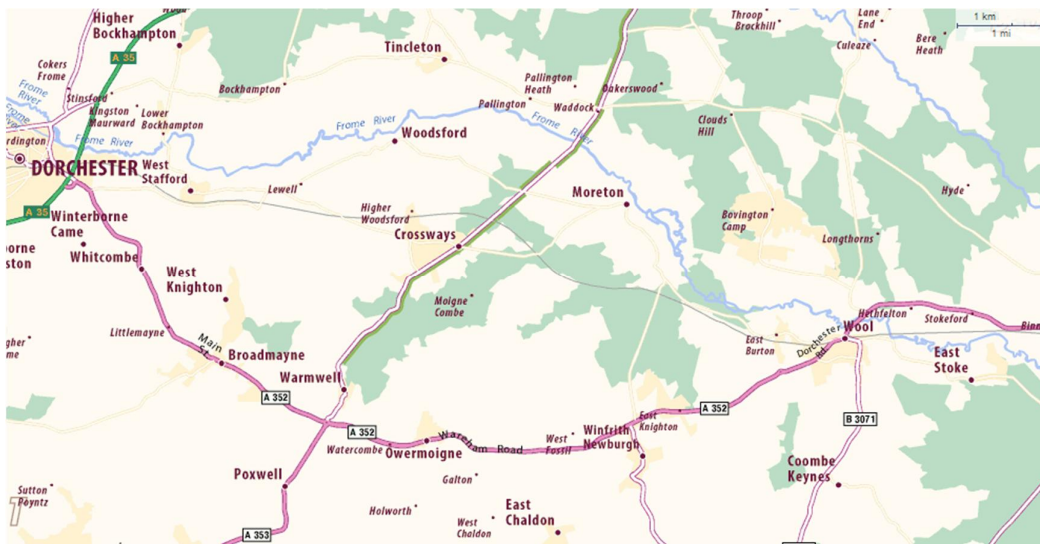
Figure 16.2 Location map of the study site

16.1.2 Flow data

Four gauging stations are located within the study area and are described in Table 16.1 and in Figure 16.3. Around Dorchester, the river Frome is divided into two separate channels, the main channel monitored at Dorchester Louds Mill and the secondary channel monitored at Stinsford. Similarly, two gauging stations are available downstream (East Stoke Flume and East Stoke Weir). Mean Daily Flow and 15 minute flows are available at those gauging stations. No rating curve was provided for these sites.

Dorchester total (http://www.ceh.ac.uk/data/nrfa/data/station.html?44004)

Combined station comprising 3 crump weirs at 2 sites: Louds Mill and Stinsford. Louds Mill has two crump profile weirs, crests 10.66m (side-spilling) and 1.52m broad. Rating includes the side channel and is modular to 10 m^3/s. The Crump profile weir at Stinsford, crest 3.04 m wide, is modular to 4.6 m^3/s but sometimes drowns due to weed growth downstream. At Stinsford the river can inundate the floodplain, and there is potential for significant floodplain flow to bypass both gauges. Minor groundwater abstractions are present in the catchment. The quality of the data at the gauging stations is described as "poor" and is not rated at high flows. Geology is characterized by predominantly chalk, with upper greensand and gault, lias and oolites in the headwaters. The land use is rural.

East Stoke total (http://www.ceh.ac.uk/data/nrfa/data/time_series.html?44001)

Combined station of East Stoke Flume (commissioned 1961): a rectangular critical depth flume, 3.05 m wide, bounded by two broad-crested weirs (local no. 445910), and East Stoke Weir (commissioned 1966), a Crump profile weir on the bypass channel, 3.565 m wide (local no. 445920). Low flood banks have been constructed on the left bank to confine all flows within the designed measuring range of the flume (21.5 m3/s) but significant bypassing occurs over ~12 m^3/s. Gaugings during bypassing have been made at a d/s location where flows are confined. The flume drowns at high flows and low flows due to downstream weed growth. The structure limit of the weir is 4.36 m^3/s. Natural runoff is equal to within 10% at the 95 percentile flow. There are no direct abstractions from river but there are substantial groundwater abstractions from the Chalk. Flows are sometimes affected by u/s research activity. The geology is characterized mainly by chalk, upper greensand and gault, lias and oolites in the headwaters, and sands, gravels and clays in the lower catchment. The land use is rural.

Table 16.1 Gauging stations located along the studied reach

Gauging station	OS location[6]	Drainage area (km²)	Station no.	Q data available
Louds Mill	370821 90353	206	445509 (fishpass) 445510	08/08/2008 to 04/12/2012 01/07/1969 to 03/12/2012
Stinsford	371160 90723		445520	01/10/1971 to 04/12/2012
East Stoke Flume	386727 86839	414.4	445910	01/10/1961 to 04/12/2012
East Stoke Weir	387232 86678		445920	01/10/1965 to 04/12/2012

---

[6] OS locations can be visualize with Streetmap.co.uk
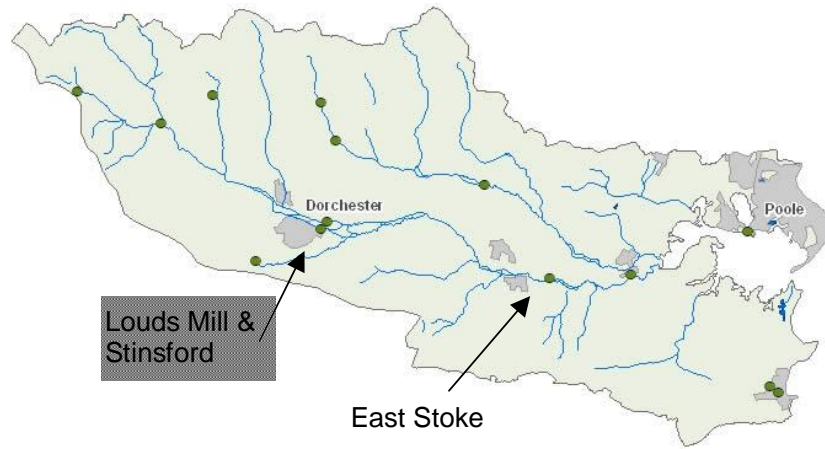
Figure 16.3   Location of the gauging stations used for the study

Time series statistics and flow duration curves, defined for average daily discharge, are detailed in Table 16.2 and in Figure 16.4. It should be noted that the Base Flow Index (BFI) mentioned differs from the baseflow (Q_{base}) used in the following paragraph. The BFI is a measure of the proportion of the river runoff that derives from stored sources (Gustard et al., 1992).

In Figure 16.5, we present a comparison between upstream and downstream discharge time series for the study reach (i.e. Dorchester total and East Stoke total) from 2008 to 2012. It appears that the dynamics for both stations are very similar with an increase in the discharge by a factor 2, approximately. Thus, there is a significant input within the reach that we cannot clearly identify, but is probably mainly attributable to groundwater upwelling through the river bed and banks.

Table 16.2   Time series statistics for Dorchester total and East Stoke total

	Dorchester total	East Stoke total
Period of Record:	1971 - 2011	1965 - 2011
Percent Complete:	95 %	100 %
Base Flow Index:	0.83	0.86
Mean Flow:	3.086 m^3/s	6.592 m^3/s
95% Exceedance	0.883 m^3/s	2.484 m^3/s
70% Exceedance	1.562 m^3/s	3.717 m^3/s
50% Exceedance	2.351 m^3/s	5.262 m^3/s
10% Exceedance	6.131m^3/s	12.47 m^3/s
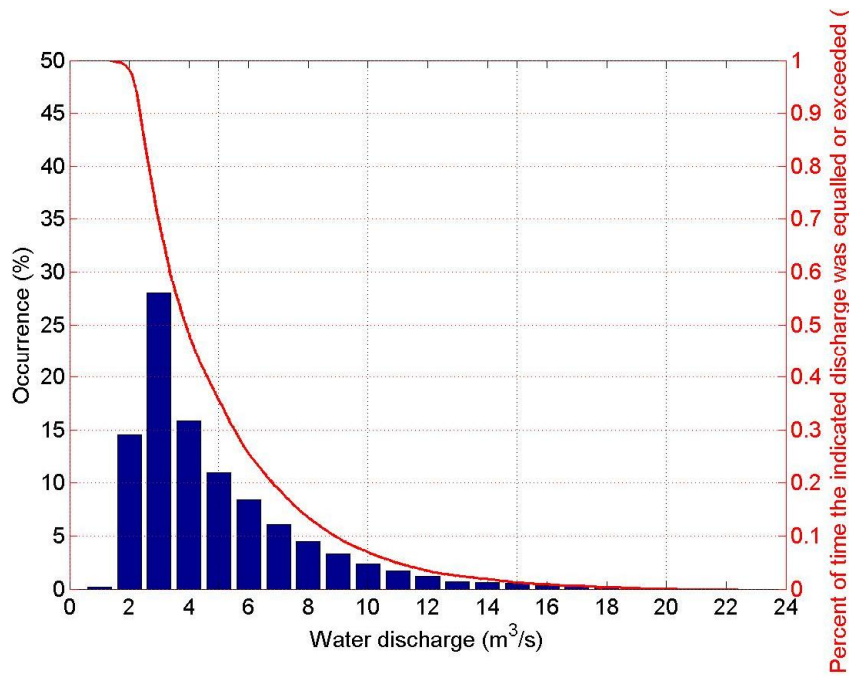
Figure 16.4   Dorchester total – Flow duration curve
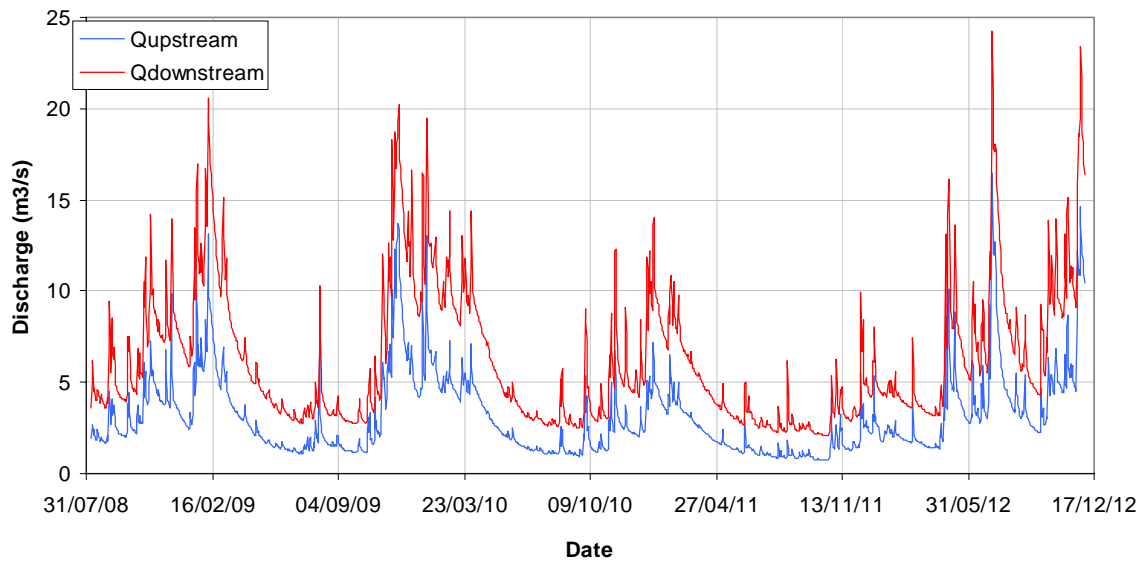
Figure 16.5   Comparison of discharges at Dorchester combined (upstream) and East Stoke combined (downstream) between 2008 and 2012.

16.1.3   Topographic and bathymetric data

Data provided by the Environment Agency (via QMUL) are listed in Table 16.3. The location of all the cross sections provided is illustrated in Figure 16.6. Only some sub-reaches of the study site can be described by the data available.
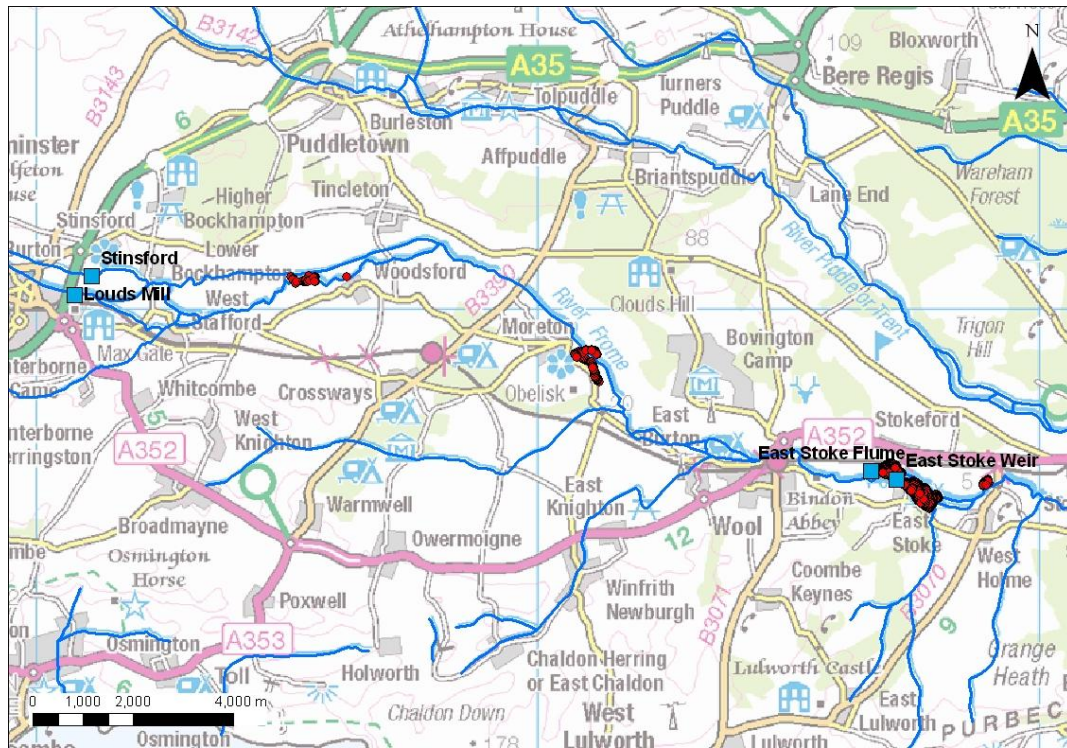
Figure 16.6   Cross sections location between Woodsford and Holme Bridge

Other data were used to complete the model, corresponding mainly to Lidar data and the River Habitat Survey. Details of RHS available on:

http://www.riverhabitatsurvey.org/?page_id=502.

Information on channel dimensions is collected as part of the River Habitat Survey. This was used to complement the model geometry (bankfull width and height, water width and water depth) as well as the valley form, the number of riffles, pools and point bars, the presence of artificial features, channel substrate, bank substrate and profile, and flow type.

There are several channel structures along the reach, which significantly modify the flow dynamics (Table 16.4).

Table I6.3 Cross section data provided by the EA (data highlighted in orange are not geo-referenced and have not been exported in GIS).

EA Job no.	Location	Date of survey	Details
EA111SVY05438	Dorchester		multi-thread river
EA111SVY05514	Dorchester – restoration		multi-thread river
EA111SVY05412 1006286.dwg 12XS and location	Woodsford, 1km D/S of Nine Hatches	July 2009	
EA111SVY05522 1006506.dwg 15 XS and long section 1006507.dwg XS location ISIS model	Moreton to Snelling Farm	08/09/2011	- The River Frome North Channel : From the confluence with the Connecting Channel for 150m downstream (2 Cross Sections). - The River Frome Moreton Channel : From just upstream of the Connecting Channel off-take to just past the weir (5 Cross Sections & 1 Long Section). - The Connecting Channel between the above (5 Cross Sections). - The Duck Pond Channel : From it's start for 75m downstream (3 Cross Sections).
EA111SVY05461 1006361 location 1006362 10 XS 1006363 9XS	Moreton House	20/07/2010	
EA111SVY05460 1006358 1006359	East Stoke Flume to Rushton Farm	July 2010	No XS but x,y,z of bed level... Survey accuracy +/- 50mm
EA111SVY05425 1006298 4 XS 1006233 location	Holme Bridge (just D/S of East Stoke gauging station)	01/09/2009	
EA111SVY05224 Dwg	East Stoke Flume	01/03/2002	Gauging station details (not georeferenced)
EA111SVY05225 Dwg	East Stoke Weir	01/02/2002	Gauging station details (not georeferenced)
EA111SVY05352 2188Y-01.Dwg 2188Y-02 - (3XS) 2188Y-03 – (3XS) pba-eaststoke sw30_estoke_001	East Stoke Flume Easter Floods PBA	Mars 2000	Some levels (not georeferenced) 3XS 3XS gauging station details some levels

Table 16.4 Flow apportionment by in-channel structures within the study reach

Structure	Flow apportionment
Pallington Tilting weir	70-80% retained in the River Frome 20-30% diverted into the North channel
Fixed crest weir near Moreton House	Majority of flow retained in river Frome but a proportion diverted into a floodplain carrier towards north channel
Bovington Tiliting weir	80% retained in north channel 20% diverted into Bovington channel
Water Barn Tilting Weir	60-70% retained in river Frome 30-40% diverted into water Barn channel
Stoney Weir	Divides flow between river Frome and Stoney Weir channel

16.2   Small scale 1D model

16.2.1   Model derivation

Due to the sparsity of the topographic data available, the geometry was defined using multiple sources, i.e., surveyed cross sections data, Lidar data, RHS information. The construction of the model necessitates the definition of the hydraulic axis along which the cross sections can be interpolated. Based on the Lidar data, the main channel was digitized in a GIS environment and points were randomly created along the polyline [Data Management tools → Feature Class → Create Random points]. X,Y coordinates were then attributed and the distance between cross sections was calculated.

For the definitions of cross sections, polylines corresponding to the location of the cross sections were drawn and converted to a point format. Using the Spatial analyst tools → extraction → extract value to points and the lidar data X,Y, Z coordinates were defined and imported in the 1D model.

The model extends from Moreton (Snelling Farm) to Holmebridge, that is a length of about 14 km. As the reach considered presents multiple channels, a multi-reach model was constructed. The RubarBE model is a classic 1D hydraulic model. The description and the notation adopted for the reach are illustrated in Figure 16.7.
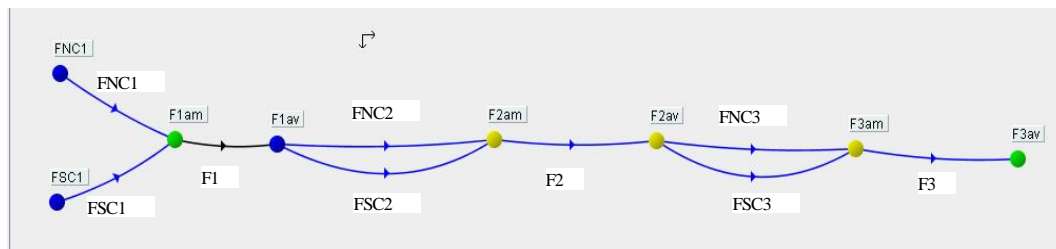
Figure 16.7   Structure of the 1D model

As the reaches considered are relatively narrow (around 10 m on average), the definition of cross sections using lidar data is relatively precise even if the level of the main channel requires to be lowered as lidar data do not describe levels below the water surface.

Adjustments to the levels of the main channel have been defined using the existing cross sections and some interpolations. Comparisons of a surveyed cross section with a cross section extracted from lidar is illustrated in Figure 16.8. Based on this type of comparison the river bed of the main channel was lowered by 0.5 m.
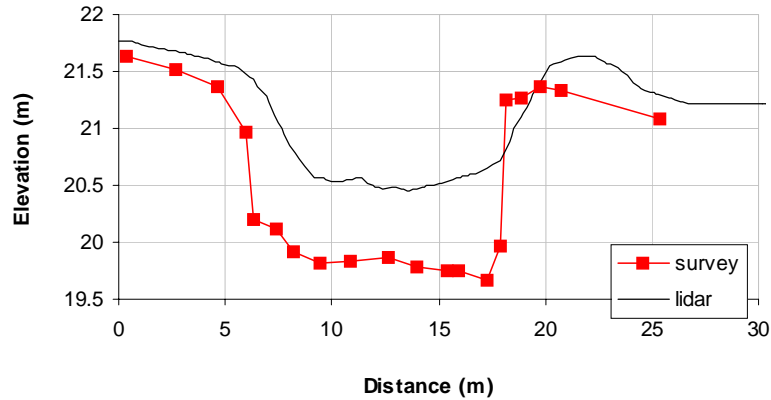
Figure 16.8 Comparison of a surveyed cross section with a lidar interpolated cross section.

16.2.2 Model calibration and validation

Few data are available for calibration and validation; the water levels recorded during the topographic surveys were used for calibration at low flows. and the flood extent provided by the EA for the 1 in 100 year flood was used for calibrating high flows. The discharges corresponding to the 1 in 100 year flood event have been estimated at 19.80 m^3/s at Dorchester (upstream) and 29.50 m^3/s at East Stoke (downstream). Data for calibration are scarce. Only the FSC1 subreach could be calibrated (K_s= 28 $m1^{/3}$/s for the main channel and K_s= 10 $m1^{/3}$/s for the flood plain) although most of the cross-sections were built using the Lidar data and only two relatively low discharges were available for the calibration (Figure 16.9). The river bed of the main channel was locally lowered by 0.35 m.

16.3 Results

16.3.1 Derivation of complementary hydraulic parameters

As detailed previously, the following discharges should be considered at the upstream station (the combined Dorchester station):

Baseflow, Qbase,defined as the flow with the highest occurrence, Q_{base} = 2.4 m^3/s

Approximately bank full Q_{bf} = 15.80 m^3/s (value defined based on the bankfull stage of 0.72 m indicated by CEH)

Approximately 50% of bank full $Q_{0.5bf}$ = 7.9 m^3/s
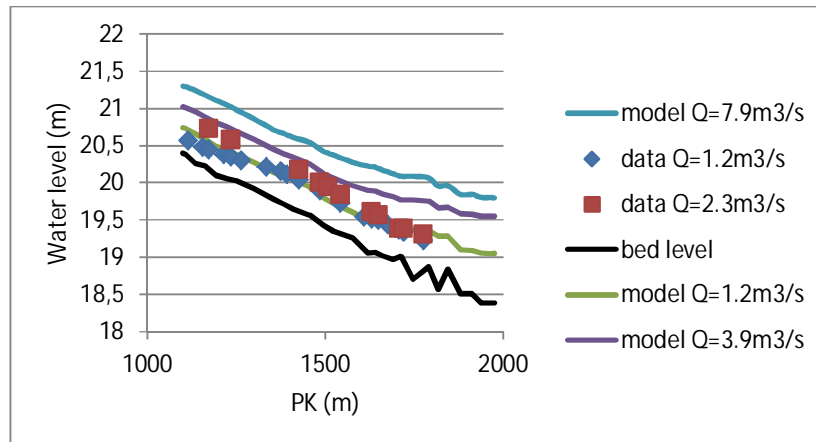
Figure I6.9   Example of calibration (subreach FSC1).

Overbank event Q_T = 20 m³/s

For each discharge specified above, the width over depth ratio (W/D), velocity U, specific stream power ω, and average boundary shear stress τ were extracted from the model or calculated (see Annex I2 for details).

Figure I6.10 shows some typical results obtained for the subreach FNC1. One can clearly observed from these results that the width to depth ratio is not sensitive to the discharge apart for extreme events during which there is overbank flow. Concerning bed shear stress and specific stream power, it appears that the spatial variability is often much higher that the temporal variability for a specific section. One section in particular (PK2900) appears to be very dynamic.

16.3.2   Sediment transport

The results presented in the previous section confirm those obtained with SIAM model (annex I1): sediment transport potentials are low for both sand and gravel. Indeed, the Frome river bed is mainly composed of gravels (d50 ≈ 20mm) with some sand (d ≈ 2mm). The critical bed shear stress for sand particles (d ≈ 2mm) is $\tau_{cr} \approx$ 1N/m² and τ_{cr} ≈ 20N/m² for gravels (Soulsby & Whitehouse, 1997). Based on Figure I6.10, it appears that the sand fraction can be transported even during low flow periods. On the other hand, gravels cannot be transported. Consequently, the potential delivery of coarse sediment to the main channel should result in net sediment deposition. On the other hand, the sand budget clearly depends on the input to the reach. If sand input were absent, it could result in an armouring of the river bed.

16.4   Conclusion

The use of a 1D model could be of interest for estimating hydraulic parameters and sediment transport along a reach. However, this requires a minimum quality for both the bathymetric data to construct the model and the hydraulic data to calibrate it, which were not available for the Frome River.

(a)   (b)

(c)   (d)
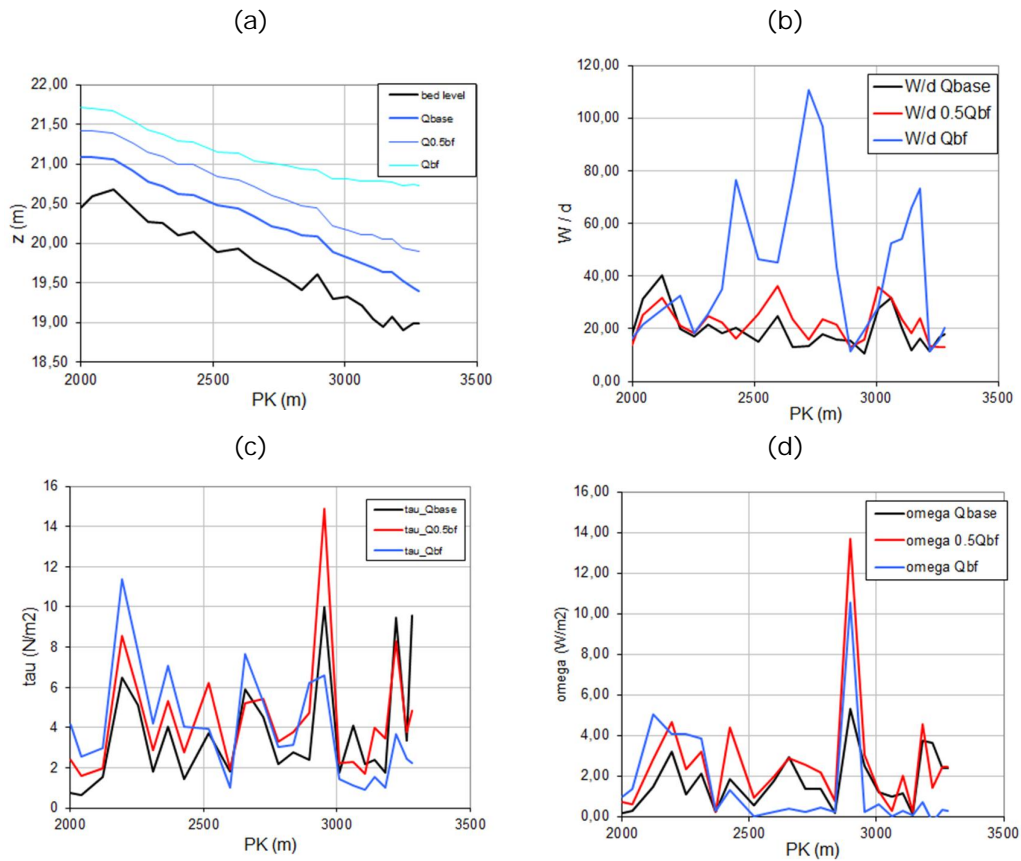
Figure 16.10 Results for the subreach FNC1 including water levels for the base flow, half bank full discharge and overbank discharge (a) and corresponding values for the width to depth ratio *W/d* (b), bed shear stress τ (c) and specific stream power ω (d).

16.5   References

Environment Agency. 2003. River Habitat Survey in Britain and Ireland – Field survey guidance manual (2003 version), 74pp.

Gustard A, Bullock A, Dixon JM. 1992. Low flow estimation in the United Kingdom. Wallingford, Institute of Hydrology, 88pp. (IH Report No.108).

Soulsby RL, Whitehouse RJSW. 1997. Threshold of sediment motion in coastal environment Proc. Pacific Coasts and Ports'97 Conf., University of Canterbury, 149-154.

Annex I7
Application of hydrodynamical and habitat evaluation models to a reach of the Lech River

Bernadette Blamauer and Helmut Habersack
BOKU, Vienna, Austria

Summary

A short reach of the Lech River was modelled using a 1D and a 2D hydrodynamic numerical model and the results were applied in a habitat evaluation model to investigate the impacts of hydro peaking on a braided river.

The simulations showed the typical behavior of braided river sections, a wide floodplain and small water depths. All habitat types were available at low flow and high flow situations, which might be an indicator for a natural river reach.

Further it could be shown that the river type is able to retain peak discharge and thus to decrease the impacts of hydro peaking. However, different outcomes were produced by the application of different models.

This study provides an example of how hydrodynamic modelling coupled with a habitat model can be used for the characterization river reaches and the investigation of different impacts such as hydro peaking.

I7.1 Introduction and objectives

Hydropeaking – artificial discharge peaks generated by the release of water from a storage basin to cover high energy demand (Moog, 1993) – causes alterations of hydrology and morphology and affects the biodiversity of the river (Gostner et al., 2011), for example by reducing biomass (e.g. a relationship between the up/downsurge ratio and the reduction of fish stocks were investigated by Jungwirth et al., 2003) or placing additional stress on fish larvae due to frequent water table fluctuations and thus changes of the wetted area and available habitats.

Important parameters to characterize hydropeaking are the absolute flow change rate (Qmax/Qmin), the frequency, and the rate of change in the rising and falling limb of the hydrograph (ramping velocity - dQ/dt). However, these parameters do not consider the river morphology, and the impacts of a certain flow change rate or ramping velocity might be different within different morphological river channel types. Therefore hydropeaking effects on different river types need to be investigated.

Thus a 1D and a 2D hydrodynamic numerical model, HEC-RAS (1D) and River 2D respectively, were set up for a 2 km long reach of the Lech River, upstream of Johannisbrücke, to gain information on hydrological, hydraulic and geomorphic parameters and to investigate the effects of hydro peaking on a braided river reach and its habitats.

The aims of the study were, therefore, within a braided reach (i) to generate information on hydro-morphological parameters; (ii) to gain insight into the hydropeaking process;

(iii) to investigate the differences of habitat availability at different flow stages, up- and downsurge respectively; and (iv) to show possible applications of a 1D and a 2D hydrodynamical model and a habitat evaluation model.

17.2 Study site

17.2.1 Lech River

The study site is located in the Austrian section of the Lech River (Figure I7.1), upstream of Johannisbrücke in Tyrol.

Figure I7.1 Location of the study site within the Danube River Basin.

The Lech originates from the confluence of several small brooks, close to lake Formarinsee (1880 m a.s.l.) in Vorarlberg. It flows north eastwards through Tyrol and leaves Austria at Weißhaus. In Germany, it flows northwards and enters the Danube at Marxheim. The catchment of the Austrian Lech is located in the Northern Calcareous Alps and experiences a temperate oceanic climate, with a mean annual precipitation of approximately 1760 mm. The topography is mountainous and characterised by steep slopes and elevations above 750 m a.s.l. The land cover is dominated by forest, scrub and herbaceous vegetation, with little or no vegetationin some areas. For further information concerning the entire Lech catchment located in Austria, see relevant Case Study in Deliverable 2.1 Part 3.

The modelled reach of the Lech River, about 2 km in length, is located in Figure I7.1. It comprises a semi-confined, braiding section of the river at about 900 m a.s.l. and with a medium slope of about 7‰.

The fish region is metharhitral and fish fauna are represented by brown trout, bullhead and grayling (Lebensministerium, 2010). Within this part of the river, a Natura 2000 protection area was established to protect rare species such as *Chondrilla chondriioides,*

Myricaria germanica, Typha minima, Cypripedium calceolus, Juniperus communis, Pinus uncinata, Charadrius dubius, Acitis hypoleucos, Bufo calamita, Cottus gobio, Austropotamobius torrentium, and so on (Tiroler-Lech, 2012).
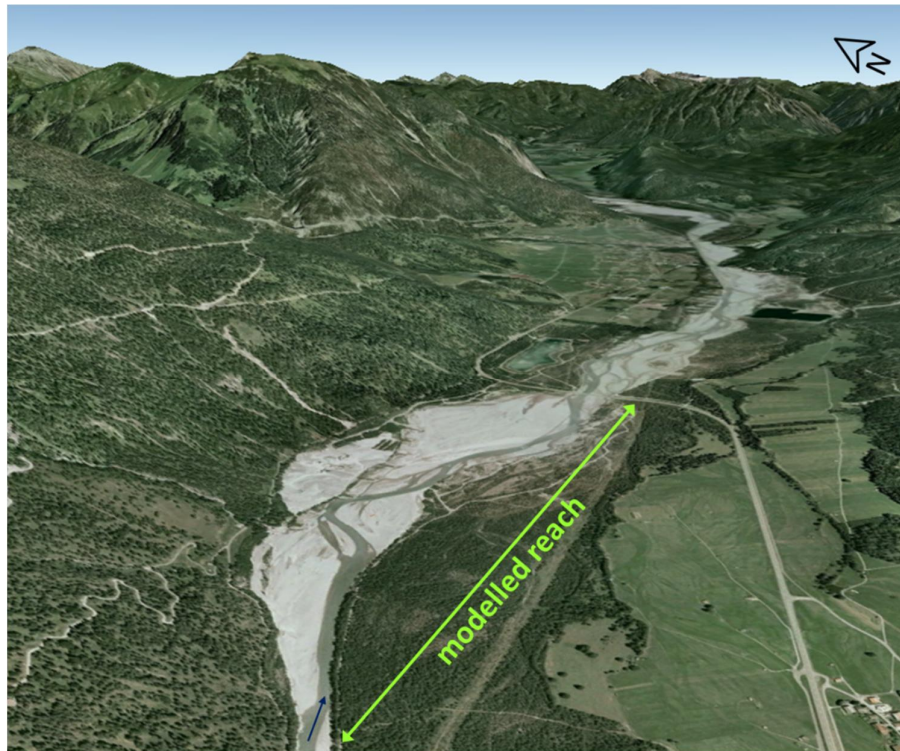
Figure 17.2   Aerial image of the modelled section of the Lech River, upstream of Johannesbrücke (data source: Google Earth 2013)

17.2.2   Hydrology

The hydrological regime of the Lech at the study site is moderate nival and the highest monthly mean discharge occurs in June. The low flow period starts in autumn and ends at the start of spring. During colder seasons, a high percentage of precipitation is stored as snow. With rising temperatures in spring, the snow melts and causes an increase in discharge.

The mean flow within the study site is approximately 32,5 m^3s^{-1}, low flow is approximately 6 m^3s^{-1} and the one year flood is approximately 193,4 m^3s^{-1} (Auer, 2012).

At the investigated section, the flow regime is natural and is not influenced by hydro peaking.

17.2.3   Substrate

The mean grain size of the surface layer of the bed within the investigated reach is approximately 21 mm and the most frequent fraction is medium to coarse gravel. The

grain size distribution and some characteristic values of sampled sediments are presented in Figure I7.3 and Table I7.1, respectively.
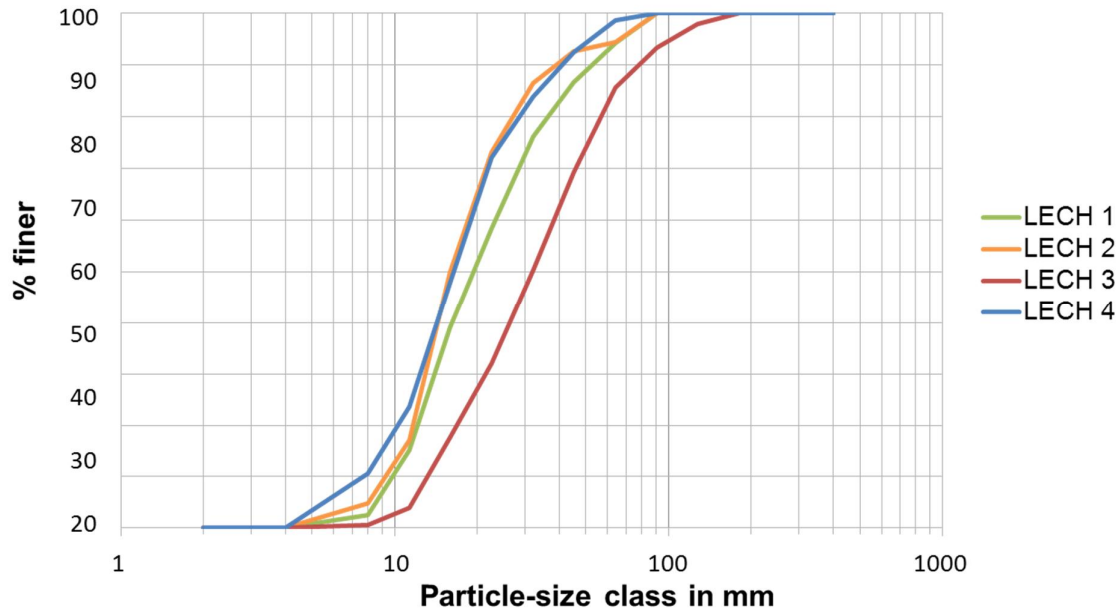
Figure I7.3 Cumulative grain size distributions of four samples taken from the bed of the Lech upstream of Johannisbrücke (Auer, 2012).

Table I7.1 Characteristic grain diameters for line samples taken in the Lech River (Auer, 2012).

Sample	d_{90} in mm	d_{50} in mm	d_{10} in mm
Lech 1	53	20	10
Lech 2	39	16	9
Lech 3	79	32	14
Lech 4	41	17	7
Mean values	53	21	10

I7.3   Method

I7.3.1   Cross sections and digital elevation model

For both hydrodynamic models (1D and 2D) terrain data is required. The digital elevation model was derived from a topographic survey of the river reach conducted using a Leica TC 805 total station, combined with existing laser scan data of the region.

Cross sections were employed for the 1D model and the digital elevation model was used to set up the 2D model and the habitat evaluation model.

I7.3.2   1D-hydrodynamic numerical model – HEC-RAS

The 1D model HEC-RAS (Version 4.1; http://www.hec.usace.army.mil/software/hec-ras/) was set up, calibrated and validated. Several discharges were modelled in a steady state condition (Table I7.2) and to investigate hydro peaking different flow change rates and durations (Table I7.3) were modelled at un-steady conditions. An example of a hydro peaking hydrograph is presented in Figure I7.4.

For each scenario the hydraulic parameters such as the mean flow velocity, mean water depth, mean bottom shear stress and water width, were evaluated and hydro peaking impacts, based on the decline rate of the water surface, were analysed. Additionally, the flow retention and the attenuation of the hydro peaking were evaluated by comparing inflow and outflow discharge.

Table I7.2 Discharges modelled at a steady state condition; MNQt mean low flow, MQ mean flow, HQ_1 one–year flood.

Characteristic value	Discharge [m^3s^{-1}]
MNQ_T	6.0
MQ	32.5
HQ_1	193.4

Table I7.3 Overview over the different hydro peaking scenarios

Flow change rate [-]	Ramping velocity [$m^3s^{-1}min^{-1}$]	Upsurge duration [min]
1:3 (5,99 m^3s^{-1} : 17,97 m^3s^{-1})	0.8	30
		60
		120
		240
		600
1:5 (5,99 m^3s^{-1} : 29,95 m^3s^{-1})	1.6	30
		60
		120
		240
		600
1:10 (5,99 m^3s^{-1} : 59,90 m^3s^{-1})	3.6	30
		60
		120
		240
		600

Figure I7.4 Example of an inflow-boundary condition to simulate hydro peaking (flow change rate 1:3, 5 different upsurge durations).

I7.3.3   2D-hydrodynamic numerical model – RIVER_2D

2D hydrodynamics were simulated with the RIVER_2D model, which was set up with the digital elevation model as basic data. The model was calibrated and validated. Similar to the application of the 1D model, different discharges at steady state (c.f. Table I7.2) and various hydrographs to simulate hydro peaking impacts (c.f. Table I7.3) were modelled.

For each model run the depth averaged flow velocity, the water depths and the bottom shear stress were evaluated. The results of the 2D model were also used as input data for the habitat modelling.

I7.3.4   Habitat evaluation model – MEM

The MEM (Mesohabitat Evaluation Model) classifies the modelled river section based on flow velocity, water depth and bottom shear stress into stable or unstable mesohabitats (pool, run, fast run, riffle, shallow water and backwater). The functionality is presented in Figure I7.5.

For each discharge scenario, the availability of mesohabitas was evaluated and compared to the other scenarios.

I7.4   Results

In this section the results of the hydrodynamic models are presented in the following way: First the results of the model runs at steady state are presented for the 1D and the 2D models. Then the results for the hydro peaking scenarios are shown for both model types, followed by the outcomes of the MEM.

x,y
<vel.dat>

x,y
<depth.dat>

x,y
<shear.dat>

1. routing:

$MH = [NC_{(d)} + NC_{(v)}] * NC_{(\tau)}$

<riffle>   <pool>   <run>   <fast run>   <low flow velocity*>

2. routing:

depth criteria: $NC(d) < g_{(4)}$; $NC(d) >/= g_{(4)}$

<shallow w.>   <backwater>

3. routing:

x,y   /   x,y
<shear.dat>   <τ_{cr} of d_m>

NhmU/AhmU **<riffle>** stable [%,A] unstable [%,	NhmU/AhmU **<pool>** stable [%,A] unstable [%,A]	NhmU/AhmU **<run>** stable [%,A] unstable [%,A]	NhmU/AhmU **<fast run>** stable [%,A] unstable [%,A]	NhmU/AhmU **<shallow w.>** stable [%,A] unstable [%,A]	NhmU/AhmU **<backwater>** stable [%,A] unstable [%,A]
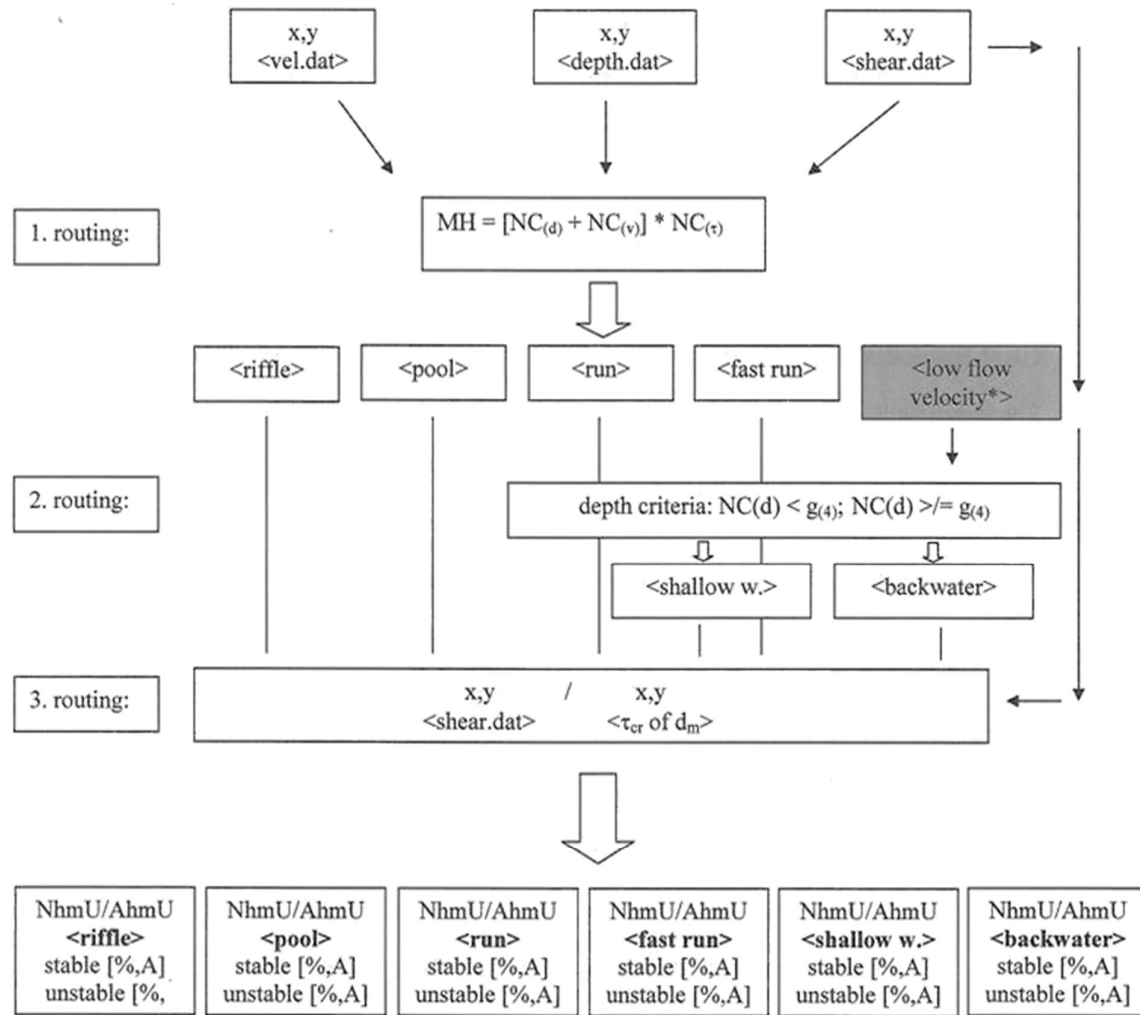
NhmU = number of hydro-morphologic units; AhmU = Area of hydro-morphologic units [m^2]; A = area [m^2]

Figure 17.5   Work flow of MEM (Hauer, 2007)

17.4.1   Steady state results

The 1D model results (Table 17.4) indicate that mean maximum water depths lie within 0.5 m and 1.5 m for discharges from low flow to a one year flood. The small water depths at high discharge might be due to the very wide section of the river. This is also indicated by the change of the maximum water surface extent from 66.5 m to 235 m, an increase of 3.5 times the low flow width.

The width to depth ratio indicates also a very wide and shallow river section. The ratio changes only slightly with increasing discharge (Figure 17.6).

Table I7.4 Simulation results of HEC-RAS (Auer, 2012). Q_{max} 1:x ... maximum discharge modelled for the flow change rate of 1:x

Discharge [m^{3}s^{-1}]	6,0 MNQ$_T$	18,0 Q$_{max}$ 1:3	30,0 Q$_{max}$ 1:5	32,5 MQ	59,9 Q$_{max}$ 1:10	193,4 HQ$_1$
Mean maximum water depth [m]	0.52	0.71	0.83	0.85	1.01	1.47
Mean flow velocity in [ms^{-1}]	0.50	0.63	0.72	0.73	0.87	1.23
Maximum water surface extent in [m]	66.5	109.1	133.5	137.3	168.9	235.0
Width/depth ratio [-]	128	154	161	162	167	160
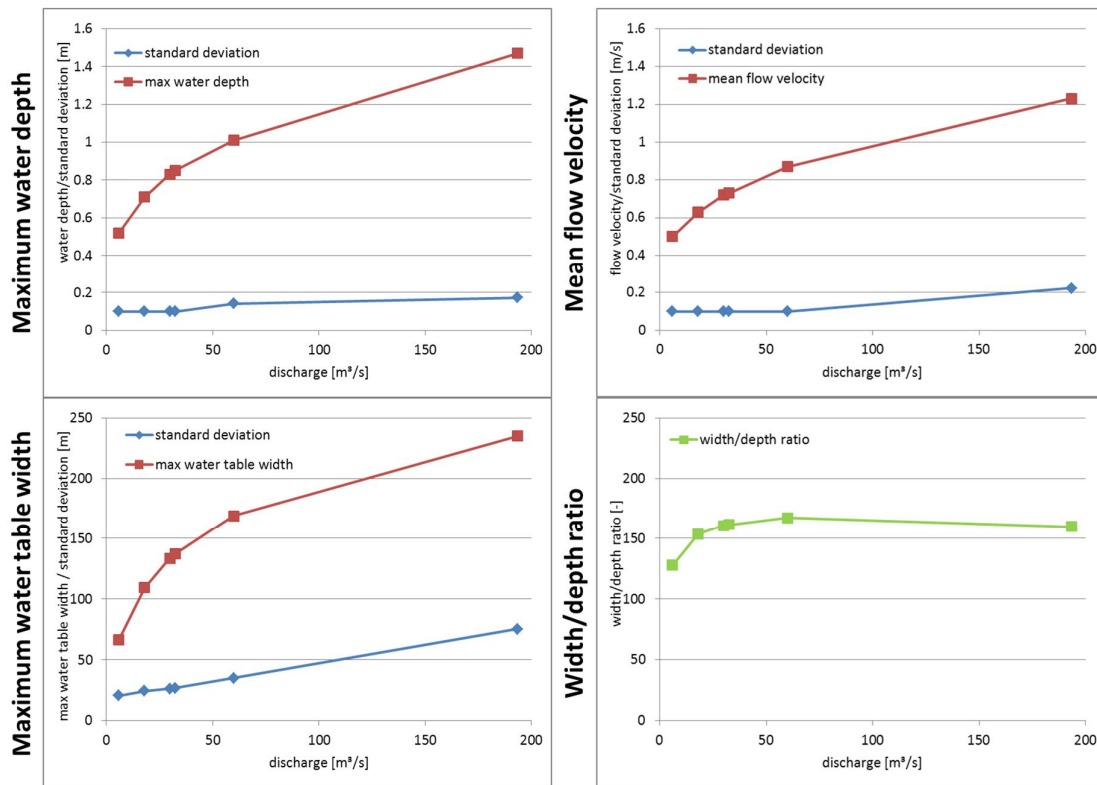
Figure I7.6 Development of different parameters as functions of the discharge (Auer, 2012).

Based on the results of the 2D model (Figure I7.7), the spatial variation in flow depths and flow velocity can be seen. In Figure I7.8 and I7.9, the frequency of flow velocity classes and water depth classes in relation to the different discharges are represented. Typically for the river type, even at higher discharges areas with low flow velocities and shallow water depths are present. However, their location changes.
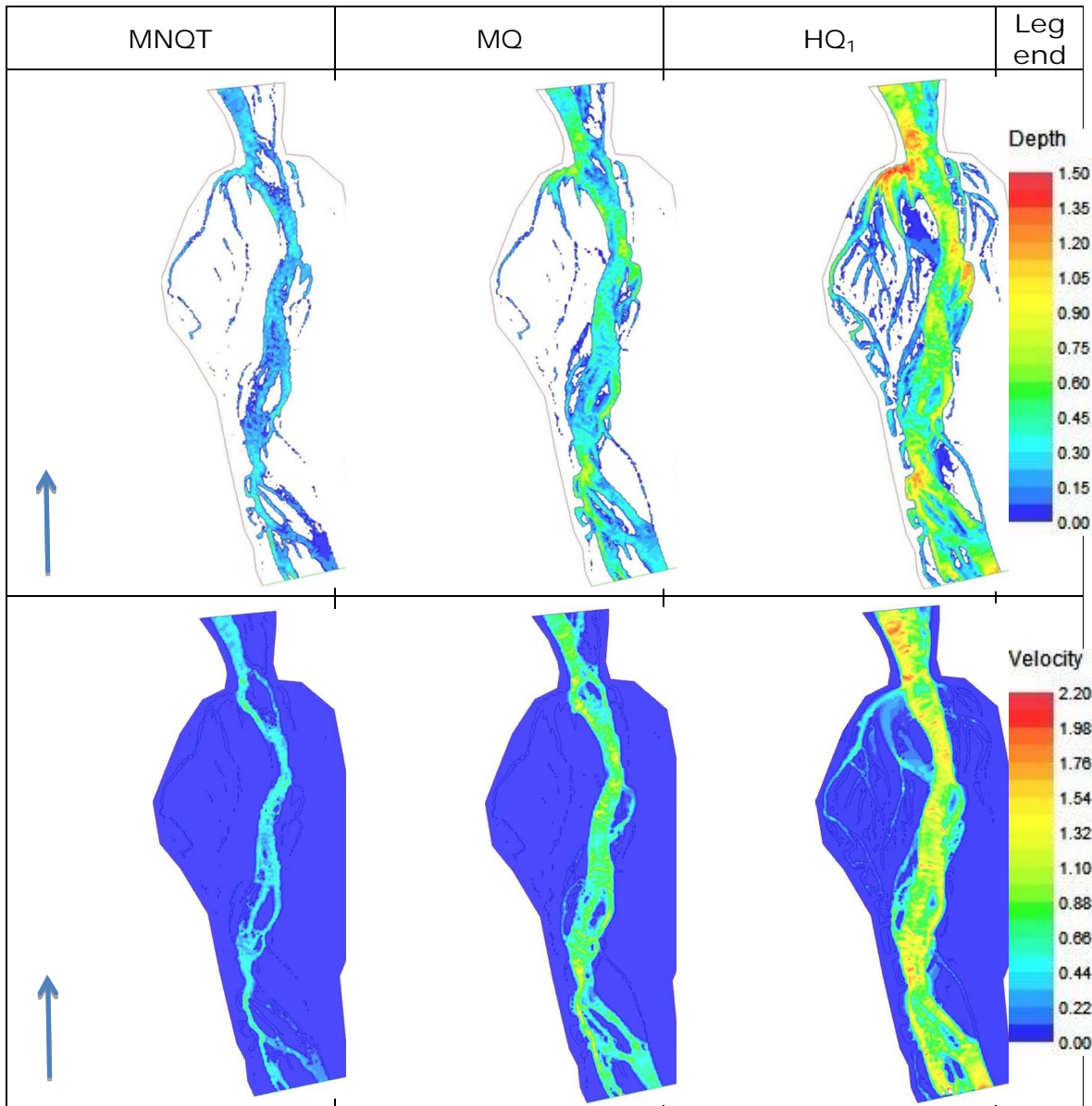
Figure I7.7 Spatial distribution of flow depth and depth averaged flow velocity at three discharges (Auer, 2012).

I7.4.2 Hydro peaking results

In the following, only selected results are presented. Details for all other scenarios can be found in Auer (2012).

In Figure I7.10 and I7.11, the inflow and outflow hydrographs for a flow change rate of 1:3 for different upsurge durations are shown. At this flow change rate the discharge increases within 15 minutes from 5.99 m^3s^{-1} to 17.97 m^3s^{-1}. It is evident that a time lag exists between the inflow and outflow hydrographs and that the peak discharge, depending on the upsurge duration, is to some extent damped.
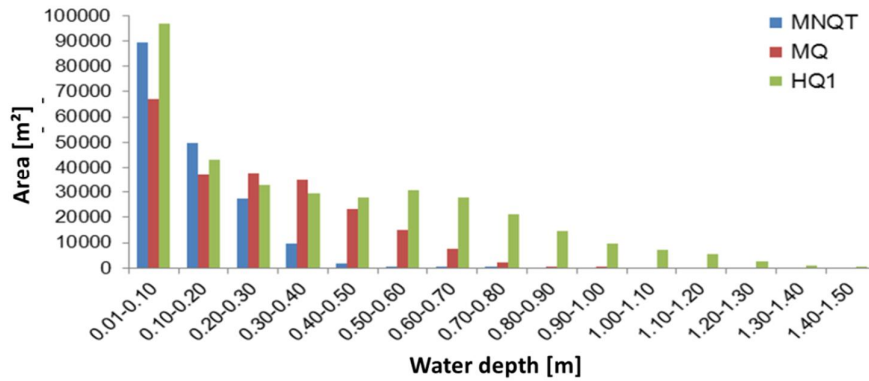
Figure I7.8 Distribution of water depth classes for three discharges (Auer, 2012).
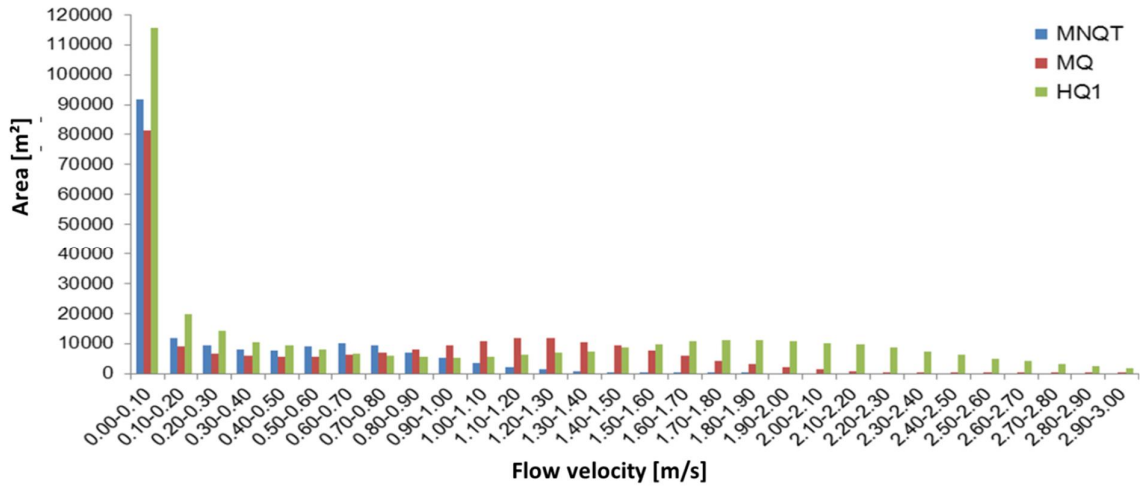
Figure I7.9   Distribution of flow velocity classes for three discharges (Auer, 2012)
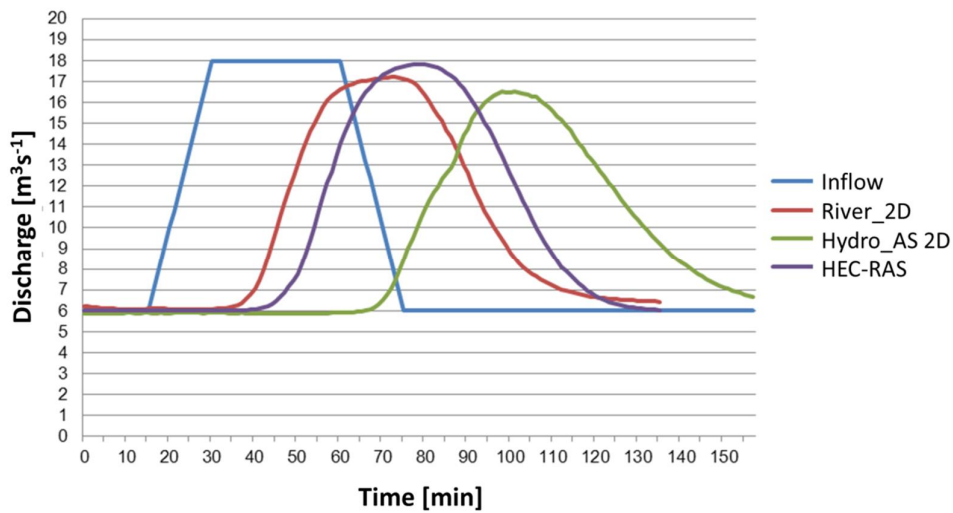
Figure I7.10   Illustration of the inflow and the simulated outflow hydrographs for a flow change rate of 1:3 and a upsurge duration of 30 minutes (Auer, 2012).
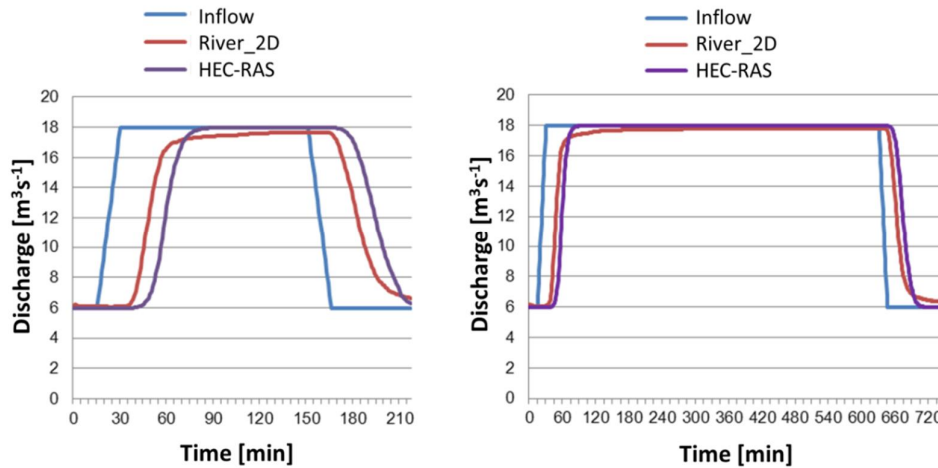
Figure I7.11   Illustration of the inflow and the simulated outflow hydrographs for a flow change rate of 1:3 and a upsurge duration of 120 minutes (left) and 600 minutes (right) (Auer, 2012).
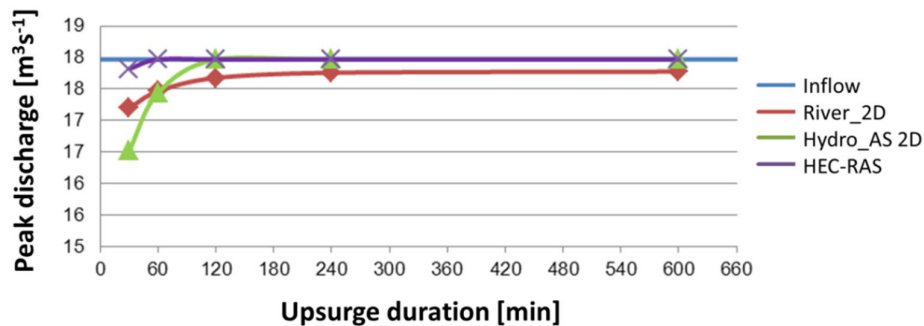
Figure I7.12 Peak discharges in relation to different upsurge durations for a flow change rate of 1:3 (Auer, 2012).

The smallest reduction in peak discharge occurs in association with at long upsurge duration (Figure I7.12). However there are also differences between outcomes of the different models used. For example, the damping of the hydro peaking is higher in the 2D model than in the 1D model. In the River 2D results, reductions in peak flow can be observed at all upsurge durations, but are highest at the smallest one. Slightly smaller ramping velocities can also be observed in the outflow hydrographs than in the inflow ones.

In Figure I7.13 the results for the flow change rate of 1:5 are presented and in Figure I7.14 the resulting peak discharges for different upsurge durations are shown. Similar to the flow change rate of 1:3, the reduction of peak discharge depends on the model that is used and becomes smaller with increasing upsurge duration. The ramping velocities of the outflow hydrographs are similar to the ones of the inflow hydrographs. Only during the falling limb of the hydrograph are the velocities slightly smaller.

The results for the flow change rate of 1:10 are illustrated in Figure I7.15. Due to numerical problems at the 2D model, the simulation was only carried out with HEC-RAS. Almost no damping of the peak discharge occurred and the ramping velocities for the rising limb of the outflow hydrograph are similar to the inflow hydrograph.
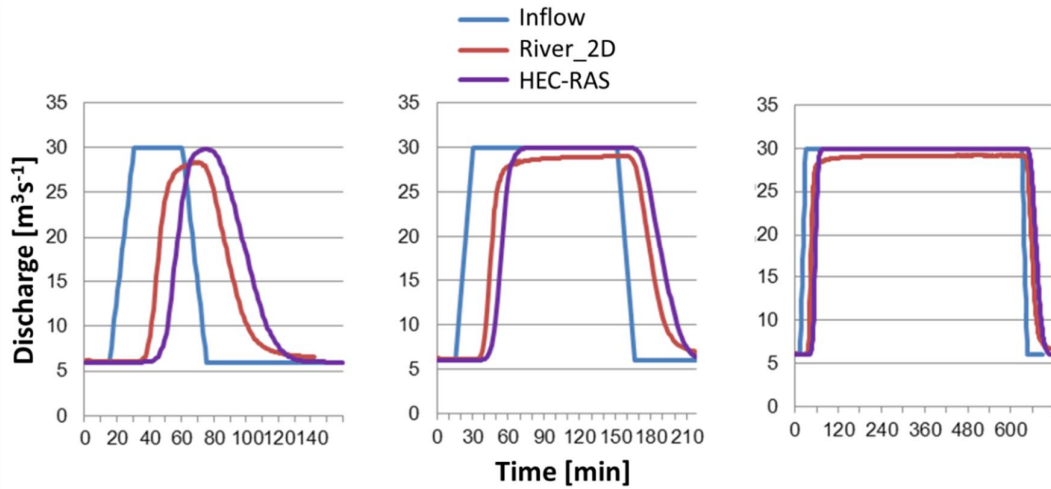
Figure I7.13   Illustration of the inflow and the simulated outflow hydrographs for a flow change rate of 1:5 and a upsurge duration of 30 minutes (left), 120 minutes (cntre) and 600 minutes (right) (Auer, 2012).

Figure I7.14 Peak discharges in relation to different upsurge durations for a flow change rate of 1:5 (Auer, 2012).
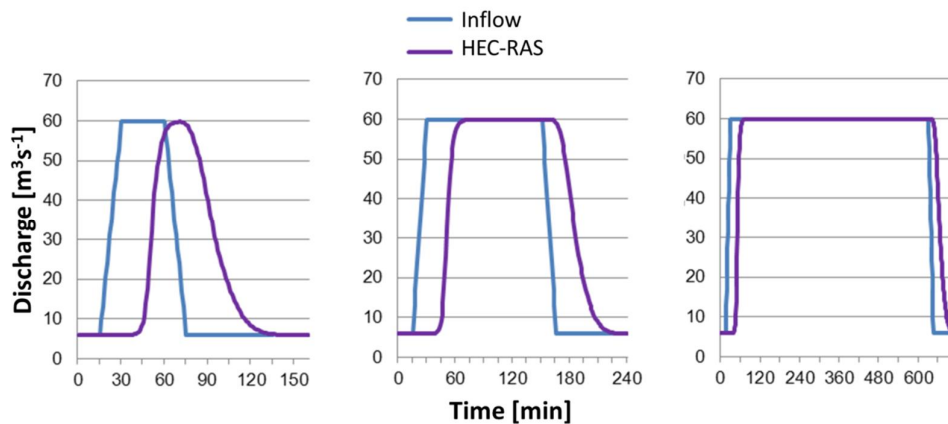
Figure I7.15   Illustration of the inflow and the simulated outflow hydrographs for a flow change rate of 1:10 and a upsurge duration of 30 minutes (left), 120 minutes (centre) and 600 minutes (right) (Auer, 2012).

I7.4.3   Mesohabitat Evaluation Model results

Similar to the results of the hydrodynamics, in this section the outcomes of the steady state simulations are presented followed by discussion of the results of the hydro peaking scenarios.

In Figure I7.17 and I7.16, the spatial distribution of mesohabitats and their relative and absolute frequency at different discharges are, respectively, shown. However, due to some inaccuracies in the digital elevation model, pools were not surveyed and are thus not represented in the model.

The highest proportion of the area is classified as shallow water and, with increasing discharge, the absolute value appears to be more or less constant. From MNQ_T to HQ_1 the wetted area almost doubles and, especially the faster flowing regions such as runs, fast runs and riffles, increase in frequency. Backwater areas start to appear at mean discharge. The distribution of the different mesohabitates is very heterogeneous.

The hydro peaking results are presented in Figure I7.18 to I7.20. The braiding river type shows a relatively constant distribution of habitats throughout the hydrograph. However, at the end of the falling limb of the hydrograph a higher value of wetted area exists compared to the area before the discharge was increased. The reason may be that the discharge in these areas, mainly shallow water habitats, may be slower to 'empty' or may become cut off from the main channels.
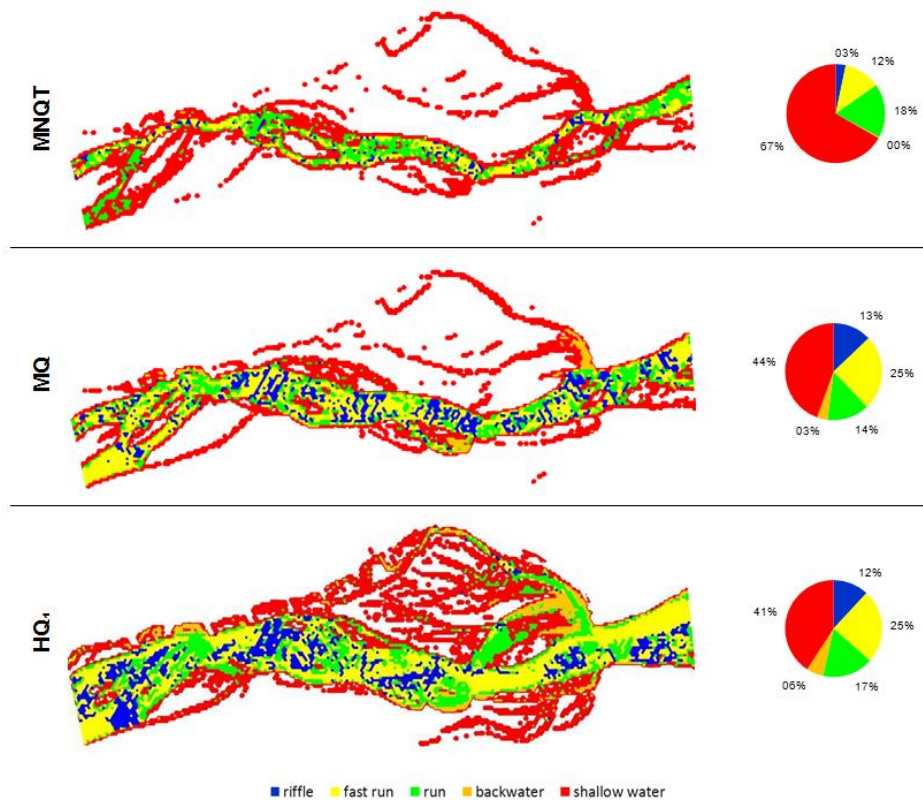
Figure I7.16   Spatial distribution and frequency of mesohabitats at different discharges (Auer, 2012).
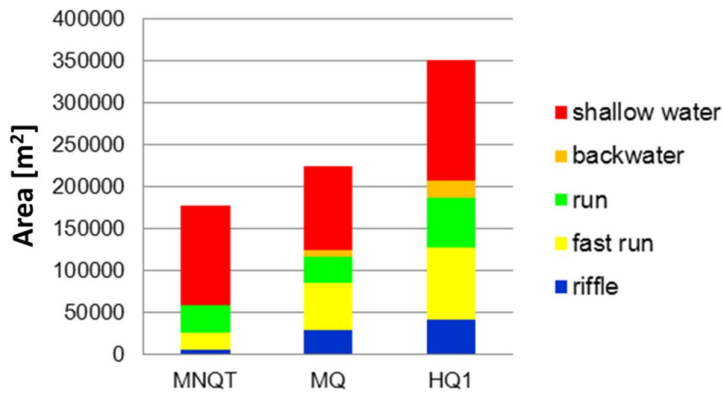
Figure I7.17   Frequency of mesohabitats at different discharges (Auer, 2012).
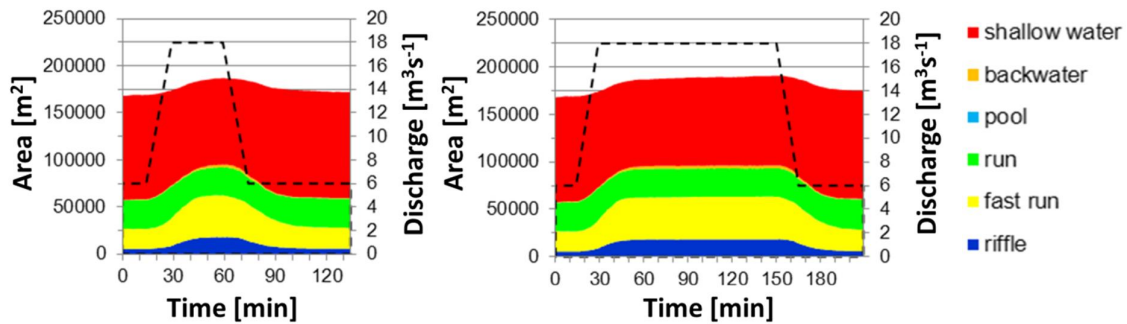
Figure I7.18   Development of mesohabitates based on hydro peaking at a flow change rate of 1:3 (Auer, 2012). The dashed line represents the inflow hydrograph and the different colours indicate the frequency of each habitat.

In Figure I7.19 the spatial distributions of habitats at low flow (downsurge) and at the peak flow (upsurge) of the hydro peaking are given. During peak flow additional arms develop and the proportions of faster flow regions increase. In some areas backwater regions establish. A comparison of the absolute frequency of mesohabitats at low and high flow for a flow change rate of 1:10 is shown in Figure I7.20.
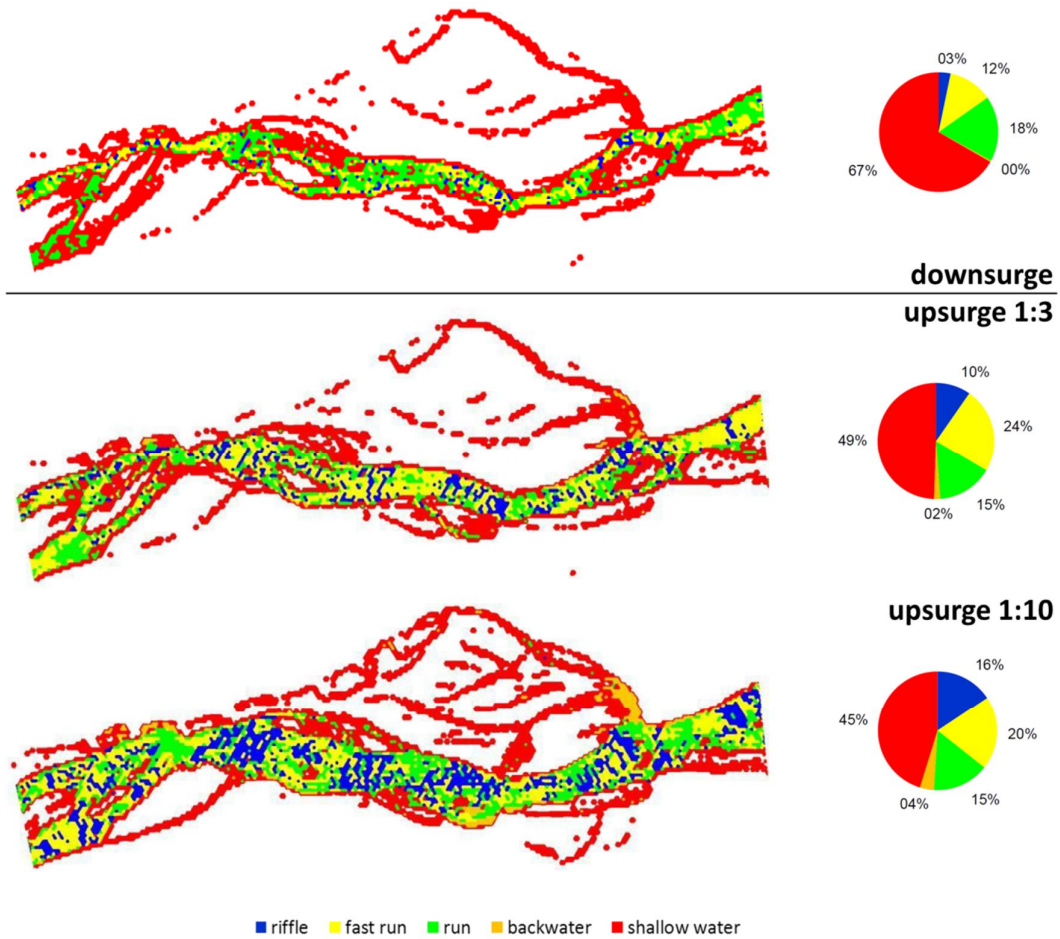
Figure 17.19   Spatial distribution and relative frequency of mesohabitats at the downsurge (5,99 m^{3}s^{-1}) and the upsurge (17,97 m^{3}s^{-1} – middle; 59,90 m^{3}s^{-1} – bottom); a flow change rate of 1:3 (middle) and 1:5 (bottom), respectively (Auer, 2012).
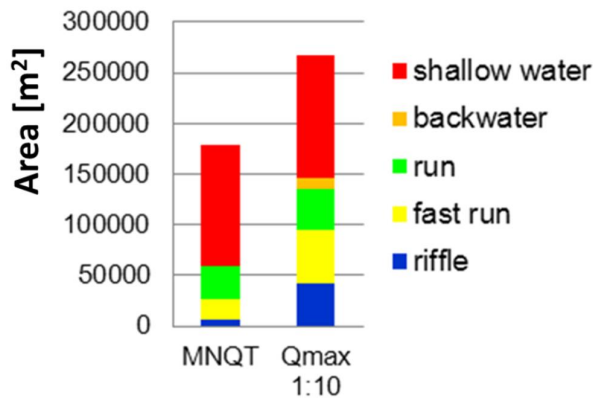
Figure 17.20   Frequency of mesohabitats low flow (downsurge) and peak flow (upsurge) for a flow change rate of 1:3 (Auer, 2012).

17.5   Discussion

The simulations of the hydraulics have shown that even at larger discharges the mean water depths stay small due to the wide flooding area. This is a typical feature of braiding river sections. When compared to other river types (e.g. single thread – straight) the differences become obvious. An example is given in Figures 17.21 and 17.22. The different behaviors of wetted width as a function of discharge for three cross sections are illustrated. A short characterization of the rivers is given in Table 17.5.

.
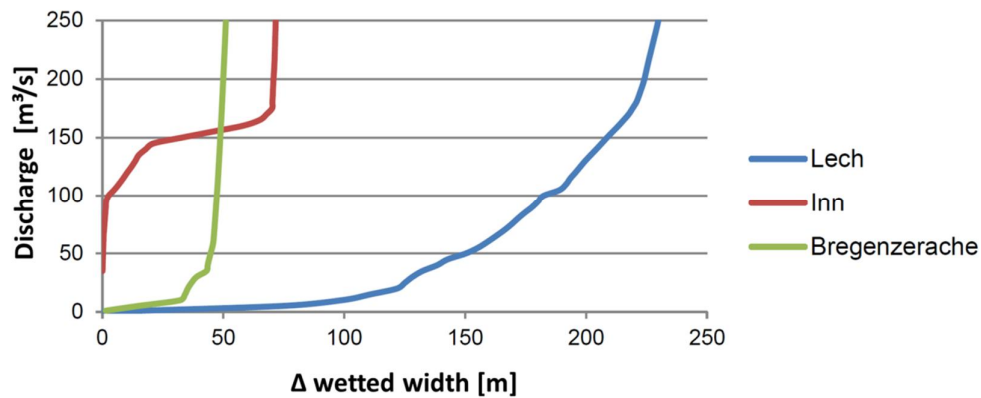
Figure 17.21   Development of wetted width as a function of discharge for three river cross sections (Auer, 2012).
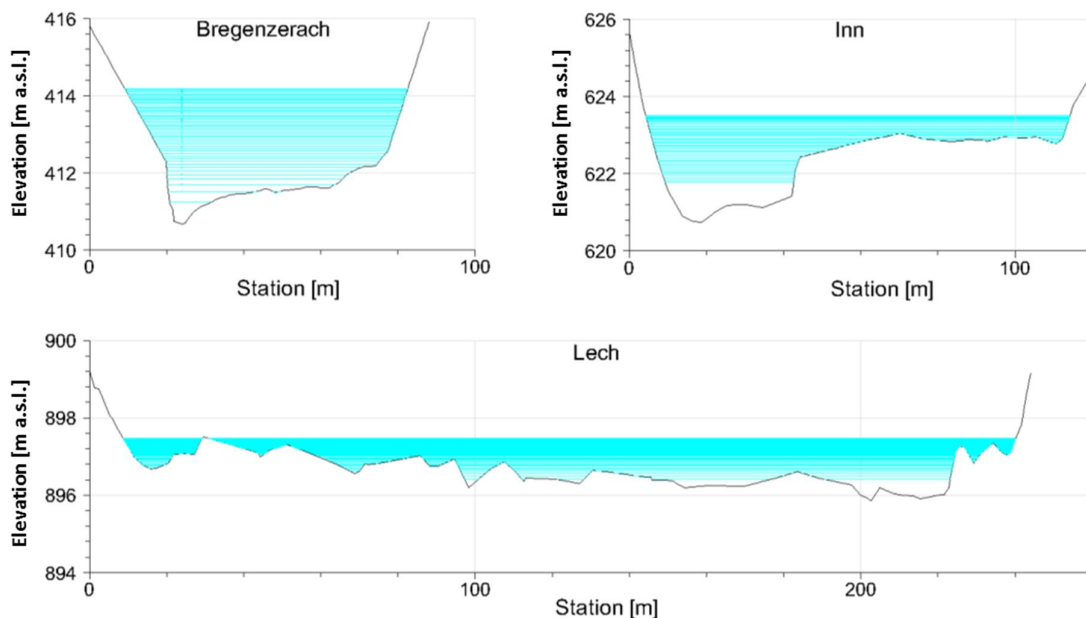
Figure 17.22   Cross sections of the investigated rivers (Auer, 2012).

Table 17.5 Characteristics of the Lech, Inn and Bregenzerach (Auer, 2012).

	Lech (Lechaschau)	Inn (Telfs)	Bregenzerach (Kennelbach)
River planform	Braiding	Single thread - straight	Single thread - straight
Catchment area	843 km²	5289 km²	826 km²
Elevation	~ 900 m a.s.l.	~620 m a.s.l.	~420 m a.s.l.
MNQT	6 m³/s	33 m³/s	5,1 m³/s
MQ	33 m³/s	156 m³/s	46 m³/s
HQ1	193 m³/s	-	480 m³/s

The evaluation of the 2D model results gives a good impression of the spatial distribution of flow parameters such as flow velocity, water depth and bed shear stress, at different discharges. These outcomes can be used for further interpretation at certain locations of the river reach in terms of flood duration, flood frequency and so on.

The models used for investigation of hydro peaking show different results in terms of peak retention. Based on the applied scenarios, it could be shown that the peak reduction depends on the upsurge duration and the flow change rate. The smaller the duration the larger is the reduction, and the higher the flow change rate the higher is the peak discharge reduction.

The application of the habitat evaluation model indicates, that at smaller flow change rates, e.g. 1:3; the relative distribution of mesohabitats is not altered significantly. However, with increasing rates (e.g. 1:10) shallow water areas decrease in favour of faster flow areas such as runs, fast runs and riffles.

In absolute numbers, the areas of shallow water seem to be more or less constant as, due to the increasing flood areas, new habitats are established.

A comparison of different river morphologies carried out by Auer (2012), indicated that the braiding section of the Lech River was more to absorb the hydro peaking, in terms of habitat availability at low and peak flow, compared to a regulated, straightened river reach of the Ill River. However, the effect of stranding of larvae due to the water level fluctuations and the accessibility of adequate habitats was not considered.

17.6 References

Auer H. 2012. Flussmorphologische Grundlagenuntersuchung am Lech zur Bewertung des Schwasseinflusses bei unterschiedlichen Flusstypen. Master, Universität für Bodenkultur.

BMLFUW (ed.) 2009. Hydrographisches Jahrbuch von Österreich 2006, Wien: BMLFUW Abteilung VII/3.

Gostner W, Lucarelli C, Theiner D, Kager A, Premstaller G, Schleiss AJ. 2011. A holistic approach to reduce negative impacts of Hydropeaking. In: Schleiss AJ, Boes RM. (eds.) Dams and Reservoirs under Changing Challenges. London: Taylor & Francis Group.

Graf M. 1992. Morphologische Beschreibung der Oberen Drau - Grundlage für ein Gewässerbetreuungskonzept. Master thesis, University of Natural Resources and Life Sciences

Hauer C. 2007. River Morphological- & Morphodynamic Aspects in Habitat Modelling and River Rehabilitation. PhD thesis, University of Natural Resources and Life Sciences.

Lebensministerium 2010. Nationaler Gewässerbewirtschaftungsplan 2009 - NGP 2009. Wien.

Mader H, Wimmer R. 1996. Abflussregime österreichischer Fließgewässer - Beitrag zu einer bundesweiten Fließgewässertypologie, Wien, Umweltbundesamt.

Moog O. 1993. Quantification of daily hydropower effects on aquatic fauna and management to minimize environmental impacts. Regulated Rivers: Research and Management, 8, 5-14.

Nachtnebel H-P, Graf M, Habersack H. 1992. Gewässerbetreuungskonzept Obere Drau, Arbeitspaket Flussmorphologie. Wien: University of Natural Resources and Life Sciences.

Nachtnebel H-P, Habersack H. 1996. Generelles Projekt zur Eindämmung der Eintiefungstendenzen and der Drau zwischen der Liesermündung und der Rosenheimer Brücke. Wien: University of Natural Resources and Life Sciences.

Tiroler-Lech. 2012. Naturpark Tiroler Lech [Online]. Verein_Naturpark_Tiroler_Lech. Available: http://www.naturpark-tiroler-lech.at/index.php?mainPid=160&c=page&s_pid=163&pid=164 [Accessed 03.2012].

Annex I.8
Application of a 2D hydrodynamical model to a reach of the Drau River

Bernadette Blamauer and Helmut Habersack
BOKU, Vienna, Austria

Summary

A two-dimensional hydrodynamic model (CCHE 2D) was applied to investigate the success of a restoration measure at the Upper Drau River. This study demonstrates that the hydrodynamic model can be used to quantify the development of different hydrodynamic parameters at different time steps and to interpret them in terms of restoration success.

Different discharges were modelled for each year and increased the knowledge of site specific parameters. Additionally, but not executed here, there is the potential to evaluate morphological parameters such as the width to depth ratio at certain locations along the modelled stretch.

This application indicates that hydrodynamic (and morphodynamic) models can be a good tool for planning of new restorations or adaptations, especially to compare different options. However, it must be kept in mind that models are only simplifications of the real world, they have limitations and different models have been developed for particular purposes and conditions.

I8.1   Introduction and objective

In 2002 a river restoration project was carried out on the upper Drau River, close to the village of Kleblach, to decrease bed incision and to improve the ecological status of the river. To evaluate the success of the measures (the river was widened and a side arm was initiated) the development of the site was monitored in the subsequent years. Additionally a hydrodynamic model was used for the comparison of hydraulic parameters based on the different bed elevation models, and this is the subject of the current study.

The aims of this study are (i) to generate additional information on hydro-morphological parameters; (ii) to compare hydrodynamic parameters before and after the river widening tocontribute to the evaluation of the river restoration; and (iii) to show possible applications of a 2D hydrodynamical model.

I8.2   Study site

I8.1.1   Drau River

The study site is located on a river widening section of the Upper Drau River close to the village of Kleblach in Carinthia, Austria (Figure I8.1).

The source of the Drau River is located between Innichen and Döblach (South Tyrol, Italy) at 1192 m a.s.l.. The Drau enters Austria at Erlach and has its confluence with the

River Isel at Lienz. The Drau runs from East Tyrol through Carinthia, leaving Austria at Lavamünd and then running through Slovenia until it joins the Danube River at Osijek in Croatia.

The Drau River within Austria follows predetermined geological structures (Alpine-Dinaric Transition Zone) with crystalline rocks in the north (Hohe Tauern, Kreuzeckgruppe,…) and carbonate rocks in the south.

The Upper Drau River is one of the last stretches of large river within the Alps that is not affected by hydropower development. Many rare and protected plant and animal species inhabit this river segment. The Drau River has been designated a Natura 2000 area, which gives great importance to protection and improvement of the state of natural processes, plant and animal species and habitats.

Figure I8.1   Location of the study site Kleblach within the Danube River Basin.

The Upper Drau River was a partly braided river section until extensive river regulations were carried out at the end of the 19th century. After flood events in 1965 and 1966, bank protection was intensified and additional regulation measures were implemented (Nachtnebel et al., 1992). The narrowing of the river channel and the prohibition of bank erosion led to a loss of habitats for fauna and flora and to a significant change in sediment transport capacity due to canalisation and consequential increased flow velocities and water depths.

At the same time sediment load was decreased by retention in the upper catchment and removal of material, so that river bed incision started to become a problem (Nachtnebel and Habersack, 1996). To stop the river degradation, several river restoration measures, in scope of the EU-LIFE projects "Auenverbund Obere Drau" and "Lebensader Obere Drau", were implemented on the Upper Drau River. One of them was river widening and the construction of a side channel at a river bend close to the village of Kleblach in 2002 (Figure I8.2).

Figure I8.2 Development of the river widening in Kleblach (aerial photos: Federal Government of Carinthia).

I8.2.2 Hydrology

The representative gauging station for the study site is situated about 8 km downstream of Klebach at the village of Sachsenburg. The catchment area is 2561.4 km² and characteristic hydrological values for the Drau River at the Sachsenburg gauging station are given in Table I8.1.

The hydrological regime, based on Mader et al. (1996), is nivo-glacial with the maximum monthly discharges in June and July, followed by August. During winter, low flow periods are characteristic for the Drau River due to the glacial influence – storage of precipitation in form of snow and ice cover.

The climate in the Upper Drau valley is affected by the pannonian climate in the east, mediterranean in the south and continental and oceanic climate in the north and west. Furthermore, the influence of altitude, relief and aspect are important (Nachtnebel et al., 1992). Temperatures fluctuate between very cold winters and hot summers and the mean annual precipitation is approximately 1000 mm (Graf, 1992).

The modelled ca. 2 km reach of the Drau River is illustrated in Figure I8.3. It is located in a semi-confined, sinuous section of the river at about 570 m a.s.l. The main bed material is gravel.

Table I8.1 Characteristic hydrological values for the Drau River at Sachsenburg (BMLFUW, 2009)

Characteristic Parameter	Discharge [m^3s^{-1}]
MNQ_T	13.2
MQ	72.6
HQ_1	1030
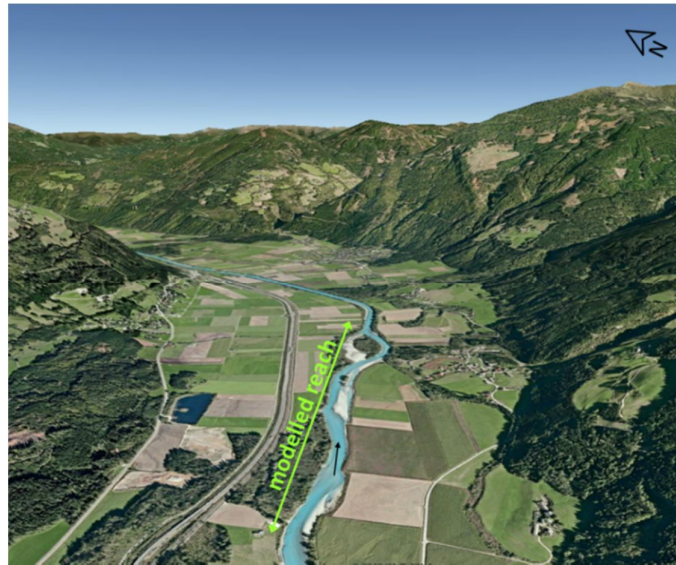
Figure I8.3   Aerial image of the modelled section of the Drau (data source: Google Earth 2013)

I8.3   Methods

I8.3.1   Digital elevation models

Digital elevation models were derived from terrestrial surveys, echo soundings and laser sans. At Kleblach four different topographies (year 2001- before river widening, and 2003, 2005 and 2008 after river widening) were considered (Figure I8.4).
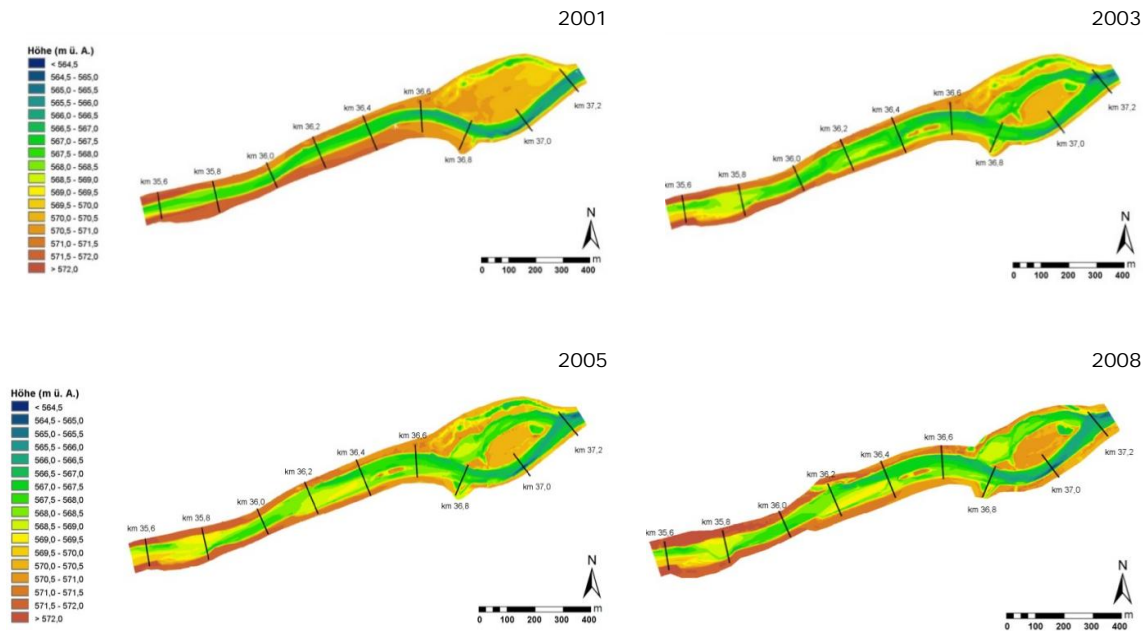

Figure I8.4   Digital elevation models of the widened river section of the Drau at Kleblach, for the years 2001, 2003, 2005 and 2008.

18.3.2   2D-hydrodynamic numerical model – CCHE 2D

Hydrodynamics were simulated with the 2D hydrodynamic numerical model CCHE 2D (http://www.ncche.olemiss.edu/cche2d).

Based on the topographies, computation meshes were generated for each year and the boundary conditions were defined. The model was calibrated and validated. Each model was run at a steady state condition and three discharges, 40 m^3s^{-1}, 73.8 m^3s^{-1} and 260 m^3s^{-1} respectively, were modelled.

The outcomes of the different years were compared and evaluated in terms of frequency, spatial distribution and variability of hydrodynamic parameters like flow velocity, water depth, bed shear stress and water table extent for the different discharges. The distribution of water depths, flow velocities and bed shear stress are indicators of the heterogeneity and quality of aquatic habitats and are thus important for the ecological condition of a water body. Additionally, the distribution of bed shear stress is important for the bed load transport capacity and thus the stability of the river bed.

18.4   Results

Some selected results of the modelling are presented below.

18.4.1   Development of the variability of flow widths and flow depths

The variability of flow width and flow depth are important indicators of the ecological condition of a river. The simulated water surfaces at different discharges enable the evaluation of the mean and maximum depths and the analysis of the water width within defined profiles. The investigation shows a clear increase in variability from the regulated (pre-widened) to the widened condition (c.f. Figure 18.5 and 18.6 and Table 18.2 for mean discharge), which seems to be similar for the years after widening.
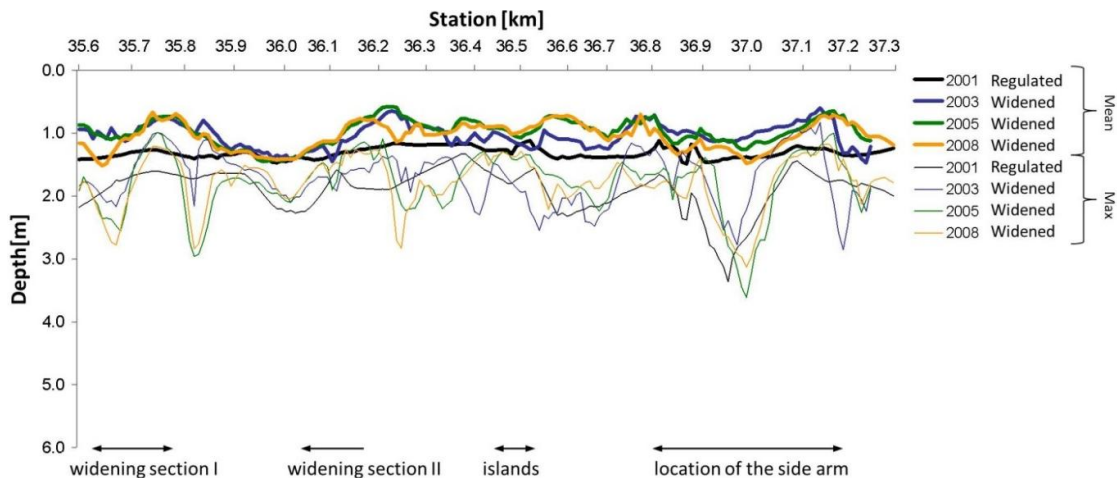

Figure 18.5   Variation of mean and maximum depth along the river at mean flow (MQ 73,8 m^3s^{-1}).
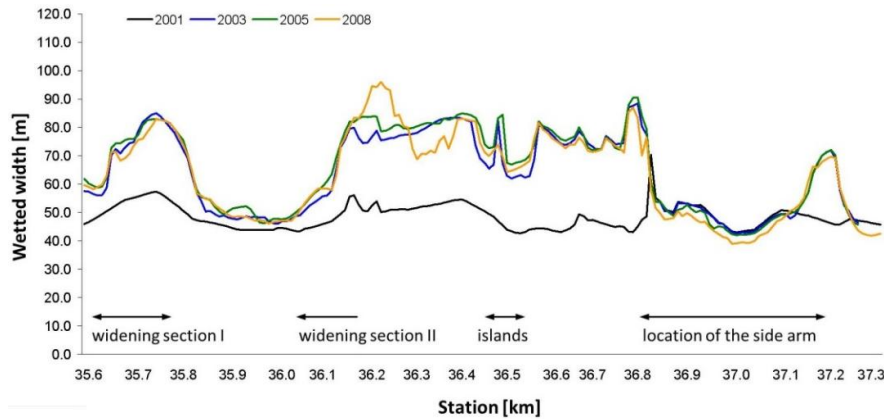
Figure 18.6   Variation of wetted width along the river at mean flow (MQ 73,8 m^{3}s^{-1}).

Table 18.2   Standard deviations of width and depth at mean flow (MQ 73,8 m^{3}s^{-1})

Year	Standard deviation (Std.) of width [m]	Std. of mean depth [m]	Std. of maximum depth [m]
2001 (regulated)	3,85	0,10	0,35
2003 (widened)	13,06	0,20	0,42
2005 (widened)	13,04	0,20	0,49
2008 (widened)	12,10	0,22	0,42

18.4.1   Development of the distribution of abiotic parameters

For the years 2001 and 2008 the frequency of hydraulic parameters such as the flow velocity, water depth and bed shear stress for several discharges, 40 m^{3}s^{-1}, 73.8 m^{3}s^{-1} and 260 m^{3}s^{-1} respectively, were evaluated.

In Figure 18.7 the spatial distribution of water depth for the mean discharge of 260 m^{3}s^{-1} are presented. The decrease in water depth in the main channel is clearly visible and also the increase in channel width can be seen.

In Figures 18.8, 18.9 and 18.10, the relative frequencies of different flow velocity, water depth and bed shear stress classes are illustrated for the year 2001 (regulated condition) and 2008 (widened condition).

For all three parameters and all discharges, the distribution is more heterogeneous for the widened river bed than for the regulated one. Thus it can be assumed that in the widened condition a higher variability of habitats exist.

At low flow conditions (40 m^{3}s^{-1} and 73,8 m^{3}s^{-1}), one flow velocity class dominates in 2001, this class is much less dominant in 2008. Another feature which becomes evident when looking at the frequency distributions of the three parameters is that all modelled discharges exhibit lower water depths, flow velocities and bed shear stress in the widened condition. Thus, the risk of further river degradation and incision is decreased.
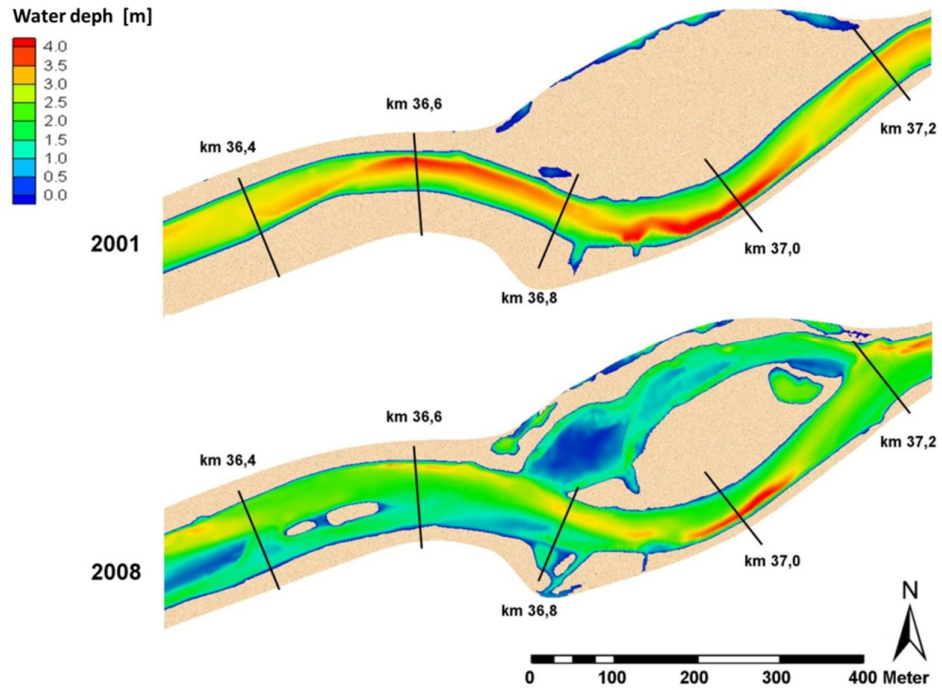
Figure 18.7   Spatial distribution of water depths at a discharge of 260 m^{3}s^{-1}.
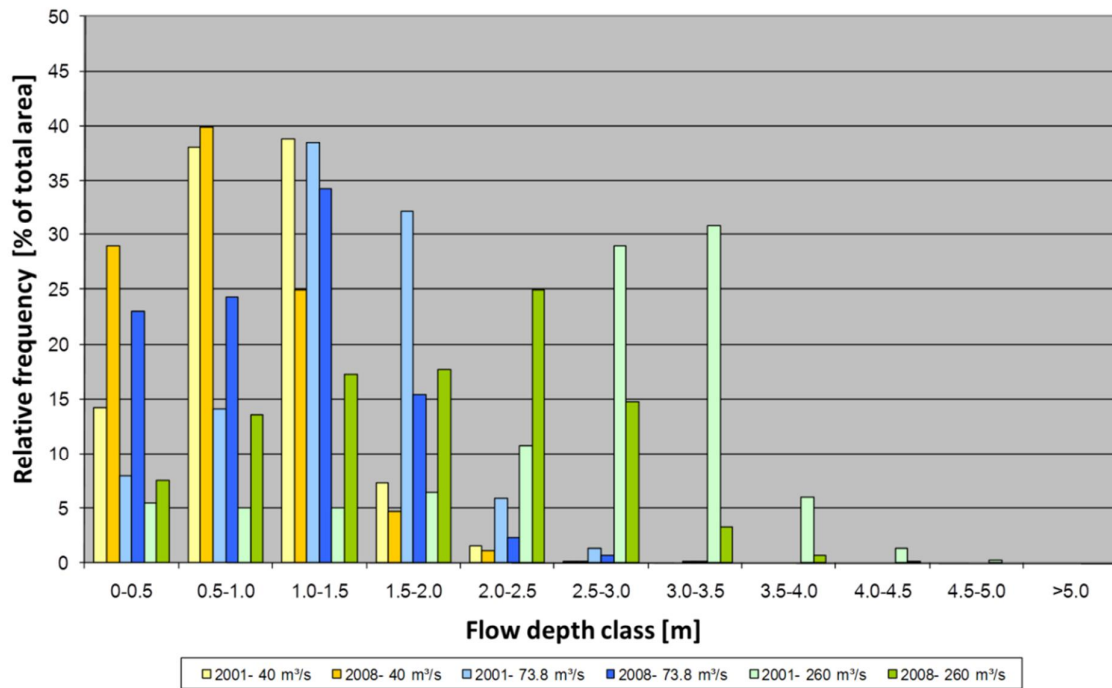

Figure 18.8   Distribution of flow depth classes modelled for the years 2001 (lighter shades of yellow, blue and green) and 2008 (darker shades) at three discharges.
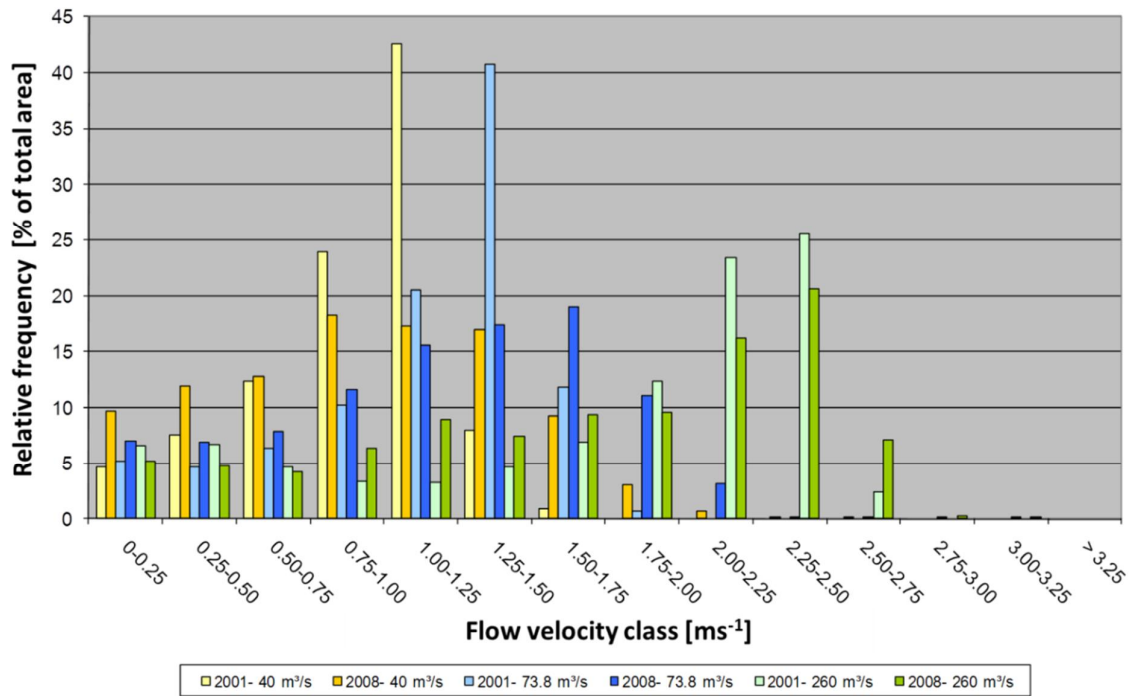
Figure 18.9   Distribution of flow velocity classes modelled for the years 2001 (lighter shades of yellow, blue and green) and 2008 (darker shades) at three discharges.
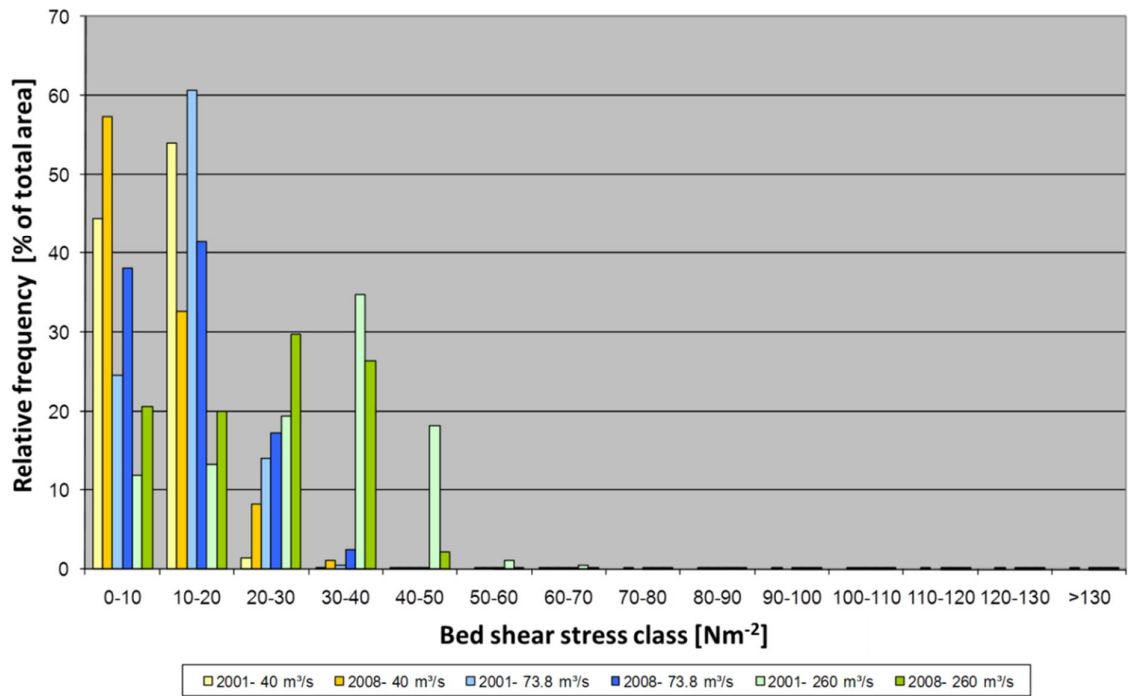

Figure 18.10   Distribution of bed shear stress classes modelled for the years 2001 (lighter shades of yellow, blue and green) and 2008 (darker shades) at three discharges.

I8.4.3 Development of the hydraulic parameters at defined cross sections

In the following figures (Figures I8.11, I8.12 and I8.13), the developments of hydraulic parameters (flow velocity and water table elevation) in defined cross sections are presented.

The differences between the regulated condition (2001, black coloured lines) and the other years are obvious. Similar to the previously-presented figures, the variability of depth averaged flow velocities and water depth are much higher within the widened cross sections than within the regulated one. Within the cross sections, the bed level development is also visible.

I8.5 Discussion

In general, the simulations showed an increase in variability of all hydrodynamic parameters (flow velocity, water depth, water table extent,…) at the widened river beds. The variability can be used as an indicator of improved ecological conditions based on habitat variability. Due to the river widening not only the variability increased, the flow velocities and water depths were also altered/reduced.

Based on the hydrodynamic simulations, a reduction in bed shear stress could be detected in the widened examples in comparison with the original regulated river bed.

Shear stress is an important parameter in the derivation of bed load transport capacity and has thus major impacts on the stability of the bed. This reduction of shear stresses in the widened river can further be interpreted as a restoration success, since bed incision is minimized.
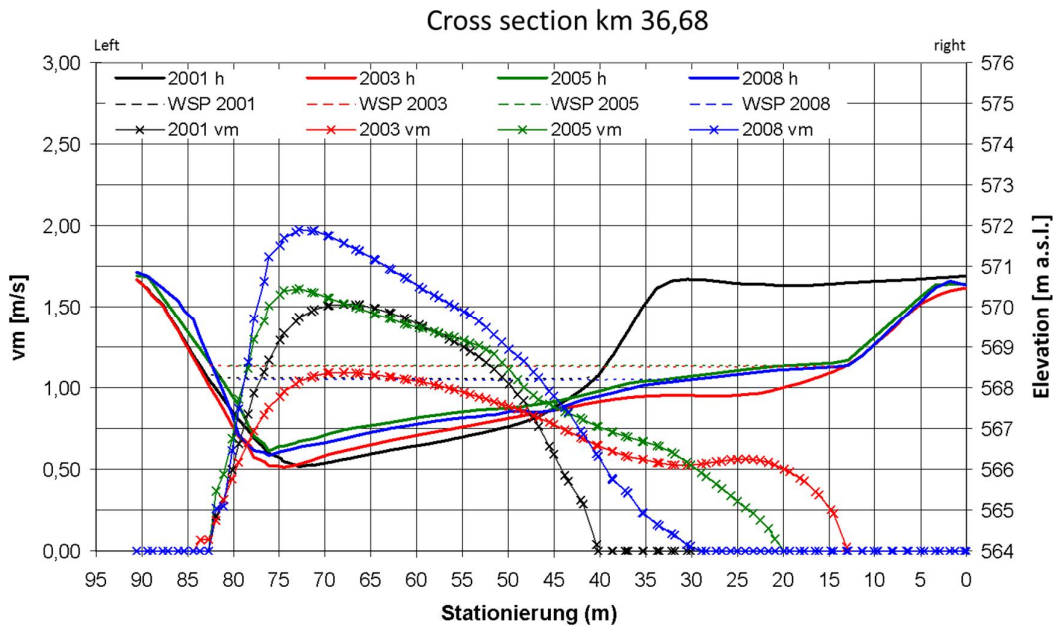

Figure I8.11   Hydrodynamic parameter at the cross section km 36,68 (widened section) for mean discharge, based on four different elevation models. h… bed elevation, WSP… water table elevation and vm… depth averaged flow velocity
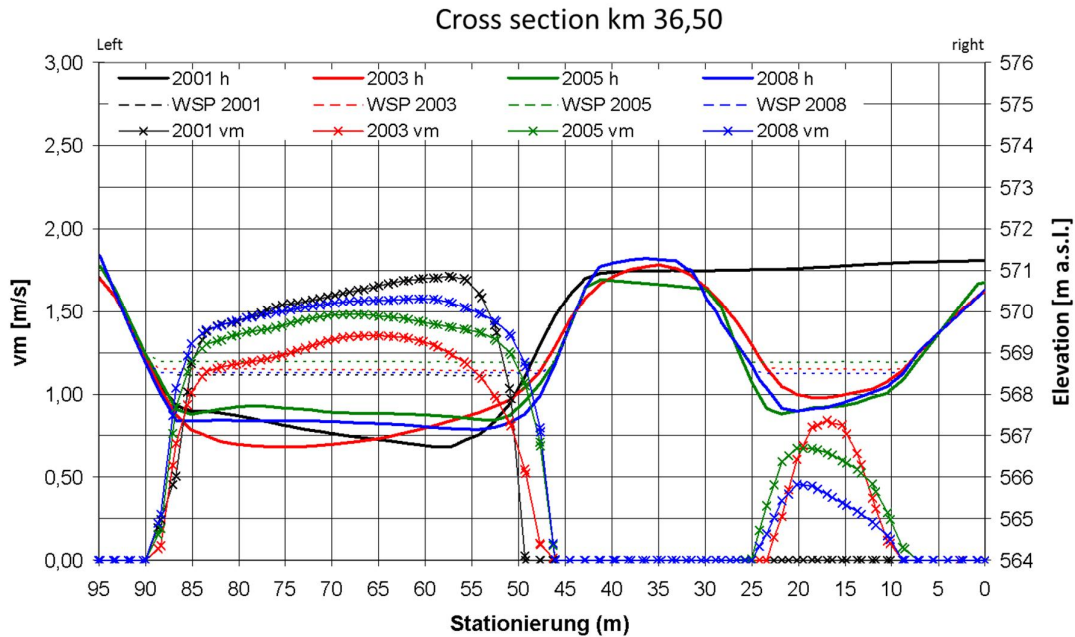
Figure I8.12   Hydrodynamic parameter at the cross section km 36,50 (widened section with island) for mean discharge, based on four different elevation models. h... bed elevation, WSP... water table elevation and vm... depth averaged flow velocity
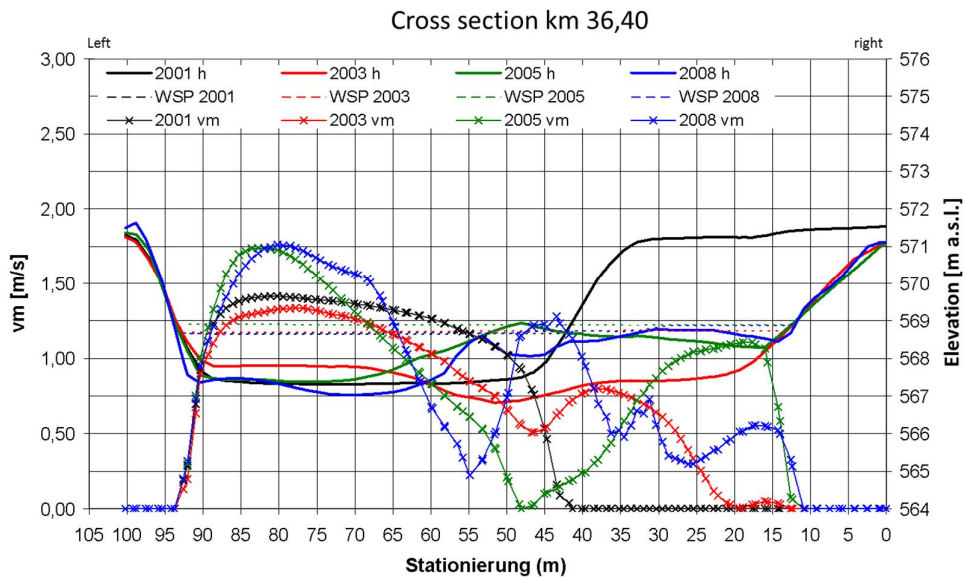

Figure I8.13   Hydrodynamic parameter at the cross section km 36,40 (widened section) for mean discharge, based on four different elevation models. h... bed elevation, WSP... water table elevation and vm... depth averaged flow velocity

18.6 References

Auer H. 2012. Flussmorphologische Grundlagenuntersuchung am Lech zur Bewertung des Schwasseinflusses bei unterschiedlichen Flusstypen. Master, Universität für Bodenkultur.

BMLFUW (ed.) 2009. Hydrographisches Jahrbuch von Österreich 2006, Wien: BMLFUW Abteilung VII/3.

Gostner W, Lucarelli C, Theiner D, Kager A, Premstaller G, Schleiss AJ. 2011. A holistic approach to reduce negative impacts of Hydropeaking. In: Schleiss, A. J. & Boes, R. M. (eds.) Dams and Reservoirs under Changing Challenges. London: Taylor & Francis Group.

Graf M. 1992. Morphologische Beschreibung der Oberen Drau - Grundlage für ein Gewässerbetreuungskonzept. Master thesis, University of Natural Resources and Life Sciences

Hauer C. 2007. River Morphological- & Morphodynamic Aspects in Habitat Modelling and River Rehabilitation. PhD thesis, University of Natural Resources and Life Sciences.

Lebensministerium 2010. Nationaler Gewässerbewirtschaftungsplan 2009 - NGP 2009. Wien.

Mader H, Wimme, R. 1996. Abflussregime österreichischer Fließgewässer - Beitrag zu einer bundesweiten Fließgewässertypologie, Wien, Umweltbundesamt.

Moog O. 1993. Quantification of daily hydropower effects on aquatic fauna and management to monimize environmental impacts. Regulated Rivers: Research and Management, 8, 5-14.

Nachtnebel H-P, Graf M, Habersack H. 1992. Gewässerbetreuungskonzept Obere Drau, Arbeitspaket Flussmorphologie. Wien: University of Natural Resources and Life Sciences.

Nachtnebel H-P, Habersack H. 1996. Generelles Projekt zur Eindämmung der Eintiefungstendenzen and der Drau zwischen der Liesermündung und der Rosenheimer Brücke. Wien: University of Natural Resources and Life Sciences.

Tiroler-Lech. 2012. Naturpark Tiroler Lech [Online]. Verein_Naturpark_Tiroler_Lech. Available: http://www.naturpark-tiroler-lech.at/index.php?mainPid=160&c=page&s_pid=163&pid=164 [Accessed 03.2012].

Annex 19

Assessing geomorphic dynamism at the reach scale to explain biotic responses using 2D models (The Curueño river, North-western Spain)

Vanesa Martínez-Fernández, Diego García de Jalón, Marta González del Tánago

Universidad Politécnica de Madrid, Spain

19.1 Introduction

At the reach scale a high diversity of hydraulic conditions (e.g. water depth and velocity) generally occurs and the intensity of erosion and deposition processes within the existing geomorphic units (e.g. pools and riffles) may be different across the range of floods that may be predicted in a reach (Schweizer et al, 2007). The identification of local variations of these processes may help to develop understanding of differences in macroinvertebrate (Brooks et al., 2005) and fish communities (Lamoroux, 1999) within the channel and differences in vegetation recruitment along the banks and riparian zones (Meier. 2008).

In the case of benthic invertebrate diversity, substrate size has been shown to be a significant predictor (Jowett, 2003). However, substrates do not supply homogeneous environments for macroinvertebrates. At a very small spatial scale, the surrounding hydraulic environment determines their distribution (Statzner et al., 1988, Hart & Finelli 1999, Jowett 2003) and community composition (Gabel, 2012), such that they are quite patchily structured.

Some hydraulic variables have been studied to describe near-bed hydraulic conditions and to predict habitat use by invertebrates, including simple variables such as flow velocity and water depth (Milhous et al., 1989), and more complex ones representing invertebrate interactions with substrate variability (Statzner et al. 1988), including Froude number, shear velocity, and shear stress (Gore 1996). Statzner et al. (1988) showed that substratum size is not as useful in describing physical habitat characteristics on the scale of a reach (0.1 – 1 m2) as is commonly believed, because the size distribution of substratum within a reach often reflects a past spate rather than present flow conditions (Lamberty and Resh, 1979).

Hydraulic modeling, could contribute to predicting the expected locations of dynamic points characterising special conditions for research on macroinvertebrate distributions and composition. In this study, a 2D hydraulic model that incorporates a sediment module is applied to estimate several hydraulic parameters at particular discharges and to locate areas where erosion and sedimentation is taking place. The aim is to locate and quantify hydromorphological processes that govern fluvial habitats.

19.2 Case study

19.2.1 Site study: The Curueño River

Following the application of the hierarchical framework defined within Deliverable 2.1, Part 1, Sections 3, 4 and 5, the study area was characterized at different spatial scales (see the relevant Case Study in Deliverable 2.1, Part 3). The reach in which the present modelling was undertaken is situated near the confluence of the Curueño river with the Porma River (Figure 19.1).
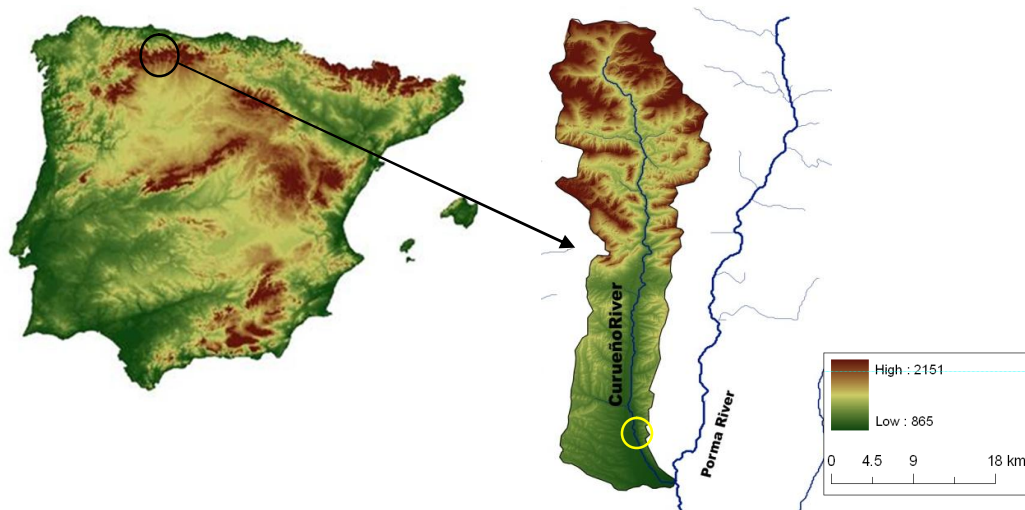

Figure 19.1   Location of the study area (Lower reach of the Curueño River) (yellow circle).

The Curueño River is a gravel bed river with a total length of 48 km and a watershed area of 293 km^2 (Figure 19.1). The river rises in the Southern slopes of the Cantabrian Mountains (2200 m altitude) and joins the Porma River at 865 m altitude. The river has a predominantly north to south flow direction. In the upper part the river flows through confined valleys where the oldest materials in the catchment can be found (cambric sedimentary rocks, with eventual calcareous rocks), whereas siliceous conglomerates from the Tertiary are predominant in the downstream part, alternating with Quaternary fluvial deposits along partially confined valleys. The study reach is located in the lower part of the river, and is characterized by a relatively high valley gradient (0.82 %) and a wide valley bottom (900-1500 m). This part of the river receives an annual rainfall between 700 and 800 mm (www.aemet.es).

19.2.2 Hydrologic and geomorphic Data

The nearest flow gauging station to the study reach has only 1-year of registered data (Ambasaguas gauge, Figure 19.2 left). At this location the Curueño River shows a temporary hydrologic regime. Annual peak flows are associated with rains during autumn and winter. There is a very sharp fluctuation in flow within the year, with almost zero discharge during the summer months. The mean annual flow is 4 m^3/s, and the

maximum and minimum flows are 37.4 and 0.02 m^3/s, respectively. Because there is only 1-year of data, records from a different gauging station situated in the upper part of the catchment is used to calculate discharge return periods (Caldas de Nocedo Gauge, Figure I9.2 right), as there are no significant tributary inputs between the two gauges.

In order to quantify the hydromorphological processes, the sediment yield of the Curueño study reach was estimated using the Meyer-Peter and Müller (1948) and Camenen and Larson (2005) formulae. For these calculations, exceedance frequencies were calculated using 'Caldas de Nocedo' data (Figure I9.3). The most frequent discharge is 1 m3/s with an occurrence of 16.9 %. The Meyer-Peter and Müller and Camenen and Larson methods predict sediment yields of 1252 and 1308 Tn per year, respectively.
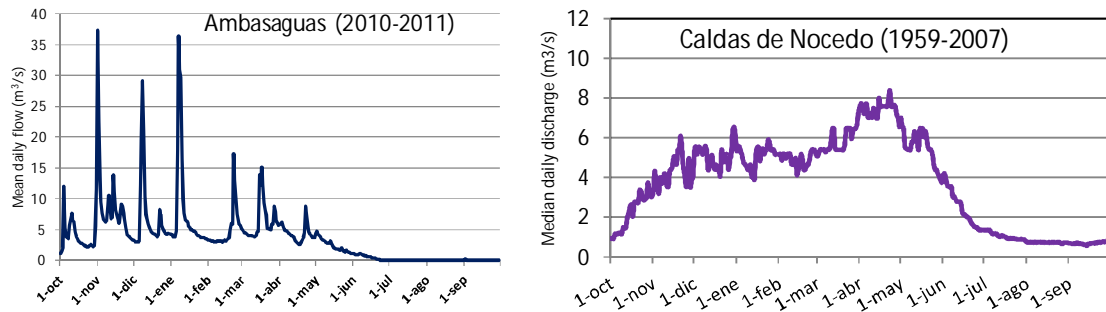

Figure I9.2 Hydrograph of mean daily discharge of the nearest gauge station to the study reach (left) and hydrograph of the gauge station with longer serial data (right).
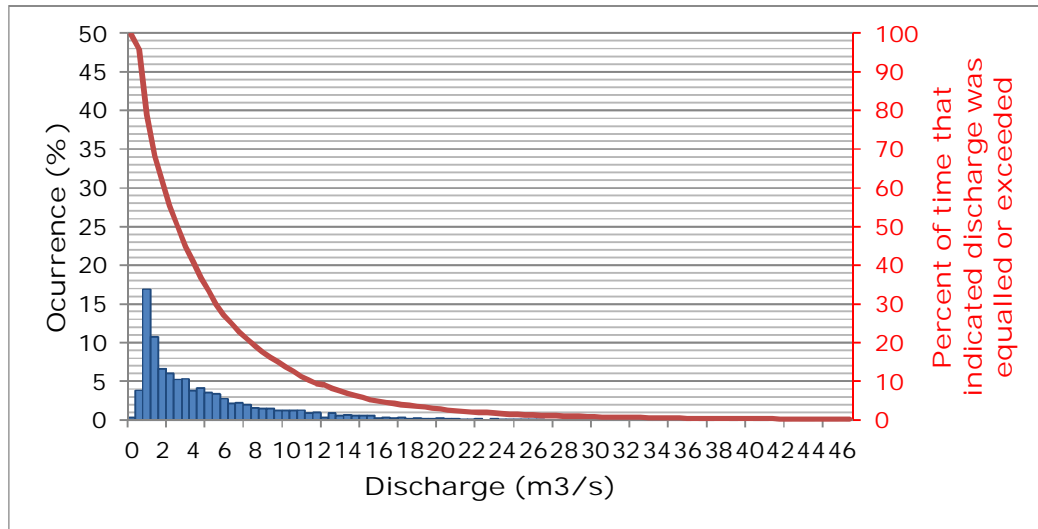

Figure I9.3   Flow duration curve to define the baseflow (Caldas de Nocedo gauging station)

Table I9.1   Discharges corresponded to return periods of interest in this study

Return period	Discharge (m^3/s)
1.5	19
2	23
5	68
10	80

19.2.3   IBER Modeling

Iber is a numerical simulation model for free surface turbulent flow in non-steady state, and environmental processes in fluvial hydraulics (CEDEX, GEAMA, FLUMEN y CIMNE 2010a, 2010b; www.iberaula.es; Bladé et al., 2014). The range of application of *Iber* includes river hydrodynamics, dam break simulations, evaluation of flood zones, calculations of sediment transport, and tidal flow in estuaries. The *Iber* model currently consists of 3 main calculation modules: a hydrodynamic module, a module of turbulence, and a sediment transport module. All modules work on an unstructured finite volume mesh formed by triangular and / or quadrilateral elements.

The present model application has two principal steps: pre-process and post-process.

In the pre-process step, a mesh is constructed over the expected surface affected by simulation with the necessary information for running the model. Each of the elements comprising the mesh (triangular elements in this case) has information about the altitude and the roughness of the surface. For the altitude information, a digital elevation model with a 5 m spatial resolution (IGN, 2011) was used. For roughness, a specific Manning´s number was assigned to each cover type that was digitised, following Chow V.T. (2000). Digisiting was implemented within ArcGIS 9.3 through the interpretation of orthophotographs from 2007 with a 0.25 – 0.5 m spatial resolution (IGN, 2011).

Once the geometry had been created, hydrodynamic parameters are fixed. (i) Discharge values are defined according to required return periods (Table 19.1) and are considered through hydrodiagrams, specifying a simulation time and time interval of 6000 s and 60 s, respectively. (ii) The sediments module is then activated and some parameters are needed including the sediment size (D_{50} in mm) and the selected bedload transport formula. In relation to the latter, two options are implemented in Iber: Meyer-Peter and Müller (1948) for gravel bed rivers with D_{50} less than 30 mm; and Van-Rjin (1984) with different expressions depending of the relevant sediment diameter.

Figure 19.4   Reach selected for simulation

For the present simulation, a reach of 1 km was selected (Figure I9.4). Granulometry information was obtained from a field survey in July 2013 that applied the Wolman (1954) methodology,which gave a D_{50} of 75 mm (Figure I9.5).
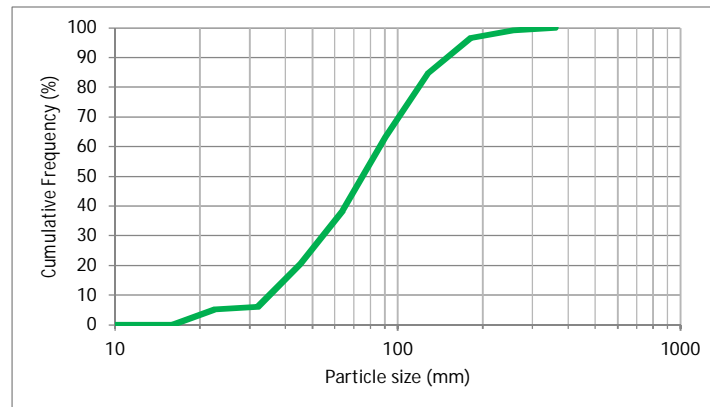

Figure I9.5   Granulometry curve for bed material at the study site.

Once preprocessing is complete, the model is run and the result are visualized in a post-process step. In the present case, water velocity, water column depth, and erosion and sedimentation rates were visualised.

I9.3   Results

I9.3.1   Hydraulics

Figure I9.6 shows some outputs from this *Iber* application in which water velocity values and water column depth distributions can be observed. For a discharge value of 1 m^3/s, which is the most frequent discharge (Figure I9.3), the maximum water velocity (1.53 m/s) is achieve in riffles (yellow circle in Figure I9.6), while the deepest zone (about 1.15 m deep, red circle in Figure I9.6) presents slower velocities. In relation to a discharge value of 19 m^3/s (1.5-years flood), water floods the floodplain in some areas, as would be expected for the bankfull discharge. The final pictures show results for a higher, 5-year flood discharge (68 m^3/s).

I9.3.2   Sediment Dynamics

For the 68 m3/s (5-y return period) discharge, the sediment module was applied with the aim of detecting areas of sediment erosion and deposition (Figure I9.7). Four locations with significant geomorphic activity were detected associated with erosion and sedimentation (if we exclude the boundary points that are affected by model).

Water velocity (m/s)   Depth water column (m)

Q =1 m³/s
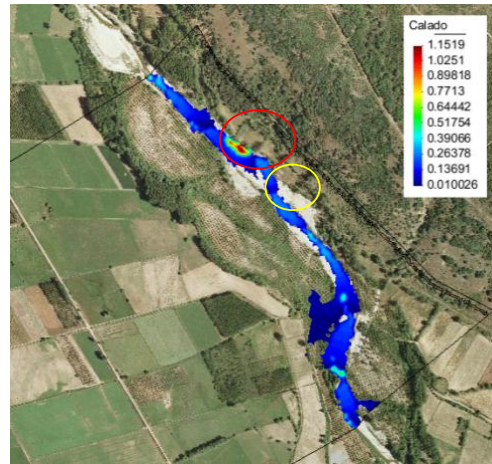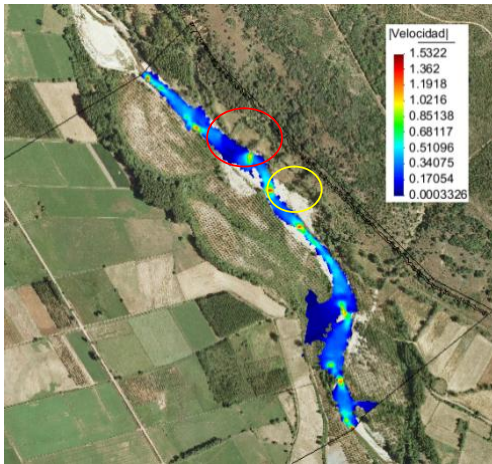

Q= 19 m³/s
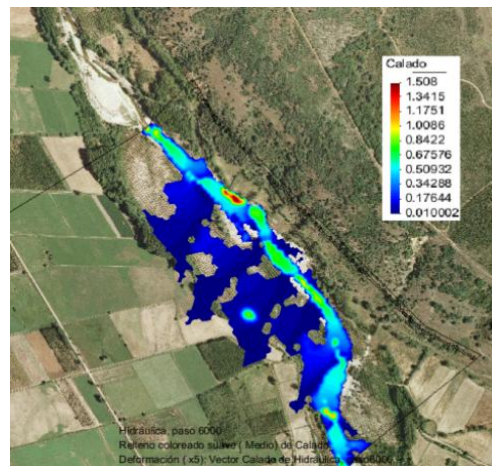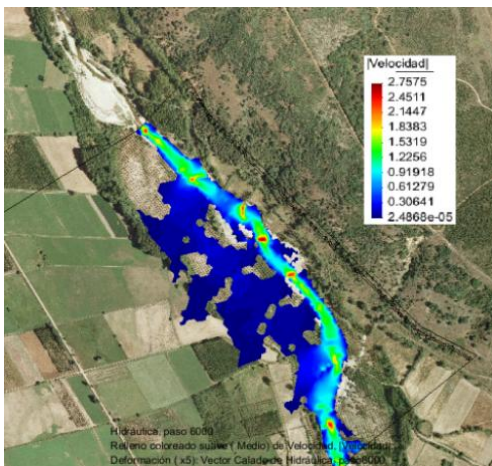
Q= 68 m³/s
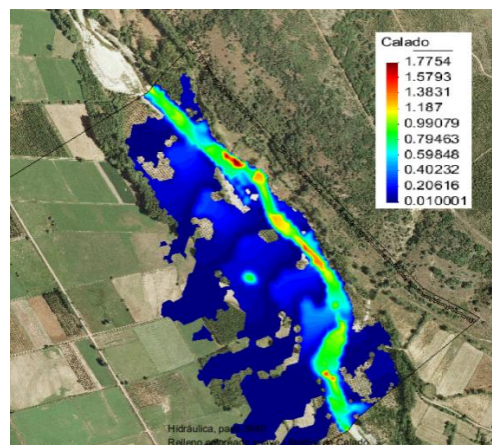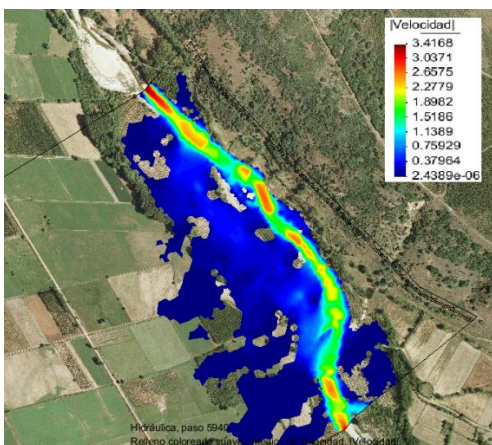
Figure 19.6   Some outputs of the model in which water velocity and depth of water column is shown through the colour legend.
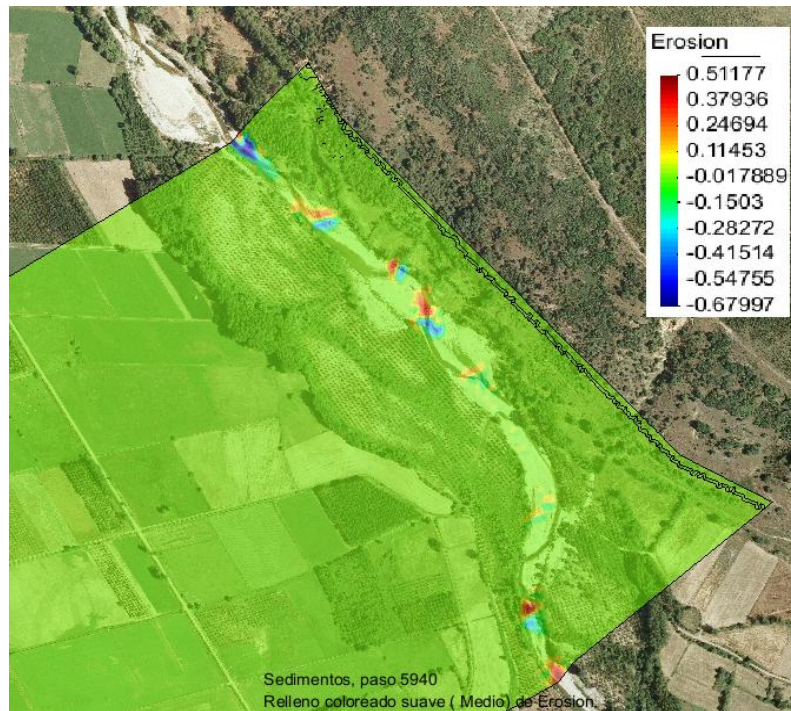
Figure I9.7 Output with the erosion (red colors) and deposition zones (blue colors) for the 5-y return period discharge, (68 m³/s).

I9.4 Conclusions

Results of the River Curueño simulation show local zones where erosion and sedimentation processes are more active and disturbances for biota may be more intense or frequent, in our case identified by the 5-y flood and representing 20 % of the studied river length. The Hydraulic simulation provides a useful tool for selecting macrobenthic sampling points where HYMO processes produce maximum stress. Also, the hydraulic conditions that characterize the microhabitat may be analyzed. The assessment of macroinvertebrate response to Hydromorphological impacts and pressures based on this type of modeling could incorporate new approaches and perspectives.

I9.5 References

Bladé E, Cea L, Corestein G, Escolano E, Puertas J, Vázquez-Cendón E, Dolz J, Coll A. 2014. Iber: herramienta de simulación numérica del flujo en ríos. Revista Internacional de Métodos Numéricos Para Cálculo Y Diseño En Ingeniería, 30(1), 1–10.

Brooks A J, Haeusler TIM, Reinfelds I, Williams S. (2005). Hydraulic microhabitats and the distribution of macroinvertebrate assemblages in riffles. Freshwater Biology 50(2): 331-344.

Camenen B, Larson M. 2005. A general formula for non-cohesive bed load sediment transport. Estuarine, Coastal and Shelf Science 63(1): 249-260.

CEDEX, GEAMA, FLUMEN y CIMNE 2010a: IBER. Modelización bidimensional del flujo en lámina libre en aguas poco profundas. Manual básico de usuario.

CEDEX, GEAMA, FLUMEN y CIMNE 2010b: IBER. Modelización bidimensional del flujo en lámina libre en aguas poco profundas. Manual de referencia hidráulico de Iber (2012)

Gabel F, Garcia XF, Schnauder I, Pusch M. 2012. Effects of ship-induced waves on littoral benthic invertebrates. Freshwater Biology 57: 2425-2435.

Gore JA, Layzer JB, Mead J. 2001. Macroinvertebrate instream flow studies after 20 years: a role in stream management and restoration. Regulated Rivers: Research and Management 17: 527-542.

Hart D, Finelli C. 1999. Physical-biological coupling in streams: the pervasive effects of flow on benthic organisms. Annual Review of Ecology and Systematics 30: 363-395.

IGN, 2011. www.ign.es

Jowett IG. 2003. Hydraulic constraints on habitat suitability for benthic invertebrates in gravel-bed rivers. River Research and Applications 19: 495-507.

Lamberti GA, Resh V. 1985. Comparability of introduced tiles and natural substrates for sampling lotic bacteria, algae and macro invertebrates.Freshwater Biology 15(1): 21-30.

Lamouroux N, Olivier J-M, Persat H., Pouilly M, Souchon Y, Statzner B, 1999. Predicting community characteristics fro habitat conditions: fluvial fish and hydraulics. Freshwater Biology 42: 275–299.

Meier CI. 2008 Cottonwood establishment in a grave bed river. PhD Thesis. University of Montana. Missoula. 149 pp.

Meyer-Peter E, Müller R. (1948, June). Formulas for bed-load transport. InProceedings of the 2nd Meeting of the International Association for Hydraulic Structures Research (pp. 39-64).

Milhous RT, Updike MA, Schneider DM. 1989. Physical Habitat Simulation System Reference Manual—Version II. Biological report 89(16). US Fish and Wildlife Service, Washington, DC.Schweizer, S., Borsuk, M.E., Jowett, I., Reichert, P., 2007. Predicting joint frequency distributions of depth and velocity for instream habitat assessment. River Research and Applications 23, 287–302. doi:10.1002/rra.980

Statzner B, Gore JA, Resh VH. 1988. Hydraulic stream ecology: observed patterns and potential applications. Journal of the North American Benthological Society 7: 307-360.

Van Rijn LC. 1984. Sediment transport, Part I: Bed load transport. Journalof Hydraulic Engineering, ASCE, 110(10): 1431-1456.

Chow VT. 2000. Hidráulica de canales abiertos. McGraw Hill.

Wolman MG. 1954. A method of sampling coarse river-bed material. American Geophysical Union.

Annex J

Improving hydromorphological assessment by remote sensing assimilations

Luca Demarchi, Simone Bizzi, Christof Weissteiner, JRC

Summary

This review provides an overview on the possibilities offered by remote sensing technology to explore and analyse river systems. Many of the river parameters judged relevant to understanding fluvial processes and described in Deliverables 2.1 and 2.2 can now be monitored through various type of remote sensing applications ranging from RADAR, multi-spectral and hyper-spectral images, and LIDAR technologies. The accuracy reached by these technologies has only recently started to satisfy the spatial and spectral resolution necessary to analyse the hydromorphological character of river systems. These novel informationsources are deeply enriching our capacity to analyse a river system, providing unprecedented quantities of continuous, spatially distributed datasets along river courses. The remote sensing datasets so derived vary in their spatial accuracy, spectral information, and cost of acquisition but they can be used for various applications in fluvial geomorphology. This review provides a perspective on these data sets for river managers, by describing the suitability of different remote sensing technologies to investigate different components of river hydromorphology.

J.1 Introduction

"*...remote sensing of rivers has come of age. Clearly, there is still much room for improving existing techniques and developing new methods. However, the range of applications and the consistent high accuracies reported in literature suggest it is time to make greater use of the existing methods in management and process studies. The field has moved beyond proof-of-concept; the time to start applying the techniques more widely is now*", (Marcus and Fonstad, 2010).

The emergence of 'Fluvial Remote Sensing' as a sub-discipline of remote sensing and river sciences is well documented in recent literature (Carbonneau and Piégay, 2012; Marcus and Fonstad, 2010). The opportunity t6 have access to remote sensing data (RS) which satisfies the spatial and spectral requirements of river science is increasing strongly. However, the convergence between technical requirements of fluvial remote sensing and RS technological innovation has still not achieved a suitable level to start applying state-of-the-art methodologies to river management. On the one hand, the acquisition of RS data covering large areas has only recently started to achieve suitable spatial and spectral resolution for fluvial audits. On the other hand, hyperspectral RS has opened up new possibilities thanks to the high spectral and spatial resolutions achieved, but its use for operational mapping remains limited because of scarce availability of data and limited coverage due to the steep costs of data aquisition. Similarly, topographic data at high-resolution are only collected from airborne platforms, resulting in limited

coverage and high acquisition costs. Under these circumstances, river managers currently have to make compromises if they are to use these technologies.

However, considering the RS technological development which has characterized recent decades, it is highly likely that new space borne missions will overcome the current limitations in the near future (Green et al., 2008; Kaufmann et al., 2006; Sacchetti et al., 2010) by providing data acquisition at resolutions and spatial extents necessary for river studies at affordable prices. In the meantime, research on RS of rivers is continuously expanding, although it is inevitably oriented towards specific research questions rather than confronting operational implementation aspects more generally.

To date, river science has been based largely on discontinuous field-derived data and (often) manual editing of geographical information. In this respect RS technology is providing a new source of spatially distributed, multi-dimensional information of high resolution. This novel availability of morphological and topographic datasets challenges existing data analysis skills and requires sophisticated statistical modeling frameworks to become suitable for river characterization and management (Alber and Piégay, 2011; Schmitt et al., 2014). Hydromorphological indices estimated from RS data are actually more robust than those derived using discontinuous field data because they rely on continuous, quantitative information, and so their assessment is more objective and less subject to the operator subjectivity (Buffington and Montgomery, 2013).

Deliverable 2.1 Part 1 provides a methodological framework for the multi-scale hydromorphological characterization of rivers, indicating which indicators are relevant for understanding channel morphological forms and processes and how these are related to natural contingency or historical human pressures. Many of these proposed indicators can be calculated using RS techniques, and the number of papers to support this type of approach is significant.

This review reports on recent studies where different sources of RS data have been used for the development of semi-automated procedures for the characterization of the hydromorphological river features listed in Deliverable 2.1 Part 1. It is strategically important to contextualize state-of-the-art research which makes use of remote sensing technology for river science, because water authorities and river managers across Europe need to plan cost-effective acquisitions campaigns of RS data at regional/national levels to contribute to modern river monitoring activities (EC, 2000). Choices concerning the kind of data acquisition and the appropriate frequency should be key questions that need to be addressed in the coming years. The answers should be a function of management objectives and resource availability, and should be taken based on scientifically sound evidence concerning the capability of specific RS technologies to characterize targeted river features and properties.

The structure of this review follows the key concepts of RS technology. RS is generally divided into two broad categories: active and passive remote sensing, which refer to the source of radiation. Passive sensors rely on an external source of radiation, the electromagnetic spectrum, which is recorded within a specified, finite range of wavelengths depending on the sensor's technical characteristics. The majority of passive sensors record reflected sunlight in the visible and shortwave infrared ranges, producing optical imageries. Although optical imagery dates back to the early 1970s, it remains an area of vibrant research in river remote sensing (Marcus and Fonstad, 2010). Key studies in fluvial remote sensing using optical imagery that focus on the extraction of some of

the indicators listed in Deliverable 2.1 Part 1 are gathered in this review, in Section J.2. In contrast, active RS relies on internally generated and emitted radiation. The key measured parameter is the time elapsed between the emission of a radiation pulse and its detected return. The best-known example of active RS is RADAR (Radio Detection And Ranging) which uses radio waves to detect the position of objects with respect to the sensor. More recently, LiDAR (Light Detection And Ranging) has rapidly become of major interest for geomorphologists. In Section J.3 we gather studies focusing on the use of active RS data for the extraction of some of the indicators reported in D2.1 Part 1.

The intent of this review is to provide a broad overview on what kind of RS data are available and their potential use for characterizing different HYMO river features ranging from catchment (e.g. land use and potential sediment supply) to reach (e.g. in-channel morphological and riparian corridor features) scales. Referring to the indicators proposed in Deliverable 2.1 Part 1, Table 8.1; Table J.1 provides a list of references to research studies where the indicators proposed have been calculated using different RS data sources. For each indicator the reported references are described in the text, grouped in relation to the RS technology used for their calculation in order to better describe RS data and its potentials for a wide range of applications. Table J.2 focuses on how different types of high resolution RS data can be used to characterize various river hydromorphological components at segment and reach scales, where the latter can be properly assessed only because of recent developments in the accuracy obtained by modern remote sensing technologies.

The literature review proposed here does not pretend to be exhaustive but aims to provide an operational overview for river managers on what is achievable by exploiting remote sensing information, a technology which recently has deeply changed the way we can view and analyse river systems.

Table J.1 A list of HYMO indicators proposed in Table 8.1 of Deliverable 2.1, volume 1 for river hydromorphological characterization that have been derived in the literature using RS data and GIS processing analyses

Spatial Unit	Assessed Criteria	Indicators with References	RS DATA
CATCHMENT	Geology	*Geological and soil type maps*: soil erodibility, soil erosion, rockiness/stoniness degree, roughness.	http://www.onegeology.org/ http://eusoils.jrc.ec.europa.eu/ http://webarchive.iiasa.ac.at/Research/LUC/External-World-soil-database/HTML/
	Landcover	*Land cover* (CORINE land cover) *Green Vegetation Fraction (fCover) of leaf area index (LAI)*: (Baret et al., 2013) .	http://www.eea.europa.eu/data-and-maps/data/clc-2006-vector-data-version-1 http://land.copernicus.eu/global/products/fcover
LANDSCAPE	Fine sediment production	*Pan/European Soil Erosion Risk Assessment model (PESERA)*: (Kirkby et al., 2004)	http://eusoils.jrc.ec.europa.eu/ESDB_Archive/pesera/pesera_download.html
	Coarse sediment production	*Coarse Sediment production*: (Bertrand et al., 2013)	High resolution multi-spectral + LIDAR
SEGMENT	Sediment supplied to the channel Sediment transport and storage	*Sediment budget*: (Lallias-Tacon et al., 2014; Notebaert et al., 2009; Wheaton et al., 2013) *Stream power*: (Barker et al., 2009; Biron et al., 2013)	LiDAR LiDAR
	Valley control on channel dynamics	*Floodplain and Terraces features*: (Notebaert and Piégay, 2013; Stout and Belmont, 2014)	LiDAR
	Riparian corridor features	*Vegetation Structural classes*: (Johansen et al., 2010c, 2007) *Plant Projective Cover*: (Johansen et al., 2010c) *Riparian zone extent and width*: (Clerici et al., 2013; Johansen and Phinn, 2006)	High resolution multi-spectral High resolution multi-spectral High resolution multi-spectral
	Potential wood delivery	*Woody debris*: (Marcus et al., 2002; Smikrud and Prakash, 2006) *Woody debris*: (Marcus et al., 2003)	High resolution multi-spectral Hyperspectral
	Flood area	*Flood extents and flood wave dynamic*: (Martinis et al., 2009; Neal et al., 2009; Pulvirenti et al., 2011)	RADAR

Table J.1 (ctd.)

Spatial Unit	Assessed Criteria	Indicators with References	RS DATA
REACH	Flow Energy	*Stream power*: (Barker et al., 2009; Biron et al., 2013)	LiDAR
	Sediment size	*Bed sediment size*: (Carbonneau et al., 2005, 2004) *Bank sediment size*: (Rainey et al., 2003)	High resolution multi-spectral data Hyperspectral
	Channel dimensions and features	*Channel morphology*: (Biron et al., 2013; Notebaert et al., 2009) *Active channel*: (Legleiter, 2012) *Active channel*: (Bertrand et al., 2013; Fisher et al., 2013) *Water depth*: (Fonstad and Marcus, 2005; Legleiter, 2012) *Water depth*: (Legleiter et al., 2009, 2004; Marcus et al., 2003) *Geomorphic features*: (Legleiter et al., 2002; Marcus et al., 2003) *Water temperature*: (Handcock et al., 2012)	LiDAR LiDAR High resolution multi-spectral data High resolution multi-spectral data Hyperspectral Hyperspectral Thermal data
	Lateral Migration, planform changes Narrowing/widening/ Bed incision/aggradation	*Lateral Migration, Channel pattern changes, Bed incision /aggradation*: (Lallias-Tacon et al., 2014; Notebaert et al., 2009; Wheaton et al., 2013)	LiDAR
	Aquatic vegetation	*Algae*: (Hick et al., 1998) *Submerged Vegetation*: (Silva et al., 2008; Williams et al., 2003)	High resolution multi-spectral data Hyperspectral
	Riparian Vegetation	*Riparian corridor features*: (Johansen et al., 2010a, 2010c; Michez et al., 2013a)	LiDAR
	Large Wood and organic debris	*Woody debris*: (Smikrud and Prakash, 2006) *Woody debris*: (Marcus et al., 2003)	High resolution multi-spectral data Hyperspectral

Table J.2 List of indicators grouped by RS data used for calculation.

RS data	Indicators with references	Assessed Criteria	Spatial Unit
High resolution multispectral	*Vegetation Structural classes*: (Johansen et al., 2010c, 2007)	Riparian corridor features	Segment
	Plant Projective Cover: (Johansen et al., 2010c)	Riparian corridor features	Segment
	Riparian zone extent and width: (Johansen and Phinn, 2006) (Clerici et al., 2013) (Weissteiner et al., 2013)	Riparian corridor features	Segment
	Woody debris: (Marcus et al., 2002; Smikrud and Prakash, 2006)	Potential wood delivery	Segment
	Woody debris: (Smikrud and Prakash, 2006)	Large Wood and organic debris	Reach
	Bed sediment size: (Carbonneau et al., 2005, 2004)	Sediment size	Reach
	Active channel: (Bertrand et al., 2013; Fisher et al., 2013)	Channel dimensions and features	Reach
	Water depth: (Fonstad and Marcus, 2005; Legleiter, 2012)	Channel dimensions and features	Reach
	Algae: (Hick et al., 1998)	Aquatic vegetation	Reach
Hyperspectral	*Woody debris*: (Marcus et al., 2003)	Large Wood and organic debris	Reach
	Bank sediment size: (Rainey et al., 2003)	Sediment size	Reach
	Water depth: (Legleiter et al., 2009, 2004; Marcus et al., 2003)	Channel dimensions and features	Reach
	Geomorphic features: (Legleiter et al., 2002; Marcus et al., 2003)	Channel dimensions and features	Reach
	Submerged Vegetation: (Silva et al., 2008; Williams et al., 2003)	Aquatic vegetation	Reach
LiDAR	*Sediment budget*: (Lallias-Tacon et al., 2014; Notebaert et al., 2009; Wheaton et al., 2013)	Sediment supplied to the channel	Segment
	Stream power: (Barker et al., 2009; Biron et al., 2013)	Sediment transport and storage	Segment
	Stream power: (Barker et al., 2009; Biron et al., 2013)	Flow Energy	Reach
	Channel morphology: (Biron et al., 2013; Notebaert et al., 2009)	Channel dimensions and features	Reach
	Active channel: (Legleiter, 2012)	Channel dimensions and features	Reach
	Lateral Migration, Channel pattern changes, Bed incision /aggradation: (Lallias-Tacon et al., 2014; Notebaert et al., 2009; Wheaton et al., 2013)	Lateral Migration, Narrowing/ widening/, Bed incision/ aggradation	Reach
	Riparian corridor features: (Johansen et al., 2010a, 2010c; Michez et al., 2013a)	Riparian Vegetation	Reach
RADAR	*Flood extents and flood wave dynamic*: (Martinis et al., 2009; Neal et al., 2009; Pulvirenti et al., 2011)	Flood area	Reach

J.2   *Passive Remote Sensing*

J.2.1   Low/medium resolution multi-spectral data

For the purposes of this review we define as low/medium spatial resolution the resolution provided by mainly long-term, established sensors (e.g. LANDSAT 8, ETM+, TM and MSS, ASTER, SPOT 4/5, MODIS) that currently enable the production of data of national and supranational extent without a major effort. We are aware that technological progress may soon shift this limit towards newer, higher resolution sensors.

The suitability of sensors for fluvial applications is determined by a number of considerations. Spatial resolution is only one such consideration: spectral, radiometric and temporal resolution (revisit time) are also important depending on the purpose of a study. Although current remote sensing studies that analyse river systems often use high resolution images (see following sections), an important strength of low/medium resolution remote sensing is that it provides data across large areas (national or worldwide), which is a scale that it is not yet covered by high resolution RS datasets.

In this section we report some examples of assessments that have been carried out at Pan-European Union scale using medium-low resolution RS data. Multispectral data, mosaics of 25 m resolution with channels in the green, red and infrared range for the year 2000 and 2006 are stored and pre-processed for the entire Europe.

Recently, more detailed data, such as a SPOT5 pan-sharpened mosaic has become available (10 m original resolution or 2.5 m final resolution). Various Pan-European indicators have been assessed using these datasets, including land cover (CORINE land cover, http://www.eea.europa.eu/data-and-maps/data/clc-2006-vector-data-version-1), and regularly (monthly/yearly) recorded indicators, such as the Green Vegetation Fraction (fCover, http://land.copernicus.eu/global/products/fcover) of the leaf area index (LAI) for trend analysis (Baret et al., 2013).

Recently, research efforts have also focused on calculating more sophisticated indicators at pan-EU scale, coupling these with precipitation, DEM (see Section J3.3 on Radar data), and soil characteristics. Geological and soil type maps providing information on soil erodibility, soil erosion, rockiness/stoniness degree, roughness have also been produced at pan-EU scale: http://www.onegeology.org/, http://eusoils.jrc.ec.europa.eu/.

A physically based soil erosion model exists at pan-EU scale that is capable of providing estimates of soil erosion rates per year for the whole of Europe (PESERA, http://eusoils.jrc.ec.europa.eu/ESDB_Archive/pesera/pesera_download.html).   In addition, the average single-sided width of riparian corridors has been calculated across Europe by Weissteiner *et al.* (2013) using an improved model to detect riparian areas after Clerici *et al.* (2013). In this case, RS data input was provided by LANDSAT imagery and ASTER data was used in the derivation of the DEM. The authors derived riparian corridor width to assess buffer capacity of riparian areas for the abatement of nutrients and, in a different study, for pesticides (Weissteiner et al., 2014).

J.2.2 High resolution multi-spectral data

Ever-accelerating advances in technology indicate that optical satellites can now provide multi-spectral data at high spatial resolution (up to 1.65 with GeoEye), while airborne imagery can cover ever-wider spatial extents, portraying rivers as continuous systems. These have the potential to transform river science by providing improved data with continuous characterization of multi-scalar variations of many stream parameters, which should allow for the development of new scientific understanding and new theories concerning river processes, eventually resulting in better guidance for river monitoring and management.

Prior to the late 1990s, image-based river maps were mainly derived using visual interpretation or photogrammetric analysis of air photos. Few researchers used multispectral satellite-based imagery for mapping river features, because large pixel sizes (up to 30 m) limited most analyses to large river settings. Multispectral mapping of smaller streams and in-stream features only emerged in the mid 1990s as airborne multispectral sensors provided pixel resolutions substantially smaller than the stream width. Since that time, the increasing availability of finer resolution imagery from satellites, aircrafts or drones, has resulted in a significant growth of investigations focusing on potential applications of optical imagery for stream characterization.

In this section we briefly synthesise established river mapping investigations from the literature that use high spatial resolution multispectral imagery, focusing on some of the stream indicators underlined in Tables 8.2 and 5.2 of Deliverable 2.1 Part 1.

Bed sediment size. Mapping bed sediment size is important for documenting in-stream habitat for fish, macroinvertebrates and other organisms, for characterizing flow resistance for hydraulic and flood inundation models, and for modeling sediment transport and channel stability. The biggest limitation in measuring sediment size is the image resolution: the smallest size that can be mapped from black and white or three-band-colour imagery is equal to the pixel resolution of the image (Carbonneau et al., 2005). For this reason, work on mapping sediment size in rivers is relatively new, and reflects the recent availability of airborne optical imagery at sufficiently fine spatial resolutions. Carbonneau and others have taken the lead in demonstrating that texture variations provide an estimation of sediment sizes (Carbonneau et al., 2005, 2004). Areas with larger sediment sizes have more shadows, which determine a more heterogeneous texture, whereas finer sediment sizes have less shadows and therefore present a more homogenous texture. A linear regression was estimated between field measurements of median particle size (D_{50}) and spectral signatures of pixels and Carbonneau et al. were able to continuously map sediment size along 80 km of the St. Marguerite River in Quebec (Figure J.1) with this technique. Managers applying the technique with panchromatic or colour imagery will almost certainly need to charter special flights to collect imagery at sufficient resolution for the sediment size of interest.

Water depth. Measuring water depth from RS data would be of great interest to river managers since this data is often scarce, discontinuous, and monitoring campaigns to measure river cross sections are resource demanding. Furthermore, continuous information on river bathymetry is needed for hydraulic modelling, habitat characterization and for monitoring the evolution of channel processes and forms. As long as water is clear enough to see the river bed, the brightness of the image at a

number of locations can be correlated with field measurements of depth at the same locations. A regression equation derived from this correlation can then be applied to the remainder of the image in order to estimate water depths continuously. Higher accuracies are achieved when multiple regressions of more than one image band (e.g., red, green and blue) are correlated to depth measurements (Gilvear et al., 2007; Lejot et al., 2007). The 'Compagnie Nationale du Rhone' is already using very high resolution imagery to map bathymetry of large, clear-water side channels using unmanned controlled platforms (Lejot et al., 2007) (Figure J.2).
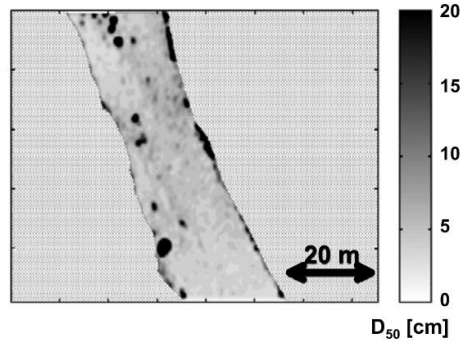

Figure J.1 D_{50} sediment size map developed from the 3 cm spatial resolution, true color imagery for the Sainte Marguerite River, Quebec, Canada (Carbonneau et al., 2005).
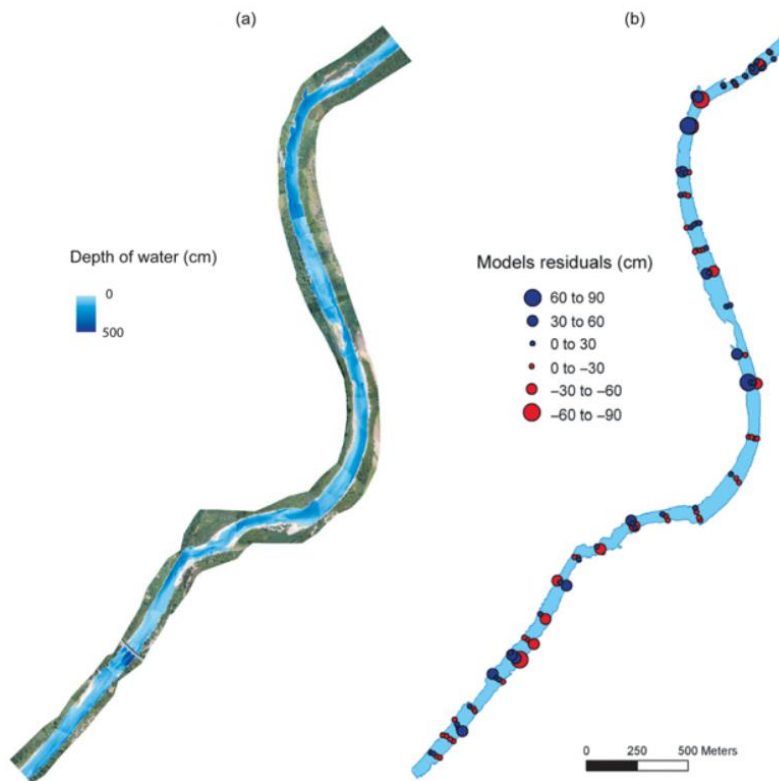

Figure J.2   Field bathymetric map of the Rhone reach calculated by multiple regression of water depth and brightness variability. (b) spatial variation of residuals models. (Lejot et al., 2007)

The major limitation of this correlation approach is the need for ground-based data at the time of image acquisition in order to avoid variations in discharge and channel shape that may modify the relationship between pixel values and depth. Recent innovations in physically-based approaches such as the hydraulically assisted bathymetry model (Fonstad and Marcus, 2005) do not require field crews or data collection specific to the acquisition project, since water depth is modeled based on equations that describe the light attenuation by the water column and the hydraulics of the open channel flow using discharge data, slope and channel width. However, water clarity is the key limitation to all techniques for estimating water depths. The maximum depth that can be remotely measured is the maximum water depth to which the light can penetrate, return to the surface and be detected by the sensor, which varies with water column optical properties, wavelength, instrument sensitivity, and substrate composition (Legleiter et al., 2004). Legleiter (2012) partially overcame this challenge by finding a reasonably strong agreement between green band radiance of optical imagery acquired at 0.4 m resolution and water depth (R^2=0.61) in higly turbid water conditions (Legleiter, 2012).

Wood. The presence of wood in rivers can force sediment deposition, transport and sorting, altering in-stream habitats and stream morphology; provides organic material for macroinvertebrates; and creates shelter for fish. Furthermore, wood emplacement is a major tool used in stream restoration, and promoting wood accumulation is often a central goal of riparian management strategies (Fox and Bolton, 2007; Kail et al., 2007). In theory, automated remote detection of wood in river channels or on exposed bars should be relatively straightforward, as long as sufficiently fine resolution imagery is available. However, because wood has a clear spectral signature that differs from other active channel features in the shortwave infrared, this task becomes more challenging if hyperspectral data are not available. In an early attempt to map wood, Marcus et al. (2002) encountered some problems: "*Our findings that four-band 1-m resolution imagery is not effective for mapping woody debris are discouraging (producer's accuracy of only 17%). It is unclear from our work, however, whether the major problems in distinguishing woody debris derive from insufficient spectral bands or from problems in coregistration of imagery and field maps at this fine spatial resolution*" (Marcus et al., 2002). Subsequent work that coupled matched filtering techniques with principal components analysis, achieved higher classification accuracy of 89%, when applied to digital air photos at submeter resolution (0.4 m) (Smikrud and Prakash, 2006).

Riparian corridor features. Riparian vegetation provides a number of important functions including: (a) nutrients to streams from litter fall, (b) root masses for stream bank stability, (c) shade to control water temperature and algal growth, (d) large wood for stream channel development, and (e) natural filtering preventing pollutants from entering waterways. Johansen et al. (2010c) have taken the lead in showing the feasibility of different sources of remotely sensed data for mapping riparian zone attributes. Vegetation indices and image texture derived from Ikonos 4 m resolution multi-spectral data were used to map riparian species composition in Australian Tropical Savannahs (Johansen and Phinn, 2006). However, the overall accuracy proved to be relatively low (55 percent), even after visual improvement led by the pan-sharpering process. On the other hand, riparian zone width could easily be identified with Ikonos data, while using the ETM+ (28m spatial resolution) resulted in an overestimation of the riparian zone width in most riparian zones wider than 50 m. At the same time, narrow riparian zones (less than 10m) were not identified from the ETM+ imagery, for obvious

spatial resolution limitations. High spatial resolution Quickbird data were later used to discriminate vegetation structural stages in riparian and adjacent forest ecosystems as defined by the British Columbia Terrestrial Ecosystem Mapping (TEM) scheme, allowing the spatial distinction of Herb/Shrub, Young/Old Forests with an overall accuracy of about 79% (Johansen et al., 2007). The final high overall accuracy was achieved by combining spectral and textural information within an object-based approach applied on the 2.8m spatial resolution Quickbird scene of (Figure J.3).
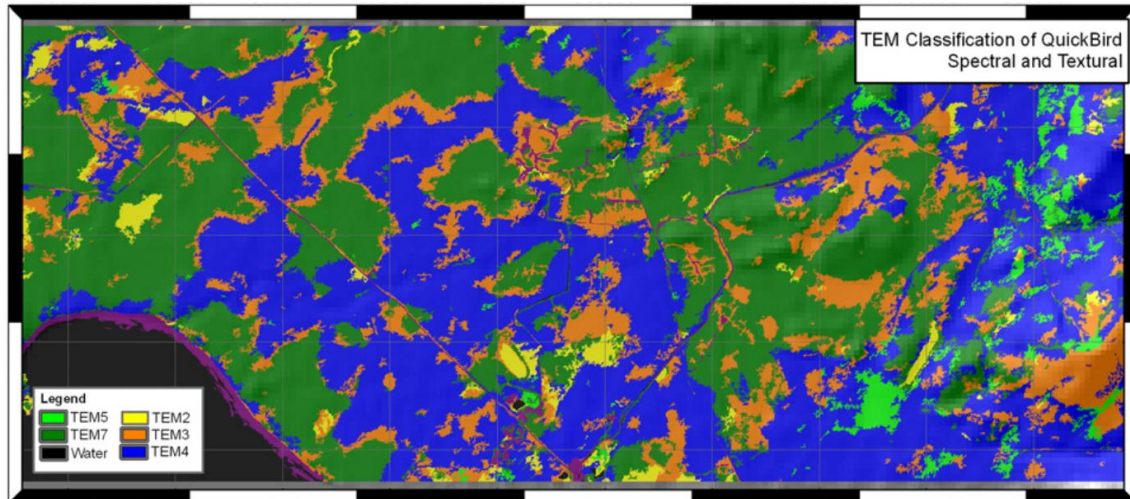

Figure J.3   Classification of vegetation structural classes using textural and spectral information extracted from a Quickbird scene (2.8 m spatial resolution). TEM classes: TEM2: Herb; TEM3: Shrub/Herb; TEM4: Pole/Sapling; TEM5: Young Forest; TEM7: Olf Forest (Johansen et al., 2007).

In following work, it was demonstrated that SPOT-5 image data was unsuitable for assessment of riparian zone attributes of 32 km of the Mimosa Creek and associated riparian zones (Johansen et al., 2010c). Even though use of SPOT-5 data was associated with the lowest costs, the mapping accuracy of all riparian attributes apart from the Plant Projective Cover (PPC) attribute and the presence/absence of vegetation proved to be too poor because of the 10 m pixel size (Johansen et al., 2010c). In order to retrieve such riparian attributes exhaustive field campaigns are also mandatory (Johansen et al., 2010c) both for the production of riparian attribute maps and for the validation of results.

Algae. High spatial resolution imagery can provide good measurements of algal blooms over time in lake settings. Hick et al. (1998) found high correlations between the 750 nm band and several parameters, concluding that only three to four bands were needed to map algal blooms over large areal extents, provided that in-water calibration data are available.

Active channel. The active channel is a key hydromorphological parameter which includes the wetted channel and the adjacent sediment bars, i.e. the portion of the channel regularly morphologically re-worked by floods at least every few years. In the

literature there are examples of automated delineations of water channels, sometimes also referred to as bankfull channels, since discerning water from vegetation and bare soils is an easy task for RS applications, including using low-medium resolution multi-spectral information. Although this type of application does not identify the active channel in a geomorphological sense, the potential to measure water width from country to world-wide scales is of increasing research interest. Despite this, channel width is almost never explicitly measured, especially in small, tectonically active systems. Fisher et al. (2013) proposed the ChanGeom methodology, which is able to efficiently and explicitly extract active channel widths at resolutions that were previously impossible using freely available imagery. Bertrand et al. (2013) also proposed a method for active channel delineation based on high-resolution multi-spectral data which defines the active channel as the combination of all low-flow water channels and unvegetated bar polygons delineated by Thiessen polygonization. This method has allowed delineation of a geomorphologically sound active channel at the regional scale in the Drome basin in France.

J.2.3   Hyperspectral data

The advent of hyperspectral sensors which are able to acquire data at high spatial and spectral resolutions, has opened up new perspectives for river science. The classical definition of Hyperspcteral data given by Goetz et al. (1985) is still valid today: "*The acquisition of images in hundreds of contiguous registered spectral bands such that for each pixel a radiant spectrum can be derived*". This definition covers all spectral regions [i.e. VIS (visible), NIR (near infrared), SWIR (shortwave infrared), MWIR (midwave infrared) and LWIR (longwave infrared)]. Compared with traditional multispectral imagery which comprises a small number of spectral bands, hyperspectral data can record up to hundreds of very narrow and contiguous wavebands. This information enables the identification of targets based on the spectral behaviour of the material in question by providing near-laboratory-quality radiance for each picture element (pixel) from a distance, and so allows the spatial recognition of physical features beyond the capability of human eyes.

Although its use for operational mapping is still limited due to high costs and limited coverage, the large increase in spectral resolution has proved to be key in many applications from urban to agricultural, in mineralogy and surveillance amongst others. The ability of providing a full-wavelength dataset at a high spatial resolution has established hyperspectral data as one of the most conspicuous river tools to emerge during the past decade, with improved capability for mapping in-stream habitats, classifying riparian vegetation and extracting water depth.

However, the aim of this section is not to report advantages and disadvantages of hyperspectral compared to multispectral data, but to synthesis published river mapping investigations using high resolution hyperspectral data that illustrate the potential to extract some of the stream indicators underlined in Tables 8.2 and 5.2 of Deliverable 2.1 Part 1.

Bank sediment size. The textural technique developed for multispectral data and presented in Section J2.2. is not applicable for mapping sediment size distributions from hyperspectral data. Instead, Rainey et al. (2003) used subpixel linear mixing models on

hyperspectral data to extract sediment sizes in estuarine sediments. This is based on the optical theory that small spaces between fine grains act as blackbody cavities, thereby filling in spectral absorption curves to a degree proportional to the grain size, enabling the estimation of sand and mud proportions, even in pixels that were 1.75 m in size (Figure J.4).
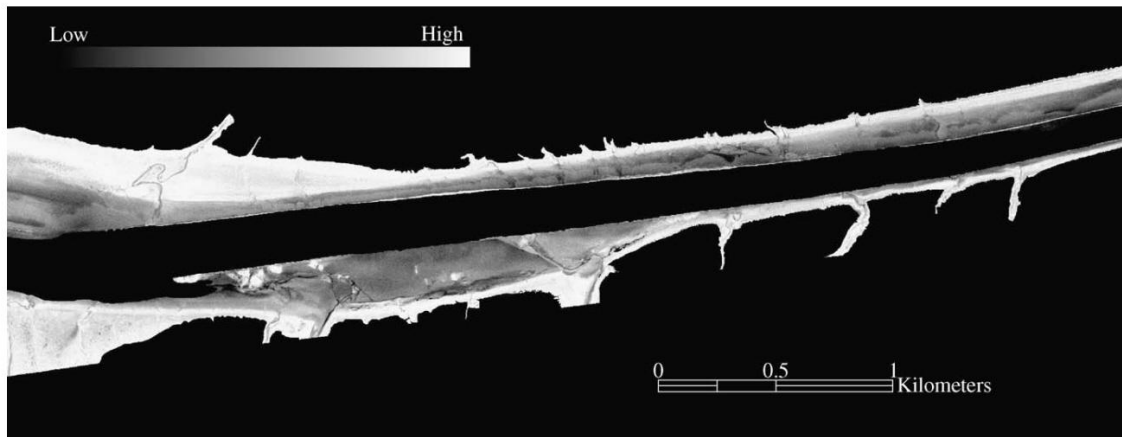

Figure J.4   Subset of the mud abundance image produced from subpixel unmixing of a hyperspectral scene acquired at 1.75 m over the Ribble Estuarine, Lancashire, UK (Rainey et al., 2003).

Water depth. Marcus et al. (2003) achieved a high accuracy of 85% with a 128-bands hyperspectral imagery covering the visible and shortwave infrared spectrum, by applying a step-wise regression for each of the biotopes (riffle, pools, glides, etc..) in order to derive depths specific to different surface turbulence regimes within the stream. Subsequent research confirms and acknowledges the challenges of making water depth estimates that are associated with variations in substrate type and in-stream vegetation. These were further corrected using band-ratios (Legleiter et al., 2004). In Legleiter et al. (2004), the band-ratio technique was used to map bathymetry from both multispectral and hyperspectral images (Figure J.5). Later, the theoretical basis of spectrally-based depth retrieval have been more closely examined with a radiative transfer model and field spectroscopy, outlining the range of conditions under which this approach would be more appropriate (Legleiter et al., 2009). Depth estimates using a band-ratio approach are most reliable when waters are shallow and clear and dominated by absorption rather than scattering of light. Furthermore, band ratios depend on wavelengths. In order to take into consideration these spectral variations, an Optimal Band Ratio Analysis specific for each sensor's wavelength pairs was defined (Legleiter et al., 2009) (Figure J.6).
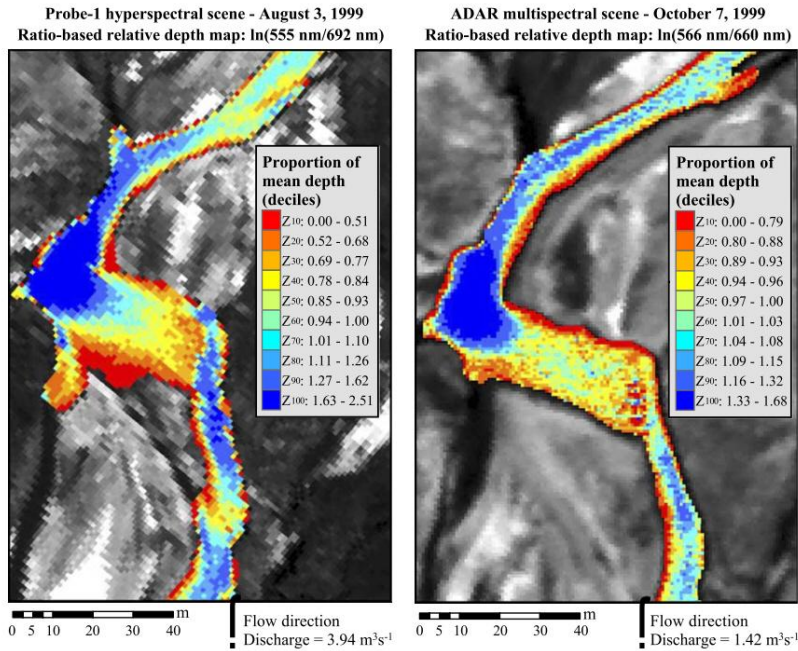
Figure J.5   Application of ratio-based bathymetric mapping to multispectral and hyperspectral images of the Soda Creek in Yellowstone National Park (Legleiter et al., 2004).
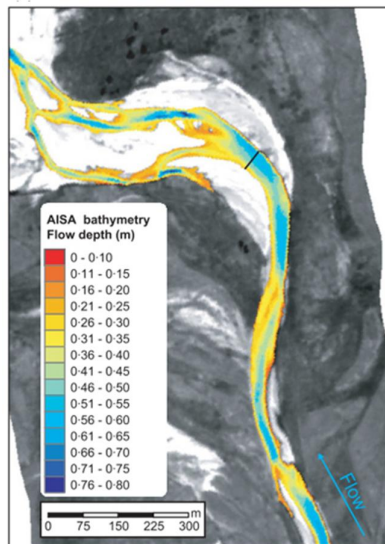

Figure J.6   Spectrally-based bathymetric map of the Lamar River, derived using the bands identified via OBRA of convolved field spectra and equation (Legleiter et al., 2009).

Wood. Automated detection of wood can be relatively simple if one has hyperspectral imagery, because the peculiar spectral signature of wood can be easily distinguished in the shortwave infrared part of the spectrum. As a first step, principal components were extracted from the hyperspectral imagery (Figure J.7) (Marcus et al., 2003). A second

step applied a matched filtering technique to the principal component images, in order to detect wood. Some wood pixels in the image are used as training pixels of the matched filter, which is then able to find similar pixels elsewhere in the image. Theoretically, the matched filter is able to detect wood in areas where it cannot be seen by the naked human eye, and if wood is clearly seen from the imagery, there is no need for field survey.


Starting at the top is the "True Color" image. The second line shows PC components 3-2-1, and also PC components 6-5-4. This image is intended to convey the broad dimensionality of hyperspectral imagery.
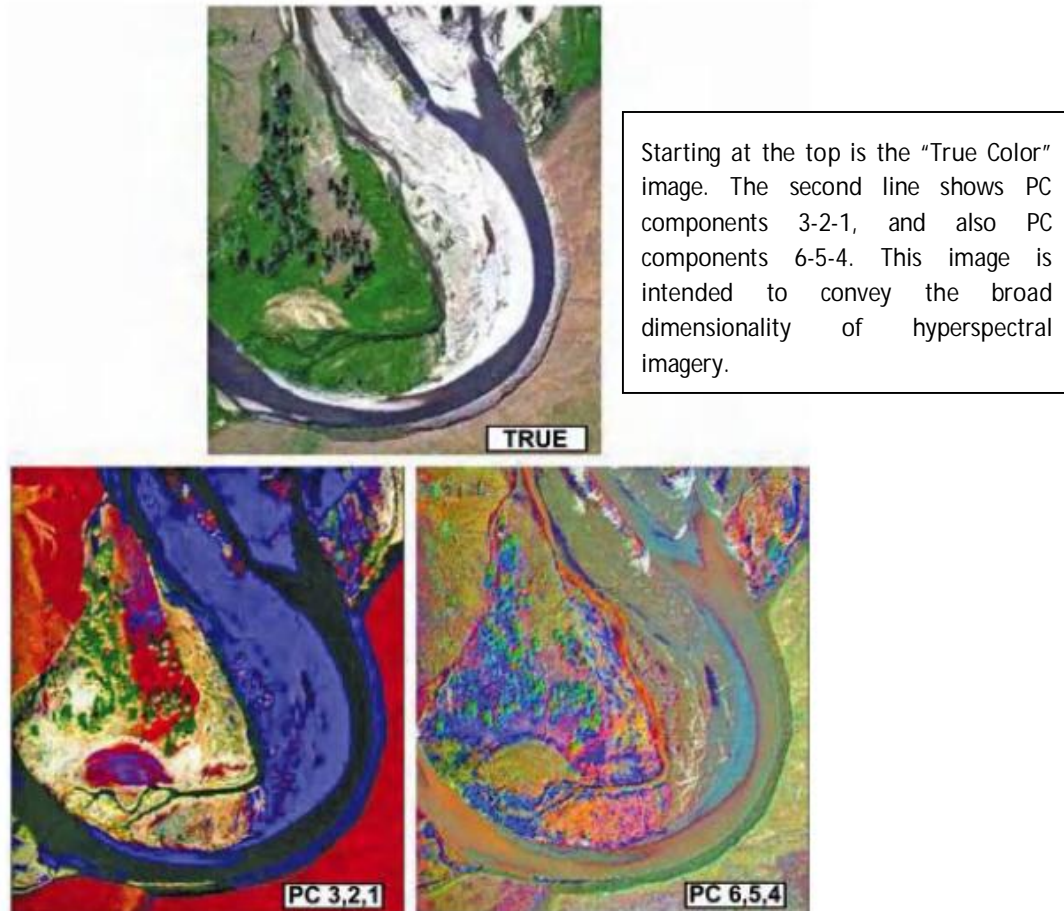
Figure J.7   An example of Pricnipal Components Analysis (PCA) processed hyperspectral image components (Carbonneau and Piegay, 2012).

Geomorphic features. Legleiter et al (2002) tested the effects of sensor resolution on mapping in-stream habitats. After achieving overall accuracies of about 60% for four habitat types, they concluded that spectral resolution was more important than spatial or radiometric resolution for this specific purpose (Legleiter et al., 2002) and that remotely sensed hyperspectral imagery might map stream morphology more effectively than field crews. In order to overcome co-registration errors of field maps and imagery noticed in a previous work (Marcus et al., 2002), Marcus et al. (2003) mapped ground truth directly to printouts of the imagery, downloaded on the same day as the flight. Removing these errors was critical for the accuracy assessment of image-based maps. The main in-stream habitats (glides, riffles, pools, and eddy drop zones) were mapped with a

supervised classification (Figure J.8) with an overall producer's accuracy ranging from 68% to 86% when going from a third order stream to a fifth order stream.
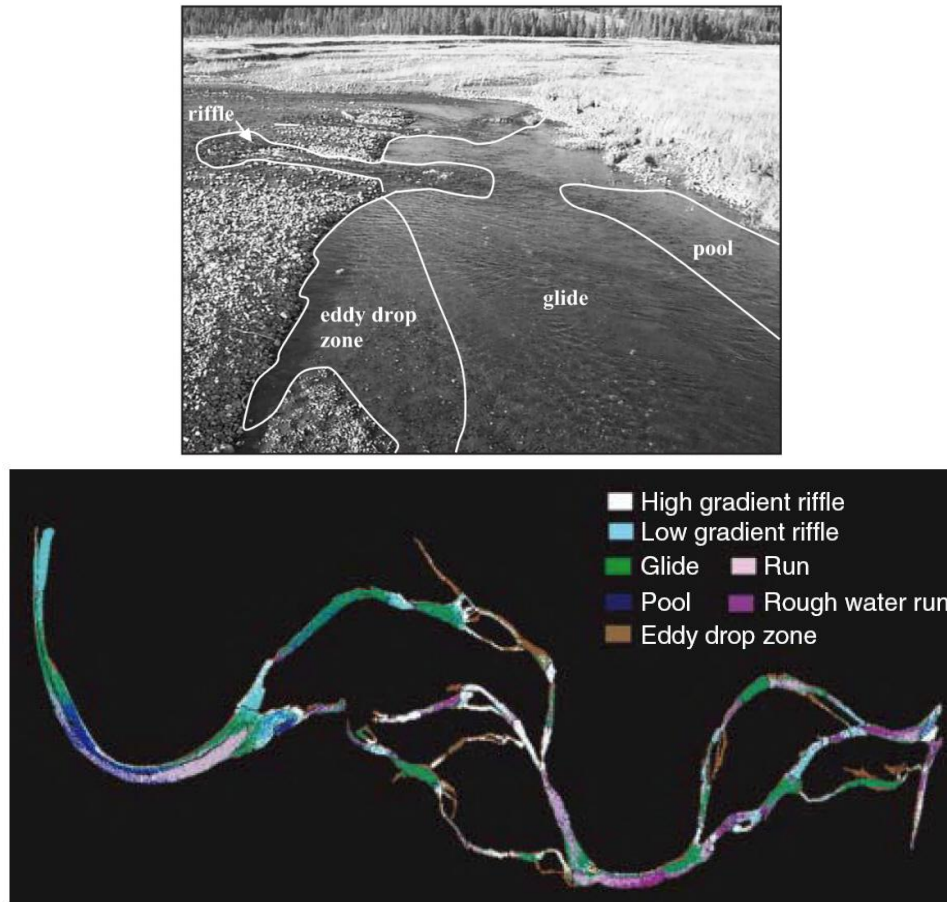

Figure J.8   Example of the four types of in-stream habitats mapped (above) and supervised classification results of a portion of the Lamar River in Yellowstone National Park (below) (Carbonneau and Piegay, 2012).

Submerged vegetation (SAV) and algae. SAV and algae are important to ecosystem health, providing food and cover for a wide range of species. On the other hand, an over abundance can be damaging to ecosystem health, water quality and human structures. Most research on remote sensing of SAV has focused on lakes, deltas, wetlands, estuaries and coastal waters, with few considering stream systems. A central issue in mapping SAV is the relatively strong absorption of optical wavelengths by water. An identical plant looks different to the sensor when it is emergent, beneath the surface or deeply submerged. Changes in plant structure, age and reflectance confuse the identification of plants, complicating the estimation of biomass. Field measurements are therefore necessary for researchers to incorporate plant and location-specific variations to develop regressions that use individual bands, band ratios, or principal components to predict biomass (Silva et al., 2008) (Figure J.9). Hyperspectral data are useful for

separating SAV and algal chlorophyll signals (Williams et al., 2003) and identifying invasive species (Underwood, 2003). However, even the enhanced spectral characteristics do not entirely overcome the issues of water turbidity, water depths and plant physiology: separation of species and mapping of parameters is problematic. For this reason, this type of application is still in a developmental rather than an operational phase.

Figure J.9 Submerged Acquatic Vegetation (SAV) and algae.

J.2.4 Thermal data

An important regional indicator of water quality is water temperature, because it is influenced directly by both ground and surface water inputs and indirectly by land use in the surrounding watershed. Coldwater fishes such as salmon and trout are sensitive to elevated water temperature and so water temperature has to be monitored to ensure it meets management guidelines and quality standards (McCullough et al., 2009). Spatially extensive measurements of water temperature are necessary to locate cool-water refuges. Water temperature has typically been measured using a sparse network of widely distributed in-stream gauges, providing limited information about the spatial distribution of water temperature (Cherkauer et al., 2005). Measurements of water surface temperature using thermal infrared remote sensing (TIR) represents an attractive alternative to *in situ* measurements of temperature, especially because TIR allows quantification of spatial patterns of water temperatures in rivers, streams, and floodplains at multiple spatial scales throughout entire watersheds (Figure J.10). However, this innovative technology can be time consuming and costly, due to the difficulties in obtaining images and to the complexities of data processing. Understand these benefits and limitations is necessary in order to determine whether TIR of water temperature is suitable for water resource management applications. The reader is referred to Handcock et al. (2012) for more insights on this topic.

J.3 Active Remote Sensing

The princinples of LiDAR and RADAR are quite similar, but instead of using radio wavelengths (1-10cm), LiDAR operates in the near-infrared, visible or ultraviolet

wavelengths of the electromagnetic spectrum (250 nm up to 11μm wavelength). As a result of the detailed measurements of terrestrial and aquatic surfaces that they are able to provide, LiDAR have rapidly become a preferred tool for geomorphologists especially in relation to its ability to provide higly accurate topographic mapping: section J3.1 presents some recent applications of LiDAR data in river science, while Section J3.2 provides an example of the employment of RADAR technology.
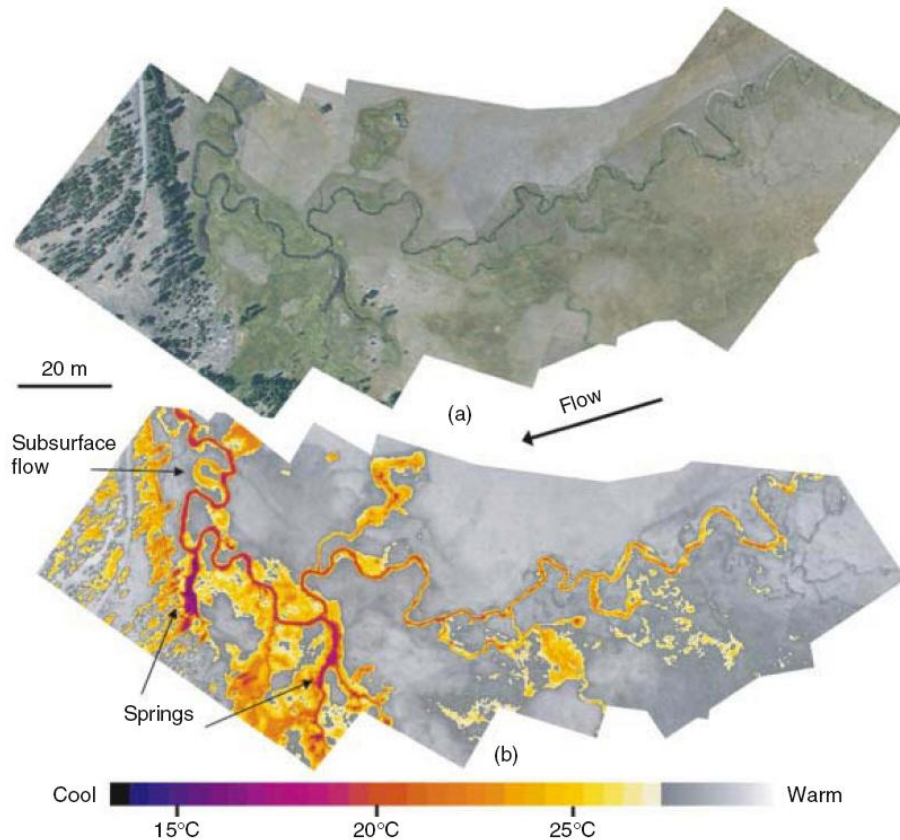

Figure J.10   Natural color and airborne TIR aerial images of groundwater springs flowing into the upper Middle Fork John Day River (Oregon, USA) in a montane meadow (Handcock et al., 2012). Complex subsurface hydrologic flow paths and areas of increased soil moisture adjacent to the wetted channel are revealed in the lower image by TIR.

J3.1   Near-infrared LiDAR

The most commonly used LiDAR, also called topographic LiDAR, uses the infrared wavelength 1064 nm. Both ground and vegetation have a high reflectance ratio in the near-infrared range (NIR), 700-1400 nm. Vegetation also has a transmission ratio in that range, which facilitates the travel of a NIR laser to the ground through vegetation, allowing of simultaneous collection of information on both the ground surface and vegetation. Because the emitted NIR laser pulses are strongly absorbed by water, these

instruments fail to provide topographic information from submerged areas of the channel, an important limitation in river science (Notebaert et al., 2009).

LiDAR for terrestrial surface measurements emits pseudo-Gaussian laser pulses and receives the sum of the pulses' energies reflected by each target that the laser beam reaches. The received waveform is therefore the sum of the response functions of the different targets, resulting in a dense point cloud coverage, where each point represents the back-scatter both from objects and from bare terrain, providing at the same time information about the vertical distribution of targets. In the case of a building, the laser will be completely reflected from the building surface, but in the case of sparse vegetation, the laser pulse will be reflected several times, the first return giving the maximum elevation of the vegetated surface while the last being the elevation of the underlying bare earth.

Channel dimensions and features. Detailed topographic data are of great importance for both quantitative and qualitative fluvial studies. Traditionally-available topographic data are not sufficiently accurate to detect differences in landforms within most floodplains (Notebaert et al., 2009). As a result of the availability of LiDAR data at larger spatial scales and the high vertical accuracy that can be achieved, applications in geomorphology have become quite common. Notebaert et al. (2009) demonstrated that the usefulness of LiDAR is strongly dependent on its resolution. 5 m resolution raster data obtained from a point dataset characterized by an average of 1 point per 20 m^2 were well suited for the qualitative recognition of larger landforms such as levees, but their resolution was insufficient for smaller landform detection such as drainage ditches or old river beds and for quantitative analysis of river channel dynamics. Furthermore, small depressions were smoothed out, but theyare well measured by a 0.5m raster produced from a point cloud having an average point density of 5-8 points/m^2 (Notebaert et al., 2009) (Figure J.11).

Given the suitability of high-resolution LIDAR (4-8 points/m^2) for describing landscape topography, its application to studying river channel geomorphological features has been an active research field. Active channel width has been calculated by Legleiter (2012). They referred to the 'active channel' as the wetted area submerged at the time the remotely sensed data were acquired, with no particular, significant geomorphic attributes. In this approach the active channel was simply delineated from the LiDAR point cloud by selecting the lower densities, where in other words the number of returns per unit area is lower, meaning that a strong absorption of the NIR wavelength has occurred (Figure J.12). After having retrieved water depth from passive optical data within the active channel, they further co-registered it with the topographic LiDAR dataset, producing an innovative hybrid LiDAR/optical product.

Channel gradient has been estimated at unprecedented spatial resolution continuously along a river (Vianello et al., 2009). Stream power has also been calculated continuously along a river course by coupling channel gradient estimates with hydrological models (Barker et al., 2009; Biron et al., 2013) allowing screening tools of river sensitivity to erosion and deposition processes to be provided (Bizzi and Lerner, 2013). Furthermore, sequential LiDAR surveys can be compared to derived sediment budgets and investigate channel patterns changes (Pirot et al., 2014; Wheaton et al., 2013) (see Figure J.13), and specific error assessments frameworks have been developed to derive the accuracy of these sediment budget estimations (Lallias-Tacon et al., 2014).
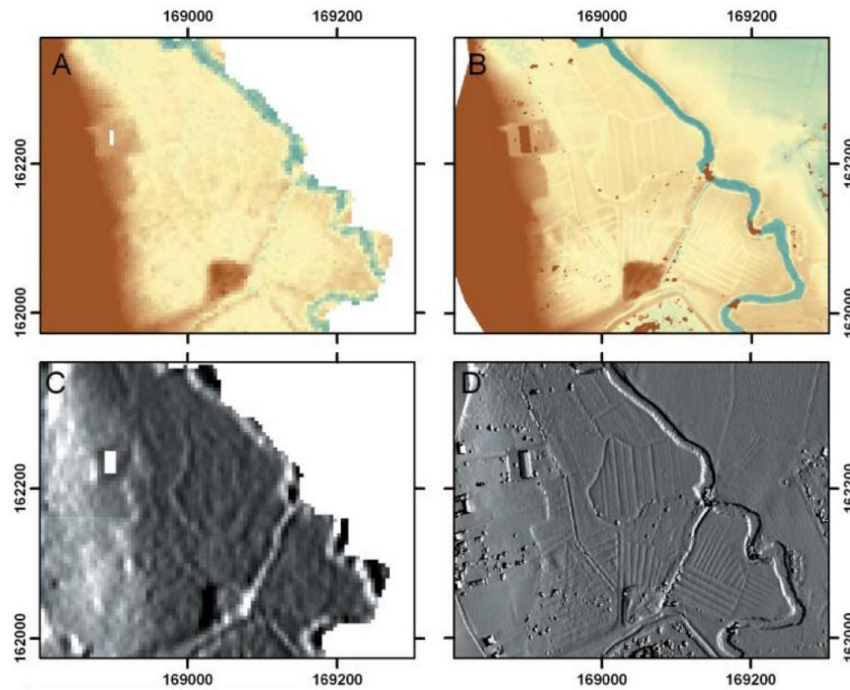
Figure J.11 Comparison of two raster products derived from a point density of 1 point/20m^2 (left) and 5-8 points/m^2 (right) (Notebaert et al., 2009).
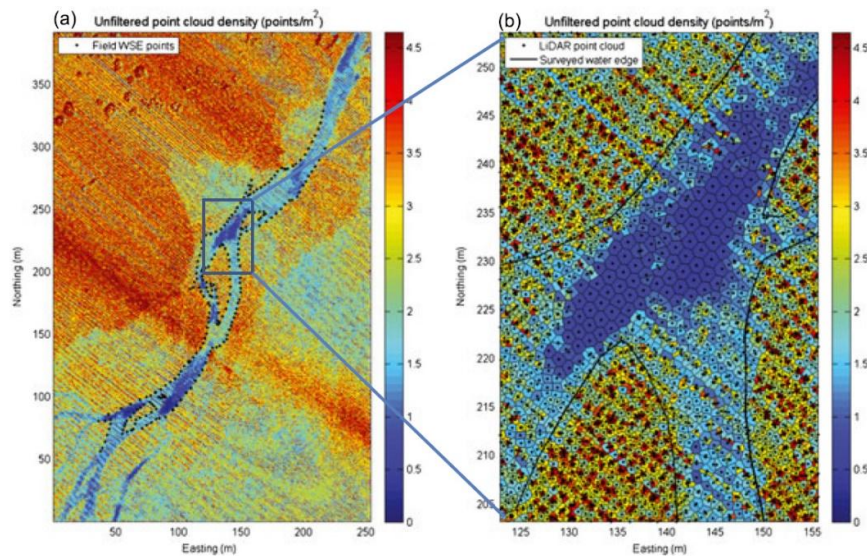

Figure J.12 LiDAR point densities for the Round Prairie reach. The contrast in point density between land and water surfaces corresponds with the active channel boundary surveyed in the field and can be used to delineate channels from the LiDAR point cloud (Legleiter, 2012).

Riparian corridor features. Johansen and others have extensively worked on this topic. In a study published in 2010, they developed an object based image analysis approach using airborne LiDAR data, and as a result several riparian attributes were continuously mapped and tested using field measurements, including longitudinal continuity, vegetation overhang, bank stability, plant projective cover (Johansen et al., 2010b). They concluded that a high density of points is needed for this kind of riparian characterization. In related work, they demonstrated that LiDAR data are more cost-effective than Quickbird and SPOT-5 image data for mapping riparian zone attributes over 26000 km of stream length (Johansen et al., 2010c) (Figure J.14). Even though the use of Quickbird was less expensive, the accuracies were not satisfactory compared to LiDAR results. Michez et al. (2013b) used a similar approach to automatically map important floodplain and riparian zone attributes for a Belgian catchment, allowing a graphical presentation of attributes that was useful for analysing the variation of upstream-downstream attributes and was, therefore, suitable for prioritizing areas for rehabilitation and conservation measures. They stressed that LiDAR data are a potential tool for planning of land and water resource management across large areas. This kind of approach could improve the hydromorphological assessment of water bodies in the context of the Water Framework Directive (EC, 2000), generating precise information on the riparian zone and riparian forest.
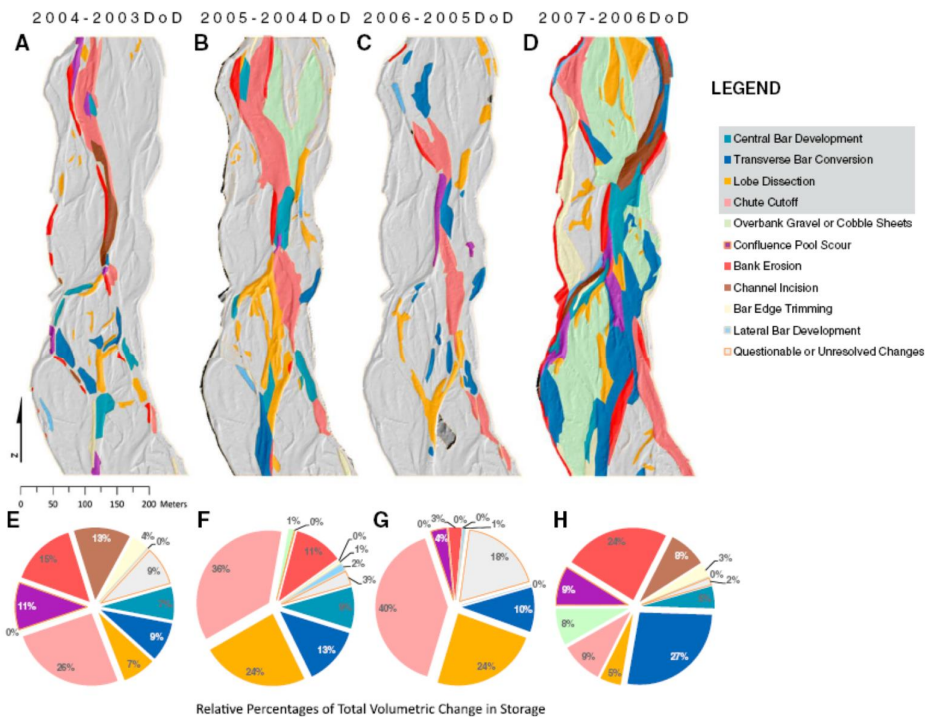

Figure J.13   Spatial aggregation of change in the sediment storage budget by braiding mechanisms and other morphodynamic signatures of change. (a–d) show the geomorphic interpretations spatially for each time period, whereas (e–h) show pie charts of corresponding relative percentages of volumetric change (Wheaton et al., 2013).
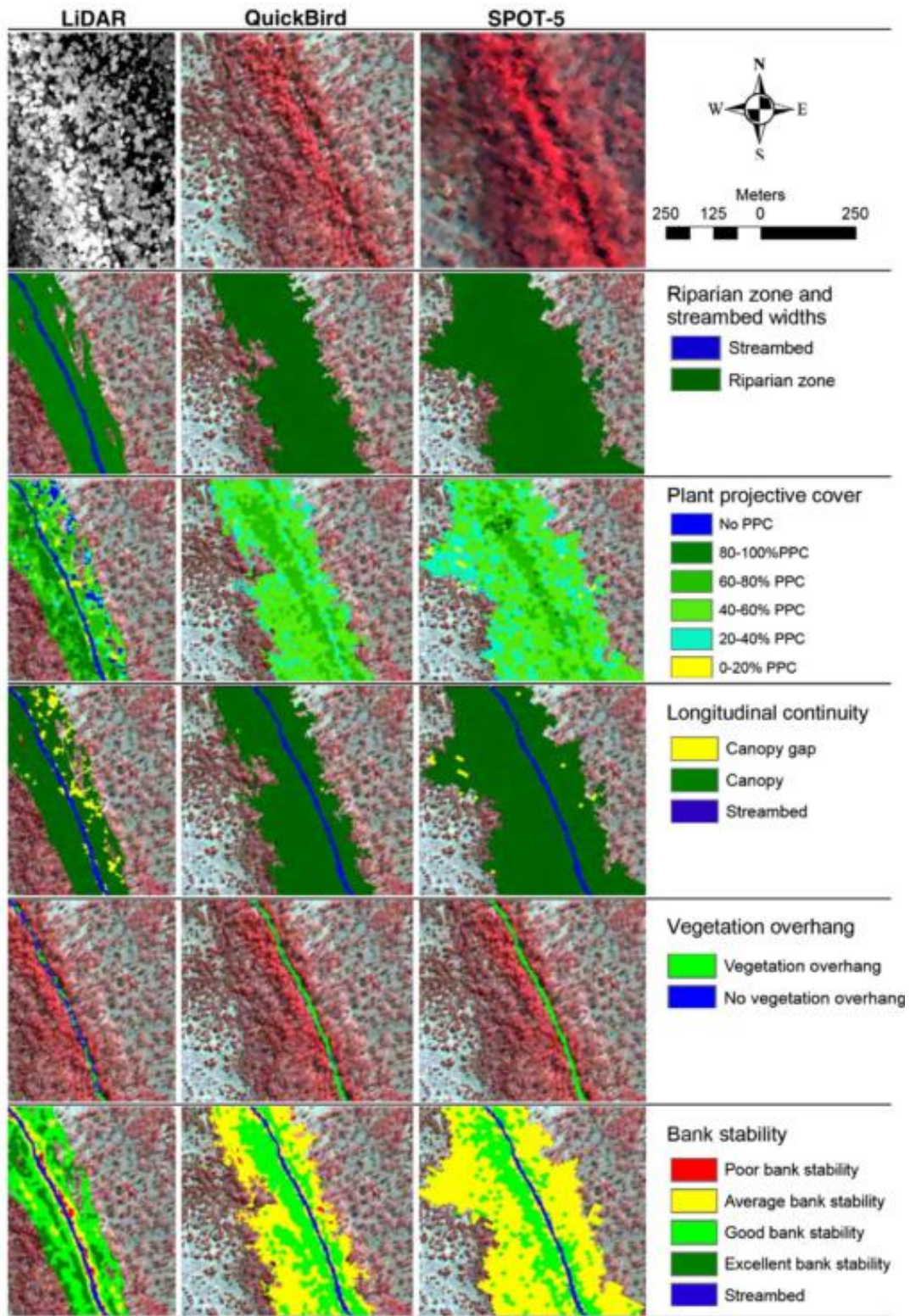
Figure J.14 Subset of the LiDAR, Quickbird and SPOT-5 images and corresponding riparian zone attributes maps (Johansen et al., 2010c).

J.3.2 Green and full-waveform LiDAR

In contrast to NIR LiDAR, shorter green wavelengths are capable of penetrating through the water column to the bed. These LiDAR systems, also called bathymetric LiDAR and originally designed for coastal environments, operate at 532 nm and only recently have been applied to rivers. The relevant portion of the bathymetric LiDAR signal corresponds to a back-scattered waveform, which usually contains two peaks, typically indicating the water surface and the bottom reflections (Bailly et al., 2012). However, most existing bathymetric LiDAR yeld a relatively coarse spatial resolution due to a large spot size and spacing and thus are not well suited to small- or medium-sized channels (Hilldale and Raff, 2008). In the work of (Allouis et al., 2010), bathymetric LiDAR proved to be highly capable of discriminating and precisely locating pools in rivers. Its great advantage is also the ability to continuously survey the topography inside and outside of the river channel.

The new generation of LiDAR instruments provides an integrated ability to acquire relatively high-resolution data describing both stream bathymetry, floodplains and the interactions across physical and biological domains over a great range of spatial scales from aquatic microhabitats covering a few square meters of a stream bed to major portions of channel networks in whole watersheds (McKean et al., 2009).

J.3.3 Radar data

Radar information was used to create the first global DEM from elevation data acquired during the Shuttle Radar Topography Mission (SRTM-DEM) at 3 arc second (90 m) spatial resolution. A DSM for the entire UK was produced using repeat pass SAR techniques applied to ERS-2 satellite data in the LandMap project (Muller, 2000), obtaining a standard deviation of height errors of ±11m and a spatial resolution of 25 m. The ASTER GDEM at 25 m target resolution (EU-DEM) isr the best available DEM at pan-European scale, and is available from the GISCO portal http://epp.eurostat.ec.europa.eu/portal/page/portal/gisco_Geographical_information_m aps/geodata/digital_elevation_model and also on http://land.copernicus.eu/in-situ/eu-dem/view.

For many current applications, optical remote sensing or active remote sensing such as Lidar provide higher resolution and richer spectral information in comparison with Radar technology and they are more suitable for characterizing riverine environments (as already noted in Section J2.1). However, radar imagery has shown interesting potential for flood inundation studies (Schumann et al., 2012). In particular, satellites and aircraft carrying Synethetic Aperture Radar (SAR) sensors are adopted since radar wavelengths can penetrate cloud cover and obtain land cover information through night and day. Satellite SAR imagery have an approximate 100m ground pixel size but the revisit time is of the range of three days and data can be obtained within 24h at low cost. For this reason these images are particularly suitable for monitoring major floods on medium to large rivers to inform flood management (Martinis et al., 2009; Pulvirenti et al., 2011). For finer resolution SAR, the revisit time can be up to 35 days so this data can be used only for major river basins. However with the recent launch of satellites carrying very fine resolution SAR (<5m) such as TerraSAR-X, RADARSAT 2 and the COSMO-SkyMed satellites, the situation is expected to change dramatically in the near future (Bates,

2006). Thus, SAR represents an alternative to optical imagery, areal photography and hydraulic models for mapping flood extent over large areas. It also provides valuable information for studying flood wave dynamics and so better supporting flood disaster management. Future potential uses will be to assimilate SAR data into hydraulic models to take advantage of this information for model parameter scaling behaviours and model optimization in general (Neal et al., 2009).

J.4 References

Alber A, Piégay H. 2011. Spatial disaggregation and aggregation procedures for characterizing fluvial features at the network-scale: Application to the Rhône basin (France). Geomorphology 125: 343–360.

Allouis T, Bailly J-S, Pastol Y, Le Roux C. 2010. Comparison of LiDAR waveform processing methods for very shallow water bathymetry using Raman, near-infrared and green signals. Earth Surf. Process. Landforms 35(6): 640-650.

Bailly J-S, Kinzel PJ, Allouis T, Feurer D, Le Coarer Y. 2012. Airborne LiDAR Methods Applied to Riverine Environments. In: Carbonneau PE, Piégay H. (Eds.), Fluvial Remote Sensing for Science and Management.

Baret F, Weiss M, Lacaze R, Camacho F, Makhmara H, Pacholcyzk P, Smets B. 2013. GEOV1: LAI and FAPAR essential climate variables and FCOVER global time series capitalizing over existing products. Part1: Principles of development and production. Remote Sens. Environ. 137: 299–309.

Barker DM, Lawler DM, Knight DW, Morris DG, Davies HN, Stewart EJ. 2009. Longitudinal distributions of river flood power: the combined automated flood, elevation and stream power (CAFES) methodology. Earth Surf. Process. Landforms 34, 280–290.

Bates PD. 2006. Invited commentary: remote sensing and flood inundation modelling. Hydrol. Process. 18: 2593–2597.

Bertrand M, Piégay H, Pont D, Liébault F, Sauquet E. 2013. Sensitivity analysis of environmental changes associated with riverscape evolutions following sediment reintroduction: geomatic approach on the Drôme River network, France. Int. J. River Basin Manag. 11: 19–32.

Biron PM, Choné G, Buffin-Bélanger T, Demers S, Olsen T. 2013. Improvement of streams hydro-geomorphological assessment using LiDAR DEMs. Earth Surf. Process. Landforms 38: 1808–1821.

Bizzi S, Lerner DN. 2013. The use of stream power as an indicator of channel sensitivity to erosion and deposition processes. available on-line, doi:10.1002/rra

Buffington JM, Montgomery DR. 2013. Geomorphic classification of river, in: Shroder, J., Wohl, E. (Eds.), Treatise on Geomorphology. San Diego, CA, pp. 730–767.

Carbonneau PE, Bergeron N, Lane SN. 2005. Automated grain size measurements from airborne remote sensing for long profile measurements of fluvial grain sizes. Water Resour. Res. 41: W11426.

Carbonneau PE, Lane SN, Bergeron NE. 2004. Catchment-scale mapping of surface grain size in gravel bed rivers using airborne digital imagery. Water Resour. Res. 40, W07202.

Carbonneau PE, Piégay H. 2012. Fluvial Remote Sensing for Science and Management. John Wiley & Sons, Ltd, Chichester, UK.

Cherkauer KA, Burges SJ, Handcock RN, Kay JE, Kampf SK, Gillespie AR. 2005. Assessing satellite-based and aircraft-based thermal infrared remote sensing for monitoring Pacific Northwest river temperature. J. Am. Water Resour. Assoc. 41(5): 1149–1159.

Clerici N, Weissteiner CJ, Paracchini ML, Boschetti L, Baraldi A, Strobl P. 2013. Pan-European distribution modelling of stream riparian zones based on multi-source Earth Observation data. Ecol. Indic. 24: 211–223.

EC, 2000. Directive 2000/60/EC of the European Parliament and of the council: establishing a framework for Community action in the field of water policy. Off. J. Eur. Communities L327: 1–71.

Fisher GB, Bookhagen B, Amos CB. 2013. Channel planform geometry and slopes from freely available high-spatial resolution imagery and DEM fusion: Implications for channel width scalings, erosion proxies, and fluvial signatures in tectonically active landscapes. Geomorphology 194: 46–56.

Fonstad MA, Marcus WA. 2005. Remote sensing of stream depths with hydraulically assisted bathymetry (HAB) models. Geomorphology 72: 320–339.

Fox M, Bolton S. 2007. A Regional and Geomorphic Reference for Quantities and Volumes of Instream Wood in Unmanaged Forested Basins of Washington State. North Am. J. Fish. Manag. 27: 342–359.

Gilvear D, Hunter P, Higgins T. 2007. An experimental approach to the measurement of the effects of water depth and substrate on optical and near infra-red reflectance: a field-based assessment of the feasibility of mapping submerged instream habitat. Int. J. Remote Sens. 28: 2241–2256.

Goetz A, Vane G, Solomon J, Rock B. 1985. Imaging spectrometry for Earth. Remote Sensing Sci. 228: 1147–1153.

Green RO, Asner G, Ungar S, Knox R. 2008. NASA Mission to Measure Global Plant Physiology and Functional Types. In: 2008 IEEE Aerospace Conference. IEEE, pp. 1–7.

Handcock RN, Torgersen CE, Cherkauer KA, Gillespie AR, Tockner K, Faux RN, Tan J. 2012. Thermal Infrared Remote Sensing of Water Temperature in Riverine Landscapes. In: Carbonneau PE, Piégay H. (Eds.), Fluvial Remote Sensing for Science and Management. pp. 85–113.

Hick P, Jernakoff P, Hosja W. 1998. Algal bloom research using airborne remotely sensed data: Comparison of high spectral resolution and broad bandwidth CASI data with field measurements in the swan river in Western Australia. Geocarto Int. 13, 19–28.

Hilldale RC, Raff D. 2008. Assessing the ability of airborne LiDAR to map river bathymetry Earth Surface Processes and Landforms 33(5): 773–783.

Johansen K, Arroyo LA, Armston J, Phinn S, Witte C. 2010a. Mapping riparian condition indicators in a sub-tropical savanna environment from discrete return LiDAR data using object-based image analysis. Ecol. Indic. 10: 796–807.

Johansen K, Arroyo LA, Armston J, Phinn S, Witte C. 2010b. Mapping riparian condition indicators in a sub-tropical savanna environment from discrete return LiDAR data using object-based image analysis. Ecol. Indic. 10: 796–807.

Johansen K, Coops NC, Gergel SE, Stange Y. 2007. Application of high spatial resolution satellite imagery for riparian and forest ecosystem classification. Remote Sens. Environ. 110: 29–44.

Johansen K, Phinn S. 2006. Mapping Structural Parameters and Species Composition of Riparian Vegetation Using IKONOS and Landsat ETM ℠ Data in Australian Tropical Savannahs. Photogramm. Eng. Remote Sens. 72: 71–80.

Johansen K, Witte C, Phinn S., 2010c. Mapping of riparian zone attributes using discrete return LiDAR, QuickBird and SPO-5 imagery: Assessing accuracy and costs. Remote Sens. Environ. 114: 2679–2691.

Kail J, Hering D, Muhar S, Gerhard M, Preis S. 2007. The use of large wood in stream restoration: experiences from 50 projects in Germany and Austria. J. Appl. Ecol. 44: 1145–1155.

Kaufmann H, Segl, K. ; Chabrillat, S. ; Hofer, S. ; Stuffier, T. ; Mueller, A. ; Richter, R. ; Schreier, G. ; Haydn, R. ; Bach, H. 2006. EnMAP – A Hyperspectral Sensor for Environmental Mapping and Analysis. Geoscience and Remote Sensing Symposium 2006, IGARSS 2006, 1617–1619.

Kirkby MJ, Jones RJA, Irvine B, Gobin A, Govers G, Cerdan O, Van Rompaey AJJ, Le Bissonnais Y, Daroussin J, King D, Montanarella L, Grimm M, Vieillefont V, Puigdefabregas J, Boer M, Kosmas C, Yassoglou N, Tsara M, Mantel S, Van Lynden G. 2004. Pan-European Soil

Erosion Risk Assessment: The PESERA Map, Version 1 , Office for Official Publications of the European Communities. Luxembourg.

Lallias-Tacon S Liébault F, Piégay H. 2014. Step by step error assessment in braided river sediment budget using airborne LiDAR data. Geomorphology 214: 307-323.

Legleiter CJ, 2012. Remote measurement of river morphology via fusion of LiDAR topography and spectrally based bathymetry. Earth Surf. Process. Landforms 37: 499–518.

Legleiter CJ, Marcus WA, Rick L. 2002. Effects of Sensor Resolution on Mapping InStream Habitats. Photogramm. Eng. Remote Sens. 68: 801–807.

Legleiter CJ, Roberts DA, Marcus WA, Fonstad MA. 2004. Passive optical remote sensing of river channel morphology and in-stream habitat: Physical basis and feasibility. Remote Sens. Environ. 93: 493–510.

Legleiter CJ, Roberts DA, Lawrence RL. 2009. Spectrally based remote sensing of river bathymetry Earth Surface Processes and Landforms 34(8): 1039–1059.

Lejot J, Delacourt C, Piégay H, Fournier T, Trémélo M, Allemand P. 2007. Very high spatial resolution imagery for channel bathymetry and topography from an unmanned. Earth Surf. Process. Landforms 32: 1705–1725.

Marcus WA, Fonstad M. 2010. Remote sensing of rivers: the emergence of a subdiscipline in the river sciences. Earth Surf. Process. Landforms 35: 1867–1872.

Marcus WA, Legleiter CJ, Aspinall RJ, Boardman JW, Crabtree RL. 2003. High spatial resolution hyperspectral mapping of in-stream habitats, depths, and woody debris in mountain streams. Geomorphology 55: 363–380.

Marcus WA, Marston RA, Colvard CR, Gray RD. 2002. Mapping the spatial and temporal distributions of woody debris in streams of the Greater Yellowstone Ecosystem, USA. Geomorphology 44: 323–335.

Martinis S, Twele A, Voigt S. 2009. Towards operational near real-time flood detection using a split-based automatic thresholding procedure on high resolution TerraSAR-X data. Nat. Hazards Earth Syst. Sci. 9: 303–314.

McCullough DA, Bartholow JM, Jager HI, Beschta RL, Cheslak EF, Deas ML, Ebersole JL, Foott JS, Johnson SL, Marine KR, Mesa MG, Petersen JH, Souchon Y, Tiffan KF, Wurtsbaugh WA, 2009. Research in Thermal Biology: Burning Questions for Coldwater Stream Fishes. Rev. Fish. Sci. 17: 90–115.

McKean J, Nagel D, Tonina D, Bailey P, Wright CW, Bohn C, Nayegandhi A. 2009. Remote Sensing of Channels and Riparian Zones with a Narrow-Beam Aquatic-Terrestrial LIDAR. Remote Sens. 1: 1065–1096.

Michez A, Piégay H, Toromanoff F, Brogna D, Bonnet S, Lejeune P, Claessens H. 2013a. LiDAR derived ecological integrity indicators for riparian zones: Application to the Houille river in Southern Belgium/Northern France. Ecol. Indic. 34: 627–640.

Michez A, Piégay H, Toromanoff F, Brogna D, Bonnet S, Lejeune, P, Claessens H, 2013b. LiDAR derived ecological integrity indicators for riparian zones: Application to the Houille river in Southern Belgium/Northern France. Ecol. Indic. 34: 627–640.

Muller J-P. 2000. The LandMap Project for the automated creation and validation of multiple resolution orthorectified satellite image products and a 1'' DEM of the British Isles from ERS tandem SAR interferometry, in: 26th Annual Conference of the Remote Sensing Society , 12-14 September. University of Leicester.

Neal J, Schumann G, Bates P, Buytaert W, Matgen P, Pappenberger F. 2009. A data assimilation approach to discharge estimation from space Hydrological Processes 23(25): 3641–3649.

Notebaert B, Piégay H. 2013. Multi-scale factors controlling the pattern of floodplain width at a network scale: The case of the Rhône basin, France. Geomorphology 200: 155-171.

Notebaert B, Verstraeten G, Govers G, Poesen J. 2009. Qualitative and quantitative applications of LiDAR imagery in fluvial geomorphology. Earth Surf. Process. Landforms 34: 217–231.

Pirot G, Straubhaar J, Renard P. 2014. Simulation of braided river elevation model time series with multiple-point statistics. Geomorphology 214: 148-156.

Pulvirenti L, Pierdicca N, Chini M, Guerriero L. 2011. An algorithm for operational flood mapping from Synthetic Aperture Radar (SAR) data using fuzzy logic. Nat. Hazards Earth Syst. Sci. 11: 529–540.

Rainey M, Tyler A, Gilvear D, Bryant R, McDonald P. 2003. Mapping intertidal estuarine sediment grain size distributions through airborne remote sensing. Remote Sens. Environ. 86: 480–490.

Sacchetti A, Cisbani A, Babini G, Galeazzi C. 2010. The Italian Precursor of an Operational Hyperspectral Imaging Mission. In: Sandau R, Roser H-P, Valenzuela A. (Eds.) Small Satellite Missions for Earth Observation: New Developments and Trends. Springer Heidelberg Dordrecht, London New York, 73–81.

Schmitt R, Bizzi S, Castelletti A. 2014. Characterizing fluvial systems at basin scale by fuzzy signatures of hydromorphological drivers in data scarce environments. Geomorphology 214: 69-83.

Schumann GJ, Bates PD, Di Baldassare G, Mason DC. 2012. The use of Radar imagery in riverine flood inundatation studies. In: Carbonneau PE, Piegay H. (Eds.) Fluvial Remote Sensing for Science and Management. Wiley-Blackwell, Chichester, p. 440.

Silva TF, Costa MF, Melack J, Novo ELM. 2008. Remote sensing of aquatic vegetation: theory and applications. Environ. Monit. Assess. 140: 131–145.

Smikrud KM, Prakash A. 2006. Monitoring Large Woody Debris Dynamics in the Unuk River, Alaska Using Digital Aerial Photography. GIScience Remote Sens. 43: 142–154.

Stout JC, Belmont P. 2014. TerEx Toolbox for semi-automated selection of fluvial terrace and floodplain features from lidar. Earth Surf. Process. Landforms 39: 569–580.

Underwood E. 2003. Mapping nonnative plants using hyperspectral imagery. Remote Sens. Environ. 86, 150–161.

Vianello A, Cavalli M, Tarolli P. 2009. LiDAR-derived slopes for headwater channel network analysis. CATENA 76: 97–106.

Weissteiner CJ, Bouraoui F, Aloe A. 2013. Reduction of nitrogen and phosphorus loads to European rivers by riparian buffer zones. Knowl. Manag. Aquat. Ecosyst. 15: article 8.

Weissteiner CJ, Pistocchi A, Marinov D, Bouraoui F, Sala S. 2014. An indicator to map diffuse chemical river pollution considering buffer capacity of riparian vegetation — A pan-European case study on pesticides. Sci. Total Environ. 484: 64–73.

Wheaton JM, Brasington J, Darby SE, Kasprak A, Sear D, Vericat D. 2013. Morphodynamic signatures of braiding mechanisms as expressed through change in sediment storage in a gravel-bed river. J. Geophys. Res. Earth Surf. 118: 759–779.

Williams, D., Rybicki, N., Lombana, A., O'Brien, T., Gomez, R., 2003. Preliminary Investigation of Submerged Aquatic Vegetation Mapping using Hyperspectral Remote Sensing. Environ. Monit. Assess. 81, 383–392. doi:10.1023/A:1021318217654